CROSS-SECTIONAL ANALYSIS OF THE MECHANICAL AND PHYSICAL PROPERTIES OF SPRUCE FOUNDATION PILES

AN INVESTIGATIVE ANALYSIS OF MOISTURE CONTENT, DENSITY, COMPRESSIVE STRENGTH, AND MODULUS OF ELASTICITY ACROSS THE CROSS-SECTION OF SPRUCE FOUNDATION PILES, WITH AN EMPHASIS ON THE PREDICTIVE PROFICIENCY OF MICRO-DRILLING METHODS

Michael Lee

MSc Thesis

Delft University of Technology

TU Delft

CROSS-SECTIONAL ANALYSIS OF THE MECHANICAL AND PHYSICAL PROPERTIES OF SPRUCE FONDATION PILES.

AN INVESTIGATIVE ANALYSIS OF MOISTURE CONTENT, DENSITY, COMPRESSIVE STRENGTH, AND MODULUS OF ELASTICITY ACROSS THE CROSS-SECTION OF SPRUCE FOUNDATION PILES, WITH AN EMPHASIS ON THE PREDICTIVE PROFICIENCY OF MICRO-DRILLING METHODS

MSc Thesis

By

Michael Lee

4746546

Supervisor:
Ir. G. Pagella *TU Delft*
Thesis committee:
Prof. Dr. Jan-Willem van de Kuilen, *TU Delft & TU Munich*
Dr. G.J.P. Ravenshorst, *TU Delft*
Dr. W. Gard, *TU Delft*
Ir. P. De Vries, *TU Delft*
Dr. Ir. Michele Mirra, TU Delft

Institution: Delft University of Technology
Place: Faculty of Civil Engineering and Geosciences, Delft

Cover Image: Foundation piles - Michael lee 2022

TU Delft

Preface

The content presented in this in these pages embodies a comprehensive two-year research exploration into the mechanical and physical properties through the cross-section of spruce foundation piles, with an emphasis on the predictive proficiency of micro-drilling methods. This master's thesis has been written to fulfil the requirements in order to attain an MSc in Civil Engineering, specifically Structural Engineering, specializing in steel, timber, and composite materials. The subject matter was introduced to me by G. Pagella, initially envisioned to encompass solely the physical attributes of spruce, namely moisture content and density, the scope of the project was subsequently broadened to encompass mechanical properties, specifically compressive strength, and modulus of elasticity. Additionally, an endeavour was made to incorporate a practical application, leading to an examination of the predictive capacities facilitated by the utilization of the IML-RESI PowerDrill apparatus. I am profoundly grateful to my daily supervisor Giorgio for his steadfast support throughout the entirety of this endeavour. His invaluable guidance, remarkable patience, and genuine care have been nothing short of extraordinary.

I extend my heartfelt thanks to Michele Mirra for his unwavering support, learning from him has been an absolute pleasure. His exceptional academic prowess continues to inspire me. I am deeply grateful also for Ruben's invaluable contribution to the journey of development and research. His remarkable pragmatism and exceptional manufacturing abilities have been the cornerstone of my progress. Working alongside you, Ruben, has not only been a pleasure but also a tremendous learning experience. Thank you for being such an integral part of this endeavour. Additionally, I express my sincere appreciation to my esteemed committee members for their unwavering enthusiasm, insightful guidance, and thought-provoking inquiries, each of which has contributed significantly to the refinement of my research. This gratitude extends to Prof. Dr. Jan-Willem van de Kuilen, Dr. G.J.P. Ravenshorst, Dr. W. Gard, and Ir. P. De Vries.

Embarking on my path at TU Delft, I quickly realised it wouldn't be an easy journey and there were times when the weight of it all, made surrender feel like my only choice. But through those trials, I discovered the true power of resilience, the unyielding strength of grit, and the enduring spirit within. My success, hard-fought and well-earned, was made possible by the unwavering support of an extraordinary group of individuals. To my beloved parents, Carole, and Philip, I am endlessly grateful for the beautiful life you have bestowed upon me. Your boundless love, invaluable lessons, and unwavering guidance have shaped me into the man I am today. I couldn't have dreamed of more extraordinary parents." To my siblings Christopher, Amy, Jonathan, Holly, and Becky, I'm reminded of a quote by Jeffrey Kluger: 'Our parents leave us too early, our spouse and our children come along too late. Our siblings are the only ones who are with us for the entire ride. Over the arc of decades, there may be nothing that defines us and forms us more powerfully than our relationship with our brothers and sisters.

There are others, not bound by blood, but woven into the fabric of my family, nonetheless. They've witnessed my evolution as an individual, standing as steadfast pillars in my journey. Among them, a cherished circle of friends who have illuminated my path, enriching my life with their unwavering presence and support. In both moments of triumph and times of adversity, their presence remains a source of comfort and strength, reminding me of the profound impact that chosen family can have on one's journey and how fortunate I am to have them. I extend this heartfelt thanks to Alex, David, Ciaran, Kevin, Gerhard, Giota, Julia, Tino, Carolin, Jamie, Zeynep, Defne, Kostandinos, Lasagne, Kosta, Alejandro, Pio, Henrique, Tal, Guiomar, Aditya, Sean, Zahid and to all the other remarkable souls I've encountered throughout this epic odyssey, thank you.

Michael Lee
October 2023

TU Delft

Summary

Numerous ancient historical constructions worldwide depend primarily on an extensive array of wooden foundation piles, as they are subject to loading conditions governed by the superstructure above. Wooden foundations transfer loads through a combination of compression and lateral resistance. The inherent strength of wood handles compressive forces, while stiffness and soil friction counteract lateral loads. Proper arrangement and maintenance ensure even load distribution. Careful design, wood quality, depth, and protective treatments are essential for longevity and load-bearing efficiency.

Amsterdam, the Netherlands' capital city, renowned for its rich artistic heritage, intricate canal infrastructure, and slender architectural dwellings, originated as a modest fishing hamlet that underwent remarkable development into a prominent global European city. During this urban transformation, less visible engineering elements, such as wooden foundation piles, were overlooked, despite their critical significance. In Amsterdam's historical core, the majority of structures including buildings, bridges, and quay walls, rely on these wooden supports. Noteworthy, the city estimates that 12 million such piles are still active. These structural components have consistently demonstrated economic efficiency and reliability. Nonetheless, the aging process affecting these foundations, with some dating back up to 500 years, introduces complexities when assessing their current load-bearing capacities and the ensuing reliability of the structures they support.

The lack of knowledge and inspection techniques of the mechanical and physical properties of these timber piles hinders a proper evaluation of the remaining life span of the foundations which could lead to possible irreplaceable structural damage to these structures. This body of research evaluates the physical and mechanical properties such as the actual moisture content, density distribution, compressive strength, and modulus of elasticity through the cross section of Spruce (*Picea abies*) foundation piles. Therefore, the overarching research question has arisen:

"How do the variations of mechanical and physical attributes manifest across the cross-sectional profile of both degraded and non-degraded spruce foundation piles and how can micro-drilling techniques be utilized to assess these characteristics?"

This will be achieved by means of small-scale compressive experimental testing of five prisms extracted from each cross-section (3 separate locations along the length of the pile) of foundation piles never driven into the soil and piles that were retrieved under bridges in the historical centre of Amsterdam that were planned to be demolished. These aforementioned retrieved piles had a service life between 100 years and 300 years, always under the water table, presenting mechanical degradation due to loading over time and in addition possible bacterial degradation of the cross section peripheral regions.

Initially, micro-drilling techniques were employed to ascertain the drilling amplitude. This step served to assess the initial quality of the wood under examination. Additionally, it aided in identifying specific points of interest for specimen extraction, including degraded wood in the peripheral regions, sound wood in the internal section, and the pith. Subsequently, the acquired data underwent thorough analysis. This analysis, combined with the micro-drilling measurements, enabled an assessment of the potential applicability of drilling amplitude in predicting the mechanical and physical properties of the pile. This sequential approach ensured a systematic and scientifically rigorous evaluation of the wood's characteristics and its implications for pile performance. The investigation was conducted to enhance the understanding of the structural performance and material characteristics of spruce foundation piles, while also evaluating the applicability of micro-drilling methods as a predictive tool in engineering assessments.

The findings revealed a consistent pattern across degraded specimens. Peripheries (Avg. Specimens 1 & 5) showed higher moisture content (233 ± 61%), lower dry density (278 ± 46 kg/m^3), resulting in reduced strength (5 ± 3 kN/m^2) and MOE (2239 ± 1398 MPa) in the softshell domain. Standard deviation indicated significant variability. Conversely, central sections (Avg. Specimens 2, 3 & 4) exhibited lower moisture content (70 ± 19%), higher dry density (399 ± 13 kg/m^3), with increased strength (11 ± 2 kN/m^2) and MOE (5894 ± 1382 MPa). Standard deviation suggested uniformity, reflecting consistent structural integrity. In summary, external regions displayed a 332% increase in

moisture content, 70% decrease in dry density, 49% decrease in strength, and 38% decrease in MOE compared to internal sections.

The examination of the non-degraded specimens revealed a discernible pattern. Peripheries (Avg. Specimens 1 & 5) exhibited higher moisture content (132 ± 22%), dry density (472 ± 46 kg/m^3), compressive strength (17 ± 2.8 kN/m^2) and MOE (9296.7 ± 1919 MPa), resulting in a slight decrease in strength and stiffness compared to internal regions. Internal sections (Avg. Specimens 2 & 4) displayed lower moisture content (54 ± 23.4%), higher dry density (513.5 ± 48.1 kg/m^3), as well as increased compressive strength (21.8 ± 2.9 kN/m^2) and MOE (12216.5 ± 2342 MPa). Samples from the pith (Sample 3) consistently showed the lowest values for moisture content (45 ± 12.4%), dry density (438 ± 47.6 kg/m^3), as well as compressive strength (13 ± 1.9 kN/m^2) and MOE (6795 ± 838.85 MPa) within the juvenile regions.

The micro-drilling signal was examined in relation to physical and mechanical properties: For degraded specimens, the average softshell thickness was 38mm, 39mm, and 41mm respectively. Linear regression showed highly significant correlations: 70% for MC, 81% for dry density, 78% for compressive strength, and 76% for MOE. An in-depth analysis focused on compressive strength and drilling amplitudes under 15% within the softshell layer resulted in an even higher R^2 value of 0.81. For non-degraded samples, regression analysis showed lower significance: 2.5% for MC, 46% for dry density, 27% for compressive strength, and 58% for MOE. This low statistical result was to be expected given the natural variability of the new wood specimens. A final analysis on all six piles together showed statistically significant correlations: 59% for MC, 69% for dry density, 53% for compressive strength, and 67% for MOE. These models enable the prediction of new properties for untested scenarios by incorporating additional drilling amplitude values.

Samenvatting

Talloze oude, historische constructies over de hele wereld zijn voornamelijk afhankelijk van een uitgebreide reeks houten funderingspalen, omdat ze onderhevig zijn aan belastingomstandigheden die worden bepaald door de bovenbouw erboven. Houten funderingen dragen belastingen over door een combinatie van compressie en laterale weerstand. De inherente sterkte van hout kan drukkrachten opvangen, terwijl stijfheid en bodemwrijving laterale belastingen tegengaan. Een juiste opstelling en onderhoud zorgen voor een gelijkmatige verdeling van de belasting. Zorgvuldig ontwerp, houtkwaliteit, diepte en beschermende behandelingen zijn essentieel voor een lange levensduur en draagvermogen.

Amsterdam, de hoofdstad van Nederland, bekend om zijn rijke artistieke erfgoed, ingewikkelde kanaalinfrastructuur en smalle architectonische woningen, ontstond als een bescheiden vissersdorpje dat een opmerkelijke ontwikkeling onderging tot een prominente Europese wereldstad. Tijdens deze stedelijke transformatie werden minder zichtbare technische elementen, zoals houten funderingspalen, ondanks hun cruciale belang over het hoofd gezien. In de historische kern van Amsterdam is het merendeel van de constructies, waaronder gebouwen, bruggen en kademuren, afhankelijk van deze houten steunen. Opmerkelijk is dat de stad schat dat er nog steeds twaalf miljoen van dergelijke palen actief zijn. Deze structurele componenten hebben consequent blijk gegeven van economische efficiëntie en betrouwbaarheid. Desalniettemin introduceert het verouderingsproces dat deze funderingen aantast, waarvan sommige al 500 jaar oud zijn, complexiteit bij het beoordelen van hun huidige draagvermogen en de daaruit voortvloeiende betrouwbaarheid van de constructies die ze ondersteunen.

Het gebrek aan kennis en inspectietechnieken van de mechanische en fysische eigenschappen van deze houten palen belemmert een goede evaluatie van de resterende levensduur van de funderingen, wat zou kunnen leiden tot mogelijk onvervangbare structurele schade aan deze constructies. Dit onderzoek zal de fysieke en mechanische eigenschappen evalueren, zoals het feitelijke vochtgehalte, de dichtheidsverdeling, de druksterkte en de elasticiteitsmodulus door de dwarsdoorsnede van funderingspalen van sparrenhout (Picea abies). Daarom is de overkoepelende onderzoeksvraag ontstaan:

“Hoe manifesteren de variaties in mechanische en fysieke kenmerken zich in het dwarsdoorsnedeprofiel van zowel aangetaste als niet aangetaste sparrenfunderingspalen en hoe kunnen microboortechnieken worden gebruikt om deze kenmerken te beoordelen?”

Dit zal worden bereikt door middel van kleinschalige experimentele drukproeven met vijf prisma's die uit elke dwarsdoorsnede (3 afzonderlijke locaties langs de lengte van de paal) worden gehaald van nooit in de grond geslagen funderingspalen en palen die onder bruggen vandaan zijn herwonnen in het historische centrum van Amsterdam die gesloopt zouden worden. Deze eerder genoemde herwonnen palen hadden een gebruiksduur tussen de 100 en 300 jaar, altijd onder de grondwaterspiegel, en vertoonden mechanische degradatie als gevolg van langdurige belasting en bovendien mogelijke bacteriële degradatie van de perifere gebieden van de dwarsdoorsnede.

Aanvankelijk werden microboortechnieken gebruikt om de booramplitude vast te stellen. Deze stap diende om de initiële kwaliteit van het onderzochte hout te beoordelen. Bovendien hielp het bij het identificeren van specifieke aandachtspunten voor de extractie van monsters, waaronder aangetast hout in de perifere gebieden, gezond hout in het interne gedeelte en het merg. Vervolgens werden de verkregen gegevens grondig geanalyseerd. Deze analyse, gecombineerd met de microboormetingen, maakte een beoordeling mogelijk van de potentiële toepasbaarheid van de booramplitude bij het voorspellen van de mechanische en fysische eigenschappen van de paal. Deze sequentiële aanpak zorgde voor een systematische en rigoureus wetenschappelijk evaluatie van de eigenschappen van het hout en de implicaties ervan voor de paalprestaties. Het onderzoek werd uitgevoerd om het inzicht in de structurele prestaties en materiaaleigenschappen van funderingspalen van sparrenhout te vergroten, evenals om de toepasbaarheid van microboormethoden als voorspellend hulpmiddel bij technische beoordelingen te evalueren.

De bevindingen onthulden een consistent patroon bij aangetaste exemplaren. De periferie (Gem. Monsters 1 & 5) vertoonde een hoger vochtgehalte (233 ± 61%), een lagere droge dichtheid (278 ± 46 kg/m^3), resulterend in verminderde sterkte (5 ± 3 kN/m^2) en MOE (2239 ± 1398). MPa) in het softshell-domein. Standaarddeviatie duidde op significante variabiliteit. Omgekeerd vertoonden

centrale secties (Gem. Monsters 2, 3 & 4) een lager vochtgehalte (70 ± 19%), een hogere droge dichtheid (399 ± 13 kg/m^3), met verhoogde sterkte (11 ± 2 kN/m^2) en MOE (5894 ± 1382 MPa). Standaardafwijking suggereerde uniformiteit, wat een consistente structurele integriteit weerspiegelt. Samenvattend vertoonden externe regio's een toename van 332% in vochtgehalte, 70% afname in droge dichtheid, 49% afname in sterkte en 38% afname in MOE vergeleken met interne secties.

Het onderzoek van het niet aangetaste monster bracht een waarneembaar patroon aan het licht. De randen (Gem. Monsters 1 & 5) vertoonden een hoger vochtgehalte (132 ± 22%), droge dichtheid (472 ± 46 kg/m^3), druksterkte (17 ± 2,8 kN/m^2) en MOE (9296,7 ± 1919 MPa), resulterend in een lichte afname in sterkte en stijfheid vergeleken met interne regio's. Interne secties (Gem. Monsters 2 & 4) vertoonden een lager vochtgehalte (54 ± 23,4%), een hogere droge dichtheid (513,5 ± 48,1 kg/m^3), evenals een verhoogde druksterkte (21,8 ± 2,9 kN/m^2) en MOE (12216,5 ± 2342 MPa). Monsters uit het merg (Monster 3) vertoonden consistent de laagste waarden voor vochtgehalte (45 ± 12,4%), droge dichtheid (438 ± 47,6 kg/m^3), evenals druksterkte (13 ± 1,9 kN/m^2) en MOE (6795 ± 838,85 MPa) binnen de juveniele regio's.

Het microboorsignaal werd onderzocht in relatie tot de fysieke en mechanische eigenschappen: voor aangetaste exemplaren was de gemiddelde dikte van de softshell respectievelijk 38 mm, 39 mm en 41 mm. Lineaire regressie liet zeer significante correlaties zien: 70% voor MC, 81% voor droge dichtheid, 78% voor druksterkte en 76% voor MOE. Een diepgaande analyse gericht op druksterkte en booramplitudes onder de 15% binnen de softshelllaag resulteerde in een nog hogere R^2-waarde van 0,81. Voor niet aangetaste monsters toonde regressieanalyse een lagere significantie: 2,5% voor MC, 46% voor droge dichtheid, 27% voor druksterkte en 58% voor MOE. Dit lage statistische resultaat was te verwachten gezien de natuurlijke variabiliteit van de nieuwe houtmonsters. Een laatste analyse van alle zes palen samen liet statistisch significante correlaties zien: 59% voor MC, 69% voor droge dichtheid, 53% voor druksterkte en 67% voor MOE. Deze modellen maken het voorspellen van nieuwe eigenschappen voor niet geteste scenario's mogelijk door aanvullende booramplitudewaarden mee te nemen.

Translation – R. Weinzierl

Index of Symbols and abbreviations

A	:Area (mm^2)
A_r	:Average cross-sectional area (mm^2)
D_{avg}	:Average diameter of the wooden pile (mm)
ε	:Strain (με)
F	:Force (in kN)
F_{max}	:Maximum force (kN)
f	:*F*requency (in Hz)
***fc*,$_{0,wet}$**	:Wet compression strength parallel to grain (N/mm^2)
***fc*,$_{0,wet,mean}$**	:Mean wet compression strength parallel to grain (in N/mm^2)
L	:Length (mm)
L0	:Span of the linear potentiometers (mm)
m	:Mass (kg)
$m_{pile,dry}$	:Calculated dry mass of the pile at MC = 0% (kg)
$m_{pile,wet}$	:Wet mass of the pile at test moisture content (kg)
MC	:Moisture content (%)
MOE_{stat}	:Modulus of elasticity parallel to the grain (N/mm^2)
MOE_{dyn}	:Dynamic modulus of elasticity parallel to the grain (N/mm^2)
ρ	:Density (kg/m^3)
$ρ_{dry}$	:Calculated dry density at MC = 0% (kg/m^3)
$ρ_{mean}$	:Mean density (kg/m^3)
$ρ_{wet}$	:Wet density at test moisture content (kg/m^3)
SD	:Standard deviation
σ	:Stress (MPa)
Vpile,dry	:Calculated dry volume of the pile at MC = 0% (m^3)
Vpile,wet	:Wet volume of the pile at test moisture content (m^3)

Contents

Introduction **1**
1.1 Background 1
1.2 Problem statement 1
1.3 Aim of the thesis 2
Literature review **3**
2.1 Introduction 3
2.2 A brief history of wooden piles 3
2.3 Wood anatomy 4
2.4 Wood Density & reaction wood. 5
2.5 Moisture content 6
2.6 Shrinkage and swelling 7
2.7 Wood Decay 7
2.7.1 Fungal decay 7
2.7.2 Bacterial decay 9
2.8 Small sample testing 9
2.9 Failure modes 11
2.10 Wooden foundation preservation 13
2.10.1 Foundation inspection protocol 13
2.10.2 Predictive models 14
2.11 Contemporary Evaluation Methods for Timber Piles 16
2.12 Micro-drilling resistance measurements 17
2.13 Soft shell calculator 18
2.14 Investigation into the application of micro-drilling (RPD) measurements. 18
2.15 State of art conclusion 19
Research Question(s), Aims & Objectives **21**
3.0 Research question 21
3.1 Research sub-question(s) 21
3.2 Research objective 21
Methodology **22**
4.1 Experimental set-up 22
4.2 Materials 22
4.3 Manufacturing of specimens 24
4.3.1 Preparation phase 24
4.3.2 Production phase 25
4.4 Moisture content ($\boldsymbol{MC}$) and Density ($\boldsymbol{\rho}$) 27
4.5 Compression tests 27
4.6 Modulus of elasticity 28
4.7 RPD Data 30
4.8 Experiment procedures 32
4.9 Individual pile selection 32

Results **33**
5.1 Introduction 33
5.2 Degraded piles 37
5.2.1 Pile 3M 37
5.2.2 Pile 2.7M 39
5.2.3 Pile 6M 41
5.2.4 Pile 6M_60mm sample 43
5.3 Non-degraded piles 45
5.3.1 Pile 3.18M 45
5.3.2 Pile 11M 47
5.3.3 New Pile 10588M 49
5.3.4 Pile 11M_60mm sample 51
5.3.5 Pile 3.18M_60mm Sample 53
5.4 Result summary 55
5.4.1 Degraded Piles: 55
5.4.2 Non-Degraded Piles: 55
5.5 Size effect 60mm vs 120mm. 57
Analysis **59**
6.1 Introduction 59
6.2 Degraded piles (2.7M, 3M, and 6M) 59
6.2.1 Moisture content vs Average drilling amplitude 59
6.2.2 Oven dry density vs Average drilling amplitude 60
6.2.3 Wet compression strength vs Average drilling amplitude 60
6.2.4 Modulus of elasticity vs Average drilling amplitude 61
6.2.5 Degraded piles analysis conclusion 62
6.3 Non-Degraded piles (3.18M, 11M, and 10588M) 62
6.3.1 Moisture content vs Average drilling amplitude 62
6.3.2 Oven dry density vs Average drilling amplitude 63
6.3.3 Wet compression strength vs Average drilling amplitude 63
6.3.4 Modulus of elasticity vs Average drilling amplitude 64
6.3.5 Non-Degraded piles analysis conclusion 64
6.4 Degraded and non-degraded piles (2.7M, 3M, 6M, 3.18M, 11M & 10588M) 65
6.4.1 Moisture content vs Average drilling amplitude 65
6.4.2 Oven dry density vs Average drilling amplitude 66
6.4.3 Wet compression strength vs Average drilling amplitude 67
6.4.4 Modulus of elasticity vs Average drilling amplitude 68
6.4.5 Degraded piles analysis conclusion 69
6.5 Predictive model for 60mm samples MOE results. 70
6.6 Predictive model for degraded sections. 71
Conclusions and outlook **72**
7.1 Main outcomes and concluding remarks. 72
7.1.1 Degraded samples 72

7.1.2 Non-degraded samples 73
7.1.3 Micro-drilling techniques 74
7.1.4 Formulas 74
7.2 Future implications and recommendations 75
7.3 Research sub-question(s) and answers 76
References 80
Appendix – Results 82
A.1 Moisture content and density through the complete section 82
A.2 - 10588M (2019) New pile HIE-P10588 87
A.3 - 11M (1922) BRU0041-PL2-P1.9 94
A.4 - 3.18M (1886)BRU0030-PL1-P3.18 105
A.5 - 3M – (1727)BRU0030-PL1-P2.13 117
A.6 - 2.7M (1727) - BRU0030 PL1 P2.7 124
A.7 - 6M (1727) - BRU0030-PL2-P2.21 131
A8 - Future predictive model strategy based on linear regression. 141
A9 - Cross-sectional bearing capacity future calculation strategy based on drilling amplitude. 144

1

Introduction

1.1 Background

Foundations are crucial to every aspect of humanity from the food we eat, to the structures that protect us. Even accumulation of knowledge and logic needs to be built on a strong foundation. For centuries, wooden pile constructions support buildings in areas with unstable soils in Europe, and many other parts of the world [1] The use of pile foundations started as early as the 15th century, when short stakes from different wood species were employed to support the erection of stone walls in Amsterdam. [2] Since then, various different foundation types were developed as our requirement for larger structures evolved which paved way for technological advancements. Thus, foundations became dimensionally larger which naturally increased the bearing capacity.

Wooden foundations had been used for hundreds of years until around the 1950's when concrete took over as the dominant material being used. The reason for this was that concrete could obtain a higher bearing capacity, logistically speaking it is easier to transport and had enhanced durability making the design of structure more flexible. However, a substantial part of the man-made building constructions are still supported on wooden piles and range in ages from decades until several centuries such as the Taj Mahal in India or even the Grand Palais in Paris. It is imperative that these buildings with such culturally significant importance are preserved. These old constructions stand as a testament that wood can be a durable material for foundations but requires attention to ensure the structures remain safe for their intended functions. [3]

1.2 Problem statement

Across the Netherlands, historical structures embellish cities, imparting cultural and economic significance, with Amsterdam serving as a prime example. The Dutch capital is currently undergoing rapid expansion, resulting in a continuous influx of new architectural designs. However, amidst this urban evolution, certain less apparent engineering aspects, like wooden foundation piles, might inadvertently receive insufficient attention despite their importance. Within Amsterdam's historic centre, the majority of structures – encompassing buildings, bridges, and quay walls – rest upon these wooden piles. Notably, the city estimates over 12 million such piles are currently in use. These structural elements have consistently demonstrated economic efficiency and reliability over time. Nevertheless, the aging process affecting these foundations, with some dating back up to 500 years, introduces challenges when evaluating present load-bearing capacities and the subsequent reliability of upper structures.

For a comprehensive evaluation of the reliability and safety of pivotal structures including bridges, quay walls, and buildings, a thorough investigation of the remaining strength of timber pile foundations proves imperative. This analytical endeavour focuses on a profound understanding of the material both biological and chemical, and also the mechanical and physical properties inherent to wooden piles. In a strategic collaboration, the Municipality of Amsterdam (*Geemente Amsterdam* in Dutch), has enlisted the specialized expertise of TU Delft's Bio-based Structures and Materials Group to embark upon an investigative venture aimed at examining the residual load-bearing capacity of the foundation piles from several different sites around the city. Two specific locations have already undertaken preparations for the replacement of the existing foundational piles of the bridges, and these identified piles will be employed as test specimens within this thesis.

The ramifications arising from the degradation of both structures and infrastructures impose substantial burdens on local residents, tourists, governmental entities, and property owners. The financial implications associated with rectifying or replacing these foundational elements can encompass a substantial proportion, potentially reaching up to 50% of the total project cost. This has prompted new research as it is estimated that the financial magnitude of the problem ranges from 1 to 40 billion Euros [3]. It also means that transit routes and public interference will be a nuisance in an already highly condensed, congested, and populated area as most of the piles are found in the historical centres. In the context of monitoring land subsidence, Amsterdam has strategically deployed measuring bolts on building facades across nearly all neighbourhoods encircled by the A10 motorway [5]. These specialized devices are instrumental in consistently assessing subsidence phenomena and maintaining vigilance over any pending developments.

Foundations often face a significant challenge in the form of biological degradation, primarily driven by bacterial decay. Up until approximately 90 years ago, there was a prevailing belief that wood remained immune to degradation under oxygen-deprived conditions; however, subsequent research discredited this notion [6]. Bacterial decay significantly modifies the chemical composition and structural characteristics of timber, consequently exerting a substantial influence on the longevity of compromised elements [7]. As a result, the evaluation of bacterial decay emerges as a pivotal factor in determining the projected service life of timber piles [8].

1.3 Aim of the thesis

The aim of this master's thesis is to develop a comprehensive approach for characterizing the distribution of the physical and mechanical properties throughout the cross section of spruce foundation piles. The piles involved in this study, obtained from beneath bridges in Amsterdam, were driven into the soil in different ages: 18th, 19th and beginning of 20th century. The research outcome will primarily encompass the establishment of an integral methodology for assessing properties such as moisture content, density, modulus of elasticity, and compressive strength. To achieve this, a series of small-scale compressive tests will be conducted parallel to the grain on clear samples extracted along the cross-section of the piles. The possible presence of biological degradation in the material will be studied with micro-drilling measurements. Micro-drilling will be used on one hand to quantify the degraded portion of the cross section, named soft shell, and on the other hand to correlate the material and mechanical properties to the micro-drilling signals. This approach will allow to determine a strength profile across the cross-sectional area, considering the influence of bacterial degradation on the compressive strength. Furthermore, this investigation aims to provide insights into the individual contributions of different mechanical and physical in order to determine if a prediction solely based on drilling amplitude can be made.

In addition to the detailed investigation of the physical and mechanical properties, an essential aspect of this thesis involves the graphical representation of these properties. To enhance the comprehensibility of the obtained data, the moisture content, density, modulus of elasticity, and compressive strength values will be meticulously plotted on graphs. These graphs will be structured to include the specific locations from which the samples were extracted along the cross-section of the spruce piles. By spatially mapping these properties, the graphical representations will provide a visual framework that correlates the variations in physical and mechanical attributes with the corresponding positions within the cross-sectional profiles of the piles. This graphical approach offers an intuitive means to identify trends, irregularities, and potential relationships that may exist across the length and depth of the piles, thus contributing to a more insightful understanding of the structural behaviour and degradation patterns of foundation elements.

2

Literature review

2.1 Introduction

Wood, a naturally occurring organic substance, is composed of intricate cell structures and serves as a complex chemical compound encompassing cellulose, hemicellulose, lignin, and various other constituents. The inherent anisotropic quality of wood stems from the elongated configuration of its cells and the alignment of its cell walls. This distinctive anisotropic characteristic requires that engineers and designers possess an in-depth comprehension of the physical and mechanical attributes of bio-based materials to facilitate the development of efficient and optimal designs [4]. Wood is classified into two primary types: coniferous, often termed softwood, and deciduous, commonly referred to as hardwood. Softwoods find greater use in the construction industry due to factors such as ease of manipulation, cost-effectiveness, and environmental sustainability. Within the context of Amsterdam's construction landscape, the majority of wooden piles originate from coniferous trees. Specifically, spruce and pine emerge as the prevalent wood species utilized for timber piles in the region. This emphasis on spruce serves as the rationale behind this thesis, which delves into the examination of its respective properties and behaviours.

2.2 A brief history of wooden piles

In the context of pile foundations within the Netherlands, a fundamental comprehension of subsurface conditions is imperative. The Netherlands, characterized as a typical deltaic region, is shaped by the convergence of the Rhine and Meuse rivers, flowing into the North Sea (Figure 1). Over the course of the Holocene epoch spanning the past 10,000 years, the contemporary landscape of the Netherlands has predominantly evolved, with sea level fluctuations and resultant soil variations primarily concentrated in its western territories. The prevailing Holocene soils consist of cohesive and soft materials, primarily marine clays combined with peat, often extending to depths of up to 16 meters across the Netherlands. Underlying the Holocene layers are stiffer soils and over-consolidated clays from the Pleistocene era. Given the limited bearing capacity of the soft Holocene strata, the application of pile foundations becomes essential, with deeper Pleistocene sand layers offering the necessary load-bearing capacity for foundational support. [5]

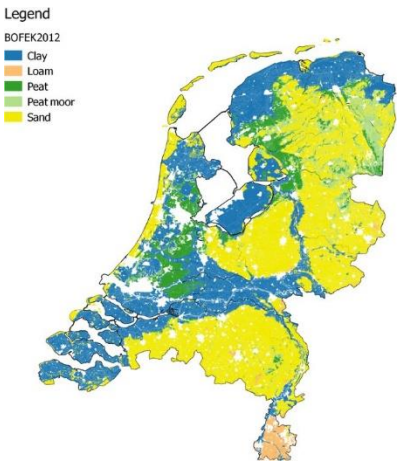

Figure 1 Soil Physical Map of the Netherlands [74]

The historical timeline from archaeological studies reveals that as early as the 15th century, small pegs were employed to bolster the construction of stone walls in Amsterdam. Subsequently, more extended, and closely spaced piles were utilized to compact the soil and enhance foundation stability. During the 17th century, the practice of embedding pile foundations, predominantly composed of pine, spruce, and alder, deeper into the stable sand layer became established. [6] This was facilitated by the introduction of a hammering system (Figure 2 left) near the close of the 17th century, involving a tripod apparatus and a weight that could be raised and then lowered onto the pile head by a team of individuals, with the weight ranging from 250 to 300 kilograms. The advent of steam engine technology revolutionized pile installation, enabling the driving of piles to greater depths. It was recognized during this era that piles fully submerged in water exhibited enhanced resistance to decay. Consequently, the 18th century saw the prominence of the

"Amsterdam foundation," (Figure 3 right) characterized by round timber piles featuring an average head diameter ranging from 180 to 200 millimetres [7].

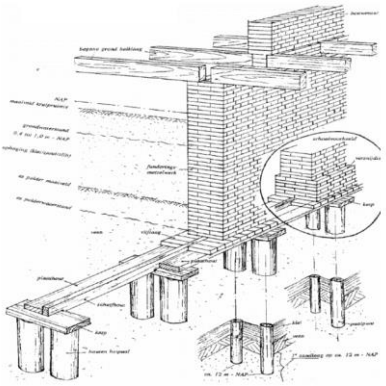

Figure 2, Left - Wooden palisades in the water were applied with manpower. [8] Figure 3, Right - Amsterdam foundation [7]

2.3 Wood anatomy

The stem of a tree serves a multitude of crucial functions that contribute to its overall health and vitality. Foremost among these roles is providing robust structural support to bear the weight of the crown, which houses the tree's leaves and branches, shielding them from the elements and allowing them to efficiently capture sunlight for photosynthesis. Furthermore, the stem acts as a lifeline for the tree, facilitating the transport of vital nutrients and water from the roots to all parts of the tree (Figure 4 Left). Notably, the tree allocates nutrients that are not utilized in the formation of wood towards the roots, where they are strategically stored for future use, ensuring the tree's resilience in times of scarcity. As the tree matures, it undergoes a dual growth process. It elongates lengthwise, while also expanding its girth, progressively widening its circumference. This growth is evident in the annual rings that develop within the cambium, the actively dividing layer just beneath the bark. These concentric rings, collectively referred to as yearly rings, chronicle the tree's age and life history in their unique patterns. The yearly rings are split into earlywood and latewood. Earlywood, formed during the tree's active growth period, tends to be lighter in density and colour. Its porous structure allows for efficient water and nutrient transport. In contrast, latewood, which forms as growth slows down, is denser and darker. The stark contrast between these two types of wood gives each yearly ring its distinct appearance. (Figure 4 Right)

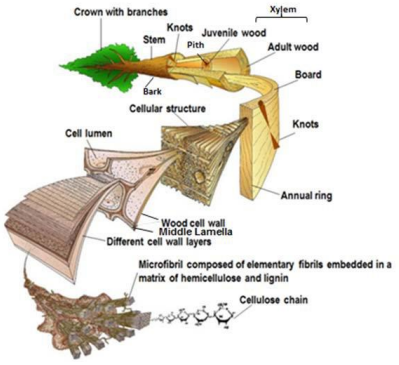

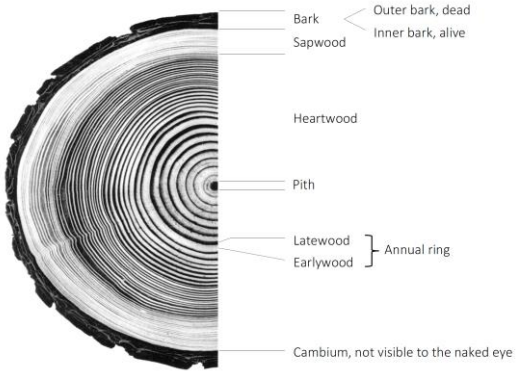

Figure 4 Left - Scheme of the hierarchical structure of coniferous wood (softwood). [9] Cross-section through a coniferous stem, Douglas fir. [10]

The internal structure of the trunk is split up into 3 sections, juvenile wood, heartwood, and sapwood. Juvenile wood is formed during the first three or so years of life of a tree is generally dominated by the so-called juvenile wood of which its properties differ from that of mature wood as it has a high anatomical variability, low-specific gravity, low density and strength, and greater longitudinal shrinkage. [12] Heartwood is the mature wood located in the central section and consists entirely of inactive tissues. This means that it is mechanically strong and also naturally resistant to decay. Sapwood, contains the living cells and is located on the outer layers of the trunk, naturally making it more prone to decomposition and decay due to the availability of nutrients and location. As trees

mature, water conduction is limited to the outer part and younger annual rings known as sapwood, which also acts as a storage area with living cells. Inner heartwood, without living cells, provides structural support. The transformation of sapwood into heartwood involves biochemical processes, changing the tree's balance and sealing cell pits. Heartwood typically has a darker colour due to its chemical composition. Lighter-coloured heartwood does not necessarily lack pulp; it simply lacks pigmented pulp. Heartwood, being sealed and non-living, is often more durable than sapwood.

2.4 Wood Density & reaction wood.

The study [11] delved into the intricate variations in wood density within Norway spruce trees, focusing on parameters like annual ring density, earlywood and latewood density, ring width, and latewood percentage. This comprehensive analysis spanned from the core to the bark and from the stem base to its apex, encompassing 85 trees from central and south-eastern Finland. The research revealed several noteworthy findings: firstly, the variation between annual rings accounted for a substantial portion (11–27%) of the total wood density variation. Secondly, differences in wood density across different stem heights were relatively small (3–6%). Most significantly, the largest variation in wood density (49–80%) was found within the annual rings. Interestingly, wood density distinctions between earlywood and latewood were more pronounced in the outer rings compared to those nearer the core. Moreover, the increase in wood density from the core outwards was closely tied to higher latewood density and latewood percentage, whereas earlywood density exhibited only marginal increases. This study not only validated existing knowledge of wood density variation but also provided crucial insights that can be instrumental in creating predictive models for wood density—a vital factor in industries relying on Norway spruce.

The academic study [12] delved into the factors influencing wood density in Norway spruce trees. It emphasized a strong link between wood density variation and tree age, highlighting the role of the cambium in older trees, leading to narrower rings with a higher late-wood proportion. Unlike prior research, this study revealed a consistent increase in wood density from the core to the outer sapwood due to a higher late-wood ratio. The research introduced 3D models illustrating the rise in wood density relative to stem position, attributed to reduced ring width along the stem radius and increased late-wood presence. These models challenged the previous notion of density decrease near the core, possibly due to sample preparation and 3D modelling limitations. Additionally, the study noted significant variations in wood density at different stem heights. While some studies suggested a decline in density at higher positions, others proposed a more uniform distribution. Compression wood, known for its notably higher density compared to standard wood, was identified as a major contributing factor.

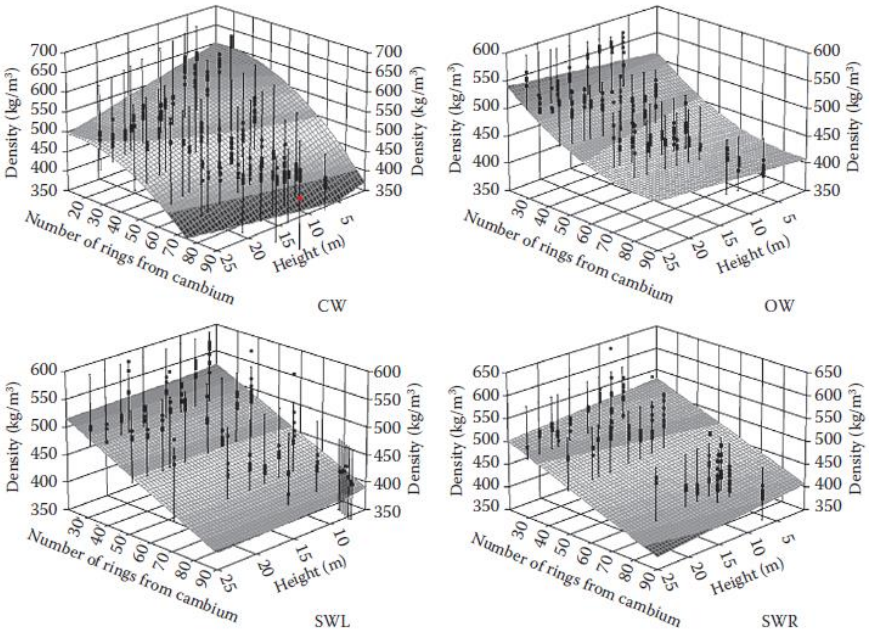

Figure 5 Wood density (w = 12%) in relation to the position in the stem [12]

The study provides empirical evidence confirming the elevated density of compression wood, at 550 kg/m³ with 12% moisture content, compared to 450 kg/m³ in the opposite zone. It acknowledges a

wide range of density values for compression wood, emphasizing the role of thick-walled compression tracheids. The unique structure of reaction compression wood results in distinct properties, particularly in terms of density. The study underscores the practical implications, noting that working with compression wood requires higher energy input. Additionally, the different visual characteristics of compression wood may necessitate specific requirements in product applications. In conclusion, this study significantly advances our comprehension of Norway spruce wood properties, especially in the context of reaction wood. It illuminates the intricate relationship between wood density and factors like tree age, stem position, and the presence of compression wood, providing valuable insights for efficient utilization in various applications.

2.5 Moisture content

Wood, like many natural materials, is hygroscopic; it absorbs water from the surrounding environment through two main processes; the transpiration stream and osmosis. The first process was first discovered by Stephen Hales as he was able to be demonstrated that plant leaves absorb air and that a portion of air is used in plant nutrition. In addition, he realized that light is necessary for growth and investigated growth rates by marking plants at regular intervals. He measured the rate of water loss (transpiration) in plants, finding that it occurred through the leaves and was responsible for an upward flow of sap in plants. [13] The second process was discovered by RJH Dutrochet (1776-1847) of which he was able to proves the movement or diffusion of solvent molecules through a selectively permeable membrane from a region of high-water potential to a region of low water potential. Once water has been absorbed by the root system they are transported through the xylem to the leaves. Therefore, the moisture content has an important influence on wood properties and performance.

Wood possesses a capillary-porous nature, wherein its porosity varies between approximately 50% and 70%, depending on its density. This characteristic results in an extensive internal surface area. The cavity system of wood exhibits hygroscopic properties, enabling it to absorb moisture present in the air. Additionally, the capillary transport processes within the cell lumen allow for the absorption of liquid water or other substances such as wood preservatives or adhesives. Based on the moisture content of the wood, three boundary conditions can be identified.

- **Oven-dry state:** Wood in the oven-dry state has a moisture content of 0%, indicating the absence of any water content.
- **Fibre saturation point:** At the fibre saturation point, the entire microsystem of the wood becomes saturated with water. This point is typically reached at around 28% moisture content and may vary slightly depending on the specific type of wood.
- **Water saturation:** During water saturation, both the microsystem and macrosystem (cell lumen) of the wood are completely filled with water.

The moisture content of wood has an impact on each property of wood which is especially evident once below fibre saturation, as wood in an oven dry state becomes brittle and stiff. This occurs because the cellulose chain in the wood helps generate strong intermolecular binding forces. As the moisture content increases the stiffness and strength decreases, sustained loading increases creep deformation and Wood becomes increasingly prone to fungal infection, particularly when the moisture content exceeds 20%. [4] The amount of water present not only influences its strength, stiffness, and mode of failure, but it also affects its dimensions [14]

Research has been extensively conducted into the relationship between strength and moisture content of wood since its inception into civil and aviation engineering. The investigations primarily focus on the effects within the hygroscopic range (22% or below) with fewer studies investigating the effects at high degrees of moisture content, up until fibre saturation. Fibre saturation is a technical term which can be loosely described as the point in which there is an absence of any free water in the cell Lumina with the cell walls are completely saturated with chemically and physically bound water. It is important to note that this is not a discreet point but rather a moisture range which may vary considerably depending on species sap- and heartwood, age, local soil and moisture conditions. [15] It is state of art to assume that the strength and stiffness properties do not change anymore beyond fibre saturation, this assumption holds true for most mechanical properties. Literature results show that in the case of compression parallel and perpendicular to fibre direction there is still some quantitatively non-negligible strength decreasing effect up to moisture contents of about 50%. [16]

2.6 Shrinkage and swelling

The natural fluctuation of moisture content in wood causes alterations in its dimensions, with swelling constituting an expansion in both size and mass, and shrinkage signifying a reduction in these properties. This phenomenon persists until the point of fibre saturation is reached, beyond which dimensions stabilize despite further increase in moisture content. The anisotropic nature of wood means that, depending on the direction, the magnitude of the shrinkage and swelling changes, which can then lead to cracking of the wood. In general, the tangential direction has the most pronounced dimension-altering effect, succeeded by the radial orientation, and finally the longitudinal orientation Empirical` figures pertaining to Spruce denote approximate shrinkage values from a green to an oven dry state (expressed as a percentage of the green dimension) as 7% for the tangential orientation, 4% for the radial orientation, and 0.3% for the longitudinal orientation as moisture content is lowered from the point of fibre saturation to 0%. Moisture content is not the only factor that influences swelling and shrinkage as higher densities also increase the magnitude of the swelling and shrinking. Low densities do the opposite. [17]

Figure 6 Left - Shrinkage directions Radial, Tangential and Longitudinal. Right – cracked circular pile sections (original photos)

2.7 Wood Decay

Wood stands as a highly beneficial naturally derived construction material, recognized by its renewability. It embodies diverse utility while also emerging as the foremost land-based contributor to carbon sequestration. Additionally, wood is also organic, heterogeneous, and biodegradable, thus serving as sustenance for wood-degrading organisms including fungi and bacteria [18]. Certain wood species have evolved chemical defences like tannins and natural oils, although resistance is species dependant, and some are more adapt than others. [19]

2.7.1 Fungal decay

Fungal activity can lead to the deterioration of wood components through the enzymatic degradation of the intricate polymers that make up the wood's structural composition. [20] The susceptibility of wood to fungal decay is contingent upon specific environmental conditions, including a moisture content surpassing 20%, accessible oxygen, temperatures within the range of 15 to 45 degrees Celsius, and an adequate supply of nutrients. In this context, wood assumes vulnerability to fungal infestations. Sapwood, characterized by its higher nutritional content, particularly in the form of carbohydrates such as sugars, is more vulnerable to fungal attacks compared to the relatively less nutritious heartwood. Consequently, the structural integrity and aesthetic attributes of outdoor wooden constructions are notably compromised by fungal decay, decreasing the wood's mechanical and aesthetic qualities and as a consequence drastically shortening the service life of the structure. [21]

A multitude of decay manifestations can emerge due to various combinations of host species, fungal species, and internal wood conditions. Amid this diversity, three primary decay categories are widely recognized: brown rot, white rot, and soft rot [22]. Each fungal species can be categorized based on its mode of degrading the fundamental components of the wood cell wall: cellulose, hemicelluloses, and lignin. Cellulose, composed of glucose units linked in a linear manner (beta-bond), is one such component, while hemicellulose, consisting of a branched arrangement of diverse sugars, constitutes

another. Lignin, on the other hand, is a complex and cross-linked polymer predominantly composed of phenylpropanoid units. This classification enables a more refined understanding of how fungal degradation processes affect the distinct components of wood's structural composition.

Figure 7 Left - Example of internal brown rot and external white rot. Right – Example of soft rot [18]

Brown-rot fungi (e.g., *Gloeophyllum trabeum or Fomitopsis pinicola, both Basidiomycota*) engage in the degradation of cellulose and hemicellulose, typically resulting in a soft crumbly surface texture on the wood or, in severe instances, encompassing the entire structure [23]. White-rot fungi, on the other hand, dismantle all three principal wood structural components, yielding a white and soft consistency. Within the realm of white-rot fungi, certain species exhibit selectivity by prioritizing the breakdown of lignin initially, followed by concurrent action on the other components. This adaptive behavior is contingent upon environmental factors and is contingent upon the specific species [24]. Soft-rot fungi (*e.g., Phialocephala dimorphospora, an Ascomycota*) operate in high-moisture environments and partially degrade all three components. This naturally results in the formation of cell wall voids in the affected areas, rendering them soft in appearance. While soft-rot fungi have a slower degradation rate compared to the previously mentioned fungi, the comprehensive disruption of cell structures renders their impact the most severe given the complete destruction of the cells [25]. A summary can be found in Figure 8

Type of Fungi	Degraded Wood Type and Components	Effect on Wood
Wood-decaying fungi		
brown-rot (Basidiomycota)	mainly softwoods; degradation of hemicelluloses and cellulose, demethylation of lignin	wood shrinkage and cracking into cubical pieces, brown colouration due to the presence of lignin remained, reduction of wood mechanical properties
white-rot (Basidiomycota)	mainly hardwoods but also softwoods; degradation of lignin and hemicelluloses, but also cellulose	fibre-like appearance and white colouration of wood due to the presence of lighter-coloured cellulose remains, wood becomes soft and spongy or stringy, its strength properties decrease along with the decay progress
soft-rot (Ascomycota, fungi imperfecti)	hemicelluloses and cellulose, less extensively lignin	formation of cavities inside the cell wall, discolouration and cracking pattern similar to brown-rot, deterioration of wood strength properties
Mould		
mould (Zygomycota or Ascomycetes)	easily available sugars, not structural polymers	superficial discolouration of wood, minor degradation of the wood surface
Blue stain		
blue stain (Ascomycota and Deuteromycota)	protein content of the parenchyma cells, easily available sugars, not structural polymers	dark discolouration of sapwood by dark-coloured hyphae, degradation of pit membranes leading to increased water permeability

Figure 8 Summary table of Fungi type and effect on the structure [26]

2.7.2 Bacterial decay

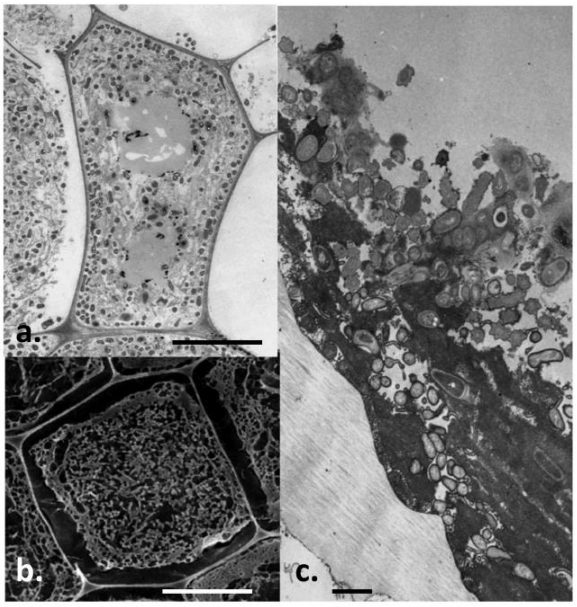

Figure 9 Micrographs show bacteria breaking down wood cells. In image "a," only the middle part of birch's secondary cell walls is being attacked. In the Cryo-FE-SEM image, bacteria, slime, and breakdown products fill the space where the cell walls and inner part used to be. In the TEM image, bacteria stick to the wood cell wall, causing erosion. [69]

Fungal decay represents merely one facet of the challenges confronting bio-based materials. Degradation also manifests within wooden piles completely submerged in water. This phenomenon was initially documented by Varossieau in 1949 at the Netherlands' Centre of Materials Research, an entity that later amalgamated with TNO, the Netherlands Organization of Applied Scientific Research. This form of degradation was observed in specimens ranging from 30 to 600 years old. At the time, degradation of this nature within anoxic environments was attributed to bacterial activity. Aged wood utilized below the groundwater level and within the soil exhibited varying degrees of bacterial decomposition. This inquiry deduced that bacterial degradation predominantly initiates during the initial few years [29].

Continued investigation delved deeper into this matter, leading to the identification of two distinct categories within wood-degrading bacteria: erosion bacteria and tunnelling bacteria. Erosion bacteria are characterized by their rod or spherical morphology, with dimensions spanning 1–4 mm in length and 0.5–1 mm in thickness. Notably, these Gram-negative cells lack flagella but possess a substantial slime layer. Their ability to move is facilitated through a gliding mechanism. A critical observation emerges that a protective slime layer envelops bacteria adhered to the cell wall, and it's only these bacteria that possess the capability to initiate wood degradation [25] Illustratively,

2.8 Small sample testing

To comprehensively assess diverse characteristics of specimens, including moisture content, density, strength, and modulus of elasticity, it is of utmost importance to establish a rigorous methodological framework and testing protocol. An illustrative instance of such an approach is referenced in [16]. The study involved conducting experiments on freshly cut spruce timber, presenting a detailed account of systematic tests and evaluations conducted on defect-free cubic specimens and fully sized round wood pile specimens. This testing methodology furnishes valuable directives for conducting tests on both small and large specimens, adhering to the specimen sizes specified in both [27] and [28] namely 20*20*120mm^3 and 30*30*60mm^3, respectively. To ascertain the moisture content, the wood was cut and cross-sectioned, followed by a two-stage vacuum treatment: an initial treatment at an absolute pressure of 20kPa for 20 minutes, succeeded by a 35-minute treatment at a pressure of 500kPa. This treatment regimen yielded a consistent moisture content of 192% ± 20% across all sections. Subsequently, specimens measuring 50*30*30mm^3 were extracted from each pile, categorized as A-E, and weighed. The oven-dry method was subsequently employed to determine the moisture content of the specimens.

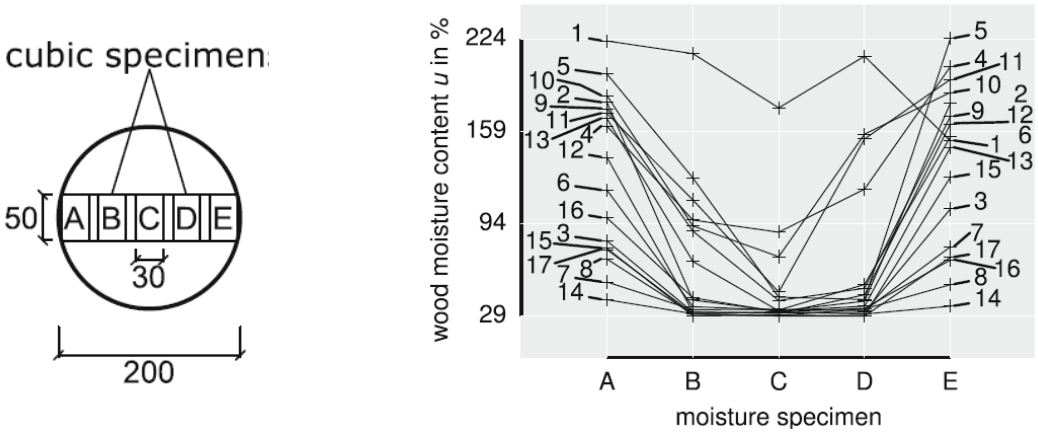

Figure 10 Cutting scheme of specimens (left). Cross- sectional moisture distribution of wet state specimens at mid-section of the piles (Right). [16]

The moisture content distribution within the specimens distinctly illustrates elevated moisture levels at the outer periphery (sapwood), gradually tapering to lower levels in the central portions (heartwood and pith). In summary, it can be stated that the minimum moisture content of the pile specimens was in majority along pile length and cross-section beyond the assumed fibre saturation limit of 30%. However, since the saturation level might be higher for some specimens and clear wood tests indicate that compressive strength drops after reaching the upper realistic saturation level of 35%, the obtained strengths of the wet log specimens should be rather higher than lower compared to long-time water submerged pile. [16] Axial compression tests were then preformed on each of the test specimens 20*20*120mm^3 conforming to the provisions in [27] and 30*30*60mm^3 specimens [28] with locations of the samples taken from the sapwood and the heartwood. The density of the sample was noted before the test started. A 100kN capacity Zwick/Roell electro-mechanical test machine was used. Unfortunately, the Modulus of elasticity was not measured.

Compression tests were executed on the 30*30*60mm^3 specimens until they reached the point of failure, revealing evident signs of damage in the form of kink bands, both in the dry and wet samples. Similarly, the 20*20*120mm^3 samples experienced failure, attributed partly to the presence of kink bands and partly to their slenderness. Notably, lateral bending manifested in 40% of the instances due to deformations occurring perpendicular to the loading axis. Failure modes will be covered in greater detail in the next section. Figure 12 presents a comprehensive statistical analysis encompassing all test series, focusing on compressive strengths, densities, and moisture contents. The key finding is that all density test series exhibited a closely aligned distribution of densities. The average density hovered around 440 kg/m3, while the 5%-quantile values spanned from 330 to 350 kg/m^3. Analysis of the compressive strength ratios unveiled that the EN specimens demonstrated approximately 5% lower strengths in comparison to the DIN specimens. This discrepancy can be attributed to the fact that the EN specimens are slenderer than their DIN counterparts, resulting in a significant influence of bending and buckling effects. It's important to note that the reduction in strength within these findings can be attributed solely to the elevated moisture content and not to any shifts in density.

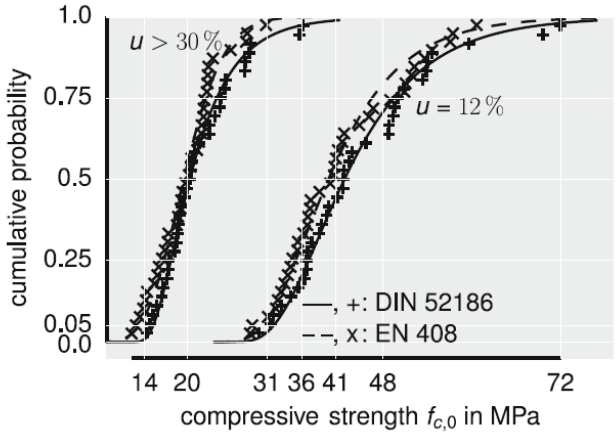

Figure 11 Compressive strength distributions parallel to the fibre of matched small defect free spruce specimens according to DIN 52185 (1976) and EN 408. (2010) [16]

Physical, mechanical property or ratio	Statistical quantity	Small scale clear wood specimens			
		Dry (MC = 12 %)		Green (MC > 30 %)	
		Specimen type		Specimen type	
		DIN 52185	EN 408	DIN 52185	EN 408
No. of specimens tested		42	42	42	42
No. of specimens used for evaluation		35	38	35	38
Moisture content in %	x_{mean} (COV in %)	13.9 (1.9)	13.9 (2.5)	200 (16)	181 (18)
Compressive strength $f_{c,0}$ in MPa	x_{mean} (std)	44.3 (9.9)	41.6 (8.5)	21.9 (5.4)	20.1 (4.4)
	COV in %	22.4	20.3	24.7	22.0
	x_{min}	30.2	29.0	14.6	12.5
	x_{max}	72.4	60.7	36.4	31.2
	x_{05}	29.3	28.4	13.9	13.0
Density ρ_{12} in kg/m^3	x_{mean} (std)	442 (75)	442 (58)	439 (64)	442 (60)
	COV in %	16.9	13.0	14.7	13.6
	x_{min}	349	334	353	348
	x_{max}	653	580	659	604
	x_{05}	326	347	337	344
Compressive strength ratio	at x_{mean} level	0.94		0.95	
$f_{c,0,EN}/f_{c,0,DIN}$	at x_{05} level	0.97		0.94	

Figure 12 Compilation of results from two different test standards for matched small clear spruce specimens tested in compression parallel to the fibre in dry and green states (DIN 52185 and EN 408) [16]

2.9 Failure modes

It has been acknowledged that the major failure mechanism limiting the compressive strength of small wooden rectangular sections is the kink banding phenomena, which is frequently seen in aligned-fibre composites subjected to compression. Kink band formation in small wooden samples refers to the localized deformation that occurs in the form of bands or zones when the wood is subjected to compression or bending forces. These bands are characterized by a concentration of microcracks and other types of damage that occur within the wood structure. The formation of kink bands is primarily attributed to the anisotropic nature of wood. Wood is composed of long, fibrous cells called cellulose fibres that are arranged in a hierarchical structure. The fibres are aligned parallel to the longitudinal axis of the tree trunk, forming grain lines. [29] This arrangement gives wood its characteristic strength and stiffness properties. However, it also means that wood has different mechanical properties in different directions. The formation of kink bands is influenced by various factors, including the density, moisture content, and specific anatomical characteristics of the wood species. Species with higher density and lower moisture content generally exhibit greater resistance to kink band formation.

This can be seen with the difference between Beech and spruce which was reported in [30]. Micrographs of the cross-section of beech Figure 13 (left) shows a semi-ring porous structure with numerous pores grouped in earlywood and solitary pores present in latewood. The fibres are thick-walled, indicating relatively high-density wood, and the rays are very large and distended along the growth ring. When observed in the tangential section, the rays appear multiseriate, with up to 25 cells wide. These ray cell aggregates suggest relatively high fibre misalignment in the (LT) plane. In the case of spruce, the cross-section (Figure 13 Right) exhibits a gradual transition between earlywood and darker latewood. The spruce fibres have fairly uniform dimensions in the tangential direction but larger dimensional variation radially due to pronounced early/latewood transition. The wall thickness of spruce fibres is thinner, implying a lesser contribution to wood strength compared to beech fibres. In the tangential section spruce fibres appear relatively slender compared to beech fibres, a characteristic that distinguishes softwood from hardwood fibres. Spruce rays are predominantly uniseriate (one cell wide) with an average height of 10 to 15 cells.

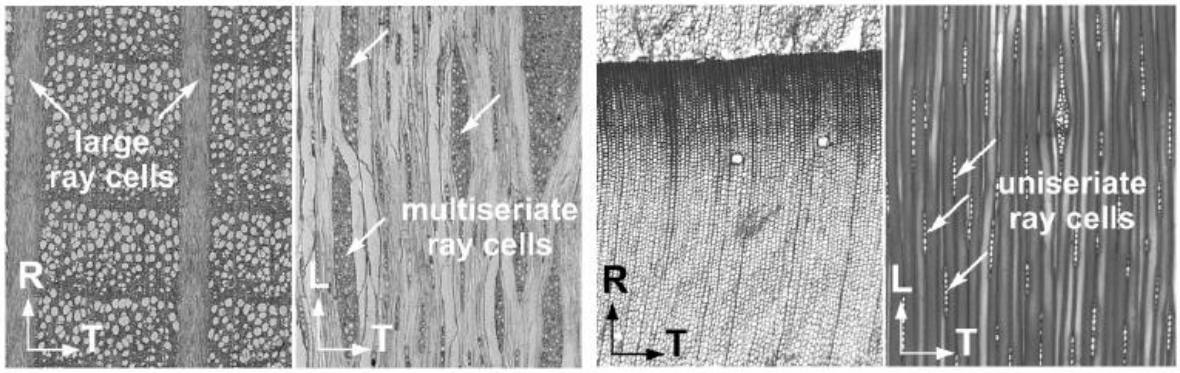

Figure 13 Micrographs showing cellular structure of beech (left) and spruce (right) in cross section (RT) and tangential section (LT)

The formation of the kink bands transpires in the following manner. After the linear elastic phase, kinking in fibre composites and wood is typically observed in three stages depicted in Figure 14. Firstly, incipient kinking occurs in localised areas around scattered ray cells in wood, causing the stress-strain curve to become non-linear. Fibre misalignment due to ray cells leads to fibre buckling and plastic shearing in the buckling region, reaching the peak stress and marking the end of incipient kinking. Wood exhibits a relatively low peak stress due to significant local fibre misalignment. Fibre misalignment and shear strength control this phase. Secondly, transient kinking follows, with stress dropping from the peak level to a steady state. Small regions of incipient kinking merge to form a dominant band with a specific orientation. Fibres within the band experience compression and rotation, with hollow wood fibres undergoing more axial compression than in fibre composites. The rotation of fibres during transient kinking contributes to the softening behaviour and overall stress drop. Rotation ceases when the lock-up angle is reached, beyond which deformation within the band becomes impossible due to volumetric constraints. [29].

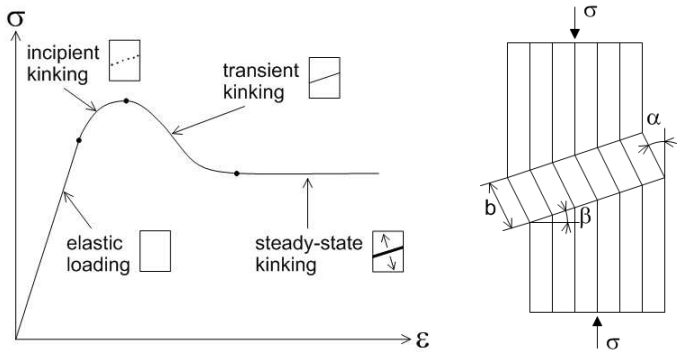

Figure 14 The overall stress-strain relationship of a compression specimen of wood with the various kinking stages (left) and the kink band geometry (right)

Other failure modes depicted in Figure 14 are as follows:

A. **Barrelling** is a failure mode seen in wood samples, where excessive compression causes the ends to move closer while the central portion bulges outward, resembling a barrel shape. It commonly occurs in long, slender wood beams or columns due to structural heterogeneity, density variations, and inadequate support. Barrelling compromises load-carrying capacity and structural integrity.

B. **Buckling** is characterised by abrupt lateral bending or bending out of the plane and is seen in wood samples subjected to compressive stresses. It happens when the load is greater than the critical buckling load, which causes the wood to become unstable and deform sideways.

C. **Shearing** is characterised by the sliding or separation of wood fibres perpendicular to the grain when subjected to shear force. It happens when the applied force is greater than the strength of the wood fibres, causing a loss of structural integrity and the possibility of the material splitting or delaminating.

D. **Homogeneous compression** is a type of wood sample failure mechanism in which the entire material is subjected to homogenous compression stress. It happens when the applied force exceeds the compressive strength of the wood, resulting in structural deformation and probable collapse. This mode is distinguished by a broad decrease in volume and a consistent reaction across the wood sample.

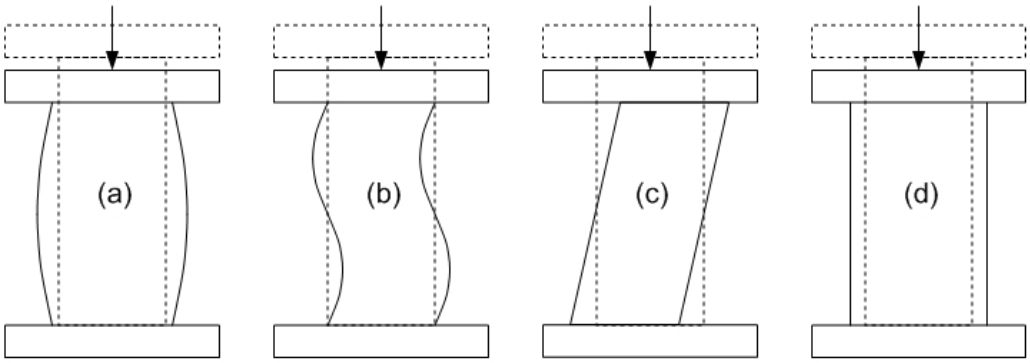

Figure 15 Modes of deformation in compression testing: a) barrelling, b) buckling, c) shearing, d) homogeneous compression [29]

2.10 Wooden foundation preservation

From February 2002 to January 2005. a Project titled "Preserving cultural heritage by preventing bacterial decay of wood in foundation piles and archaeological sites" was commissioned. The main objective of this project "was to provide basic knowledge on the impact of bacterial degradation on wood stored under different environmental conditions like foundations." Practical preservation methods were also to be developed to increase the lifespan of foundation piles and to further advance our understanding and of bacterial decay and to identify it. This was an extensive project with an in-depth analysis of Bacterial decay. Chapter 2 Focuses on historical foundation types and state of the art analyses techniques for engineering firms to conduct thorough investigations into foundations of existing buildings. The inspection of foundations in many cities in the Netherlands is required before the purchase of a property and the cost to replace a foundation could be upwards of 50% of the full cost of renovation. [31] Presently, the examination of foundations has attained standardization through the national protocol known as "foundation inspections." The following overview outlines the procedural steps: Initially, an assessment of the ground adjacent to the structure is conducted, facilitating the identification of areas with potential issues. Once these problematic zones are pinpointed, it becomes of utmost importance to cross-reference the foundation's layout with the architectural drawings. To gain access to the foundations, an excavation is executed, while also ensuring the provision of a pump for draining groundwater. Subsequently, a sample can be extracted from the pile, following these steps.

2.10.1 Foundation inspection protocol

1. A 10 mm increment borer is bored from bark to pith of the pile at 500mm from pile head.
2. The sample is then removed and put in a plastic tube with water, sealed and then sent to the laboratory for testing.
3. Once received the sample is cut into 15mm segments.
4. Microscopic analysis is conducted in order to deduce the species and degree/type of degradation.
5. Wood density and moisture content is determined from the weight of wet-dry samples.

The report also encompasses a methodology designed to assess the quality of the piles. This involves the utilization of a penetrometer, commonly known as a wood test hammer. This straightforward tool is user-friendly and can be operated by individuals with minimal expertise. The penetrometer is positioned approximately 150mm away from the pile's head, and a consistent force is exerted from the device, causing it to penetrate the wood. The depth of penetration is subsequently measured and documented. This sequence is repeated three times, and the outcomes offer an indication of the extent of wood decay. Leveraging this extensive set of samples, it became feasible to investigate the correlation between density, moisture content, and compressive strength—a pivotal facet of this research. The resulting data allows for an analysis of the compression strength of Pine relative to the quotient of density and moisture content. This graph, presented in Figure 16, portrays the outcomes of this compression strength assessment.

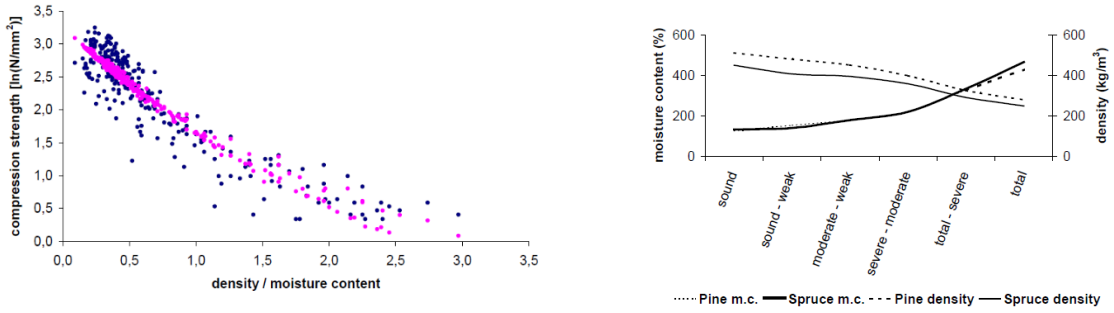

Figure 16 Left-Relationship between compression strength and the quotient of density and moisture content for Pine. Blue dots are measured data, pink dots are estimated data. Right relationship between categories of decay and moisture content and density for Pine and Spruce. [32]

The report highlighted a robust correlation between the extent of degradation and the Density/Moisture content quotient. For specimens in good condition, higher density and lower moisture content were observed. Conversely, severely degraded piles exhibited elevated moisture content and decreased density. This trend is clearly illustrated in the graph provided below. Additionally, the degradation pattern was visually represented through a frequency diagram, allowing for more intricate analysis. The assessment of degradation was conducted in 10mm increments spanning from the outermost layer (bark) to the centre of the cross-section (pith). The graphs were generated for both Spruce and Pine, introducing an intriguing element of variation in degradation levels at the species level. The graph unveils that less than 5% of all Pine piles remain unaffected by degradation, while 90% of the piles show severe degradation in the outermost 10 mm layer. Notably, about half of all Pine piles exhibit significant degradation in the outermost section of around 40 mm, a substantial proportion given the mean pile diameter of approximately 100 mm. The situation for Spruce is comparatively better: 10% of Spruce piles exhibit no degradation, and around 70% of all piles manifest severe degradation in the outermost 10 mm. Roughly half of the Spruce piles display notable degradation in the outermost 20 mm layer.

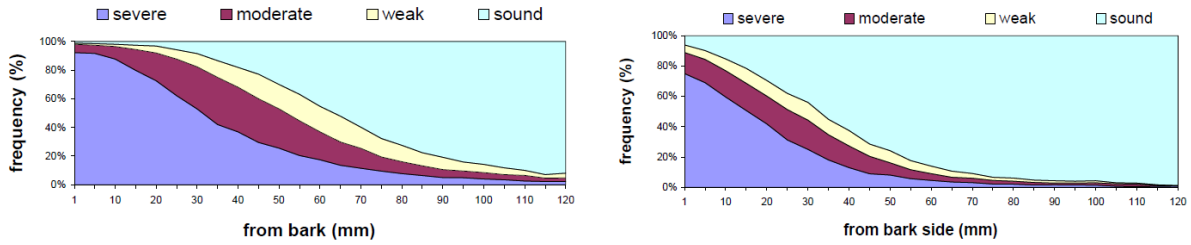

Figure 17 frequency diagram based on 803 Pine piles (left) and 789 spruce piles (right) [31]

2.10.2 Predictive models

Between 1995 and 2005, about 2000 wooden foundation piles were sampled and assessed as per the national standard for the examination of wooden pile structures [33]. These evaluations aimed to deepen the comprehension of bacterial decay in such piles. The majority of these samples were derived from the underpinnings of historical structures, primarily located in Amsterdam but also in other cities across the Netherlands. The process involved extracting cores from each pile, situated 50 cm below the pile head, using a hand-driven increment borer (10 mm). These cores were collected radially from the exterior toward the centre of the pile. For transportation, each core was enclosed in a sealed plastic tube with a small amount of groundwater [6].

This research led to the formulation of a model presented in Klaassen [6], where a predictive model for the compression strength of pine foundation piles was constructed. This model was developed based on the interrelation between compression strength, moisture content, specific gravity, and the degree of degradation. One of the critical factors in evaluating the stability of foundation piles is their compression strength. However, assessing the strength of currently in-use piles poses challenges. To address this, a model was sought that could forecast compression strength using easily extractable cores from the pile head. Key variables influencing compression strength – specific gravity, moisture content, and degree of degradation – were all tested to determine if they could be used to predict compression strength from cores obtained at the pile head.

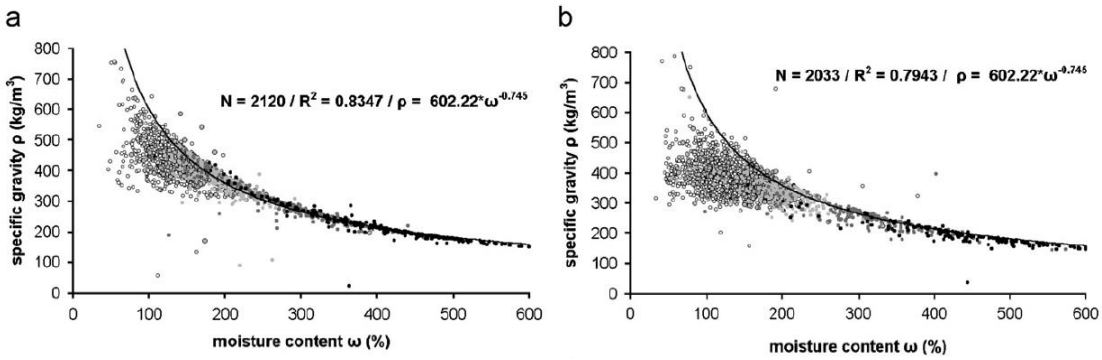

Figure 18 Relationship between specific gravity and moisture content for: (a) pine and (b)spruce. [6]

The assessment of deterioration was deemed subjective and unpredictable, making it an unreliable predictor for the compression strength of the wood among the three factors considered. In contrast, moisture content demonstrated the closest correlation with compression strength. Consequently, a "simple model" for pine was developed (Figure 19). However, a similar model has not yet been established for spruce, indicating the need for further experiments to ascertain such a relationship.

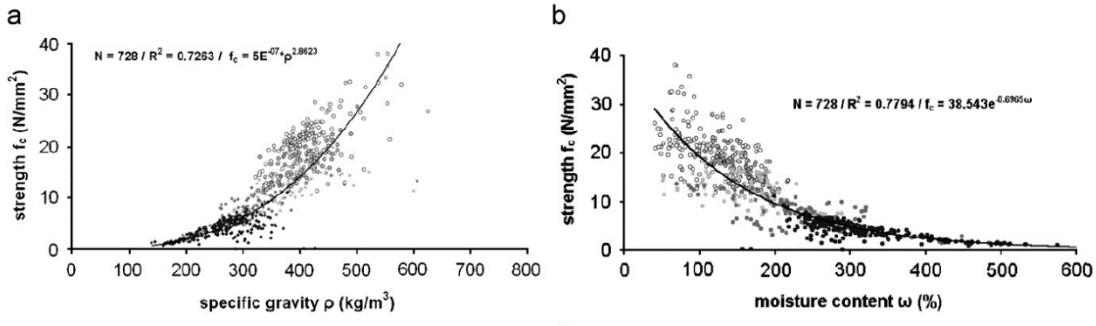

Figure 19 Relationship between compression strength and specific gravity and moisture content, (a and b) pine. [6]

In the assessment of degradation levels, the age of the wood was considered by comparing the compressive strength and specific gravity measurements of non-degraded piles that had been in service for over 80 years with those of freshly sawn timber [6]. The outcomes indicated that "no significant differences could be found for either pine or spruce between sound wood that had been in use for more than 80 years and freshly sawn timber." This conclusion holds notable significance; however, it's important to note that numerous piles within historical cities have suffered significant degradation and are confronted with various additional challenges. This context underscores the compelling rationale for pursuing further research that delves into older and degraded piles.

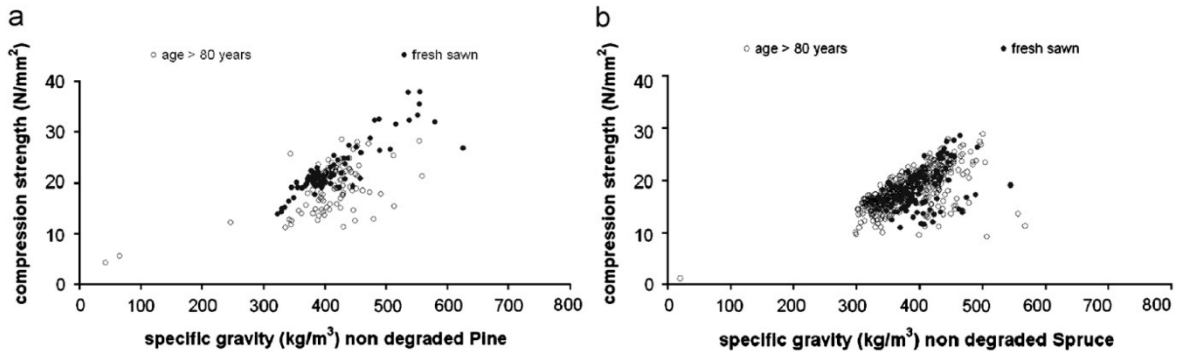

Figure 20 Comparison of relationship between compression strength and specific gravity in piles that are 480 years in service and freshly sawn material [22]

2.11 Contemporary Evaluation Methods for Timber Piles

This master's thesis forms a crucial component of an expansive research initiative with the overarching objective of comprehensively understanding the complex elements that contribute to the current condition of wooden foundations and their anticipated remaining service life. This all-encompassing initiative's goal is to "capture many of the aspects that determine the current state of wooden foundations as well as their remaining service life estimate. This includes analysis of loading conditions, age of the structure, assessing the mechanical properties of wood, inspection techniques and remaining service life model development." The choice between conducting in-situ measurements or sending materials to a laboratory for more detailed scrutiny hinges on the specific technology employed and the scale of analysis, whether it be on a smaller or larger level. Within a laboratory setting, it becomes feasible to uncover the mechanical traits of the samples and gain insights into the nature and extent of degradation. The accurate identification of the wood species takes on paramount importance due to the changing prevalence of bacterial degradation among different species. A comprehensive array of equipment and methodologies is at disposal for appraising timber constructions or wood sourced from existing structures, with a comprehensive compilation available in reference [34].

Figure 21 Left - Impact hammers – Pilodyn. Right- IML-RESI PowerDrill [35]

Currently, impact hammers like Pilodyn [35] and micro drilling equipment (Figure 21) have emerged as the fundamental tools for on-site assessments. Micro-drilling techniques, exemplified by the IML-RESI PD, represent a subset of non-destructive and in-situ technologies employed for wood examination, which will be elaborated further in the literature review. The micro-drilling procedure involves the use of a needle-equipped drill, such as the IML-RESI PD, which is inserted into the cross section of the target wooden trunk. As the needle advances through the material, the energy required for its movement is quantified as drilling resistance. In the specific case of IML-RESI PD, the needle is designed with a tip diameter of 3mm and a shaft diameter of 1.5mm. The resulting dataset is presented as resistances plotted against distance, revealing a distinct wave pattern characterized by amplitude displacements corresponding to variations in density. (Figure 22)

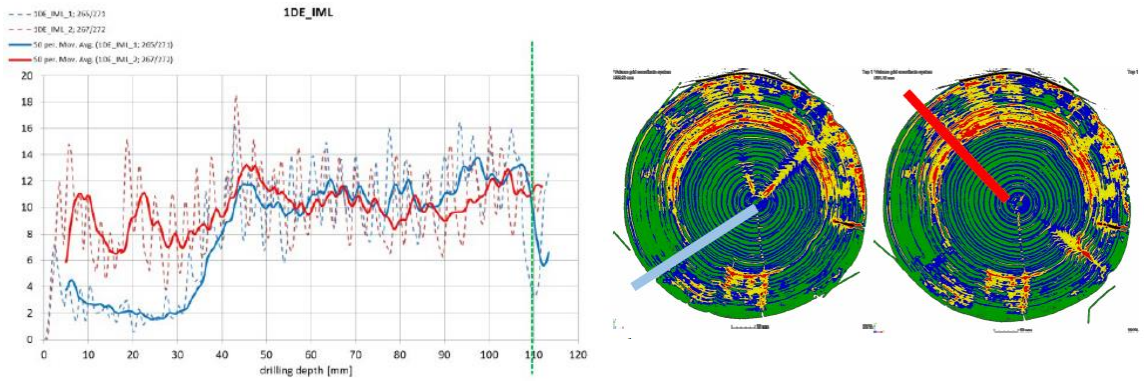

Figure 22 Right: drilling resistance profile created from micro drill test data. Left: CT-cross sectional image with location of micro-drill profile from the top graph. High density knots and sapwood with high moisture content (yellow/red), with juvenile and heartwood (green/blue) in the centre. [34]

Both of the approaches outlined above produce data that may be turned into density profiles along the cross sections of the piles. These graphs depict yearly ring profiles, with highest amplitudes indicating latewood ring and minimum amplitudes indicating earlywood rings. There are also extreme maximums and minimums on occasion. Higher value extremes are related with knots and other high-density anatomical abnormalities, whereas lower value extremes are associated with piths and cracks.

Furthermore, because density is inversely proportional to moisture content, drill amplitude minimums designate a point within the cross section with wood. The images below provide an example of the readings taken by the drill and highlight the main flaw with this type of examination tool which simply put is the results are based locally and are not always representative of the global cross section. The blue line represents high levels of decay and red represents an area with no decay. [36] Further issues were presented in [37] of which areas within the pile with poor natural density or strength complicate matters. Low natural density wood with a light amount of decay can have drill resistance values comparable to high density wood. Plots between resistance values and compression strength were recorded with a correlation coefficient at 0.62.

Computer Tomography (CT) scanning is another in-depth way of analysing wood quality. Since the 1980s, this non-destructive technology has been utilised for wood testing [18]. It has since been used to calculate density, wood quality, and moisture content. CT scans may produce very detailed 3D pictures that identify knots, fractures, heartwood, and sapwood. The moisture content while scanning is a problematic factor as it is clear that denser sapwood with a high moisture content has the same density as high-density knots. This is not representative of the actual density. Therefore, reducing the moisture content enables for unambiguous identification of wood quality, particularly whorls, which influence compression strength in general. When determining a pile's load carrying capability such weak points need to be addressed as to get an accurate result. The best results can be found in the CT scans when the samples are dry as the degraded parts can be easily recognised with a low density. [34]

2.12 Micro-drilling resistance measurements

The study [38] predominantly focuses on hydraulic structures, including lock gates and quay walls. These structures face challenging environmental conditions such as exposure to brackish and contaminated water, drying-out, and mechanical impacts. Given these demanding circumstances, it's imperative to closely monitor the deterioration processes to ensure their service life performance. Micro-drilling has previously demonstrated effectiveness in assessing softwoods and various medium-density hardwoods. In this research, the goal was to investigate the extent to which different types of defects within the cross-section of hardwood beams can be accurately and reliably identified. The utilization of drilling resistance measurements on Eucalypt and azobé wood species facilitates the detection of issues like decay and fractures, as well as the identification of high- and low-density zones due to variations in growth rates and the presence of juvenile wood regions. Achieving these results requires meticulous calibration of the micro-drilling process, particularly concerning parameters such as drilling depth, wood cross-section, and wood species. [38]

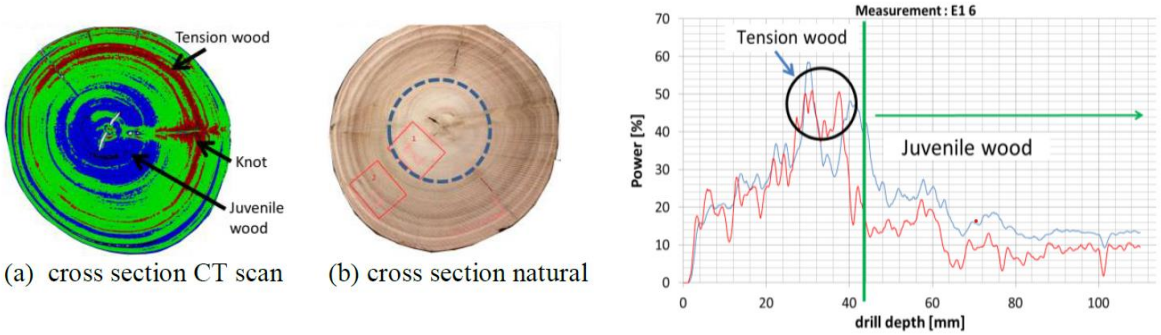

Figure 23 Left-Eucalypt cross section: 3D CT scan, relative density: high density red>green>blue low density (a); indication of juvenile area, blue dashed line (b). Right - Resistance profile of eucalypt cross section; red line = feed speed amplitude, blue line = drill feed speed amplitude; high dense area (tension wood). [38]

Micro drilling employs a dual-force mechanism involving pressure and torsion to effectively penetrate wood. The pressure force ensures the drill head maintains friction with the wood, facilitating cutting when the torsional force is applied. The energy required to shear wood fibres varies depending on the direction. Cutting fibres parallel to the grain necessitates a fraction of the energy needed for cutting fibres perpendicular to the grain. Consequently, it is logical to consistently drill perpendicular to the grain direction [39]. As mentioned earlier, experimentation was conducted on both Azobé and Eucalypt wood. The latter possesses a circular cross-section and features a prominent central pith. The juvenile wood surrounds the core and exhibits lower density compared to the adult wood. Through 3D CT scans, two 500mm-long sections of timber piles were scanned. This process facilitated the

identification of zones within the wood exhibiting significant density variations. In the resulting images, distinct colours represent varying density levels. Notably, red zones exhibit a density approximately 50% higher than that of blue zones, as visually evident in the image below.

2.13 Soft shell calculator

The definition of the soft shell was developed on the basis of the results from Klaassen [6], as issued by the municipality of Amsterdam: “A drill core (in this report called HM from the Dutch term Houtmonster) is taken until approximately half of the pile diameter and will be divided in segments that are analysed. The maximum moisture content of each of these segments is determined. Based on this maximum moisture content the compression strength of each segment is determined by calculation. The soft-shell thickness is the summation of the length of the segments seen from the outside of the pile, for which the deter-mined compression strength is lower than or equal to 8 N/mm2 “. This procedure to determine the soft shell is currently called the “Amsterdam method” and did not include RPD signals.

The soft-shell calculator in Figure 24 is a tool for deciphering RPD signals (drill samples) and was created by the Biobased Structures and Materials division at TU Delft for Ingenieursbureau Amsterdam. RPD data will then be transferred to the *“soft shell calculator”* Which will give values of the zones based on the diameter from each RPD signal which is sub-divided over the length of the pile diameter. The method assumes that the wood in the pile's core is sound and is based on variances in signal levels rather than absolute values. As a result, using the maximum values of this characteristic on both sides, an incremental outwards moving average (IOMA) is generated on both sides starting from the centre. Zones 1, 2, 3, and 4 on each side are then determined as 20%, 40%, 60%, and 80% of the moving average value in relation to the IOMA's maximum value on that side, which is used as a benchmark for sound wood, accordingly. The total of the zones, whose number is established during the calibration step, this is how the soft shell is ultimately computed. This makes it feasible to evaluate the zone allocation compared to each measurement. The allocation of zones 1+2 based on the RPD signals provides the best fit with the soft shell determined with the Amsterdam method. [40] The soft shell calculator is a new tool and therefore it is possible that further refinement is required, it is important to note that the calculator can only give a reliable value for the soft shell if the signal is of sufficient quality. This requires experience from the user to assess this.

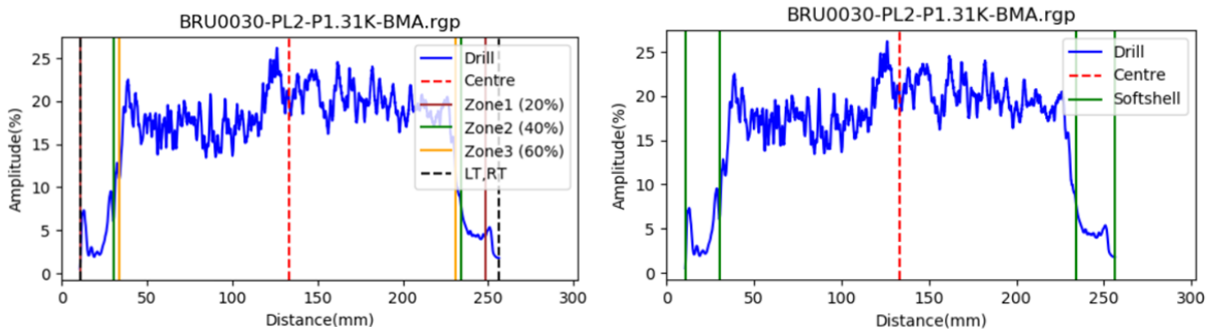

Figure 24 Left - Soft shell is determined on the left as SHL = Zone 1 left + Zone 2 left and on the right as SHR = Zone 1 right + Zone 2 right. Right – Full soft-shell area. [41]

2.14 Investigation into the application of micro-drilling (RPD) measurements.

This research investigates the use of micro-drilling (RPD) measurements as a replacement for the present approach of extracting drill cores (Houtmonsters, HM) to calculate the soft shell using the Amsterdam method which in essence is the extraction of drilled cores which subsequently are analysed to determine the highest moisture content. The moisture content is then used to determine an estimate for the compressive strength based on a connection established via experiments on samples of pine wood in [6]. This research was conducted in two steps. The soft-shell allocations based on RPD (microdrill) measurements are calibrated on the soft-shell allocations based on the HM (Houtmonster) analysis and checked on an additional dataset in the first stage. The RPD and HM results are then compared to a reference benchmark, the density distribution of dry wood derived from CT (computer tomography) images, in the second stage. [40]

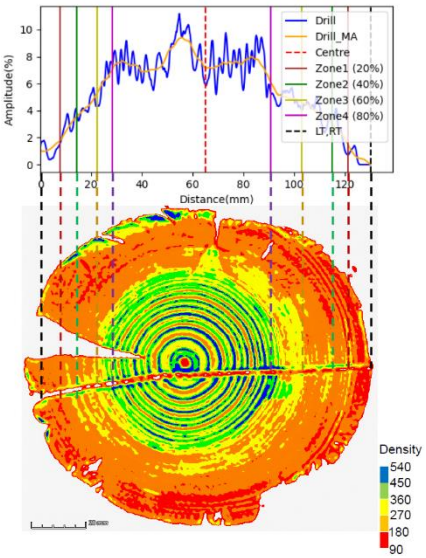

Figure 25 Comparison between the zones of the RPD signal and the CT scan on the same cross section for the tip of pile BRU30-PL1-P2.13. [40]

In the first stage, A soft shell calculator was developed which is an algorithm which determines 4 different zones (levels of quality of the wood) over the diameter of the pile at the position of the measurement. Figure 25 depicts each one of the zones present in both the RPD graph and also along the cross section of a CT scan. The number of zones providing the best fit with the soft shell determined using the Amsterdam method was calibrated on an initial dataset of 117 matched RPD signals and HM analyses, and then validated with an extended dataset of 189 matched in-situ measurements. The Amsterdam method's optimum fit for the soft shell is achieved by allocating zones 1+2 based on RPD signals. Naturally as scatter is found but this perhaps can be explained due to cutting lengths of specimens. [41]

Since bacterial decay of wood reduces local dry density, a relationship to this physical property can be used as a benchmark when assessing the RPD signals' predictive power. CT scans can be used to precisely calculate the dry density for pile components. Five pile segments were used in this study which one highly degraded result can also be seen in image Figure 25, and the findings indicate that the RPD signals can predict local dry density fluctuations in a manner similar to that found in CT scans. The report ended with an essential conclusion that the physical properties of wood could be predicted with an element of accuracy from the RPD data. Further investigation into related properties, like strength and stiffness over the cross section of a wooden pile, is made possible by this opportunity.

2.15 State of art conclusion

Following an in-depth analysis of the literature review, it is evident that various methodologies have been devised to quantify essential parameters like moisture content, density, compression strength, and modulus of elasticity over the cross section . Notably, these methodologies are predominantly rooted in non-destructive approaches, underlining the industry's tendency for minimizing structural intervention while assessing the integrity of such vital infrastructure elements. However, it is apparent that a more profound comprehension of the overall residual strength and structural health of foundation piles, particularly in distinct states of degradation, could be gathered through destructive testing methods. Such insights could be invaluable in not only understanding the underlying mechanisms of degradation but also in more accurately predicting the remaining service life of these critical structural components.

Building upon the methodologies and insights extracted from the literature, there is a recipe to develop a structured methodological approach. The goal here is not only to replicate the successes achieved through non-destructive methods but also to go beyond the current understanding. A rigorous testing protocol, considering both cross-sectional and longitudinal variations, could provide a comprehensive and multi-dimensional perspective on the condition of these foundation piles. In pursuit of these goals, the envisaged testing protocol for spruce foundation piles will encompass a range of mechanical and physical attributes, including moisture content, wet and dry density, compression strength parallel to the grain, and modulus of elasticity. However, what sets this proposed approach apart is its integration with drilling amplitude data derived from the RPD (micro-drilling) technique. This integration represents a novel attempt to bridge the gap between non-destructive measurements and the fundamental mechanical properties of the piles, potentially revolutionizing the way we understand and assess foundation piles.

By establishing a robust correlation between drilling amplitude and key physical and mechanical attributes, a significant leap could be achieved in terms of predictive capabilities. The implications of this are extensive; a simple and non-intrusive micro-drilling measurement could potentially serve as a gateway to predicting vital properties. This predictive capacity would not only streamline assessment processes but could also play a pivotal role in more informed decision-making regarding maintenance, repair, or replacement strategies. The research stands as a bridge between conventional non-destructive techniques and comprehensive destructive testing. By merging these dimensions, the research strives to enrich our comprehension of foundation pile behaviour, offering insights that are not

only theoretically significant but also practical for the field of structural engineering and infrastructure management.

3

Research Question(s), Aims & Objectives

3.0 Research question

The main research question of this thesis is.

"How do the variations of mechanical and physical attributes manifest across the cross-sectional profile of both degraded and non-degraded spruce foundation piles and how can micro-drilling techniques be utilized to assess these characteristics?"

3.1 Research sub-question(s)

The sub-questions will primarily focus on the acquirement of knowledge and then experimental and analytical work in order to deduce conclusions.

1. What research has already been conducted in a comparable project and what data is currently available?
2. What impact does an elevated moisture content have on timber and how can this be related to timber piles?
3. What are the levels and types of degradation, how can it be quantified?
4. What type of experiments need to be conducted? What is possible and available for testing in the required time frame? How many experiments need to be done? What type of data needs to be collected and what is the procedure?
5. What is the actual moisture content and density distribution in the cross section of wooden foundation piles both New/old non-degraded piles and visibly degraded piles? What difference and similarities do they possess?
6. What is the correlation between moisture content, density, compressive strength, and modulus of elasticity and how can it be modelled with the micro-drilling measurements to provide information on level of degradation of piles in service?
7. What effect does the size of the specimen ($20*20*120mm^3$ &$20*20*60mm^3$) have on the results?
8. Can the mechanical properties and in particular the compressive strength profile be related to micro-drilling signals?
9. Is it possible to predict the compressive strength of a timber pile by analysing the amplitude of micro-drilling signals conducted through the cross section?

3.2 Research objective

The objective of this research is to characterize the cross-sectional mechanical and physical properties of foundation piles both degraded and non-degraded by means of physical experimentation which will be conducted on small cross-sectional samples ($20*20*120mm^3$ & $20*20*60mm^3$) in order to determine moisture content, density, compressive strength, and the modulus of elasticity. Additionally, an in-depth analysis will be conducted in order to determine a link between micro-drilling signals (drilling amplitude) and the mechanical and physical properties through the spruce foundation piles.

4

Methodology

4.1 Experimental set-up

The following experiments have been conducted within the laboratory facilities of TU Delft adhering to the established protocols and practices mandated by the university, as outlined in [42]. These experiments have been undertaken with the primary objective of precisely cutting and sectioning local cross-specimens, which will subsequently undergo weighing, volumetric determination (wet and oven dry) and subsequent compression testing. The overarching purpose of these experiment is to quantitatively assess the mechanical and physical properties in six distinct piles across their respective heights. The selected piles for assessment encompass three different conditions, specifically, those in a new state, those that are aged but exhibit a relatively low level of degradation, and those that are both aged and substantially degraded. The assessment of degradation levels is contingent upon the analysis of the drilling amplitude data, subsequently considering the extent of soft-shell presence in the piles under investigation. Notably, the age range of the evaluated piles spans from 0 to 300 years, with the material of interest being limited to spruce wood, reflective of its prevalence within the city of Amsterdam.

4.2 Materials

The specimens were retrieved in various locations from the foundations of two demolished bridges in Amsterdam (Bridge 30 and 41). In total 60 foundation piles were extracted of which 55 were Spruce (*Picea abies*) and 5 Fir (*Abies)* driven in 1727,1886 and 1922. The assessment of the mechanical properties of the full 60 piles can be found in [43]. This project in total will determine the physical and mechanical properties of 6 piles of which 5 piles are taken from these bridges, 3 from 1727, 1 from 1887 and 1 from 1922. The remaining pile is from 2019 and therefore has not been driven in the ground but will serve as a baseline for the results. Further details of the piles can be found below.

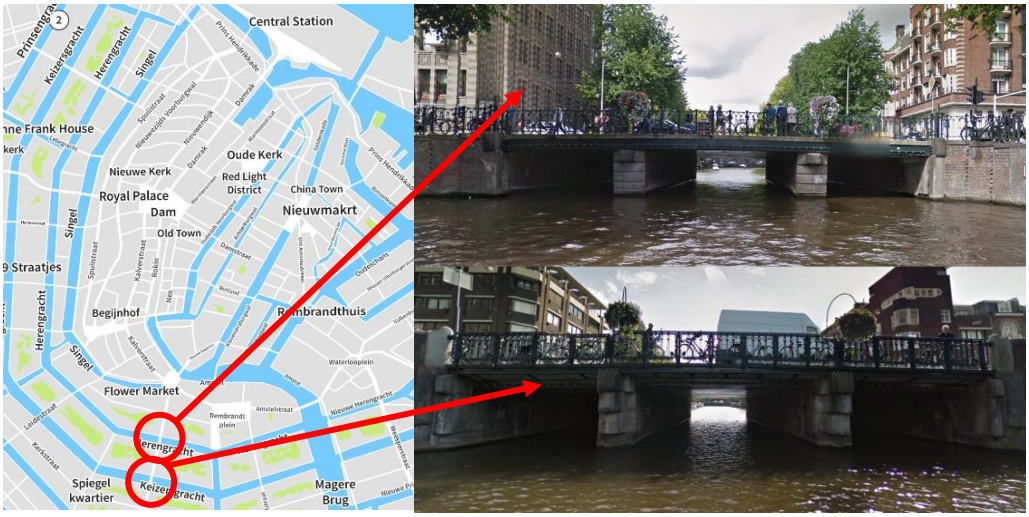

Figure 26 Left - Map of Amsterdam. Right- Bridge 30 and 41.

The locations of the bridges can be seen above, and the piles were removed from the piers. The full-length specimens were 9500 mm to 13500 mm in length, with an average head diameter of 230 mm and a tip diameter of 145 mm. Following the extraction, the timber piles were transported in a barge while submerged in water to the municipality of Amsterdam's storage facility. At the storage location, all piles were measured and tested along their entire length. Acoustic frequency response measurements were used to determine the dynamic modulus of elasticity parallel to the grain (MOEdyn). Following that, the 60 piles were divided into three sections and submerged in containers under water. Following that, the water was drained and the containers with piles were delivered to the TU Delft Stevin 2 laboratory. Upon arrival, all of the piles were chopped into 201 segments. The pile's head, middle, and tip were sawed into the segments as shown below.

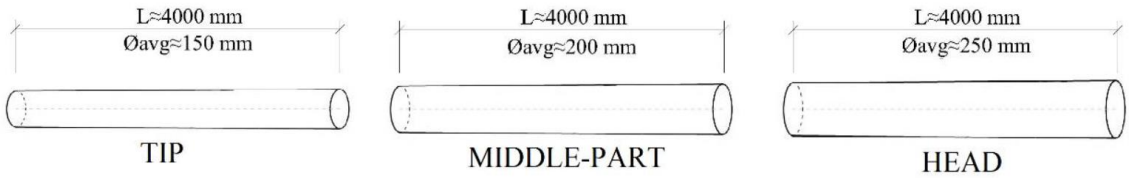

Figure 27 Full-pile subdivision in head, middle-part and tip. [43]

Table 1 Full pile data from [43]

Full pile ID	Segment code - container	year	length (mm)	D_{avg} (mm)	species	dry density (kg/m^3)	m.c. (%)	MOE_{dyn} (Mpa)	MOE_{stat} (Mpa)	f_{c,0,wet} (Mpa)
BRU0030-PL1-P2.13	K3M-228	1727	1350	176	spruce	290	190	7700	8400	7.1
	M3M-228		1350	155		270	170	3900	3700	5.3
	V3M-228		900	131		260	220	4000	2900	5.1
BRU0030-PL2-P2.21	K6M-228	1727	1350	212	spruce	370	100	8600	8300	9.8
	M6M-228		1350	184		340	120	5700	4600	6.3
	V6M-228		900	145		340	135	4700	4200	6.6
BRU0030 PL1 P2.7	K2.7-115	1727	1350	197	spruce	320	100	5000	5000	6.1
	M2.7-115		1350	205		290	105	2700	2600	4.1
	V2.7-115		900	138		300	175	4300	3900	5.8
BRU0030-PL1-P3.18	K3.18-115	1886	1350	241	spruce	410	55	11400	10800	14.9
	M3.18-115		1350	222		430	50	10900	10200	14.2
	V3.18-115		1350	182		400	85	10400	9000	12.1
BRU0041-PL2-P1.9	K11M-228	1922	1800	233	spruce	460	80	13300	12500	16.9
	M11M-228		1350	208		440	75	12600	12200	16.3
	V11M-228		1350	172		510	75	12200	11100	15.4
HIE-P10588	K10588M	2019	1800	247	Spruce	560	80	13200	11900	23.1
	M10588M		1350	197		550	103	13500	11900	22.5
	V10588M		1350	179		450	125	9600	8900	17

4.3 Manufacturing of specimens

4.3.1 Preparation phase

Wooden piles, each approximately 12 meters in length, underwent segmentation into 4-meter sections within Amsterdam. Subsequently, these segmented piles were transported to TU Delft, with the logistical arrangements coordinated by IB Amsterdam. The transportation process involved the utilization of lifting equipment such as industrial ropes to lift the piles onto a forklift, which facilitated their transfer into the laboratory premises. Throughout this transportation phase, laboratory technicians provided supervision to ensure the safe and secure execution of the operation, strictly adhering to relevant safety protocols and guidelines.

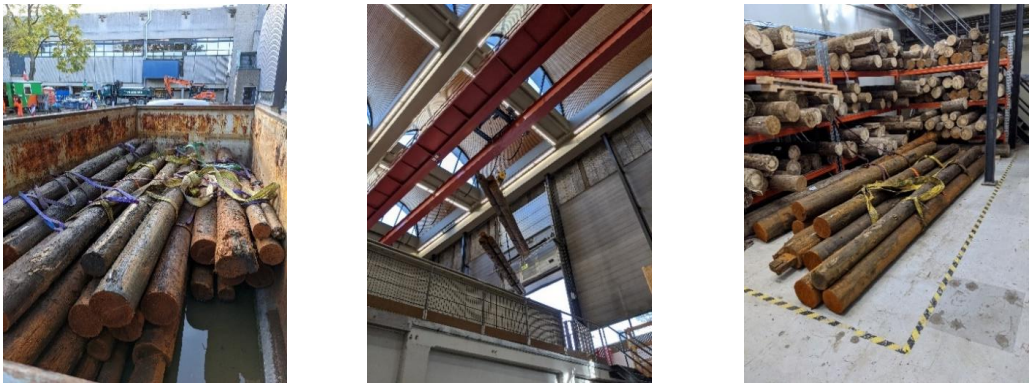

Figure 28 Pile delivered in shipping containers (Left) Piles transported safely to the basement awaiting assortment (Centre, Right)

Upon the arrival of the piles in the basement pit, they underwent a preliminary cutting process into three distinct segments: the top part, the middle part, and the foot section. This rough cutting operation was carried out by a trained specialist who was equipped with appropriate protective gear, including protective clothing, safety goggles, and multi-layer noise-cancelling earmuffs. Following the segmentation, each of the resulting segments was securely affixed to supports using a clamp mechanism to ensure stability and facilitate subsequent testing procedures.

Figure 29 Pre-cut 4m pile segments and cut foundation piles submerged in water.

Initial measurements were carried out on the central segments of each section to assess various parameters, including dimensions, weight, and frequency (utilized for the determination of Modulus of Elasticity - MOEdyn). Subsequently, a comprehensive compression test was conducted on the entire pile segment to ascertain its strength. Following the completion of this compression test, the pile underwent further segmentation, a necessary step for the production of specimens required for subsequent analyses. Achieving precise and accurate wood cuts was paramount, and this precision was attained through the utilization of a laser line to ensure that the cuts were both level and parallel. In accordance with the specifications outlined in [27] for the preparation of clear specimens, the length of these segments measured 120mm. For each full 12-meter pile, three 4-meter-long sections were designated for testing, facilitating the acquisition of representative results for compression strength across the cross-section. It was noteworthy that one cross-section from the middle part of each 4-meter segment was specifically chosen for examination to ensure the attainment of uniform and consistent results.

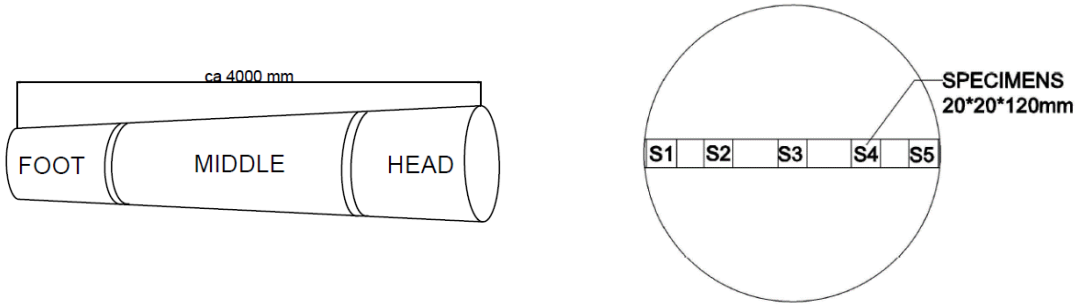

Figure 30 AutoCAD drawings of Pile segment (left) and the cross section of the pile with locations of where each sample will be approximately located with sample numbers (S) 1-5.

The middle segments of the piles underwent complete submersion in water for a duration of 10 days. This immersion was essential to ensure that the pile samples attained full saturation, replicating the environmental conditions typically encountered beneath the groundwater table. Following the saturation process, the disk-shaped cross sections were meticulously measured and labelled, employing a water-resistant marker to maintain legibility in the wet environment. For each cross section, a total of 5 specimens were extracted from the middle section, each possessing dimensions of approximately 20*20*120mm^3. Additionally, to assess the size effect of samples, specimens measuring 20*20*60mm^3 were also prepared. The selection of specimen locations was a critical aspect in obtaining accurate results, as shown in Figure 30. Specifically, two specimens were sourced from the edges of the cross section, where the sapwood was present. Two additional specimens were taken from the heartwood, and one was extracted from the pith or juvenile wood region. The demarcation of these boundaries was facilitated through the use of RPD data.

4.3.2 Production phase

The process of sample production was of paramount importance to ensure the precision and accuracy of results. It necessitated meticulous care and a high degree of skill to guarantee that each sample was cut perpendicular to the grain and exhibited identical dimensions. Initially, a rough cut was executed, typically at approximately 150mm from the original segment. To ensure uniformity, a laser was employed to measure the distance on each side accurately. Subsequently, the rough cross sections were obtained, as visually represented in the image below.

Figure 31 Procedure involving the cutting, preparation, and labelling of cross-sections.

Subsequently, the cross sections had to be clearly marked to indicate the locations of the specimens, which were labeled as 1, 2, 3, 4, and 5. These labels corresponded to sapwood, heartwood, and juvenile wood regions. At this stage, RPD measurements could be taken in alignment with the positions of the sample locations. Following the marking and measurement process, a skilled operator performed a rough cut along the outermost part of the marked lines. To achieve precision and uniformity, a sander was then utilized to level the specimens and ensure that they conformed to the correct dimensions. This meticulous procedure guaranteed the accuracy and consistency of the samples for subsequent analysis.

Figure 32 Sample location established, initial cut and sanding.

At this stage, what remained was a rectangular section that could subsequently be further divided to attain the prescribed length of 120mm. Furthermore, each specimen could then be meticulously separated individually. This procedural sequence had been proficient in guaranteeing the precise size of each specimen to the required dimensions. The final step in this protocol entailed the determination of the wet weight of each sample, followed by its placement within a sealed container to maintain the moisture content (MC) at a consistent level. These sealed samples were stored within a temperature-controlled environment, specifically in a refrigerator, until the designated time for conducting the intended testing procedures.

Figure 33 Samples being levelled, final product & plastic wrap to keep moisture content.

It was important to note that the samples had undergone manual cutting and preparation, resulting in slight variations among individual specimens. However, it was essential to underscore that, within the context of these specific experiments, the provided samples exhibited a high level of quality, imparting confidence in their capacity to yield accurate results. The accompanying image, presented below, elucidated the diverse sample locations and effectively delineated the contrasting wood types distributed across the specimens. Notably, the discernible presence of sapwood, heartwood, and juvenile wood within the sample was apparent. Visual differentiation of these wood types in the cross-sectional context could often pose challenges. Therefore, the utilization of the micro-drilling technique served as an invaluable tool, enhancing the precision and reliability of such determinations.

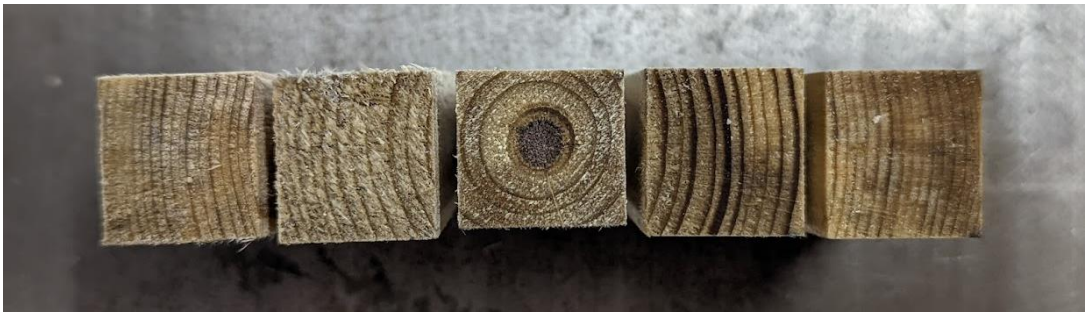

Figure 34 Sapwood, Heartwood and juvenile wood can be visually identified.

4.4 Moisture content (MC) and Density (ρ)

The two fundamental physical characteristics to be assessed in this study are moisture content and density. To obtain a comprehensive understanding of moisture content and density throughout the complete cross-section of a pile, it is essential to adhere to the sample preparation methodology outlined in section 4.2.2. The determination of moisture content involves measuring the wet weight immediately after sample cutting and subsequently assessing the dry weight following oven drying. The computation of both wet and dry density necessitates the utilization of the respective wet and dry mass measurements, in conjunction with volume measurements. This rigorous approach is essential to ensure the precision and accuracy of the results obtained. The detailed procedure for conducting these assessments is highlighted below, while the outcomes of these experiments are prominently featured and discussed in Chapter 5. Furthermore, for illustrative purposes, an exemplification of the moisture content (MC) and density alterations is provided in the annex A1. This example specifically pertains to two new, non-degraded piles, namely 010640M and 010584M, each encompassing section of 120mm and 60mm.

Test procedure

1. Two cross sections of lengths 60mm and 120mm are to be cut from the pile.
2. The sample locations are then drawn on the cross section at 20mm width each.
3. The samples are then individually manufactured.
4. The wet volume (V_{wet}) and weight (m_{wet}) of the wet samples is then recorded using a digital calliper and scale.
5. The samples are then put in the oven at 103 degrees until the rate of weight change was less than 1% through periodic measurements.
6. The dry volume (V_{dry}) and weight (m_{dry}) of the samples is then recorded using a digital calliper and scale.

The moisture content ω and Density ρ can be calculated from a simple formula as follows:

$$\boldsymbol{MC = \frac{m_w - m_{dy}}{m_{dy}} \cdot 100} \qquad \boldsymbol{\rho_{dry} = \frac{m_{dry}}{v_{dry}} \qquad \rho_{wet} = \frac{m_{wet}}{v_{wet}}}$$

$MC = Moisture\ content\ (\%)$ $\qquad \rho = Density\ (kg/m^3)$

$m_{wet} = mass\ of\ wood\ wet\ (g)$ $\qquad m = mass\ (g)$

$m_{dry} = mass\ of\ wood\ dry\ (g)$ $\qquad v = volume\ (m^3)$

After recording the mass and volume measurements of the samples in a tabulated format, the data can be employed to construct graphical representations illustrating the variations in moisture content and density across the cross-section. These plots will be generated for distinct segments within the pile, allowing for a more detailed analysis of the moisture content and density profiles.

4.5 Compression tests

Compliance with the testing standard EN408 necessitates that the length of the specimen be six times the dimension of its cross-section. The primary objective of the compression tests is to derive essential parameters, including the maximum applied compression force and the displacement of each sample. These measurements enable the determination of internal stress and strain, thereby facilitating the computation of ultimate strength and Modulus of Elasticity (MOE). The configuration of the compression test setup is depicted below. A hinge mechanism is employed to ensure that the applied force is concentrated at the midpoint of the top portion of the sample. This design mitigates the introduction of unwanted moments on the specimen, thereby reducing the likelihood of buckling. Such an approach aligns with the principles outlined in EN408, which stipulate that “The test piece shall be loaded concentrically using spherically seated loading-heads or other devices, which permit the application of a compressive load without inducing bending. After load pick up the loading-heads shall be locked to prevent angular movement.”

Figure 35 Compression test set-up; Left- compression machine with sample. Middle- K3M with attached LVDTs. Right- Sample after shear failure.

The load throughout the test will be kept constant and the loading equipment used can measure the load to an accuracy of 1 % of the load applied. Two Linear variable differential transformer (LVDT's) shall be used and positioned at the two sides of the specimen to minimize the effects of distortion and to find an accurate reading for the displacement. The data obtained can then be used to plot the load/deformation graph. Sections between $0.1 * f_{max}$ and $0.4 * f_{max}$ will be used for the regression analysis. EN408 also states the load/deformation linear regression correlation coefficient should be greater than 0,99 and the MOE shall be calculated to an accuracy of 1%. To ensure results are consistent a cycle load of $0.1 - 0.4 * f_{max}$ will be applied at the start of the experiment which will yield better results. Naturally the result for f_{max} will change throughout the cross section and therefore a spare sample should also be cut from the cross section in order to determine a base result for $F_{max.}$

The standard formulas below are used to determine the results:

The compressive strength $f_{c,0}$ is given by the equation:

$$f_{c,0} = \frac{F_{MAX}}{A_{wet}}$$

$$F_{MAX} = Maximum\ applied\ force\ (kN)$$
$$A_{wet} = Area\ of\ wet\ sample$$

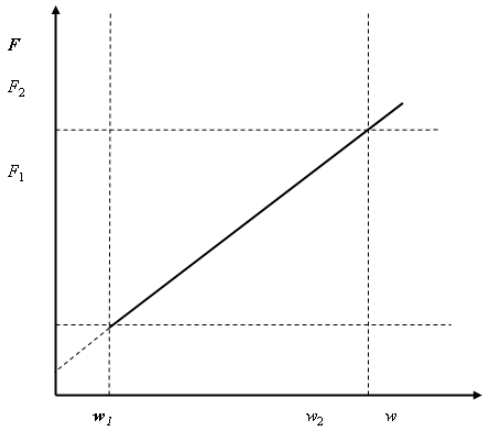

Figure 36 Load-deformation graph within the range of elastic deformation

The modulus of elasticity in compression $E_{C,0}$ is given by the equation:

$$E_{c,0} = \frac{l_1(F_2 - F_1)}{A(w_2 - w_1)}$$

Where:

$f_2 - f_1$ is an increment of load on the straight-line portion of the load deformation curve, in Newtons.
$w_2 - w_1$ is the increment of deformation corresponding to $f_1 - f_2$, in millimetres.

4.6 Modulus of elasticity

The Modulus of Elasticity plays a pivotal role in comprehending how stiffness varies across the cross-section of the material. This variation can be effectively determined through the utilization of strain gauges, potential meters, or Linear Variable Differential Transformers (LVDTs). Preliminary testing has indicated that relying solely on internal displacements of the compression machine is an inaccurate method for measuring strains in the specimens. The results obtained through this approach did not align with values observed in the literature study. This discrepancy primarily arises from the presence of a soft layer at the top and bottom of the specimens, which does not accurately reflect the actual strain distribution. To achieve precise strain measurement, four rectangular metallic blocks are affixed to the

sample, positioned 15mm away from both the top and bottom edges. These metallic blocks serve a dual purpose. Firstly, they allow for the measurement of the original length, which is the distance between the two metallic blocks. Additionally, they provide an initial clamping force necessary for the secure attachment of the LVDTs. Two LVDTs are deployed on either side of the specimen, connected to the metallic blocks by applying adhesive at the top of the LVDT and bonding it firmly to the metallic block. This bonding ensures a rigid and reliable connection between the LVDT and the sample, enhancing the accuracy and precision of strain measurements.

The standard formula is then used.

$$\lambda = \frac{Stress}{Strain} = \frac{\sigma}{\epsilon}, \sigma = \frac{f_{MAX}}{A_{wet}}, \epsilon = \frac{\Delta L}{L}$$

Where:

$$f_{MAX} = maximum\ compressive\ force$$
$$A_{wet} = Area\ of\ wet\ sample$$
$$L = original\ length$$
$$\Delta L = change\ of\ length$$

The computer software installed on the laboratory computers has been specifically tailored to capture and record the compression force and displacement data obtained from the two LVDTs, visually represented in blue and green in the screenshot below. The red line in the graphical depiction signifies the computed average values. In the presented experiment, which features a 20*20*60mm specimen extracted from K6M, the slopes curve can be utilized for the determination of the Modulus of Elasticity (MOE). It has been observed that achieving a more accurate slope for MOE determination can be attained by subjecting the specimen to three cycles of a quarter of the predicted maximum load, thereby enhancing the reliability of the results.

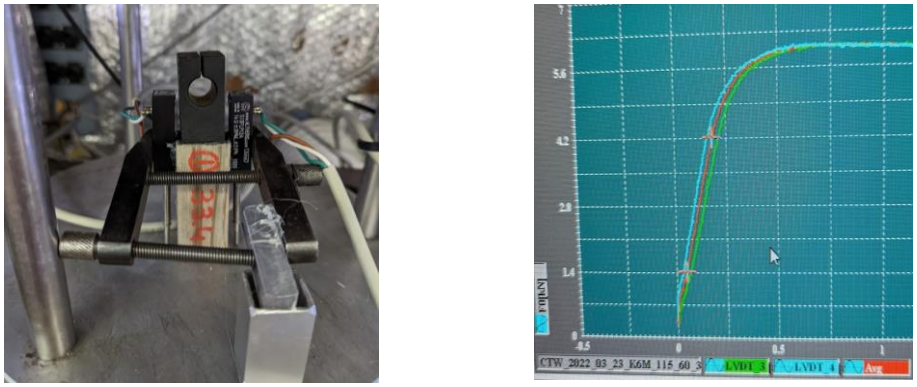

*Figure 37 Compression experiment of K6M 20*20*60 and Load vs displacement graph.*

To determine the Modulus of elasticity, the elastic range of the specimen needs to be determined. This can be achieved by plotting the compressive force vs displacement graph. Figure 38 shows the full cycle of the specimen from initial cycle loading to a uniform gradient and finally full failure of the specimen. The gradient of this graph is not accurate so another graph with the elastic range needs to be plotted to ensure an accurate representation is realised. This can be seen in figure 39 with an R^2 value of 0.99 and gradient of 39.73. To calculate the MOE the following formula can be used.

$$MOE = \lambda = \frac{dy}{dx} * (\frac{original\ length}{area})$$

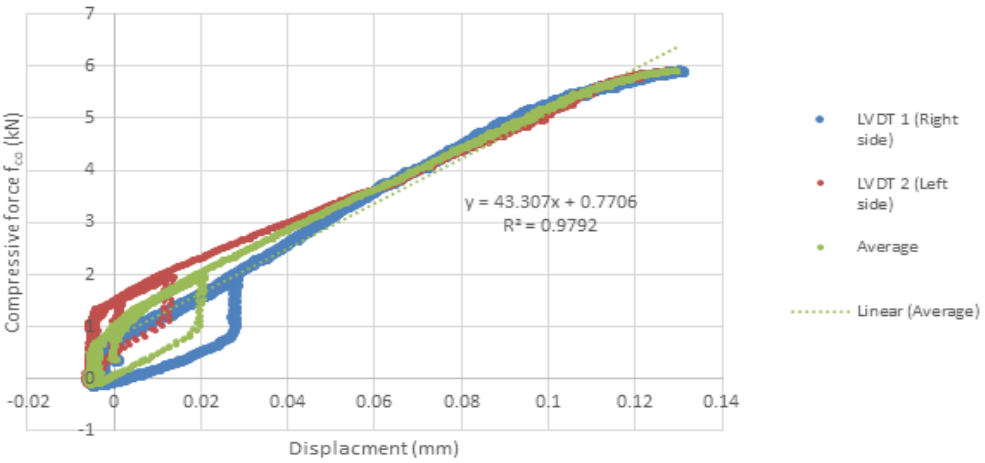

Figure 38 Compressive force and displacement of test sample using 2 LVDT's.

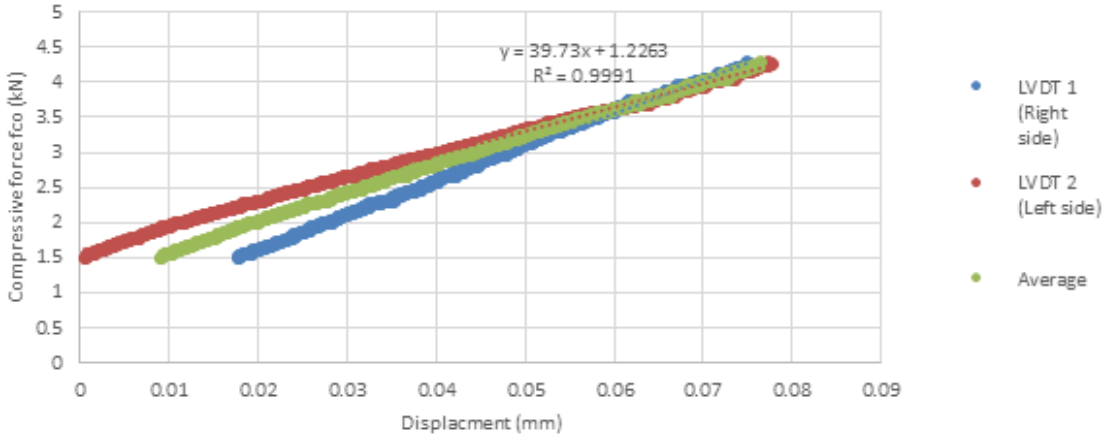

Figure 39 Elastic range for 'test specimen without initial cyclic loading.

4.7 RPD Data

The RPD Drilling amplitude is one of the most crucial parts of the experimentation campaign as prior to samples being cut and the subsequently tested, RPD tests can give a good indication of the quality of the wood being tested. As a visual inspection can be used to determine if a piece of wood is degraded but the extent of which cannot be examined visually. RPD data can be used to determine the soft shell of a material which is the degraded zone of the pile. This degraded area would have a high moisture content, but low density/compressive strength as opposed to the non- degraded zones. RPD data is first transferred to the *"soft shell calculator"* Which will give values of the zones based on the diameter from each RPD signal which is sub-divided over the length of the pile diameter. This can be seen in the image below.

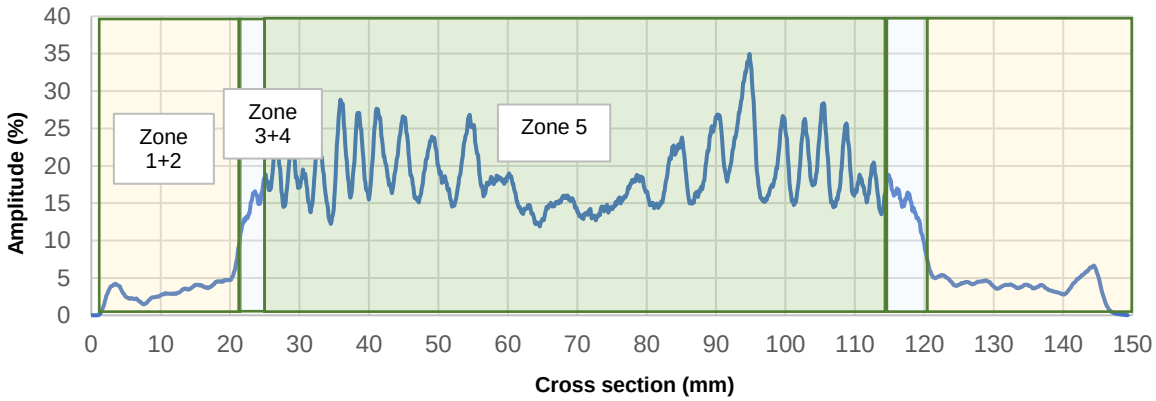

Figure 40 Example RPD data with the 5 different zone locations created by the IOMA's algorithm.

The reason the location of the zone is important is that ideally if samples could be collected at each location, then the physical properties could be estimated at each zone. The issue with this is that the zones can change rapidly over the cross section as can be seen above in Figure 40 which doesn't give enough space for a full 20mm sample in zones 3 and 4. Instead two samples will be taken from zone 1,2,3 & 4 and another two taken from the location of the highest amplitudes of each side of the pith. The final location is situated in the juvenile zone/pith. The results will therefore be representative for how the strength will change over the cross section. The intended final result can be seen below in Figure 41 which demonstrates how the compression strength changes throughout the cross section with a much lower value found in the degraded soft shell and a much higher value found in the heartwood.

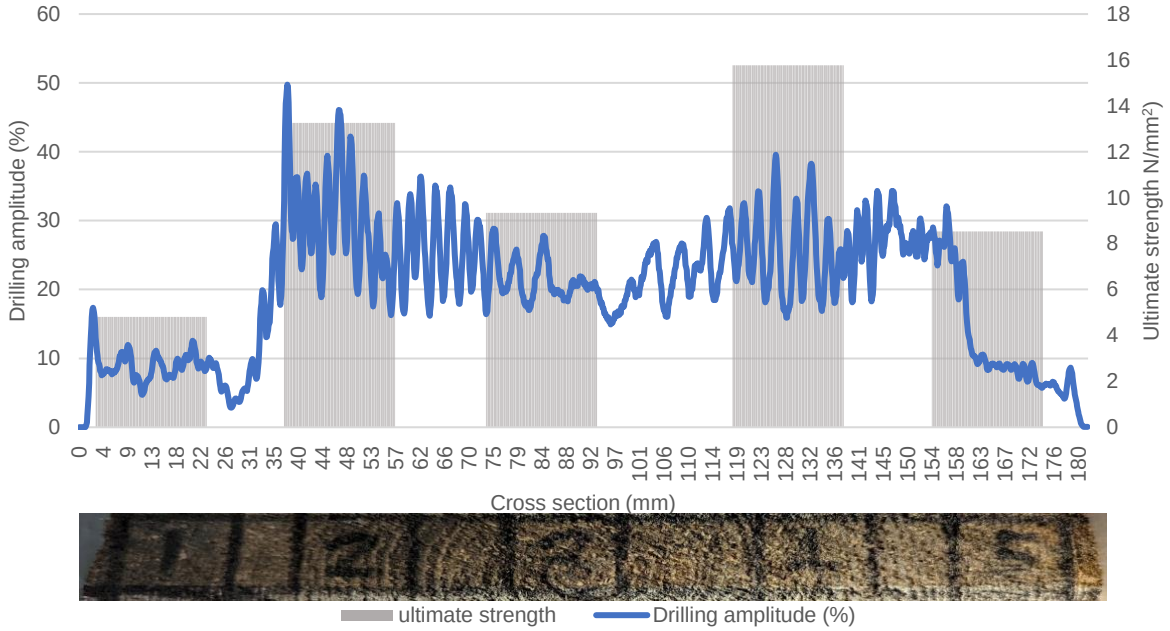

Figure 41 Example RPD data with ultimate strength, drilling amplitude and sample location

4.8 Experiment procedures

The methodological framework has undergone a meticulous refinement process, drawing insights from a comprehensive literature review, on-site experimental trials, and collaborative progress meetings that have leveraged expertise from diverse domains. These iterative efforts have culminated in the development of a comprehensive experimental procedure, which is delineated below. This procedure is categorized into two distinct phases: the preparation phase and the experimental procedure phase.

Pre-Experimental preparation procedure

1. Roughly set out the location of the RPD drill location
2. Conduct RPD measurement.
3. Analyse RPD data to determine locations for Heartwood, Sapwood and Juvenile wood/pith.
4. Measure distances between zones and prepare cross section.
5. Each specimen must be clearly labelled with 1, 2, 3, 4, and 5.
6. Cut each sample.
7. Weigh the wet specimens separately immediately after cutting.
8. Record the weight in the tables.
9. Record the Volume in the table using a calliper.
10. Place samples in a sealed bag to retain the moisture content.

Experimental procedure

1. Weigh the wet specimens to ensure the same weight as before, note any differences.
2. Use the Glue gun to attach four rectangular cross sections to each side of the specimen.
3. Record the distance between the cross sections using a calliper.
4. Attach glue to the top of the potential metre ensuring that it is flush against the specimen.
5. Conduct compression test (see details above) with initial cyclic load.
6. Record Max compression strength & dy/dx of the curve.
7. Photograph and record failure mode.
8. Save and export excel file sheet for gradient analysis.
9. Collect the specimen into a dish and transport to the ovens.
10. The samples are then put in the oven at 103 degrees until the rate of weight change was less than 1% through periodic measurements.
11. Weigh the dry specimen and then using a calliper record the dry volume.

4.9 Individual pile selection

A pivotal aspect of this research entails the examination of various piles exhibiting diverse levels of degradation to establish a correlation between physical and mechanical properties and drilling amplitude. The selection of piles possessing specific physical attributes is of paramount importance in this regard. This selection process was guided by the analysis of drilling amplitudes associated with various piles. For instance, piles 3M and 2.7M exhibit average soft-shell thicknesses of 41mm and 39mm, respectively, signifying their suitability for yielding results representative of old, degraded samples. Pile 6M, while possessing a relatively high average soft-shell thickness of 38mm, exhibits an uneven distribution of this characteristic throughout the pile. Consequently, it is employed as a transitional source of results, bridging the gap between old, degraded, and old, sound piles. Pile 3.18M, categorized as an old pile, features a minimal level of degradation, evidenced by an average soft-shell thickness of 6.4mm. Pile 11M, also an old pile, stands out with a complete absence of soft shell (0mm). The variance in age and degradation levels among these selected piles is anticipated to yield a comprehensive range of results, thereby offering valuable insights into the progression of decay. The inclusion of a new pile from 2019 serves as a baseline for the results, facilitating comparative assessments.

5

Results

5.1 Introduction

This chapter encompasses all the relevant data collected by the experimental campaign conducted in the laboratory of TU Delft. This extensive dataset encompasses various dimensions of the research, each contributing significantly to the overarching objectives of the study. The data includes pictures of the locations of the specimens to document cross section location. The results of experimental measurements, Contain the essential parameters for the physical and mechanical characteristics such as moisture content, density, ultimate compression strength, and the Modulus of Elasticity. These measurements offer crucial insights into the composition, structural integrity, load-bearing capacity, and elasticity of the foundation piles under investigation. Furthermore, the dataset includes invaluable Micro-drilling amplitude data which is used to determine a relationship for predictive purposes.

A total of six piles will be presented. Five of these piles have been meticulously selected from historic bridges, with three dating back to 1727, one from 1887, and another from 1922. The sixth pile, dating from 2019, has not been driven into the ground and will serve as a foundational reference point for the study's outcomes. A detailed explanation of the methodological processes and sample manufacturing procedures can be found in Section 4 of this thesis. It is noteworthy that the complete set of results is presented in annex A2-A7, and for analytical purposes, an averaged result, accompanied by the standard deviation calculated from the three segments, will be employed.

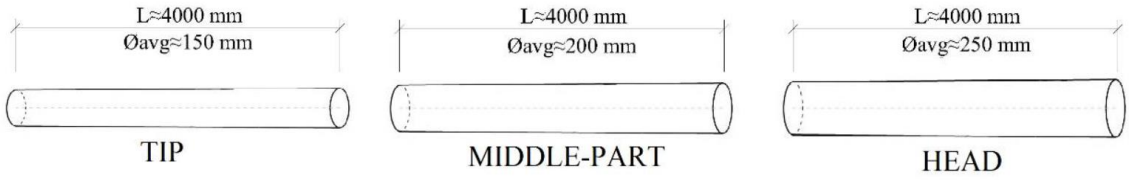

Figure 42 Full-pile subdivision in head, middle-part and tip. [43]

Full pile ID	Segment code - container	year	length (mm)	D_{avg} (mm)	species	dry density (kg/m^3)	m.c. (%)	MOE_{dyn} (Mpa)	MOE_{stat} (Mpa)	f_{c,0,wet} (Mpa)
BRU0030-PL1-P2.13	K3M-228	1727	1350	176	spruce	290	190	7700	8400	7.1
	M3M-228		1350	155		270	170	3900	3700	5.3
	V3M-228		900	131		260	220	4000	2900	5.1
BRU0030-PL2-P2.21	K6M-228	1727	1350	212	spruce	370	100	8600	8300	9.8
	M6M-228		1350	184		340	120	5700	4600	6.3
	V6M-228		900	145		340	135	4700	4200	6.6
BRU0030 PL1 P2.7	K2.7-115	1727	1350	197	spruce	320	100	5000	5000	6.1
	M2.7-115		1350	205		290	105	2700	2600	4.1
	V2.7-115		900	138		300	175	4300	3900	5.8
	K3.18-115	1886	1350	241	spruce	410	55	11400	10800	14.9

BRU0030-PL1-P3.18	M3.18-115		1350	222		430	50	10900	10200	14.2
	V3.18-115		1350	182		400	85	10400	9000	12.1
BRU0041-PL2-P1.9	K11M-228	1922	1800	233	spruce	460	80	13300	12500	16.9
	M11M-228		1350	208		440	75	12600	12200	16.3
	V11M-228		1350	172		510	75	12200	11100	15.4
HIE-P10588	K10588M	2019	1800	247	Spruce	560	80	13200	11900	23.1
	M10588M		1350	197		550	103	13500	11900	22.5
	V10588M		1350	179		450	125	9600	8900	17

RPD Data

The attainment and analysis of the drilling amplitude data play a pivotal role in this project. The utilization of RPD instrumentation offers a non-invasive approach that is particularly advantageous when testing foundations, as it minimizes potential damage to the pile. By relying on RPD signals, it becomes possible to gather valuable insights into the structural integrity and behaviour of the pile without compromising its stability. In this context, the drilling amplitude serves as a crucial parameter that provides vital information about the pile's response to the applied forces. To ensure accuracy and reliable correlation with the photographic documentation of the samples, the drilling amplitude is collected at two distinct locations—specifically, the left and right sides of the target sample. This approach enables precise matching of the signal data with the corresponding images, facilitating a comprehensive analysis of the pile's characteristics. To maintain the integrity of the test samples, it is deemed impractical to drill through them directly. This decision arises from the fact that the samples possess a relatively small size, with dimensions of only 20mm in length and width. Moreover, the needle head employed for drilling has a diameter of approximately 1mm. Drilling through the test samples would reduce the cross-sectional area, potentially introducing unwanted variables that could undermine the accuracy of the analysis.

Examining the RPD signals obtained from the left and right sides of the K3M and V2.7M samples reveals noteworthy patterns. The inherent organic nature of wood contributes to natural variations in the signals. Additionally, the path taken by the drill as it traverses the cross section introduces further variability. It is worth mentioning that the right-side amplitude exhibits a distinct dip in the middle of the K3M sample, indicating that the drill penetrated the pith during the drilling process. This observation underscores the sensitivity of the RPD technique in identifying such occurrences. In quantifying the drilling amplitude, a comparative analysis between the left and right sides of V2.7M reveals a negligible difference of only 3%. The average drilling amplitude on the right side is determined to be 14.2, while on the left side, it amounts to 14.6. Such close alignment in values suggests a high level of consistency and reinforces the notion that a single reading obtained through the cross section is sufficient for conducting a comprehensive analysis of the average drilling amplitude. By leveraging the RPD signal data, obtained through a non-invasive approach and carefully considering the limitations of drilling through the test samples, this project ensures an accurate evaluation of the pile's behaviour and structural properties. Such insights with additional physical and mechanical test results will contribute to a more informed decision-making process when assessing the integrity and performance of the foundation.

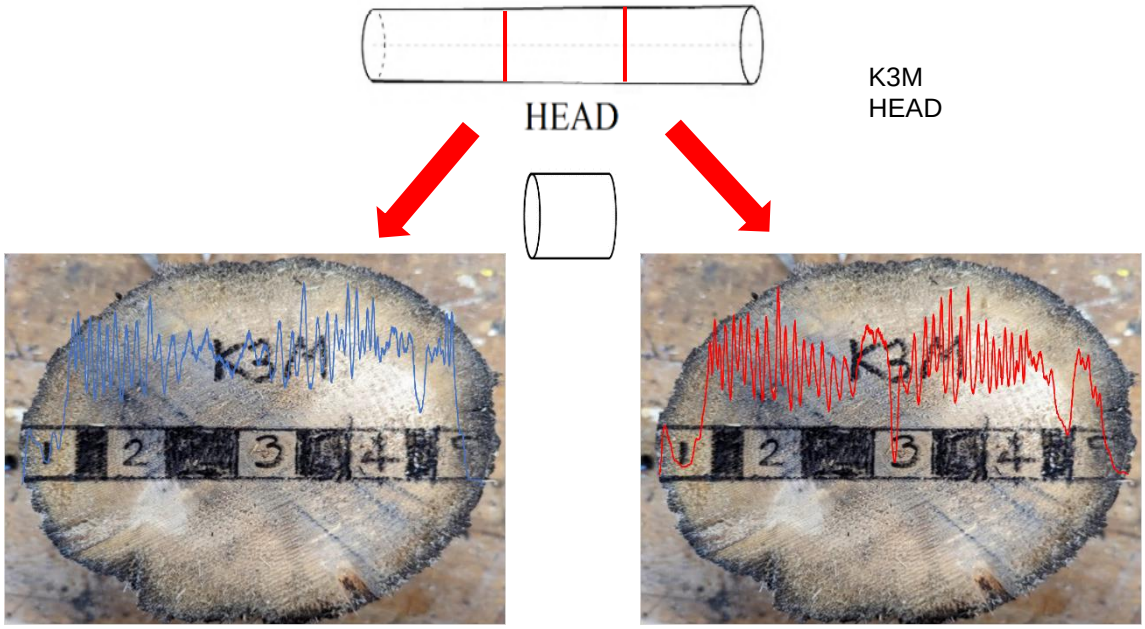

Figure 43 RPD drilling locations on samples in the same orientation.

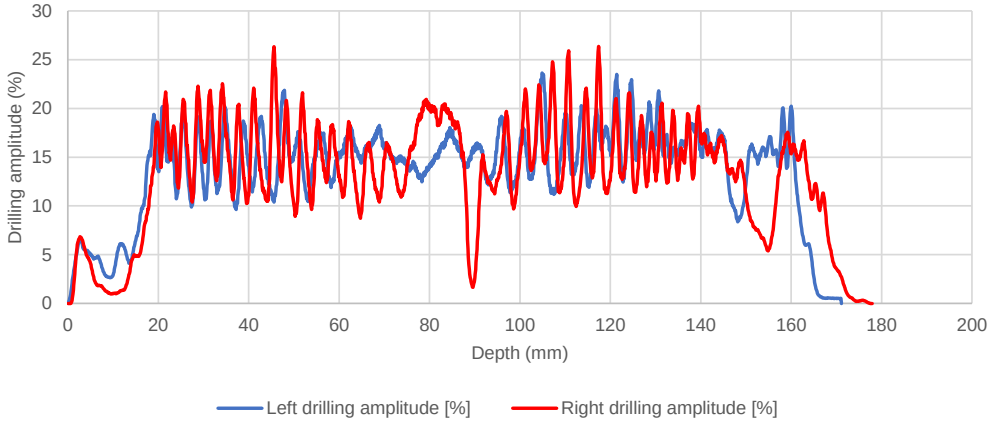

Figure 44 _K3M Drilling amplitude comparison between the left and right side of the sample.

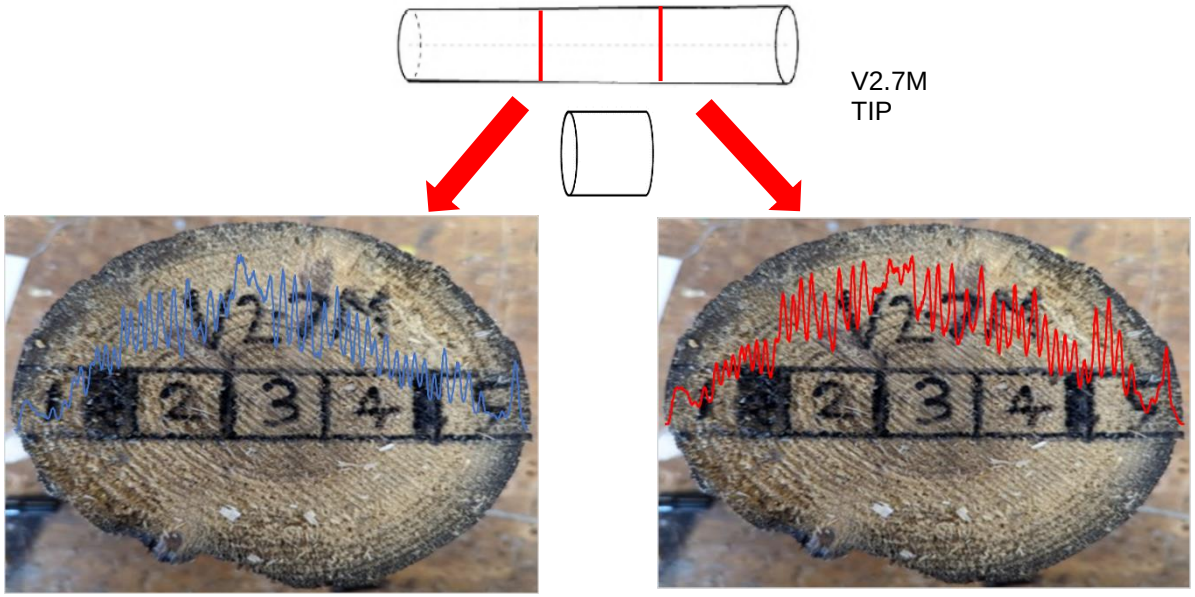

Figure 45 V2.7M Drilling amplitude comparison between the left and right side of the sample.

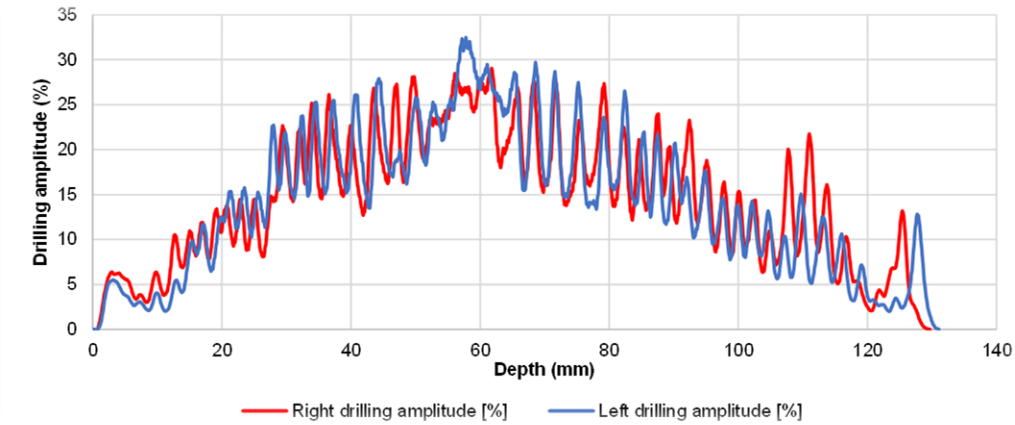

Figure 46 _V2.7M Drilling amplitude comparison between the left and right side of the sample.

5.2 Degraded piles

5.2.1 Pile 3M

The subsequent findings pertain to Pile BRU0030-PL1-P2 derived from the year 1727, specifically identified by a segment code of 3M and originating from container 228. Evaluations of the soft shell in terms of thickness reveal measurements of 13mm, 47mm, and 54mm for the head, middle part, and tip, respectively. Therefore, the average softshell for this pile is 38mm. It is worth noting that this particular pile exhibited extensive degradation, as evidenced by discernible alterations in its visual appearance, physical attributes, and mechanical characteristics.

Moisture content

Samples 1 and 5, positioned at the peripheral regions of the cross section within the soft-shell zone, exhibit the highest moisture content values. Sample 1, in particular, demonstrates the highest average moisture content at 280% with a standard deviation of 83.5%. The intermediate section yields comparable MC results, displaying a slight difference between 63% and 72%. Furthermore, samples 2 and 4 showcase smaller standard deviations, implying a tightly clustered distribution of data points around the mean. This coherence signifies enhanced precision and reliability within these datasets. The obtained results, when graphically represented, exhibited a distinctive W-shaped pattern, aligning with previous findings in the research literature. (Figure 47)

Density oven dry (0% MC)

The analysis reveals notable distinctions between Samples 1 and 5, positioned within the softshell region, and Samples 2, 3, and 4. Specifically, Samples 1 and 5 exhibit lower densities and higher standard deviations, indicating a state of degradation within the outer layer. Intriguingly, the density exhibits an increasing trend within the heartwood region, followed by a subsequent decrease in the middle portion where juvenile wood is located, thus giving rise to an M-shaped pattern within the results. The collective average dry density for the five samples is determined to be 319 kg/m³, which falls below the typical range of 400-500 kg/m³ observed for spruce wood. (Figure 47)

Modulus of elasticity and compression strength parallel to the grain

The observed trend in both stiffness and strength within the cross section follows an M-shaped pattern, indicating that the outermost layers exhibit significantly lower levels of strength and stiffness compared to the internal regions. On average, the strength of samples 1 and 5 is found to be approximately 35% of the average strength exhibited by samples 2, 3, and 4. Similarly, the stiffness of samples 1 and 5 is approximately 27% of the average stiffness observed in samples 2, 3, and 4. This intriguing outcome is further complemented by the fact that the amplitude of drilling in the outer layers is only 23% of the amplitude observed in the interior regions. This promising result suggests that it could be possible to match the RPD data to that of the mechanical properties. (Figure 47)

Drilling amplitude vs Compression strength

The statistical analysis conducted on the relationship between fc,0,wet and drilling amplitude of wooden samples yielded a coefficient of determination (R^2) value of 0.77 see Figure 49. This indicates that approximately 77% of the observed variation in the ultimate compression strength can be explained by changes in the drilling amplitude. The assessment of drilling amplitude presents a valuable measurement for evaluating the compressive strength characteristics. This assertion is substantiated by the significant correlation coefficient (R^2) observed.

Table 2 Average result and standard deviation for the head, middle part & tip.

Average result	Moisture Content	SD	Density dry	SD	Density wet	SD	fc,0,wet	SD	MOE	SD	RPD drilling average	SD
[#]	[%]	[#]	[kg/m^3]	[#]	[kg/m^3]	[#]	[N/mm^2]	[#]	Mpa	[#]	[%]	[#]
3M_1	280	83.5	251	49.0	811	8.0	4	3.0	1289	1117.1	4	1.5
3M_2	63	7.3	374	6.3	534	11.1	12	2.3	5793	1133.8	23	7.4
3M_3	72	15.1	338	20.4	515	45.5	7	1.9	3699	743.3	16	0.3
3M_4	70	9.1	383	5.0	564	40.5	11	1.7	5663	858.9	19	5.7
3M_5	253	43.6	252	32.3	759	26.9	3	1.1	1447	734.5	5	1.5

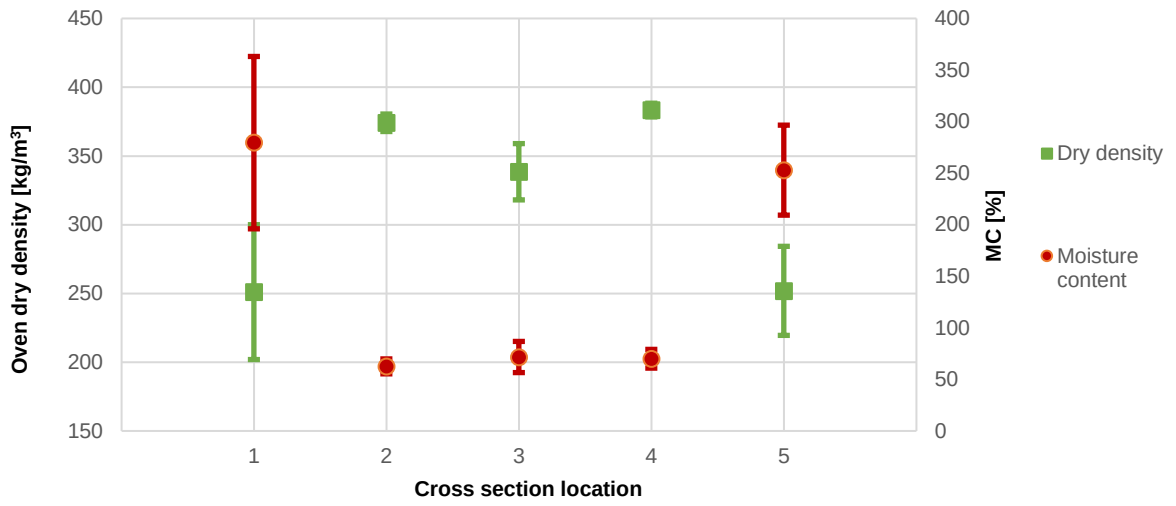

Figure 47 Average values and standard deviations of oven dry densities (0% MC) and moisture contents above fibre saturation were obtained across the cross section (1-5) for the head, middle part, and tip.

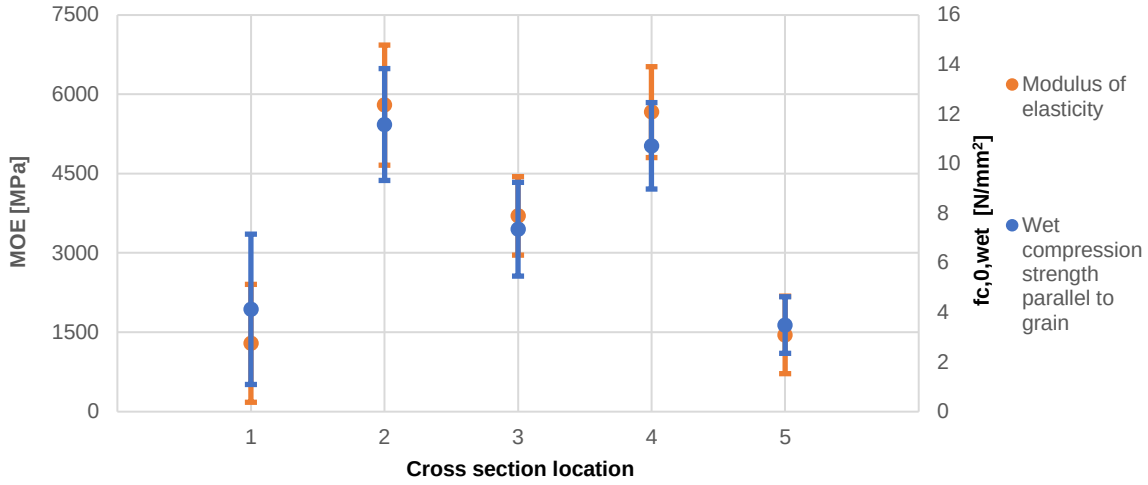

Figure 48 Average values and standard deviations of MOE (Mpa) and wet compression strength parallel to the grain (N/mm²) above fibre saturation were obtained across the cross section (1-5) for the head, middle part, and tip.

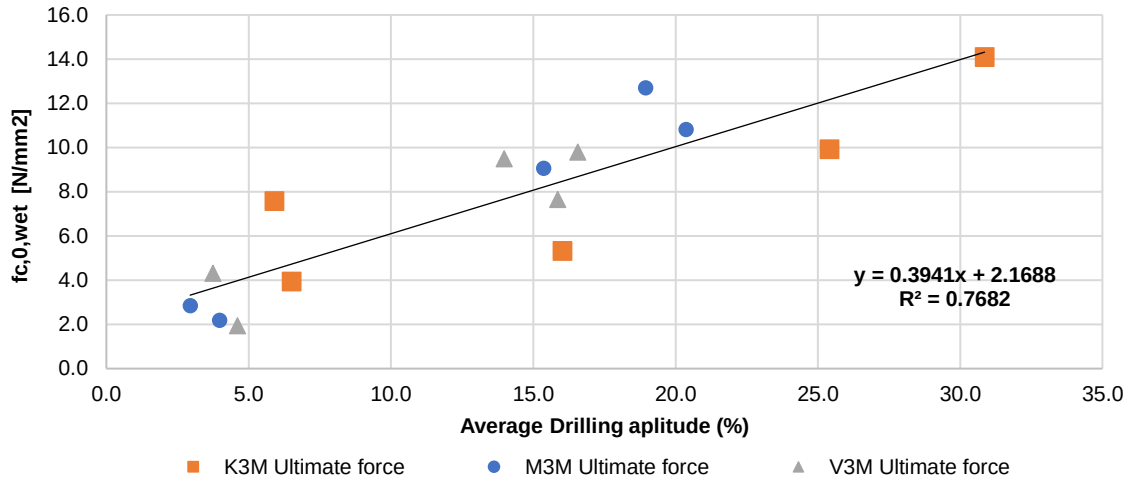

Figure 49 Wet compression strength parallel to the grain (N/mm²) vs Average drilling amplitude (%)

5.2.2 Pile 2.7M

The subsequent findings pertain to Pile BRU0030 PL1 P2.7 derived from the year 1727, specifically identified by a segment code of 2.7M and originating from container 115. Evaluations of the soft shell in terms of thickness reveal measurements of 29mm, 54mm, and 34mm for the head, middle part, and tip, respectively. Therefore the average softshell for this pile is 39mm. It is worth noting that this particular pile exhibited extensive degradation, as evidenced by discernible alterations in its visual appearance, physical attributes, and mechanical characteristics.

Moisture content

Samples 1 and 5, positioned at the peripheral regions of the cross section within the soft-shell zone, exhibit the highest moisture content values. Sample 1, in particular, demonstrates the highest average moisture content at 264% with a standard deviation of 32%. The intermediate section yields comparable MC results, displaying a difference between 61% and 98%. Furthermore, samples 3 and 4 showcase smaller standard deviations, implying a tightly clustered distribution of data points around the mean. This coherence signifies enhanced precision and reliability within these datasets. The obtained results, when graphically represented, exhibited a distinctive U-shaped pattern, aligning with previous findings in the literature research. (Figure 50)

Density oven dry (0% MC)

The analysis reveals notable distinctions between Samples 1 and 5, positioned within the softshell region, and Samples 2, 3, and 4. Specifically, Samples 1 and 5 exhibit lower densities but similar standard deviations, indicating a state of degradation within the outer layer. The density exhibits an increasing trend within the heartwood region, followed by a uniform result in the centre of the pile where juvenile wood is located, thus giving rise to an n-shaped pattern within the results. The collective average dry density for the five samples is determined to be 344.2 kg/m³, which falls below the typical range of 400-500 kg/m³ observed for spruce wood. (Figure 50)

Modulus of elasticity and compression strength parallel to the grain

The observed trend in both stiffness and strength within the cross section follows an M-shaped pattern, indicating that the outermost layers exhibit significantly lower levels of strength and stiffness compared to the internal regions. On average, the strength of samples 1 and 5 is found to be approximately 40% of the average strength exhibited by samples 2, 3, and 4. Similarly, the stiffness of samples 1 and 5 is approximately 20% of the average stiffness observed in samples 2, 3, and 4. This intriguing outcome is further complemented by the fact that the amplitude of drilling in the outer layers is only 20% of the amplitude observed in the interior regions. This promising result suggests that it could be possible to match the RPD data to that of the mechanical properties. (Figure 51)

Drilling amplitude vs Compression strength

The statistical analysis conducted on the relationship between fc,0,wet and drilling amplitude of wooden samples yielded a coefficient of determination (R^2) value of 0.89 see Figure 52. This indicates that approximately 89% of the observed variation in the ultimate compression strength can be explained by changes in the drilling amplitude. The assessment of drilling amplitude presents a valuable measurement for evaluating the compressive strength characteristics. This assertion is substantiated by the significant correlation coefficient (R^2) observed.

Table 3 Average result and standard deviation for the head, middle part & tip.

Average result	Moisture Content	SD	Density dry	SD	Density wet	SD	fc,0,wet	SD	MOE	SD	RPD drilling average	SD
[#]	[%]	[#]	[kg/m^3]	[#]	[kg/m^3]	[#]	[N/mm^2]	[#]	Mpa	[#]	[%]	[#]
2.7M_1	177	19.8	263	14.9	666	28.3	5	0.9	1517	407.0	5	1.1
2.7M_2	98	51.0	397	28.0	679	124.9	12	2.0	6206	1693.8	20	3.4
2.7M_3	57	15.8	409	10.4	567	42.4	11	2.2	6055	1832.7	21	2.5
2.7M_4	61	16.8	412	17.9	582	77.6	12	1.3	7347	1342.9	18	1.1
2.7M_5	264	31.9	240	25.7	789	4.6	4	1.2	1179	383.8	3	0.4

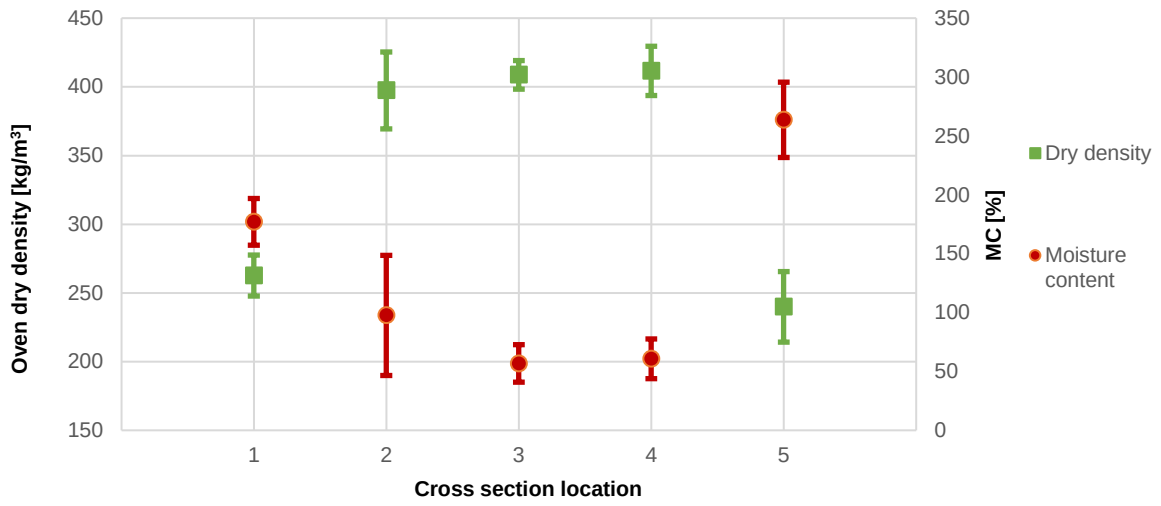

Figure 50 Average values and standard deviations of oven dry densities (0% MC) and moisture contents above fibre saturation were obtained across the cross section (1-5) for the head, middle part, and tip.

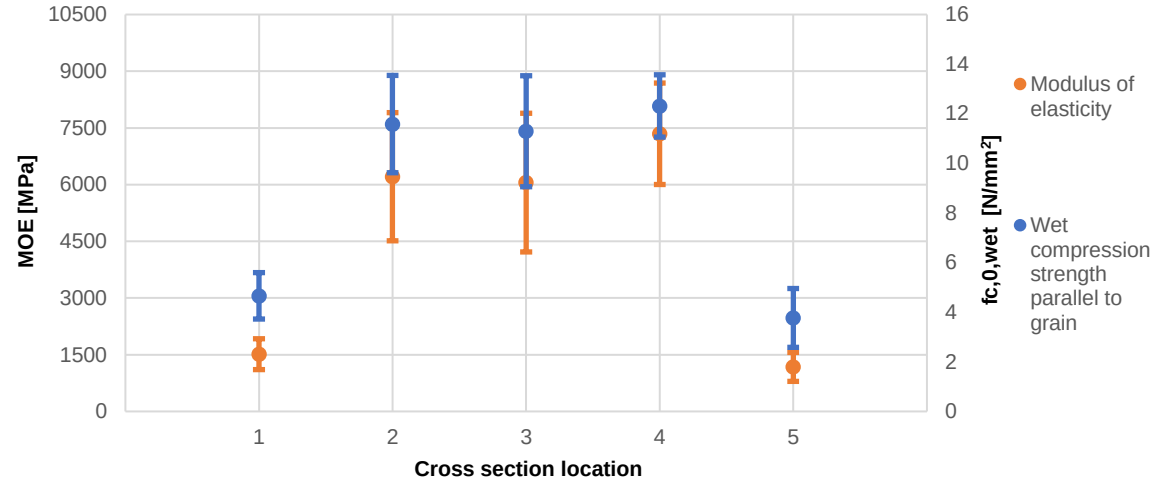

Figure 51 Average values and standard deviations of MOE (Mpa) and wet compression strength parallel to the grain (N/mm²) above fibre saturation were obtained across the cross section (1-5) for the head, middle part, and tip.

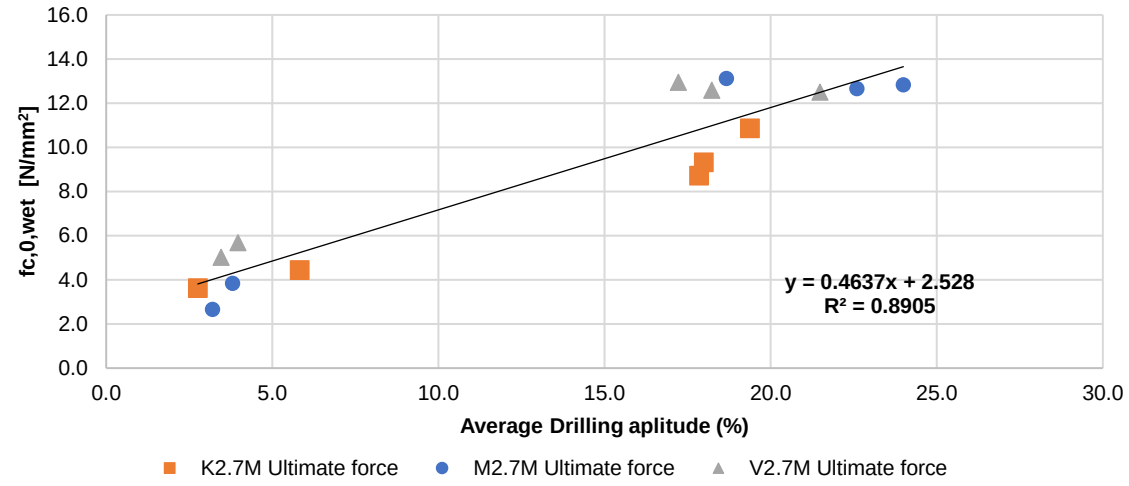

Figure 52 Wet compression strength parallel to the grain (N/mm²) vs Average drilling amplitude (%)

5.2.3 Pile 6M

The subsequent findings pertain to Pile BRU0030-PL2-P2.21 derived from the year 1727, specifically identified by a segment code of 6M and originating from container 228. Evaluations of the soft shell in terms of thickness reveal measurements of 30mm, 52mm, and 42mm for the head, middle part, and tip, respectively. Therefore the average softshell for this pile is 41mm. It is worth noting that this particular pile exhibited extensive degradation, as evidenced by discernible alterations in its visual appearance, physical attributes, and mechanical characteristics.

Moisture content

Samples 1 and 5, positioned at the peripheral regions of the cross section within the soft-shell zone, exhibit the highest moisture content values. Sample 1, in particular, demonstrates the highest average moisture content at 216% with a standard deviation of 80.5%. Sample 5 has a larger SD at 105.8% and a similar 212% MC. A high SD means a greater amount of variability in the results. The intermediate section yields comparable MC results, displaying a change between 62% and 89%. Furthermore, samples 2 to 4 showcase smaller standard deviations, implying a tightly clustered distribution of data points around the mean. This coherence signifies enhanced precision and reliability within these datasets. The obtained results, when graphically represented, exhibited a distinctive W-shaped pattern, aligning with previous findings in the literature research. (Figure 53)

Density oven dry (0% MC)

The analysis reveals notable distinctions between Samples 1 and 5, positioned within the softshell region, and Samples 2, 3, and 4. Specifically, Samples 1 and 5 exhibit lower densities but larger standard deviations, indicating a state of degradation within the outer layer. As anticipated, the density exhibits an increasing trend within the heartwood region, followed by a lower result in the centre of the pile where juvenile wood is located, thus giving rise to an M-shaped pattern within the results. The collective average dry density for the five samples is determined to be 388 kg/m³, which falls below the typical range of 400-500 kg/m³ observed for spruce wood. (Figure 53)

Modulus of elasticity and compression strength parallel to the grain

The observed trend in both stiffness and strength within the cross section follows an M-shaped pattern, indicating that the outermost layers exhibit slightly lower levels of strength and stiffness compared to the internal regions. On average, the strength of samples 1 and 5 is found to be approximately 69% of the average strength exhibited by samples 2, 3, and 4. Similarly, the stiffness of samples 1 and 5 is approximately 67% of the average stiffness observed in samples 2, 3, and 4. This intriguing outcome is further complemented by the fact that the amplitude of drilling in the outer layers is only 52% of the amplitude observed in the interior regions. (Figure 53)

Drilling amplitude vs Compression strength

The statistical analysis conducted on the relationship between fc,0,wet and drilling amplitude of wooden samples yielded a coefficient of determination (R^2) value of 0.68 see Figure 52. This indicates that approximately 68% of the observed variation in the ultimate compression strength can be explained by changes in the drilling amplitude. The assessment of drilling amplitude presents a valuable measurement for evaluating the compressive strength characteristics. This assertion is substantiated by the significant correlation coefficient (R^2) observed.

Table 4 Average result and standard deviation for the head, middle part & tip.

Average result	Moisture Content	SD	Density dry	SD	Density wet	SD	fc,0,wet	SD	MOE	SD	RPD drilling average	SD
[#]	[%]	[#]	[kg/m^3]	[#]	[kg/m^3]	[#]	[N/mm^2]	[#]	Mpa	[#]	[%]	[#]
6M_1	216	80.5	304	38.5	842	105.6	8	5.2	3691	2450.1	12	8.7
6M_2	89	20.5	439	13.9	708	90.0	12	2.2	6028	1988.5	24	2.6
6M_3	62	14.4	402	6.8	574	75.1	10	3.1	5039	1864.9	23	0.7
6M_4	63	24.4	439	12.5	616	108.6	13	0.2	7218	982.5	25	2.6
6M_5	212	105.8	358	112.7	889	29.8	8	5.3	4312	3298.0	13	9.1

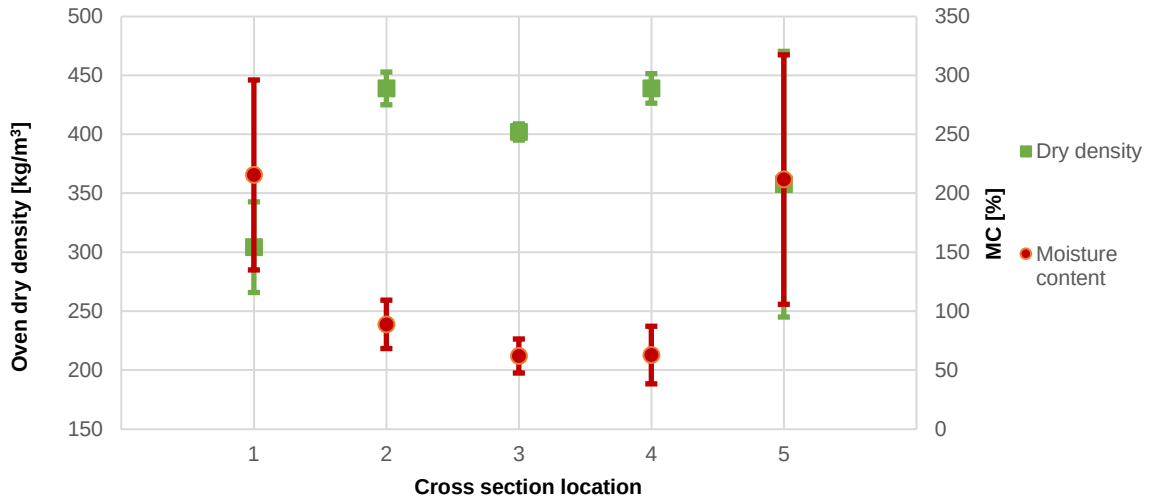

Figure 53 Average values and standard deviations of oven dry densities (0% MC) and moisture contents above fibre saturation were obtained across the cross section (1-5) for the head, middle part, and tip.

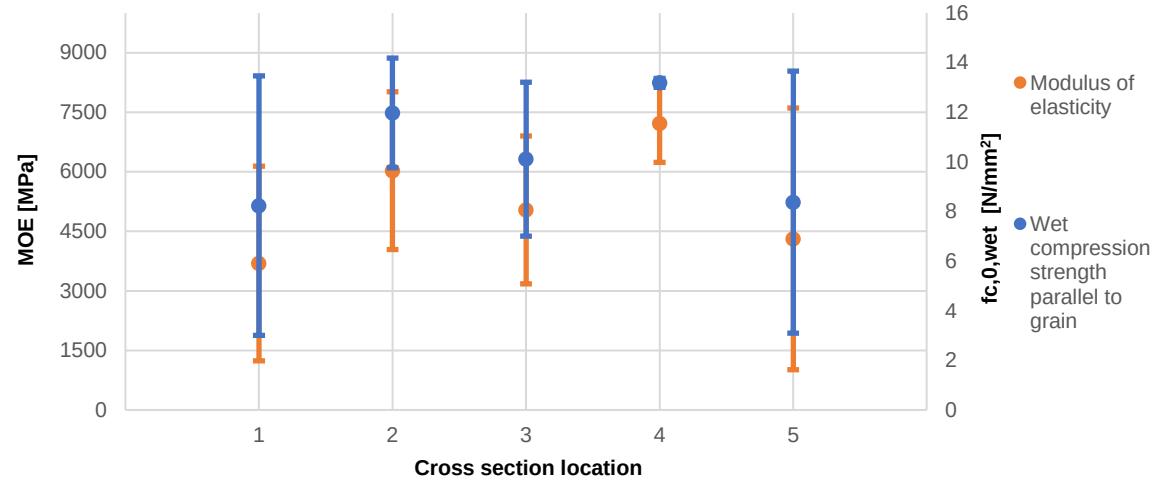

Figure 54 Figure 42 Average values and standard deviations of MOE (Mpa) and wet compression strength parallel to the grain (N/mm²) above fibre saturation were obtained across the cross section (1-5) for the head, middle part, and tip.

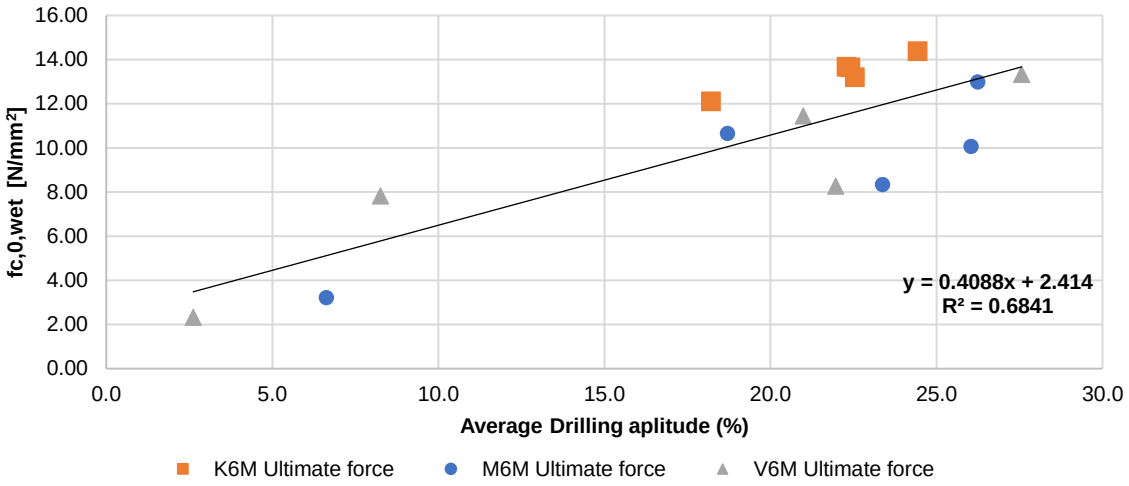

Figure 55 Wet compression strength parallel to the grain (N/mm²) vs Average drilling amplitude (%)

5.2.4 Pile 6M_60mm sample

The subsequent findings pertain to Pile BRU0030-PL2-P2.21 derived from the year 1727, specifically identified by a segment code of 6M and originating from container 228. This is the small 60mm sample results.

Moisture content

Samples 1 and 5, positioned at the peripheral regions of the cross section within the soft-shell zone, exhibit the highest moisture content values. Sample 1, in particular, demonstrates the highest average moisture content at 189% with a standard deviation of 81%. Sample 5 has a larger SD at 84% and a lower 146% MC. A high SD means a greater amount of variability in the results. The intermediate section yields comparable MC results, displaying a difference between 52% and 60%. Furthermore, samples 2 to 4 showcase smaller standard deviations, implying a tightly clustered distribution of data points around the mean. This coherence signifies enhanced precision and reliability within these datasets. The obtained results, when graphically represented, exhibited a distinctive W-shaped pattern, aligning with previous findings in the literature research.

Density oven dry (0% MC)

The analysis reveals notable distinctions between Samples 1 and 5, positioned within the softshell region, and Samples 2, 3, and 4. Specifically, Samples 1 and 5 exhibit lower densities but larger standard deviations, indicating a state of degradation within the outer layer. As anticipated, the density exhibits an increasing trend within the heartwood region, followed by a lower result in the centre of the pile where juvenile wood is located, thus giving rise to an M-shaped pattern within the results. The collective average dry density for the five samples is determined to be 391.4kg/m³, which falls below the typical range of 400-500 kg/m³ observed for spruce wood.

Compression strength parallel to the grain

The observed trend in strength within the cross section follows an M-shaped pattern, indicating that the outermost layers exhibit slightly lower levels of strength compared to the internal regions. On average, the strength of samples 1 and 5 is found to be approximately 63% of the average strength exhibited by samples 2, 3, and 4.

Drilling amplitude vs Compression strength

The statistical analysis conducted on the relationship between fc,0,wet and drilling amplitude of wooden samples yielded a coefficient of determination (R^2) value of 0.78 see Figure 52. This indicates that approximately 78% of the observed variation in the ultimate compression strength can be explained by changes in the drilling amplitude. The assessment of drilling amplitude presents a valuable measurement for evaluating the compressive strength characteristics. This assertion is substantiated by the significant correlation coefficient (R^2) observed.

Table 5 Average result and standard deviation for the head, middle part & tip.

Average result	Moisture Content	SD	Density dry	SD	Density wet	SD	fc,0,wet	SD	RPD drilling average	SD
[#]	[%]	[#]	[kg/m^3]	[#]	[kg/m^3]	[#]	[N/mm^2]	[#]	[%]	[#]
6M_60mm_1	146	84	315	59	658	101	7.5	2.3	9.6	1.4
6M_60mm_2	52	18	436	61	557	67	13.8	2.0	25.2	4.4
6M_60mm_3	60	6	403	15	551	11	10.8	1.9	22.6	1.7
6M_60mm_4	58	21	452	8	620	74	13.7	0.9	24.0	2.0
6M_60mm_5	189	81	351	113	811	110	8.6	5.5	13.7	8.8

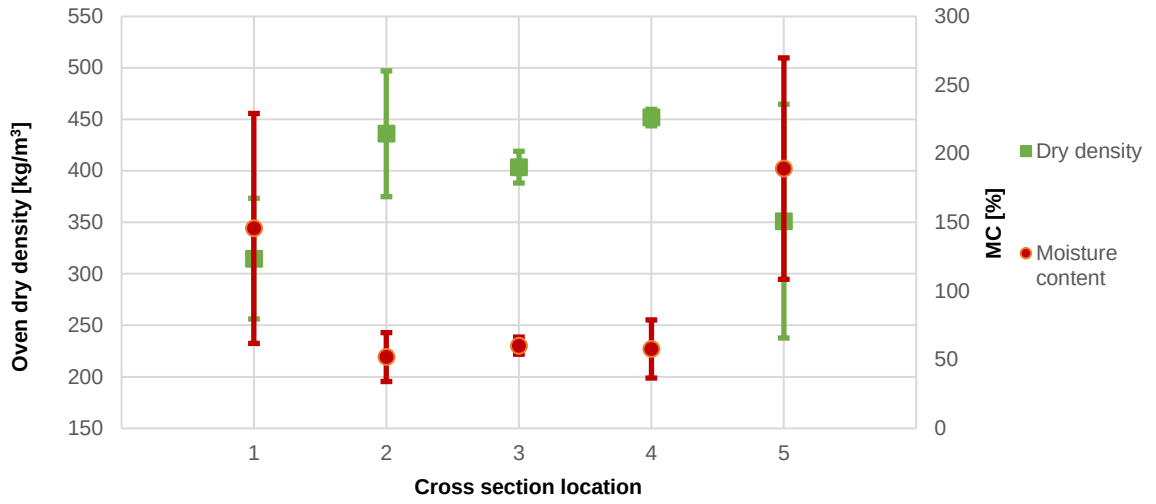

Figure 56 Average values and standard deviations of oven dry densities (0% MC) and moisture contents above fibre saturation were obtained across the cross section (1-5) for the head, middle part, and tip.

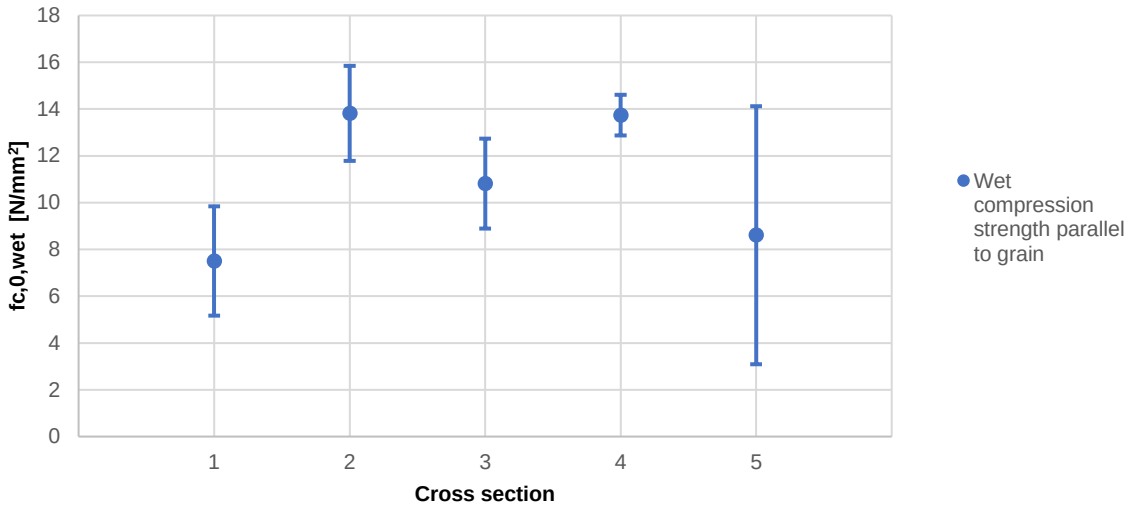

Figure 57 Figure 42 Average values and standard deviations of the wet compression strength parallel to the grain (N/mm²) above fibre saturation were obtained across the cross section (1-5) for the head, middle part, and tip.

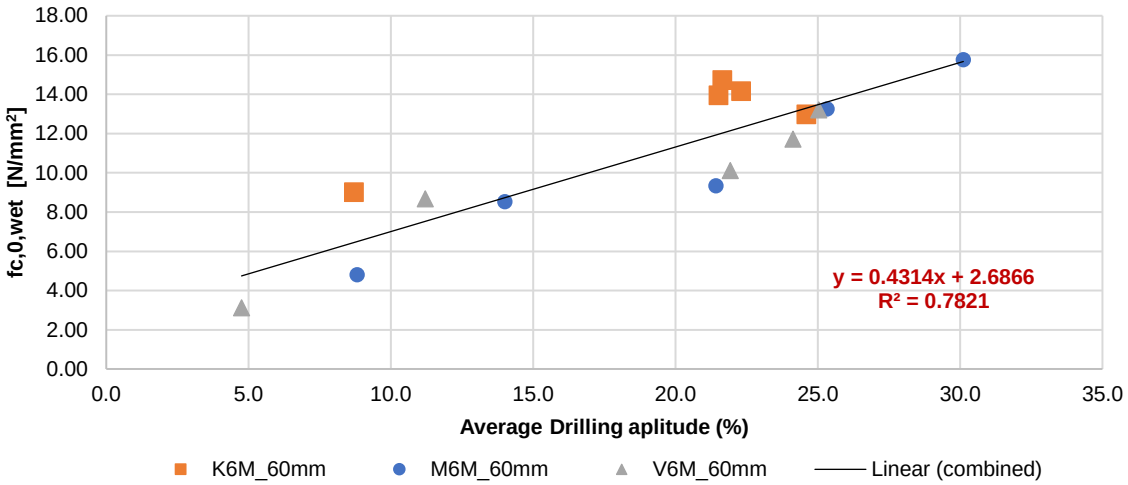

Figure 58 Wet compression strength parallel to the grain (N/mm²) vs Average drilling amplitude (%)

5.3 Non-degraded piles

5.3.1 Pile 3.18M

The subsequent findings pertain to Pile BRU0030-PL1-P3.18 derived from the year 1886, specifically identified by a segment code of 3.18M and originating from container 228. The measured softshell thickness values for the head, middle part, and tip of the soft shell were determined to be 13.8mm, 2mm, and 4mm, respectively. Importantly, this particular pile exhibited no significant signs of degradation, evident through its well-preserved visual appearance, intact physical attributes, and sound mechanical characteristics.

Moisture content

The moisture content plotted in Figure 59 has a uniform result for each of the 5 samples with no clear trend being established. The minimum MC of samples was 44 found in sample 2 with a maximum MC found in sample 4 of 58. It is important to note that samples 1 and 4 had a high standard deviation in comparison to their mean which means there was quite a lot of variability with the results. The average MC along the pile was 52% which is the lowest MC of all the experiments conducted.

Density oven dry (0% MC)

The dry density plotted in Figure 59 reveals notable distinctions between Samples 1 and 5, positioned at the edges of the cross-section region, with a notably higher dry density than the interior samples 2, 3, and 4. The collective average dry density for the five samples is determined to be 414 kg/m³, which falls below the typical range of 400-500 kg/m³ observed for spruce wood.

Modulus of elasticity and compression strength parallel to the grain

The observed trend in both stiffness and strength plotted in Figure 60 within the cross section follows a U-shaped pattern, indicating that the outermost layers exhibit significantly higher levels of strength and stiffness compared to the internal regions. On average, the strength of samples 1 and 5 is found to be approximately 140% of the average strength exhibited by samples 2, 3, and 4. Similarly, the stiffness of samples 1 and 5 is approximately 169% of the average stiffness observed in samples 2, 3, and 4. This intriguing outcome is further complemented by the fact that the amplitude of drilling in the outer layers is 123% of the amplitude observed in the interior regions. This promising result suggests that it could be possible to match the RPD data to that of the mechanical properties.

Drilling amplitude vs Compression strength

The statistical analysis conducted on the relationship between fc,0,wet and drilling amplitude of wooden samples yielded a coefficient of determination (R^2) value of 0.73 see Figure 52. This indicates that approximately 73% of the observed variation in the ultimate compression strength can be explained by changes in the drilling amplitude. The assessment of drilling amplitude presents a valuable measurement for evaluating the compressive strength characteristics. This assertion is substantiated by the significant correlation coefficient (R^2) observed.

Table 6 Average result and standard deviation for the head, middle part & tip.

Average result	Moisture Content	SD	Density dry	SD	Density wet	SD	fc,0,wet	SD	MOE	SD	RPD drilling average	SD
[#]	[%]	[#]	[kg/m^3]	[#]	[kg/m^3]	[#]	[N/mm^2]	[#]	Mpa	[#]	[%]	[#]
3.18M_1	52	16.5	496	33.7	640	55.0	17	3.0	8553	3158.9	19	1.1
3.18M_2	44	2.2	378	9.6	477	9.4	14	1.0	6742	1117.3	16	0.3
3.18M_3	55	7.0	373	4.9	519	27.0	9	1.5	3420	635.7	14	1.3
3.18M_4	58	27.6	372	18.3	515	99.6	11	0.8	4143	527.3	15	1.8
3.18M_5	51	5.7	453	5.8	579	39.8	15	0.9	7532	1336.5	18	2.3

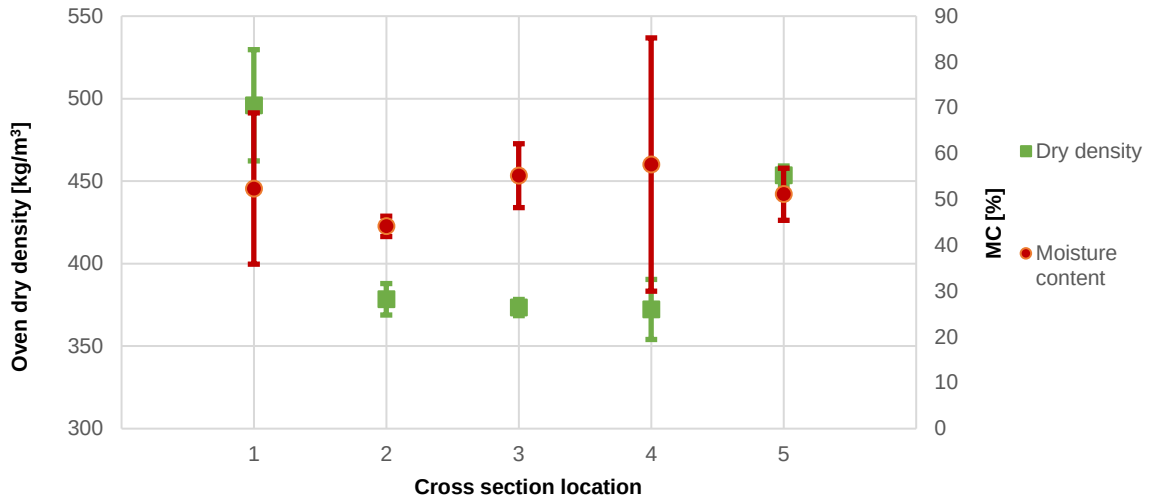

Figure 59 Average values and standard deviations of oven dry densities (0% MC) and moisture contents above fibre saturation were obtained across the cross section (1-5) for the head, middle part, and tip.

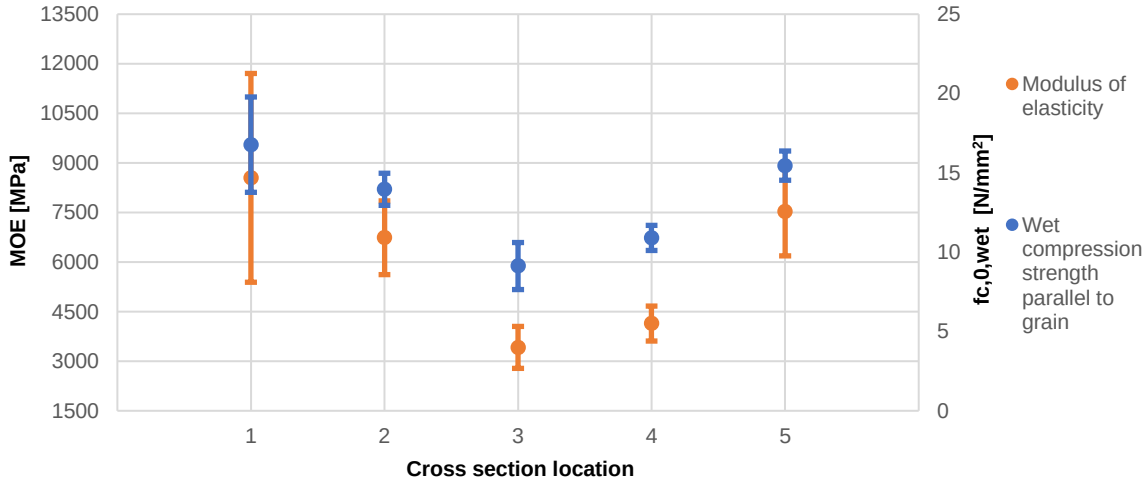

Figure 60 Figure 42 Average values and standard deviations of MOE (Mpa) and wet compression strength parallel to the grain (N/mm²) above fibre saturation were obtained across the cross section (1-5) for the head, middle part, and tip.

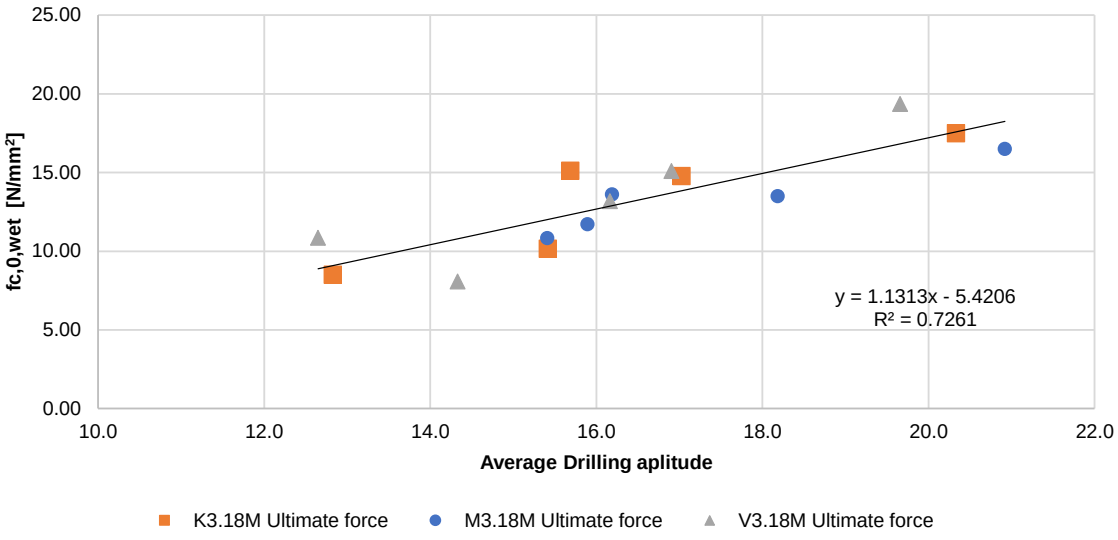

Figure 61 Wet compression strength parallel to the grain (N/mm²) vs Average drilling amplitude (%)

5.3.2 Pile 11M

The following results are related to Pile BRU0041-PL2-P1.9, which originated in the year 1922 and can be specifically identified by the segment code 11M from container 228. Measurements were taken for the softshell thickness at the head, middle part, and tip, yielding a value of 0mm. It is noteworthy that this particular pile showed no significant signs of degradation, as evidenced by its well-preserved visual appearance, intact physical attributes, and sound mechanical characteristics.

Moisture content

Samples 1 and 5, positioned at the peripheral regions of the cross section within the Sapwood zone, exhibit the highest moisture content values. Sample 5, in particular, demonstrates the highest average moisture content at 143% with a standard deviation of 24.9(%). The intermediate section yields comparable results, displaying a difference between 46% and 59%. Furthermore, samples 2 and 3 showcase smaller standard deviations, implying a tightly clustered distribution of data points around the mean. This coherence signifies enhanced precision and reliability within these datasets. The obtained results, when graphically represented, exhibited a distinctive U/W-shaped pattern, aligning with previous findings in the literature research. (see Figure 62)

Density oven dry (0% MC)

The analysis reveals notable distinctions between Samples 1 and 5, positioned within the Sapwood region, and Samples 2, 3, and 4. Specifically, Samples 1 and 5 exhibit lower densities and similar standard deviations. Intriguingly, the density exhibits an increasing trend within the heartwood region, followed by a subsequent decrease in the middle portion where juvenile wood is located, thus giving rise to an M-shaped pattern within the results. The collective average dry density for the five samples is determined to be 477 kg/m³, which falls within the typical range of 400-500 kg/m³ observed for spruce wood. (see Figure 62)

Modulus of elasticity and compression strength parallel to the grain

The observed trend in both stiffness and strength within the cross section follows an M-shaped pattern, indicating that the outermost layers and pith/Juvenile in the centre of the wood exhibit significantly lower levels of strength and stiffness compared to the heartwood regions. On average, the strength of samples 1,3 and 5 is found to be approximately 72%% of the average strength exhibited by samples 2, and 4. Similarly, the stiffness of samples 1,3 and 5 is approximately 69% of the average stiffness observed in samples 2 and 4. This intriguing outcome is further complemented by the fact that the amplitude of drilling follows the same trajectory. This promising result suggests that it could be possible to match the RPD data to that of the mechanical properties. (see Figure 62)

Drilling amplitude vs Compression strength

The statistical analysis conducted on the relationship between fc,0,wet and drilling amplitude of wooden samples yielded a coefficient of determination (R^2) value of 0.44 see Figure 52. This indicates that approximately 44% of the observed variation in the ultimate compression strength can be explained by changes in the drilling amplitude. The assessment of drilling amplitude presents low measurement for evaluating the compressive strength characteristics. This assertion is substantiated by the significant correlation coefficient (R^2) observed.

Table 7 Average result and standard deviation for the head, middle part & tip.

Average result	Moisture Content	SD	Density dry	SD	Density wet	SD	fc,0,wet	SD	MOE	SD	RPD drilling average	SD
[#]	[%]	[#]	[kg/m^3]	[#]	[kg/m^3]	[#]	[N/mm^2]	[#]	Mpa	[#]	[%]	[#]
11M_1	120	22.2	487	4.5	906	92.9	15	1.8	9650	1641.6	29	5.4
11M_2	46	9.4	510	26.2	632	34.1	19	2.5	12634	1933.8	31	1.8
11M_3	49	8.3	460	51.2	597	35.8	13	2.3	8003	1103.1	26	2.0
11M_4	59	25.0	499	6.8	683	91.6	20	2.5	12996	1940.8	30	0.4
11M_5	143	24.9	428	29.9	904	71.7	14	1.9	8813	1797.3	25	3.7

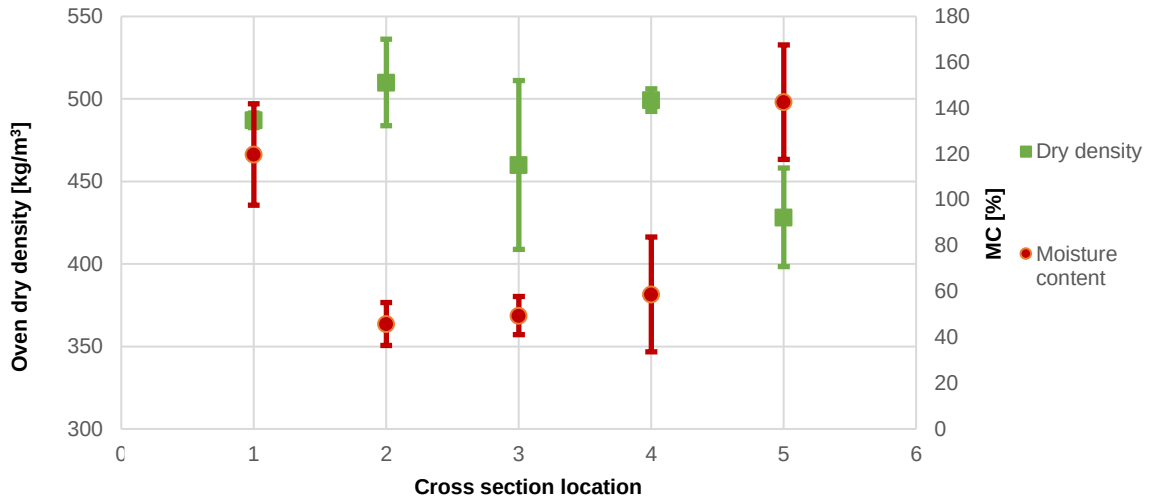

Figure 62 Average values and standard deviations of oven dry densities (0% MC) and moisture contents above fibre saturation were obtained across the cross section (1-5) for the head, middle part, and tip.

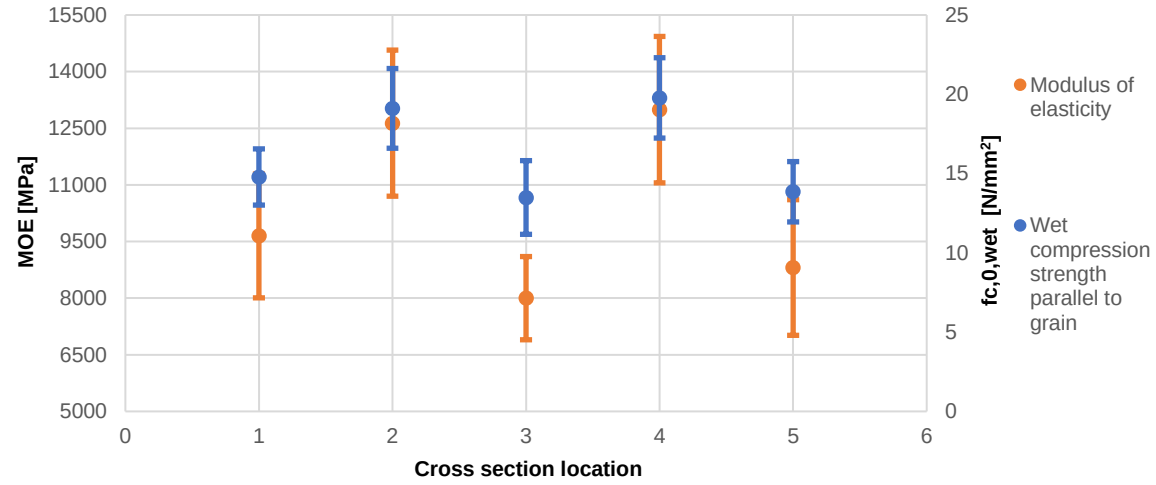

Figure 63 Figure 42 Average values and standard deviations of MOE (Mpa) and wet compression strength parallel to the grain (N/mm²) above fibre saturation were obtained across the cross section (1-5) for the head, middle part, and tip.

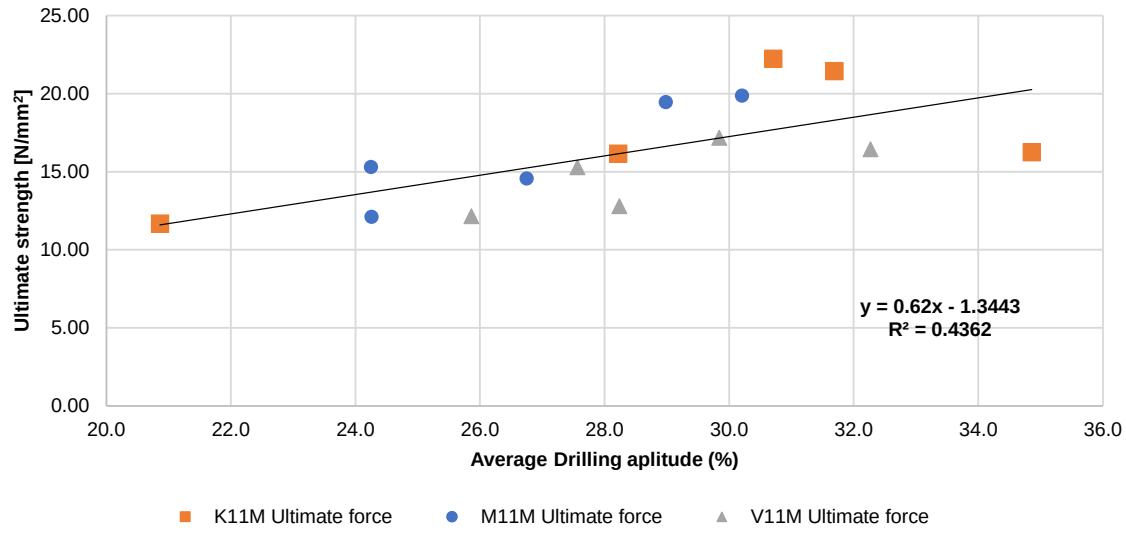

Figure 64 Wet compression strength parallel to the grain (N/mm²) vs Average drilling amplitude (%)

5.3.3 New Pile 10588M

The following results are related to Pile HIE-P10588, which is a new pile that has never been driven into the ground and can be specifically identified by the segment code 10588M. Measurements were taken for the softshell thickness at the head, middle part, and tip, yielding a value of 0mm. It is noteworthy that this particular pile showed no signs of degradation, as evidenced by its visual appearance, intact physical attributes, and sound mechanical characteristics.

Moisture content

Samples 1 and 5, positioned at the peripheral regions of the cross section within the Sapwood zone, exhibit the highest moisture content values. Sample 1, in particular, demonstrates the highest average moisture content at 135% with a standard deviation of 29(%). The intermediate section yields comparable results, displaying a difference between 41% and 63%. The obtained results, when graphically represented, exhibited a distinctive U-shaped pattern, aligning with previous findings in the literature research. (Figure 65)

Density oven dry (0% MC)

The analysis reveals notable distinctions between Samples 1 and 5, positioned within the Sapwood region, and Samples 2, 3, and 4. Specifically, Samples 1 and 5 exhibit lower densities and similar standard deviations. Intriguingly, the density exhibits an increasing trend within the heartwood region, followed by a subsequent decrease in the middle portion where juvenile wood is located, thus giving rise to an M-shaped pattern within the results. The collective average dry density for the five samples is determined to be 486 kg/m³, which falls within the typical range of 400-500 kg/m³ observed for spruce wood. (Figure 65)

Modulus of elasticity and compression strength parallel to the grain

The observed trend in both stiffness and strength within the cross section follows an M-shaped pattern, indicating that the outermost layers and pith/Juvenile in the centre of the wood exhibit lower levels of strength and stiffness compared to the heartwood regions. On average, the strength of samples 1 and 5 is found to be approximately 81%% of the average strength exhibited by samples 2, and 4. Sample 3 located in the juvenile wood had only 54% of strength in comparison to 2 and 4. Similarly, the stiffness of samples 1 and 5 is approximately 76% of the average stiffness observed in samples 2 and 4 Sample 3 once again had 48% stiffness compared to 2 and 4. This intriguing outcome is further complemented by the fact that the amplitude of drilling follows the same trajectory. This promising result suggests that it could be possible to match the RPD data to that of the mechanical properties.

Drilling amplitude vs Compression strength

The statistical analysis conducted on the relationship between fc,0,wet and drilling amplitude of wooden samples yielded a coefficient of determination (R^2) value of 0.58 see Figure 52. This indicates that approximately 58% of the observed variation in the ultimate compression strength can be explained by changes in the drilling amplitude. The assessment of drilling amplitude presents a measurement for evaluating the compressive strength characteristics. This assertion is substantiated by the significant correlation coefficient (R^2) observed.

Table 8 Average result and standard deviation for the head, middle part & tip.

Average result	Moisture Content	SD	Density dry	SD	Density wet	SD	fc,0,wet	SD	MOE	SD	RPD drilling average	SD
[#]	[%]	[#]	[kg/m^3]	[#]	[kg/m^3]	[#]	[N/mm^2]	[#]	Mpa	[#]	[%]	[#]
10588M_1	135	29.0	482	95.1	1021	68.3	20	5.4	9990	2466.1	20	4.7
10588M_2	47	25.3	548	87.9	736	51.5	24	2.4	11697	2413.9	23	3.3
10588M_3	41	16.5	416	44.0	546	66.0	13	1.5	5587	574.6	18	2.1
10588M_4	63	34.0	497	71.6	740	152.6	24	4.0	11539	3079.6	23	2.9
10588M_5	128	12.5	489	53.2	1029	21.9	19	1.9	8734	1769.2	22	3.5

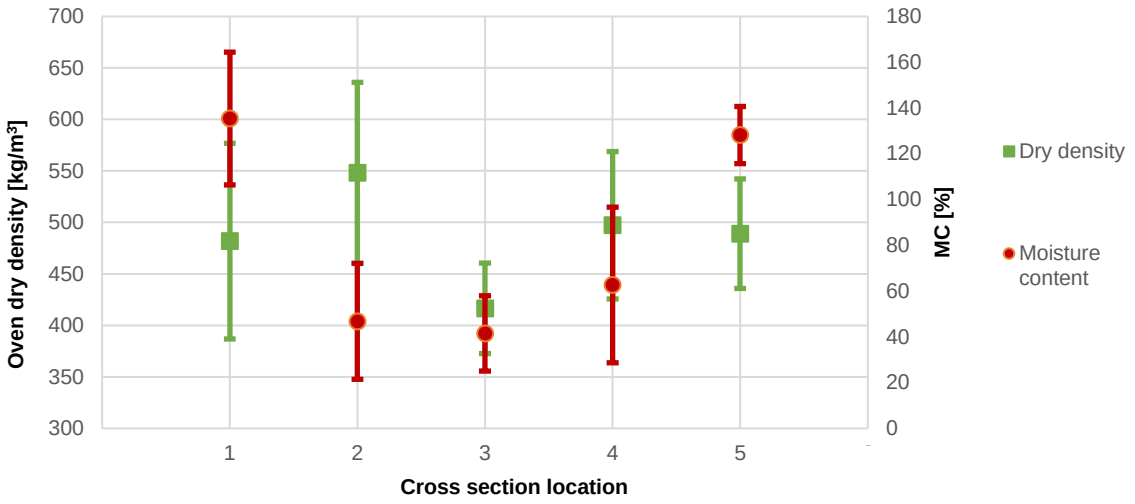

Figure 65 Average values and standard deviations of oven dry densities (0% MC) and moisture contents above fibre saturation were obtained across the cross section (1-5) for the head, middle part, and tip.

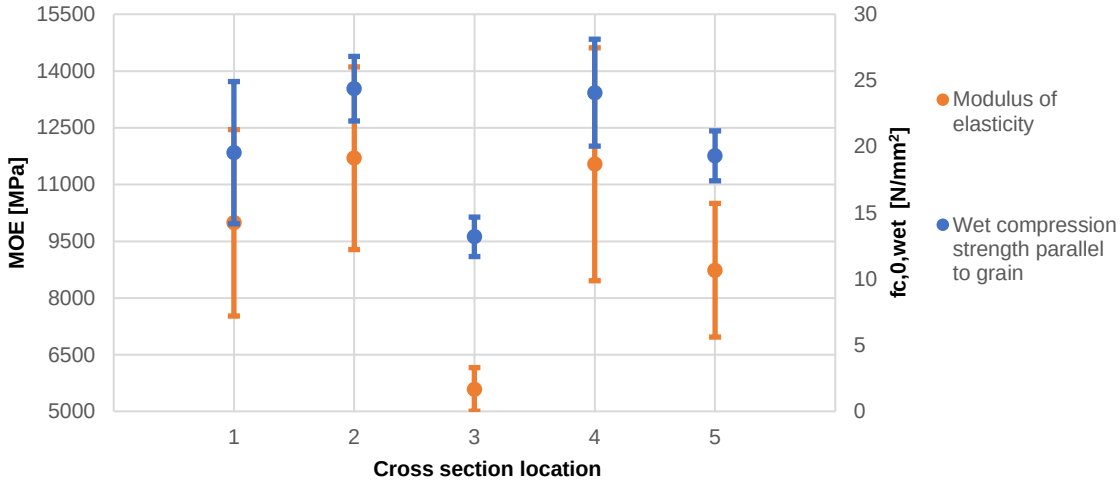

Figure 66 Figure 42 Average values and standard deviations of MOE (Mpa) and wet compression strength parallel to the grain (N/mm²) above fibre saturation were obtained across the cross section (1-5) for the head, middle part, and tip.

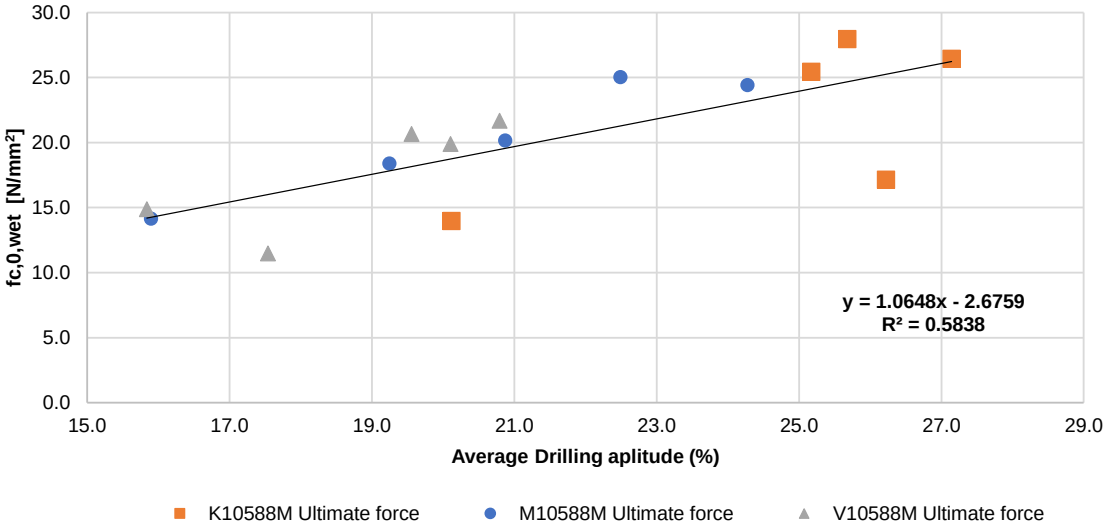

Figure 67 Wet compression strength parallel to the grain (N/mm²) vs Average drilling amplitude (%)

5.3.4 Pile 11M_60mm sample

The following results are related to Pile BRU0041-PL2-P1.9, which originated in the year 1922 and can be specifically identified by the segment code 11M from container 228. This is the small 60mm sample results.

Moisture content

Samples 1 and 5, positioned at the peripheral regions of the cross section within the Sapwood zone, exhibit the highest moisture content values. Sample 1, in particular, demonstrates the highest average moisture content at 117% with a standard deviation of 34(%). The intermediate section yields comparable results, displaying a slight variance between 44% and 74%. Furthermore, the obtained results, when graphically represented, exhibited a distinctive U-shaped pattern, aligning with previous findings in the literature research.

Density oven dry (0% MC)

The analysis reveals notable distinctions between Samples 1 and 5, positioned within the Sapwood region, and Samples 2, 3, and 4. Specifically, Samples 1 and 5 exhibit lower densities and similar standard deviations. Intriguingly, the density exhibits an increasing trend within the heartwood region, followed by a subsequent decrease in the middle portion where juvenile wood is located, thus giving rise to an M-shaped pattern within the results. The collective average dry density for the five samples is determined to be 496 kg/m³, which falls within the typical range of 400-500 kg/m³ observed for spruce wood.

Compression strength parallel to the grain

The observed trend in strength within the cross section follows an M-shaped pattern, indicating that the outermost layers exhibit slightly lower levels of strength compared to the internal regions.

Drilling amplitude vs Compression strength

The statistical analysis conducted on the relationship between fc,0,wet and drilling amplitude of wooden samples yielded a coefficient of determination (R^2) value of 0.27 see Figure 52. This indicates that approximately 27% of the observed variation in the ultimate compression strength can be explained by changes in the drilling amplitude. The assessment of drilling amplitude presents a measurement for evaluating the compressive strength characteristics. Such a weak relationship suggests that drilling amplitude is not a substantial predictor of the ultimate compression strength in wooden samples.

Table 9 Average result and standard deviation for the head, middle part & tip.

Average result	Moisture Content	SD	Density dry	SD	Density wet	SD	fc,0,wet	SD	RPD drilling average	SD
[#]	[%]	[#]	[kg/m^3]	[#]	[kg/m^3]	[#]	[N/mm^2]	[#]	[%]	[#]
11M_60mm_1	117	34	436	57	805	27	13.5	3.0	23.9	5.6
11M_60mm_2	74	42	503	45	743	113	21.4	7.6	30.2	0.4
11M_60mm_3	44	4	489	57	606	64	17.1	2.4	29.8	4.7
11M_60mm_4	61	19	502	49	687	39	19.1	3.1	29.9	1.7
11M_60mm_5	111	16	450	43	809	54	14.5	4.6	27.4	7.3

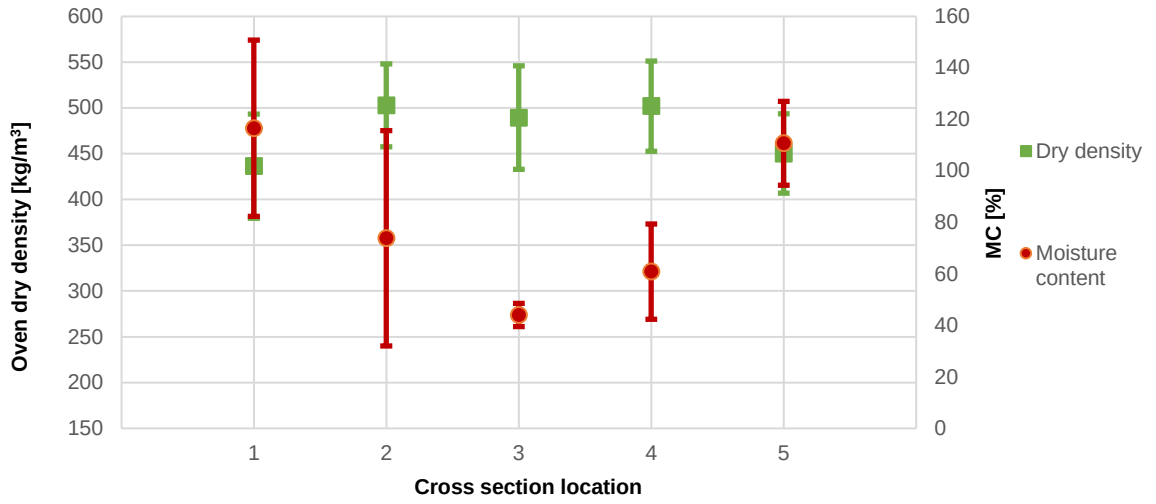

Figure 68 Average values and standard deviations of oven dry densities (0% MC) and moisture contents above fibre saturation were obtained across the cross section (1-5) for the head, middle part, and tip.

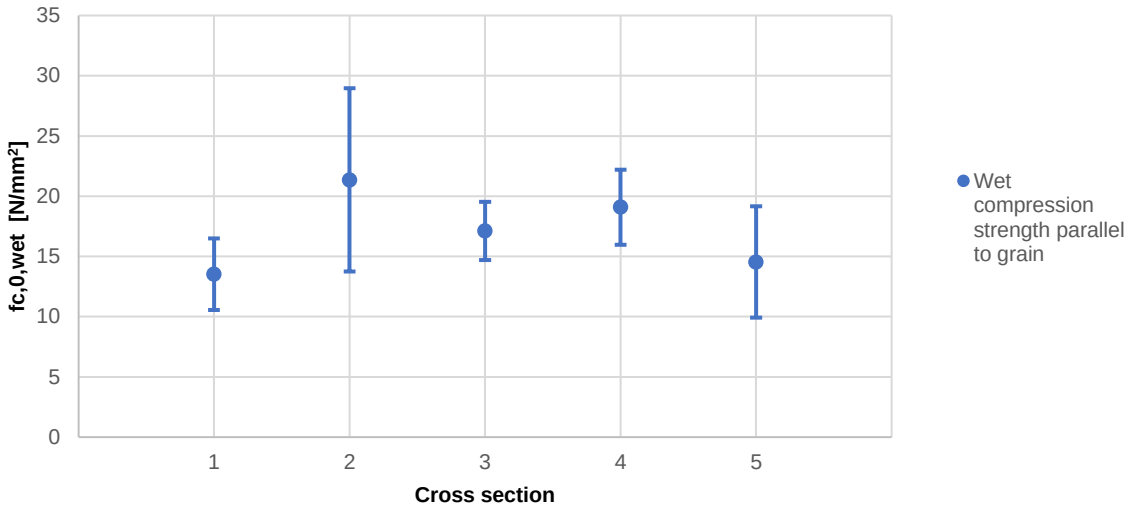

Figure 69 Figure 42 Average values and standard deviations of the wet compression strength parallel to the grain (N/mm²) above fibre saturation were obtained across the cross section (1-5) for the head, middle part, and tip.

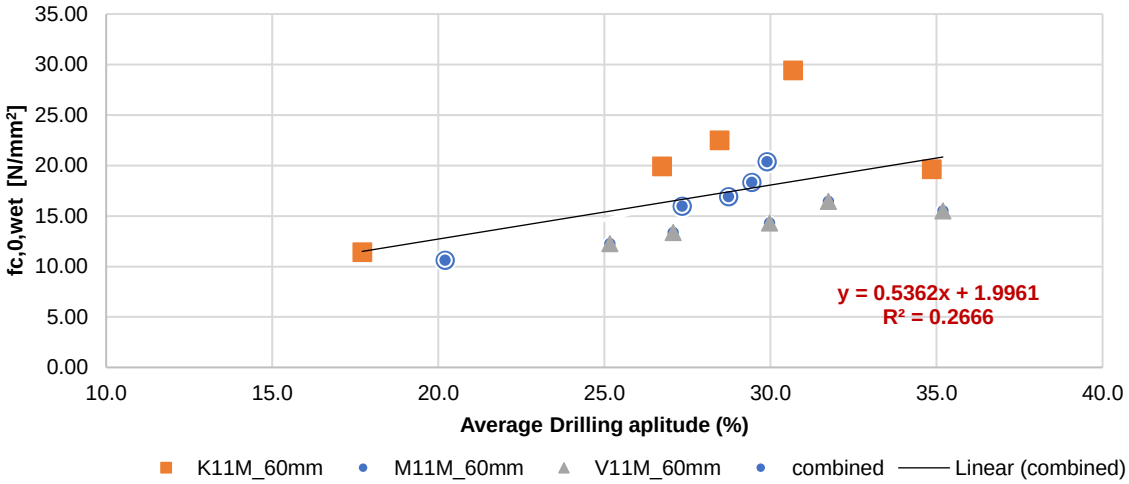

Figure 70 Wet compression strength parallel to the grain (N/mm²) vs Average drilling amplitude (%)

5.3.5 Pile 3.18M_60mm Sample

The subsequent findings pertain to Pile BRU0030-PL1-P3.18 derived from the year 1886, specifically identified by a segment code of 3.18M and originating from container 228. The measured softshell thickness values for the head, middle part, and tip of the soft shell were determined to be 13.8mm, 2mm, and 4mm, respectively. Importantly, this particular pile exhibited no significant signs of degradation, evident through its well-preserved visual appearance, intact physical attributes, and sound mechanical characteristics. Note this is the 60mm sample.

Moisture Content:

The moisture content exhibited consistent results across the five samples, displaying a W-shaped trend. Sample 2 and 4 demonstrated the minimum moisture content of 41, while sample 3 exhibited the maximum MC of 65. Notably, samples 3 and 5 displayed a relatively high standard deviation in comparison to their mean, indicating substantial variability in the results. The average MC along the pile was 49.4%, representing the lowest MC among all conducted experiments.

Density (Oven Dry - 0% MC):

Analysis reveals notable distinctions between samples 1 and 5, located within the sapwood region, and samples 2, 3, and 4. Samples 1 and 5 exhibited higher densities, albeit with larger standard deviations. Such variability is commonly observed in the sapwood region of newly formed wood. The collective average dry density for the five samples was determined to be 420 kg/m³, falling within the typical range of 400-500 kg/m³ observed for spruce wood.

Compression Strength (Parallel to the Grain):

The observed trend in strength across the cross-section followed a U-shaped pattern, indicating that the outermost layers demonstrated slightly higher levels of strength compared to the internal regions.

Drilling Amplitude vs. Compression Strength:

A statistical analysis conducted on the relationship between fc,0,wet (ultimate compression strength) and drilling amplitude of wooden samples yielded a coefficient of determination (R^2) value of 0.7 (see Figure 73) This implies that approximately 70% of the observed variation in ultimate compression strength can be explained by changes in drilling amplitude. The assessment of drilling amplitude provides a means for evaluating the compressive strength characteristics, a relationship substantiated by the significant correlation coefficient (R^2) observed.

Table 10 Average result and standard deviation for the head, middle part & tip.

Average result	Moisture Content	SD	Density dry	SD	Density wet	SD	fc,0,wet	SD	RPD drilling average	SD
[#]	[%]	[#]	[kg/m^3]	[#]	[kg/m^3]	[#]	[N/mm^2]	[#]	[%]	[#]
3.18M_60mm_1	55	2	460	31	609	39	14.6	2.5	17.3	2.8
3.18M_60mm_2	41	5	398	23	484	38	15.1	0.4	15.5	0.2
3.18M_60mm_3	65	22	382	9	560	89	10.4	1.3	13.6	0.9
3.18M_60mm_4	41	2	374	7	456	23	13.0	0.4	14.7	0.4
3.18M_60mm_5	45	12	488	34	605	25	17.9	3.0	19.6	1.1

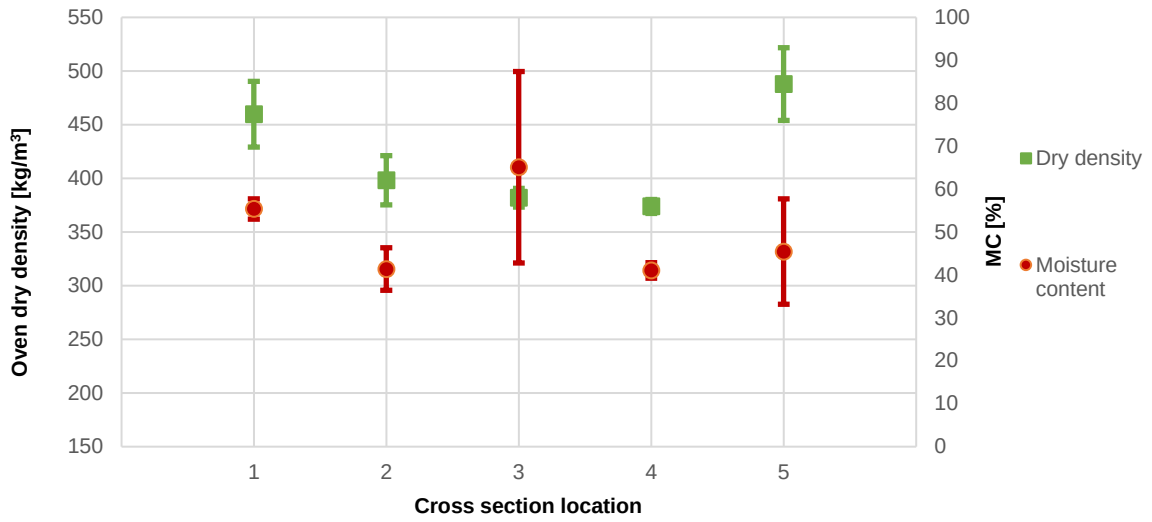

Figure 71 Average values and standard deviations of oven dry densities (0% MC) and moisture contents above fibre saturation were obtained across the cross section (1-5) for the head, middle part, and tip.

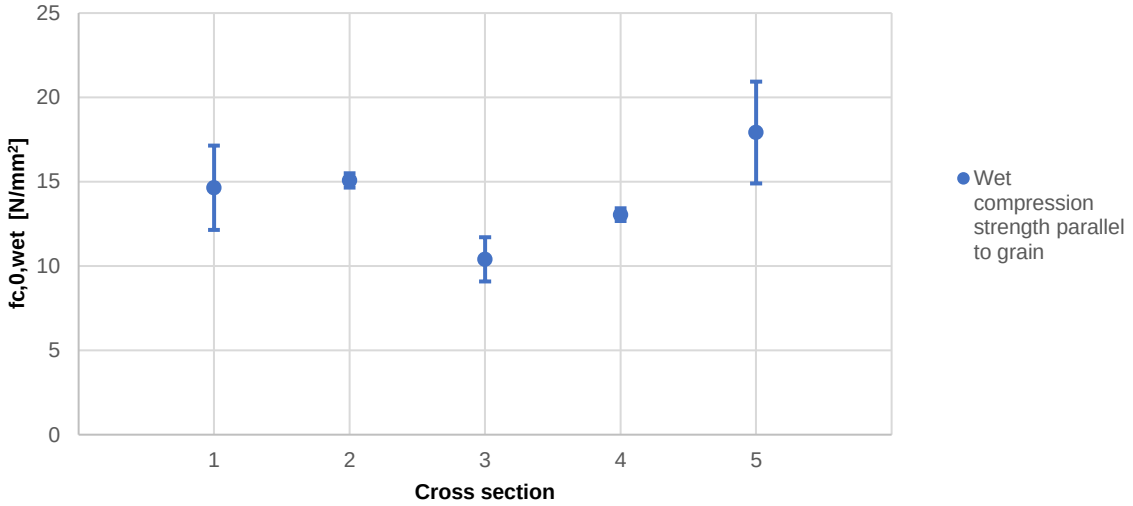

Figure 72 Figure 42 Average values and standard deviations of the wet compression strength parallel to the grain (N/mm²) above fibre saturation were obtained across the cross section (1-5) for the head, middle part, and tip.

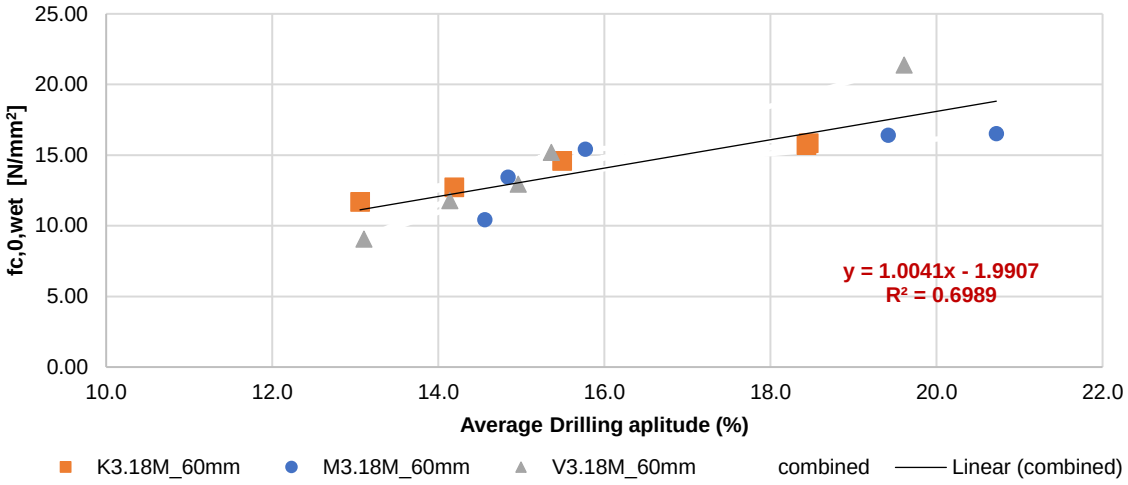

Figure 73 Wet compression strength parallel to the grain (N/mm²) vs Average drilling amplitude (%)

5.4 Result summary

The investigation aimed to comprehensively analyse the moisture content, oven dry density, compression strength parallel to the grain and modulus of elasticity distribution across multiple cross-sections of wooden foundation piles, emphasizing various segments and conditions. A wide array of samples was meticulously examined, encompassing both degraded and non-degraded piles, and encompassing regular-sized and smaller (60mm) samples. Noteworthy trends and discernible distinctions emerged from this detailed analysis.

5.4.1 Degraded Piles:

Pile 3M:

Moisture Content: The samples obtained from the periphery exhibited the highest moisture content levels, with Sample 1 standing out by showcasing the most substantial average (280%) alongside notable variability. Sections positioned in the intermediate range displayed comparable albeit lower moisture content percentages (ranging from 63% to 72%).

Density (Oven Dry): Within Pile 3M, Samples 1 and 5 were characterized by lower densities and elevated standard deviations, indicative of degradation within the outer layer. The density increased significantly within the heartwood region, followed by a gradual decrease in density across the middle portion. The calculated average density settled at 319 kg/m³.

Compression Strength: (Samples 1 and 5): Approximately 35% of the average strength and Modulus of Elasticity (Samples 1 and 5): Approximately 27% of the average stiffness exhibited by samples 2, 3, and 4.

Pile 2.7M:

Moisture Content: Mirroring the observations from Pile 3M, a similar trend was observed in Pile 2.7M, where Sample 1 exhibited the highest average moisture content (264%), while sections in-between displayed varying moisture content percentages (ranging from 61% to 98%).

Density (Oven Dry): The density distribution in Pile 2.7M paralleled that of Pile 3M, with Samples 1 and 5 showcasing diminished densities and a gradual upsurge in density as one moved towards the heartwood region. The calculated average density stood at 344.2 kg/m³.

Compression Strength: (Samples 1 and 5): Approximately 40% of the average strength and Modulus of Elasticity (Samples 1 and 5): Approximately 20% of the average stiffness exhibited by samples 2, 3, and 4.

Pile 6M (60mm Sample):

Moisture Content: Sample 1 within Pile 6M displayed the highest average moisture content (189%), accompanied by a significant degree of variability. Furthermore, Samples 1 and 5 exhibited lower moisture content percentages (146% and 212%, respectively).

Density (Oven Dry): Analogous degradation patterns were evident in Pile 6M, with Samples 1 and 5 exhibiting reduced densities and a discernible trend of density increment towards the heartwood regions. The average density was determined to be 391.4 kg/m³.

Compression Strength: (Samples 1 and 5): Approximately 69% of the average strength and Modulus of Elasticity (Samples 1 and 5): Approximately 67% of the average stiffness exhibited by samples 2, 3, and 4.

5.4.2 Non-Degraded Piles:

Pile 3.18M:

Moisture Content: Pile 3.18M showcased a relatively uniform moisture content across the various samples, though with a degree of variability that prevented the establishment of a clear trend. The computed average moisture content settled at 52%.

Density (Oven Dry): Notable density differences emerged between samples obtained from the periphery and those from the interior, with higher densities found in the former. The calculated average density stood at 414 kg/m³.

Compression Strength: (Samples 1 and 5): Approximately 140% of the average strength and Modulus of Elasticity (Samples 1 and 5): Approximately 169% of the average stiffness exhibited by samples 2, 3, and 4.

Pile 11M:

Moisture Content: Peripheral samples extracted from Pile 11M exhibited elevated moisture content levels, with Sample 5 displaying the highest average (143%), while intermediate sections demonstrated moderate variability, ranging from 46% to 59%.

Density (Oven Dry): Pile 11M presented peripheral samples with higher densities, coupled with heartwood regions showing an ascending density trend. The average density was calculated to be 477 kg/m³.

Compression Strength: (Samples 1, 3, and 5): Approximately 72% of the average strength and Modulus of Elasticity (Samples 1, 3, and 5): Approximately 69% of the average stiffness exhibited by samples 2 and 4.

New Pile 10588M:

Moisture Content: Analogous to previous observations, peripheral samples from New Pile 10588M displayed elevated moisture content levels, with Sample 1 again having the highest average (135%). Intermediate sections exhibited variations in moisture content percentages, ranging from 41% to 63%.

Density (Oven Dry): Comparable to the trend in other cases, peripheral samples from New Pile 10588M exhibited higher densities, while the heartwood region demonstrated an escalating density trend. The average density settled at 486 kg/m³.

Compression strength: Samples 1 and 5 demonstrate roughly 81% and 76% of the average strength respectively compared to samples 2 and 4, while Sample 3 indicates a reduced strength of 54% and stiffness of 48% in comparison to samples 2 and 4.

Pile 11M_60mm Sample:

Moisture Content: Moisture content trends remained consistent, with peripheral samples displaying higher moisture content (117% for Sample 1), and intermediate sections showing slight variations, ranging from 44% to 74%.

Density (Oven Dry): The density distribution within Pile 11M_60mm Sample resembled previous patterns, with peripheral samples presenting higher densities and a noticeable density increase within the heartwood region. The calculated average density was 496 kg/m³.

Compression Strength: Outermost layers slightly lower than internal regions.

Pile 3.18M_60mm Sample:

Moisture Content: Moisture content observations in Pile 3.18M_60mm Sample followed a distinct W-shaped pattern, characterized by variability. Sample 3 emerged with the highest moisture content (65%).

Density (Oven Dry): Peripheral samples within Pile 3.18M_60mm Sample exhibited higher densities, accompanied by greater variability, and heartwood regions showcased a progressive density increase. The average density was 420 kg/m³.

Compression Strength: Outermost layers slightly higher than internal regions.

In summary, the analysis clarified that degraded piles consistently demonstrated lower densities and higher moisture content, showcasing distinct degradation patterns across cross-sections. In contrast, non-degraded piles displayed more uniform moisture content and density distributions, aligning with established wood characteristics. The insights garnered from these findings shed valuable light on the structural and material attributes of wooden foundation piles across varying conditions. Degraded wooden foundation piles display cross-sectional compression strength and modulus of elasticity variations, characterized by diminished values in the outer layers compared to internal regions, following discernible M-shaped patterns indicative of structural deterioration. Conversely, non-degraded piles distinctive structural behaviours: The variations observed in the indicate that the strength and stiffness of the wood material differs significantly across the cross-sections of the piles. In some cases, the outer layers of the piles exhibit lower compression strength compared to the inner regions, while in other cases, the outer layers show slightly higher compression strength. This suggests that the structural integrity and load-bearing capacity of the piles can vary significantly depending on their internal composition and degradation level.

5.5 Size effect 60mm vs 120mm.

The size effect of specimens in wood samples is an important consideration in materials testing and research. Wood is a natural and heterogeneous material, and the mechanical properties of wood can vary significantly depending on the size and orientation of the wood grain. One significant size effect in wood samples is related to the density of the wood. In general, as the size of the wood specimen decreases, the proportion of the material made up of surface area and defects increases. This can result in lower mechanical properties, such as lower stiffness and strength, in smaller wood samples. It is therefore important to determine the difference between specimens with a height of 120mm compared to 60mm. Another important consideration in the size effect of wood samples is related to the moisture content of the wood. Wood is a hygroscopic material, meaning it can absorb and release moisture from the environment. Changes in moisture content can cause significant dimensional changes in the wood, which can impact the mechanical properties.

To determine the extent of the size effect from the 120mm and 60mm samples a comparison of the average results for the moisture content, area, density, strength, and average drilling amplitude. The results show that the results are relatable with most results having a difference less than 5% which given the natural variation in wood this is comparable. The following results were found between the 3 piles:

- Moisture content exhibited an average difference of 14.1%.
- Area (wet) displayed an average difference of 1.4%.
- Wet density exhibited a difference of 6.7%, while dry density showed a difference of 2.3%.
- Ultimate force exhibited a difference of 6.6%, and ultimate strength showed a difference of 6.8%.

Notably, the moisture content demonstrated the highest degree of variation. This can be attributed to the faster drying rate of the smaller 60mm samples compared to the 120mm specimens. Consequently, the differences in moisture content have an impact on both wet density and strength, explaining the relatively higher disparities observed in these parameters. Based on these findings, it is recommended to preferentially employ the 120mm samples. The larger samples facilitate the attachment of Linear Variable Differential Transformers (LVDTs) for precise strain measurements, enabling the determination of the modulus of elasticity. Moreover, the usage of 120mm samples aligns with local codes of practice [27], ensuring consistency and compatibility with established standards in the field of wood materials testing.

The investigation of the size effect in wood samples, encompassing aspects such as moisture content, area, density, strength, and drilling amplitude, contributes valuable insights to both scientific research and practical applications. Further exploration of the underlying mechanisms and additional factors contributing to the size effect can enhance our understanding of wood behaviour and aid in the development of improved design and engineering practices concerning wood structures and materials. Expanding the research to consider other relevant parameters and exploring the implications of the size effect across a broader range of wood species and environmental conditions would be beneficial for advancing knowledge in this field.

Table 5.2.1_Pile 11M Percentage difference between 120mm and 60mm samples

Section	Moisture Content	Area (wet)	Density wet	Density dry	Ultimate force	Ultimate strength	RPD drilling average
[N/A]	[%]	[mm^2]	kg/m^3]	kg/m^3]	[kN]	[N/mm^2]	[%]
K11M_60_Avg	77	431	759	500	8.9	20.6	27.7
K11M_120_Avg	73	436	711	486	7.7	17.6	29.3
Percentage difference	4%	-1%	6%	3%	14%	15%	-6%
M11M_60_Avg	81	437	704	467	7.2	16.4	27.1
M11M_120_Avg	87	431	748	461	7.0	16.3	26.9
Percentage difference	6%	1%	6%	1%	2%	1%	1%
V11M_60_Avg	86	431	727	462	6.2	14.4	29.8
V11M_120_Avg	90	435	774	484	6.6	14.8	28.8

Percentage difference	-5%	-1%	-6%	-5%	-6%	-3%	4%

Table 5.2.2_3.18M Percentage difference between 120mm and 60mm samples

Section	Moisture Content	Area (wet)	Density wet	Density dry	Ultimate force	Ultimate strength	RPD drilling average
[N/A]	[%]	[mm^2]	[kg/m^3]	[kg/m^3]	[kN]	[N/mm^2]	[%]
K3.18M_60_Avg	50	416	532	411	5.9	14.1	15.9
K3.18M_120_Avg	53	418	540	410	5.5	13.2	16.3
diff	-5%	-1%	-1%	0%	6%	6%	-2%
M3.18M_60_Avg	46	423	530	421	6.1	14.4	17.1
M3.18M_120_Avg	47	418	530	411	5.5	13.2	17.3
diff	4%	1%	0%	2%	9%	8%	-2%
V3.18M_60_Avg	53	413	566	429	5.8	14.1	15.4
V3.18M_120_Avg	56	410	568	422	5.5	13.3	15.9
diff	-6%	1%	0%	2%	6%	5%	-3%

Table 5.2.3_6M Percentage difference between 120mm and 60mm samples

Section	Moisture Content	Area (wet)	Density wet	Density dry	Ultimate force	Ultimate strength	RPD drilling average
[N/A]	[%]	[mm^2]	[kg/m^3]	[kg/m^3]	[kN]	[N/mm^2]	[%]
K6M_60_Avg	73	432	618	420	5.6	13.0	19.8
K6M_120_Avg	123	432	745	402	5.8	13.4	22.0
diff	-69%	0%	-21%	4%	-3%	-3%	-11%
M6M_60_Avg	107	437	654	394	4.5	10.3	19.9
M6M_120_Avg	123	456	712	390	4.2	9.1	20.2
diff	15%	-4%	9%	1%	8%	12%	-1%
V6M_60_Avg	123	429	647	360	4.0	9.4	17.4
V6M_120_Avg	138	440	721	373	3.8	8.7	16.3
diff	-13%	-3%	-12%	-3%	5%	8%	7%

6

Analysis

6.1 Introduction

In the result section it became apparent that a substantial contrast exists in the outcomes between the deteriorated piles and the intact piles concerning their physical and mechanical characteristics. The historical pile specimens originating from the year 1727, on average, exhibit elevated moisture content, reduced oven dry density, diminished compressive strength parallel to the grain, and decreased modulus of elasticity. These specimens encompass a variety of pile types as well as various states of degradation. Hence, it is of utmost significance to establish a correlation between the drilling amplitude (the independent variable) and the physical and mechanical properties. This will be accomplished through the use of linear regression analysis. The analysis will be conducted separately on the degraded and non-degraded piles and then finally the combined results. The primary objective emerges as the development of a dependable method to predict the characteristics of forthcoming piles based solely on their drilling amplitude results. By capitalizing on the established correlations between drilling amplitude and the intricate array of physical and mechanical attributes displayed by piles, the aim is to construct a predictive framework.

6.2 Degraded piles (2.7M, 3M, and 6M)

The purpose of creating the following graphs is to explore the potential relationship between the physical and mechanical properties of degraded spruce foundation piles and the corresponding average drilling amplitude. These piles are all from 1727 making these pile 296 years old .Among these piles, the soft shell was present in all of them. By examining these graphs, the aim is to uncover any discernible patterns or trends that may exist between the physical and mechanical characteristics of the piles and the average drilling amplitude. This analysis will contribute to our understanding of the relationship between these variables and potentially provide insights into the behaviour and performance of degraded spruce foundation piles in different time periods.

6.2.1 Moisture content vs Average drilling amplitude

The power trendline plotted below in Figure 74 with equation $y = 658.01x^{-0.723}$, with x values representing the average drilling amplitude and y indicating the moisture content, suggests a strong relationship between these variables. The negative exponent of -0.723 which implies an inverse relationship, meaning that as the average drilling amplitude increases, the moisture content decreases. The linear regression analysis of the results for the old, degraded specimens yields a coefficient of determination R^2 value of 0.7. This represents the proportion of the variance in the dependent variable (moisture content) that can be explained by the independent variable (average drilling amplitude). In this case, an R^2 of 0.7 suggests that approximately 70% of the variability in moisture content can be attributed to changes in the average drilling amplitude for degraded samples. Based on this analysis, using additional drilling amplitude values to determine moisture content appears to be a valid approach. The power trendline equation provides a mathematical model that describes the relationship between drilling amplitude and moisture content. With a reasonably high R^2 value, it indicates that the model captures a significant portion of the moisture content variability. It is interesting to note as the MC falls below 100% the trendline starts to become linear, this signifies that the MC is less dependent on the drilling amplitude as the quality of the wood improves.

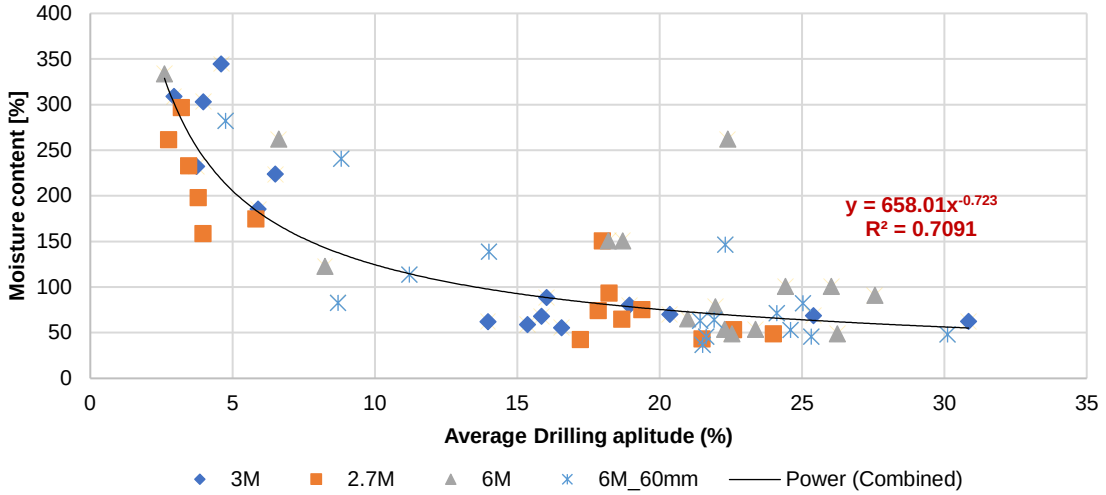

Figure 74 Figure 51 Combined piles from 1727 (3M, 2.7M & 6M). Moisture content (%) vs Average drilling amplitude (%).

6.2.2 Oven dry density vs Average drilling amplitude

The data analysis focused on examining the relationship between average drilling amplitude (x) and oven dry density (y) in old, degraded spruce specimens from 1727. A power trendline found in Figure 75 with equation, $y = 166.27x^{0.2901}$. The power function $x^{0.2901}$ was employed to model the observed data. To assess the strength of the relationship, a linear regression analysis was conducted, yielding an R^2 value of 0.817. The coefficient of determination, R^2, signifies the proportion of variance in oven dry density that can be explained by changes in average drilling amplitude. The obtained R^2 value of 0.817 indicates that approximately 81.7% of the variation in oven dry density can be attributed to variations in drilling amplitude. This analysis suggests a robust association between average drilling amplitude and oven dry density in the old, degraded spruce specimens. The power trendline equation, along with the high R^2 value, provides a potentially reliable mathematical model for understanding and predicting the relationship. Based on this model, it is possible to estimate the oven dry density of new tests by inputting additional drilling amplitude values into the power equation, $y = 166.27x^{0.2901}$.

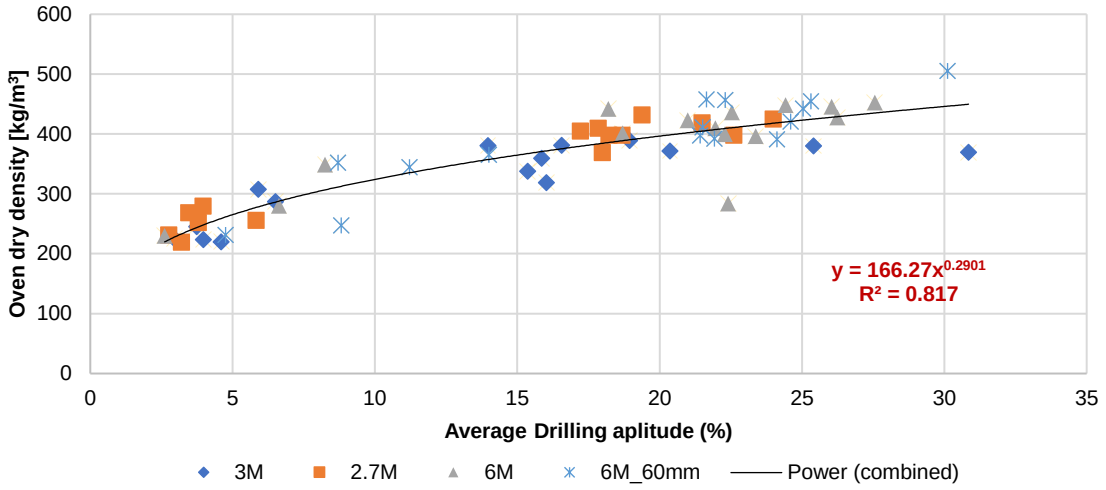

Figure 75 Combined piles from 1727 (3M, 2.7M & 6M). Oven dry density (%) vs Average drilling amplitude (%).

6.2.3 Wet compression strength vs Average drilling amplitude

The data analysis focused on investigating the relationship between average drilling amplitude (x) and wet compression strength parallel to the grain (y) in old, degraded spruce specimens from 1727. A linear trendline equation, $y = 0.4166x + 2.4282$, was derived to represent this relationship found in Figure 76. The equation indicates that for every unit increase in average drilling amplitude, the wet compression strength parallel to the grain is predicted to increase by 0.4166, with a baseline value of

2.4282. To assess the strength of the relationship, a linear regression analysis was conducted, resulting in an R^2 value of 0.78. The coefficient of determination, R^2, represents the proportion of variance in wet compression strength parallel to the grain that can be explained by changes in average drilling amplitude. In this case, an R^2 value of 0.78 indicates that approximately 78% of the variability in wet compression strength parallel to the grain can be attributed to variations in drilling amplitude. Based on this analysis, it can be inferred that there is a moderately strong association between average drilling amplitude and wet compression strength parallel to the grain in the old, degraded spruce specimens. The linear trendline equation, along with the relatively high R^2 value, provides a reliable mathematical model for understanding and predicting this relationship.

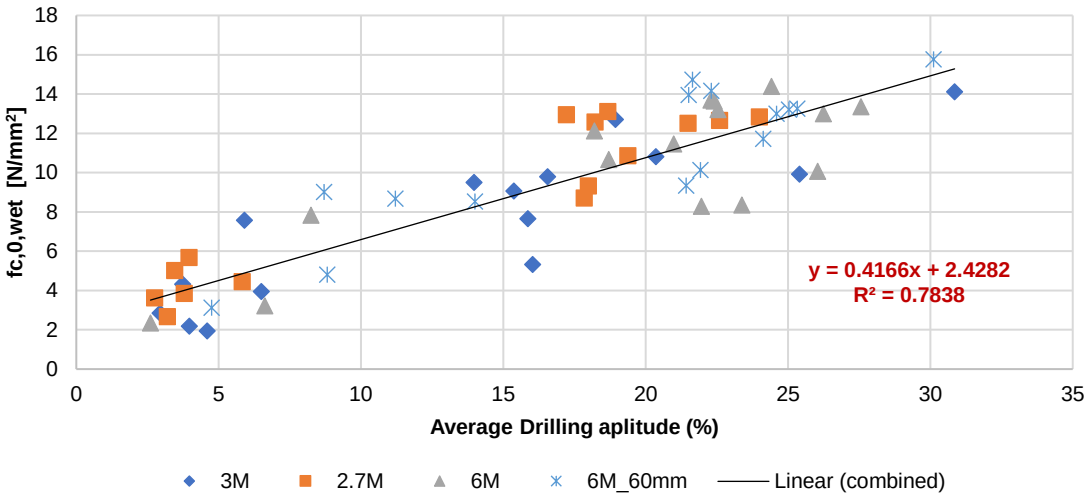

Figure 76 Combined piles from 1727 (3M, 2.7M & 6M). Compression strength parallel to the grain (N/mm2) vs Average drilling amplitude (%).

6.2.4 Modulus of elasticity vs Average drilling amplitude

The present data analysis focused on exploring the correlation between average drilling amplitude (x) and the modulus of elasticity (y) in old, degraded spruce specimens of dimensions 20mm20mm120mm, dating back to 1727 found in Figure 77. The investigation employed a linear trendline equation, y = 257.92x + 457.17, as a representation of this relationship. This equation implied that a unit increase in drilling amplitude was associated with a projected increase of 257.92 in the modulus of elasticity, with a baseline value of 457.17. The subsequent linear regression analysis yielded an R^2 value of 0.76, signifying that approximately 76% of the variability in the modulus of elasticity could be accounted for by fluctuations in drilling amplitude. These findings denote a moderate-to-strong connection between average drilling amplitude and the modulus of elasticity in the aged spruce specimens.

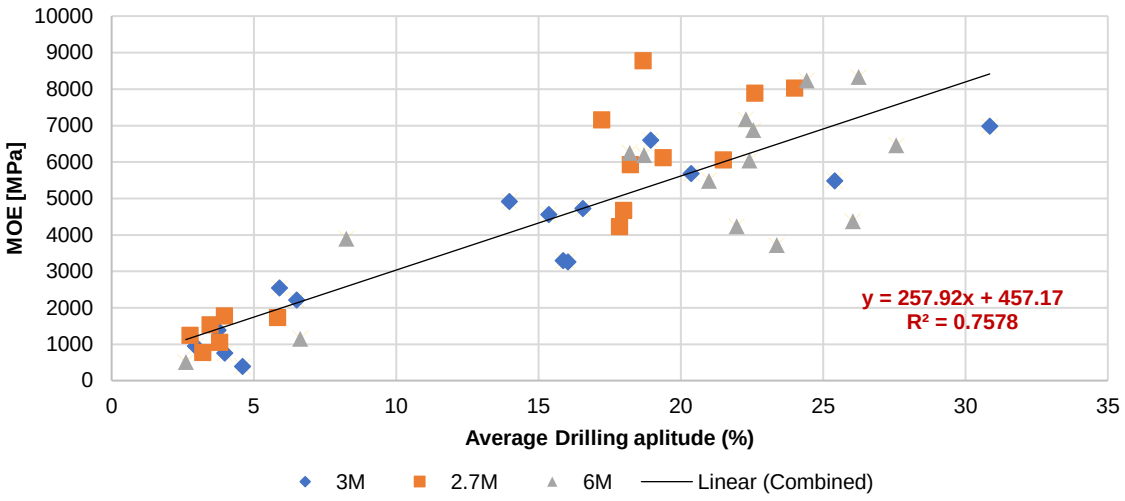

Figure 77 Combined piles from 1727 (3M, 2.7M & 6M). MOE (Mpa) vs Average drilling amplitude (%).

6.2.5 Degraded piles analysis conclusion

The moisture content, dry density, compression strength, and modulus of elasticity graphs exhibit coefficient of determinations (R^2 Values) exceeding 70% in linear regression analysis denoting a robust relationship. In each case, the drilling amplitude serves as the independent variable, while the physical or mechanical property under examination functions as the dependent variable. Consequently, these models facilitate the prediction of novel mechanical and physical properties for untested scenarios through the integration of supplementary drilling amplitude values into the equations. However, it is imperative to exercise caution, as the accuracy of such prediction's hinges on the assumption that the association between drilling amplitude and physical/mechanical properties remains consistent for new tests. Thus, it becomes crucial to validate the model further by comparing with actual measurements or conducting additional experiments to ensure its applicability and reliability in novel test scenarios Hence, the existing predictability constraints arise from the utilization of deteriorated spruce piles dating back to 1727, featuring an average softshell value of 39mm (6M-41mm, 3M-38mm, & 2.7M-39mm).

6.3 Non-Degraded piles (3.18M, 11M, and 10588M)

The purpose of creating the following graphs is to explore the potential relationship between the physical and mechanical properties of non-degraded spruce foundation piles and the corresponding average drilling amplitude. These piles represent three specific time periods: a 3.18M pile from 1886, an 11M pile from 1922, and a 10588M pile from 2019. Among these piles, the soft shell was only present in the 3.18M pile, with an average soft-shell measurement of 6.6mm along its length. By examining these graphs, the aim is to uncover any discernible patterns or trends that may exist between the physical and mechanical characteristics of the piles and the average drilling amplitude. This analysis will contribute to our understanding of the relationship between these variables and potentially provide insights into the behaviour and performance of non-degraded spruce foundation piles in different time periods.

6.3.1 Moisture content vs Average drilling amplitude

The analysis conducted on the non-degraded specimens revealed a power trendline equation of $y = 24.942x^{0.2966}$, where y represents the moisture content and x denotes the average drilling amplitude in Figure 78. The linear regression analysis yielded a coefficient of determination, R^2, of 0.025. Interpreting the results, the R^2 value of 0.0254 indicates a very weak relationship between the average drilling amplitude and moisture content. This suggests that only about 2.5% of the variability in the moisture content can be explained by the average drilling amplitude. Given this low R^2 value, it implies that the average drilling amplitude alone may not be a reliable predictor for determining moisture content in non-degraded specimens. Therefore, relying solely on additional drilling amplitude values to estimate moisture content may not yield accurate results, as the relationship between the two variables is weak.

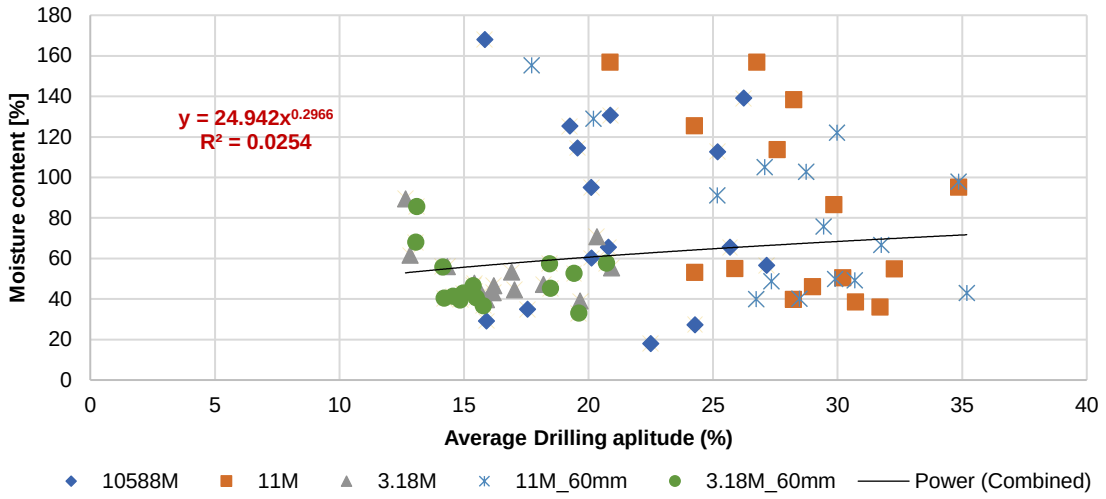

Figure 78 Figure 51 Combined piles (3.18M, 11M & 10588M). Moisture content (%) vs Average drilling amplitude (%).

6.3.2 Oven dry density vs Average drilling amplitude

The power trendline equation, $y = 165.1x^{0.3288}$, describes the relationship between the average drilling amplitude (x) and the oven dry density (y) of non-degraded spruce specimens in Figure 79. The linear regression analysis yielded an R^2 value of 0.446, which provides insight into the fit of the power model to the data. An R^2 value of 0.446 indicates that approximately 44.6% of the variation in the oven dry density can be explained by the average drilling amplitude using this power model. This suggests a moderate level of correlation between the two variables. However, it also suggests that there is a significant amount of unexplained variation in the relationship between drilling amplitude and dry density. It's important to acknowledge that natural variability introduces challenges in establishing reliable correlations. For instance, sound wood typically falls within a range of 350-550 kg/m³, making it harder to precisely link this range to drilling amplitude. This doesn't imply that the method is incapable of explaining the variation, but rather, it provides a general overview of the characteristics "on average" for the sound piles. This understanding should be considered when interpreting the results and when applying the model to new data sets.

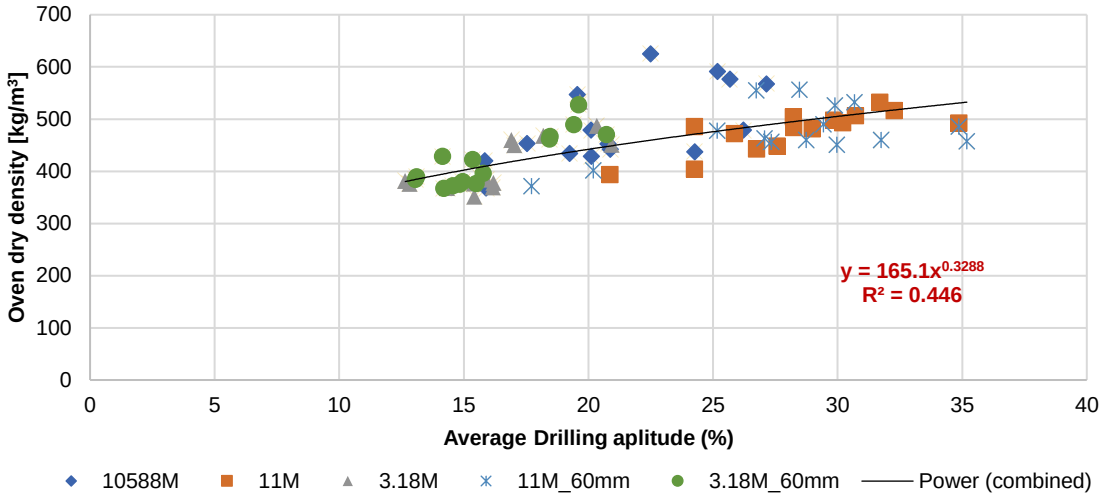

Figure 79 Combined piles (3.18M, 11M & 10588M). Oven dry density (%) vs Average drilling amplitude (%).

6.3.3 Wet compression strength vs Average drilling amplitude

The data analysis was focused on investigating the relationship between average drilling amplitude (x) and wet compression strength parallel to the grain (y) in non-degraded spruce specimens, measured in N/mm². A linear trendline equation in Figure 80, y = 0.3764x + 7.8576, was derived to represent this relationship. According to this equation, for every unit increase in average drilling amplitude, the wet compression strength parallel to the grain was predicted to increase by 0.3764 N/mm², with a baseline value of 7.8576 N/mm².In order to assess the strength of this relationship, a linear regression analysis was conducted, resulting in an R^2 value of 0.27. In this context, an R^2 value of 0.27 indicates that approximately 27% of the variability in wet compression strength parallel to the grain can be attributed to variations in drilling amplitude. However, it's important to recognize that natural variability introduces challenges in establishing reliable correlations. This range highlights the inherent variability in this property. Consequently, while the method provides an overview of the characteristics "on average" for sound spruce specimens, it may not fully capture the nuanced variations in wet compression strength due to other influencing factors. This understanding should be taken into account when interpreting the results and applying the model to new data sets.

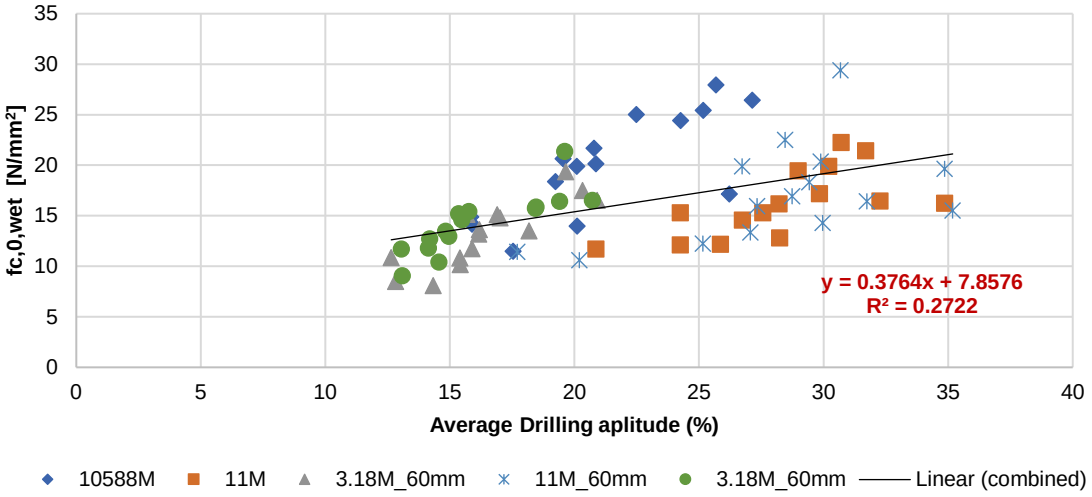

Figure 80 Combined piles (3.18M, 11M & 10588M). Compression strength parallel to the grain (N/mm2) vs Average drilling amplitude (%).

6.3.4 Modulus of elasticity vs Average drilling amplitude

The present data analysis focused on exploring the correlation between average drilling amplitude (x) and the modulus of elasticity (y) in non-degraded spruce specimens of dimensions 20mm20mm120mm. The resulting equation of the trendline is y = 420.62x - 613.36, and the coefficient of determination (R^2) for the linear regression analysis is 0.5796. The linear trendline equation suggests that there is a proportional association between the average drilling amplitude and the modulus of elasticity. As the drilling amplitude increases, the modulus of elasticity is expected to increase as well, given the positive slope coefficient of 420.62. Conversely, as the drilling amplitude decreases, the modulus of elasticity is expected to decrease, as indicated by the negative constant term of -613.36. The coefficient of determination (R^2) provides valuable insights into the goodness of fit of the model. In this case, an R^2 value of 0.5796 indicates that approximately 58% of the variance in the modulus of elasticity can be explained by variations in the average drilling amplitude. While this signifies a moderate level of correlation between the two variables, it also suggests that there is a substantial amount of unexplained variability in the modulus of elasticity, not accounted for by drilling amplitude alone.

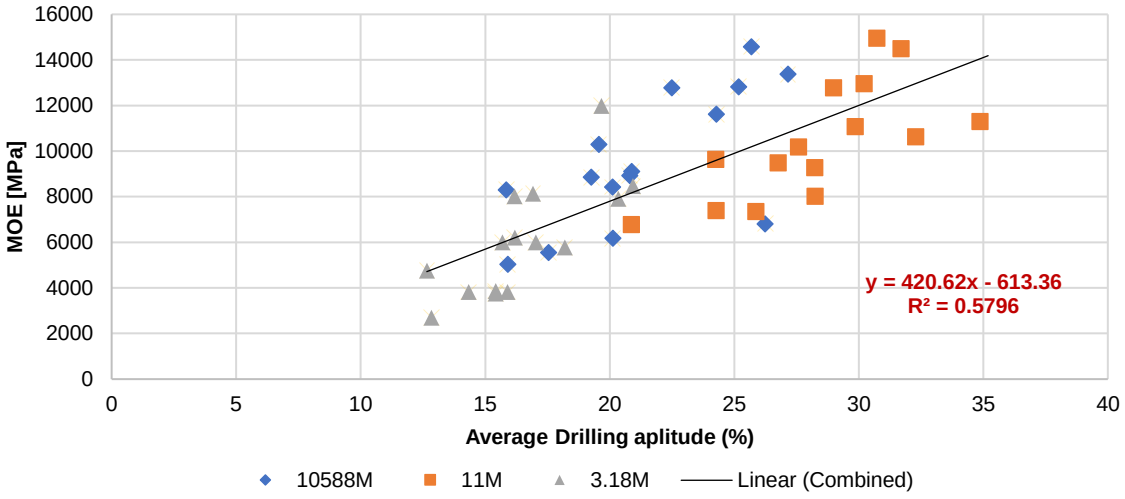

Figure 81 Combined piles (3.18M, 11M & 10588M). MOE (MPa) vs Average drilling amplitude (%).

6.3.5 Non-Degraded piles analysis conclusion

In conclusion, the linear regression analysis on the relationship between the average drilling amplitude and various properties of non-degraded spruce samples has provided valuable insights into the correlations between these variables. The coefficient of determination (R^2) values for moisture content, oven dry density, wet compression strength, and modulus of elasticity indicate varying degrees

of association. Moisture content shows a non-existent correlation $R^2 = 0.025$, while oven dry density has a weak $R^2 = 0.27$ correlation and wet compression strength exhibit moderate correlation $R^2 = 0.46$. Notably, the modulus of elasticity demonstrates the highest correlation ($R^2 = 0.5796$), suggesting that the model has relatively better predictive capabilities for this property however this model only includes the 20*20*120mm samples. While the R^2 value of 0.5796 for the modulus of elasticity indicates a moderate correlation with average drilling amplitude, it is important to interpret this result with caution. The model may be suitable for predicting the modulus of elasticity within the range of drilling amplitude values used in the analysis. However, the model's predictive accuracy might diminish when extrapolating to new drilling amplitude values, particularly at the extremes or outliers.

However, it's important to recognize that natural variability introduces challenges in establishing reliable correlations. This range highlights the inherent variability in this property. Consequently, while the method provides an overview of the characteristics "on average" for sound spruce specimens, it may not fully capture the nuanced variations in the physical and mechanical properties due to other influencing factors. This understanding should be considered when interpreting the results and applying the model to new data sets.

To improve the model's reliability and expand its applicability, additional data points encompassing a wider range of drilling amplitude values should be collected and incorporated into the analysis. In summary, the linear regression analysis highlights the relationships between average drilling amplitude and various properties of non-degraded spruce samples. It emphasizes the importance of understanding the varying degrees of correlation and the limitations of the model's predictive capabilities. To enhance the accuracy and robustness of the model for determining the modulus of elasticity in new tests based on additional drilling amplitude values, further data collection and model validation are essential. This iterative process will contribute to a more comprehensive understanding of the relationships between these variables and facilitate better predictions in practical applications.

6.4 Degraded and non-degraded piles (2.7M, 3M, 6M, 3.18M, 11M & 10588M)

The purpose of creating the following graphs is to explore the potential relationship between the physical and mechanical properties of combined degraded and non-degraded spruce foundation piles with the corresponding average drilling amplitude. These piles are the combined summation of all the tests that were conducted. By examining these graphs, the aim is to uncover any discernible patterns or trends that may exist between the physical and mechanical characteristics of the piles and the average drilling amplitude. This analysis will contribute to our understanding of the relationship between these variables and potentially provide insights into the behaviour and performance of degraded spruce foundation piles in different time periods.

6.4.1 Moisture content vs Average drilling amplitude

The power trendline plotted below in Figure 82 with equation $y = 473.83x^{-0.639}$, with x values representing the average drilling amplitude and y indicating the moisture content, suggests a strong relationship between these variables. The negative exponent of -0.639 which implies an inverse relationship, meaning that as the average drilling amplitude increases, the moisture content decreases. The linear regression analysis of the results for the old, degraded specimens yields a coefficient of determination R^2 value of 0.6. This represents the proportion of the variance in the dependent variable (moisture content) that can be explained by the independent variable (average drilling amplitude). In this case, an R^2 of 0.6 suggests that approximately 60% of the variability in moisture content can be attributed to changes in the average drilling amplitude for degraded samples. Based on this analysis, using additional drilling amplitude values to determine moisture content appears to be a valid approach. The power trendline equation provides a mathematical model that describes the relationship between drilling amplitude and moisture content. With a reasonably high R^2 value, it indicates that the model captures a significant portion of the moisture content variability. It is interesting to note as the MC falls below 100% the trendline starts to become linear, this signifies that the MC is less dependent on the drilling amplitude as the quality of the wood improves.

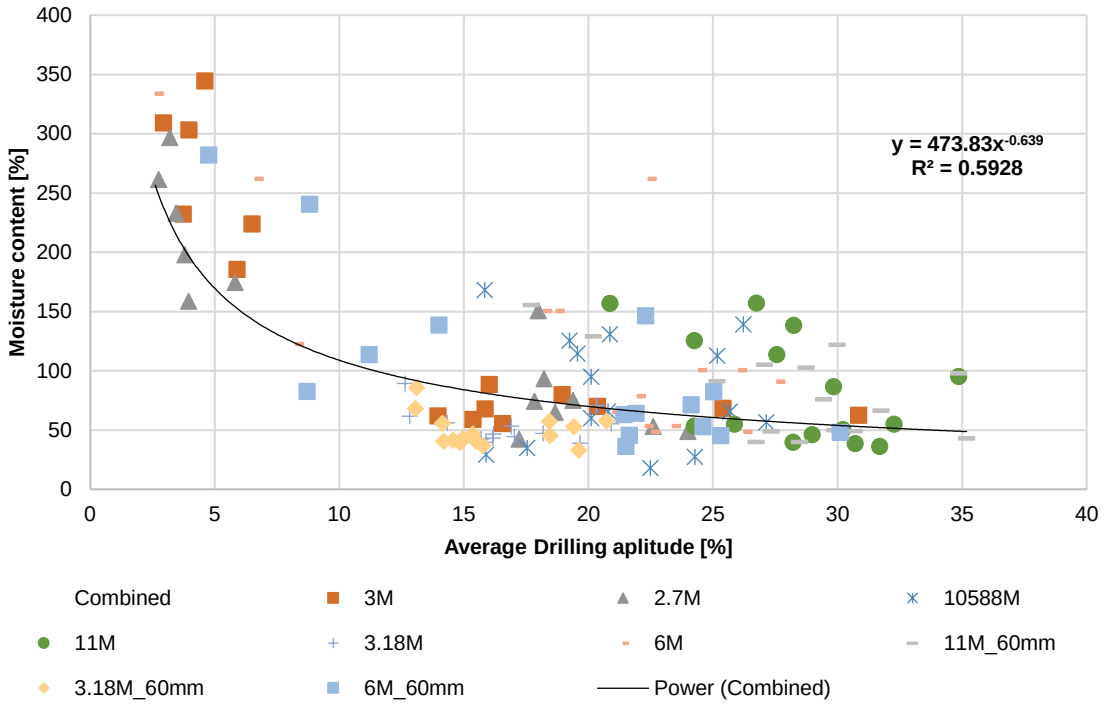

Figure 82 Combined piles (2.7M, 3M, 6M, 3.18M, 11M & 10588M). Moisture content (%) vs Average drilling amplitude (%).

6.4.2 Oven dry density vs Average drilling amplitude

The data analysis focused on examining the relationship between average drilling amplitude (x) and oven dry density (y). A power trendline found in Figure 83 was derived with the equation $y = 156.48x^{0.3331}$. This power function was employed to model the observed data. To assess the strength of the relationship, a linear regression analysis was conducted, resulting in an R^2 value of 0.6936. The coefficient of determination, R^2, signifies the proportion of variance in oven dry density that can be explained by changes in average drilling amplitude. The obtained R^2 value of 0.6936 indicates that approximately 69.36% of the variation in oven dry density can be attributed to variations in drilling amplitude. This analysis suggests a robust association between average drilling amplitude and oven dry density in the spruce specimens. The power trendline equation, along with the high R^2 value, provides a potentially reliable mathematical model for understanding and predicting the relationship. Based on this model, it is possible to estimate the oven dry density of new tests by inputting additional drilling amplitude values into the power equation, $y = 156.48x^{0.3331}$.

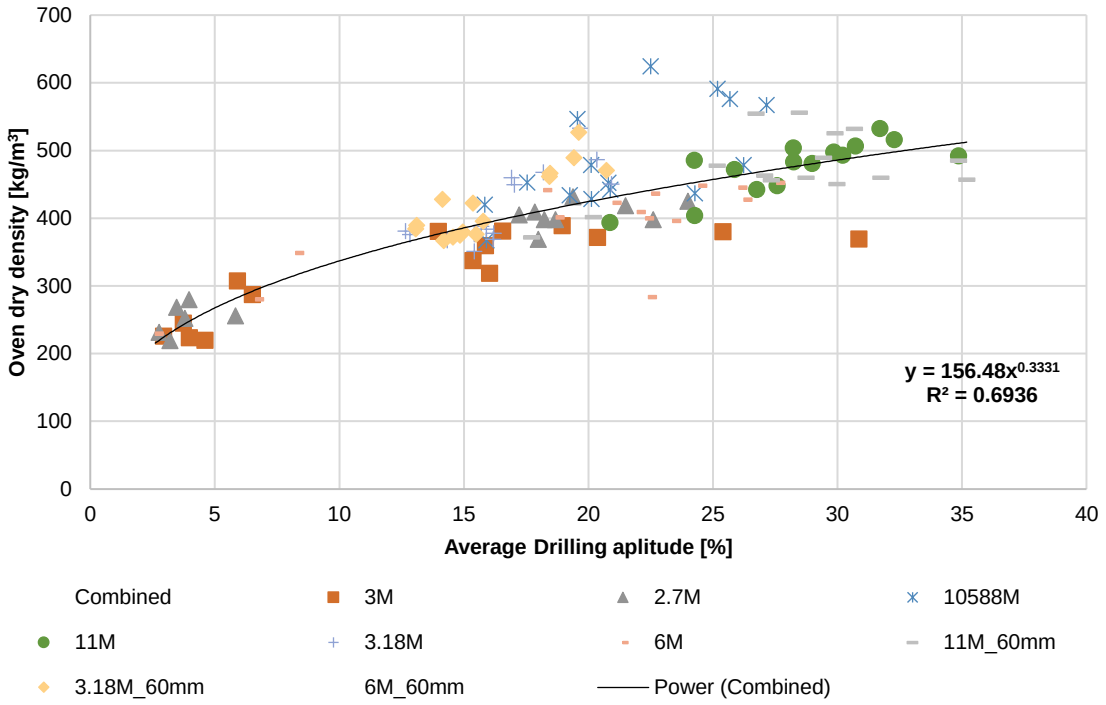

Figure 83 Combined piles (2.7M, 3M, 6M, 3.18M, 11M & 10588M). Oven dry density (%) vs Average drilling amplitude (%).

6.4.3 Wet compression strength vs Average drilling amplitude

The data analysis focused on investigating the relationship between average drilling amplitude (x) and wet compression strength parallel to the grain (y) in the combined spruce specimens. A linear trendline equation, y = 0.5096x +3.1937, was derived (Figure 84) to represent this relationship. The equation indicates that for every unit increase in average drilling amplitude, the wet compression strength parallel to the grain is predicted to increase by 0.5096, with a baseline value of3.1937. To assess the strength of the relationship, a linear regression analysis was conducted, resulting in an R^2 value of 0.53. The coefficient of determination, R^2, represents the proportion of variance in wet compression strength parallel to the grain that can be explained by changes in average drilling amplitude. In this case, an R^2 value of 0.53 indicates that approximately 23% of the variability in wet compression strength parallel to the grain can be attributed to variations in drilling amplitude. Based on this analysis, it can be inferred that there is a moderate association between average drilling amplitude and wet compression strength parallel to the grain in the spruce specimens. The linear trendline equation, along with the relatively moderate R^2 value, provides a reliable mathematical model for understanding and predicting this relationship.

It's worth highlighting the significance of observing that beyond a drilling amplitude threshold of 15%, a discernible trend emerges wherein the dispersion of data points becomes more pronounced. This phenomenon is particularly evident when examining the subset of samples that belong to a relatively younger cohort. The trend of increased dispersion aligns well with expectations, given the distinct statistical patterns present in the analysis of the more recently collected sample set as they have a diminished linear regression coefficient (R^2 =0.27) in comparison to their counterparts from 1727 (R^2 = 0.78) .

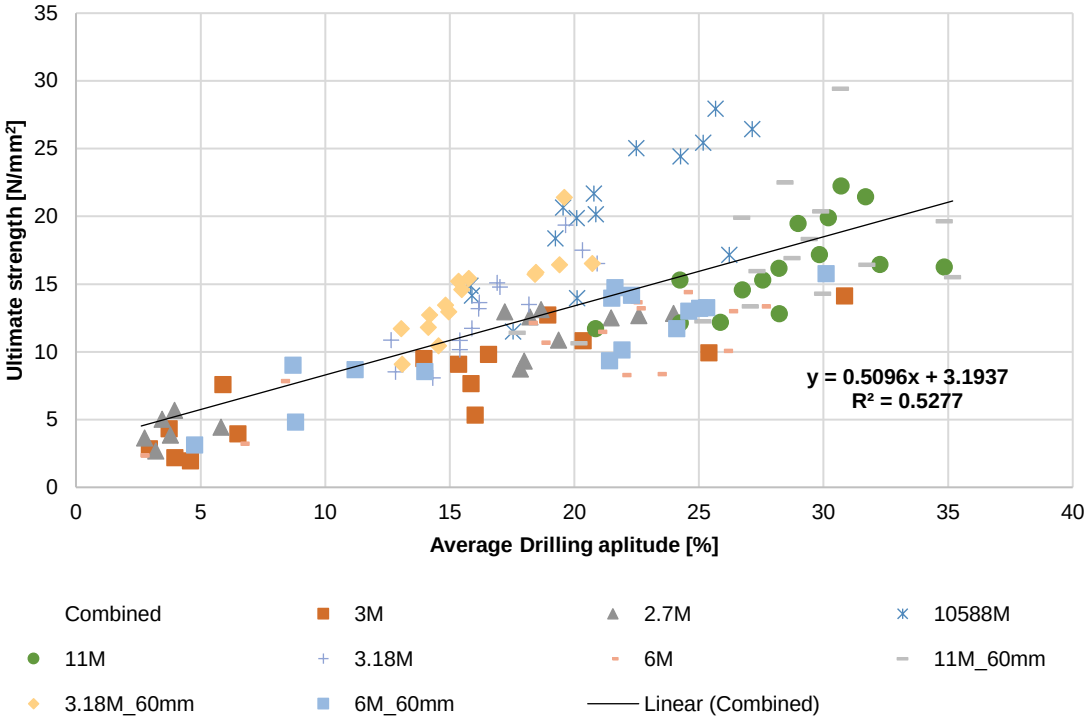

Figure 84 Combined piles (2.7M, 3M, 6M, 3.18M, 11M & 10588M).Compression strength parallel to the grain (N/mm²) vs Average drilling amplitude (%).

6.4.4 Modulus of elasticity vs Average drilling amplitude

The present data analysis focused on exploring the correlation between average drilling amplitude (x) and the modulus of elasticity (y) in old, degraded spruce specimens of dimensions 20mm20mm120mm, dating back to 1727. The investigation employed a linear trendline in Figure 85 equation, y = 367.72x - 340.52, as a representation of this relationship. Employing a linear equation, y = 367.72x - 340.52, as a representation of this relationship, the subsequent linear regression analysis yielded an R^2 coefficient of determination valued at 0.67. This R^2 value indicates that approximately 67% of the variability witnessed in the modulus of elasticity can be attributed to fluctuations in drilling depth. In other words, changes in drilling depth account for a substantial portion of the observed differences in the stiffness characteristics of the studied aged spruce samples.

Notably, there's an important observation: when the drilling amplitude exceeds 15%, a clear trend emerges—the data points spread out more noticeably. This effect is especially visible in the younger sample group. This trend of increased spread aligns with what was expected based on the specific statistical patterns found in the recent sample analysis. Importantly, these newer samples have a weaker linear regression coefficient (R^2 = 0.58), unlike the samples from 1727, which had a higher coefficient (R^2 = 0.76). The lower R^2 value for the newer samples indicates that the drilling amplitude explains a smaller proportion of the variance in modulus of elasticity compared to the older samples. This comparison indicates a potential shift or change in the nature of the relationship over time, which has statistical implications for understanding the underlying dynamics.

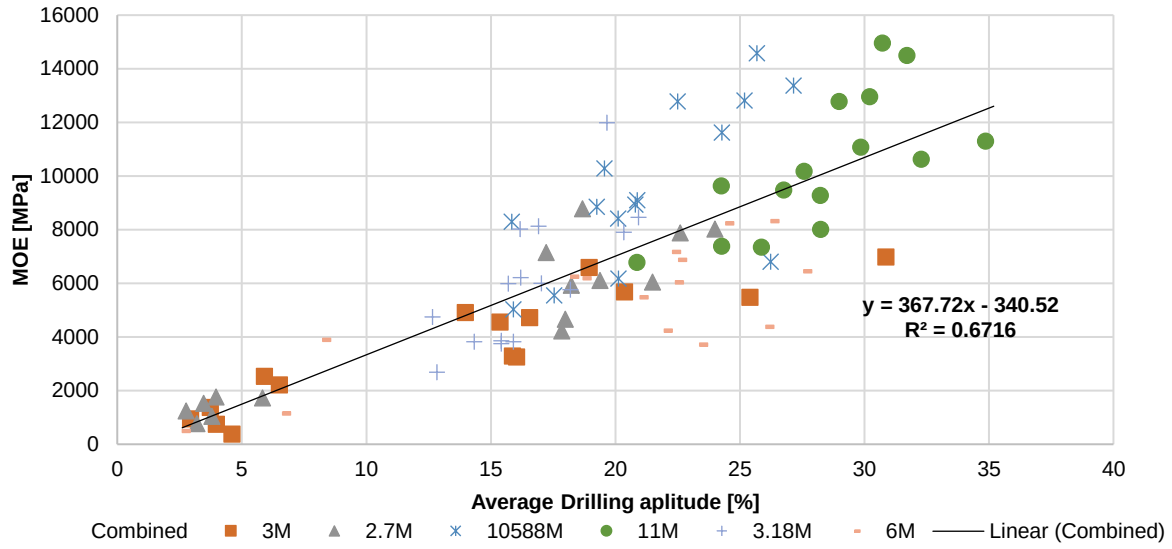

Figure 85 Combined piles (2.7M, 3M, 6M, 3.18M, 11M & 10588M).MOE (MPa) vs Average drilling amplitude (%).

6.4.5 Degraded piles analysis conclusion

The moisture content, dry density, compression strength, and modulus of elasticity graphs exhibit coefficient of determinations (R^2 Values) exceeding 53% in linear regression analysis denoting a robust relationship. In each case, the drilling amplitude serves as the independent variable, while the physical or mechanical property under examination functions as the dependent variable. Consequently, these models facilitate the prediction of novel mechanical and physical properties for untested scenarios through the integration of supplementary drilling amplitude values into the equations. However, it is imperative to exercise caution, as the accuracy of such prediction's hinges on the assumption that the association between drilling amplitude and physical/mechanical properties remains consistent for new tests. Thus, it becomes crucial to validate the model further by comparing with actual measurements or conducting additional experiments to ensure its applicability and reliability in novel test scenarios Hence, the existing predictability constraints arise from the utilization of degraded and non-degraded spruce piles dating back to 1727.

6.5 Predictive model for 60mm samples MOE results.

In this study, a prediction model for the modulus of elasticity (MOE) of wood samples was developed based on the results obtained from 120mm wood samples. The model utilizes linear regression analysis, with wet compression strength perpendicular to the grain (x-axis) and the modulus of elasticity (y-axis).The linear regression analysis yielded an R-squared (R^2) value of 88%. The equation of the regression line was determined to be y = 572.74x - 714.58, where y represents the predicted MOE and x represents the compression strength. The high R^2 value indicates that the regression line provides a good fit to the data, explaining 88% of the variability in the MOE based on the compression strength.

Using this prediction model, the MOE of smaller 60mm wood samples can be estimated based on their compression test values. It is worth noting that there was 6.8% difference observed for the compression strength between the 60mm and 120mm samples, allowing for the assumption that they can be equated given the natural with variations in composition and material properties. However, it is crucial to acknowledge that MOE was not directly tested in the 60mm samples due to limitations in attaching LVDTs (Linear Variable Differential Transformers) for strain measurements. By applying the regression equation derived from the 120mm samples to the compression test values of the 60mm samples, the model enables the prediction of the MOE for the smaller wood samples. This prediction approach proves valuable in situations where direct measurement of MOE in the 60mm samples is not feasible, providing an alternative means to estimate their elastic properties based on their compression strength values.

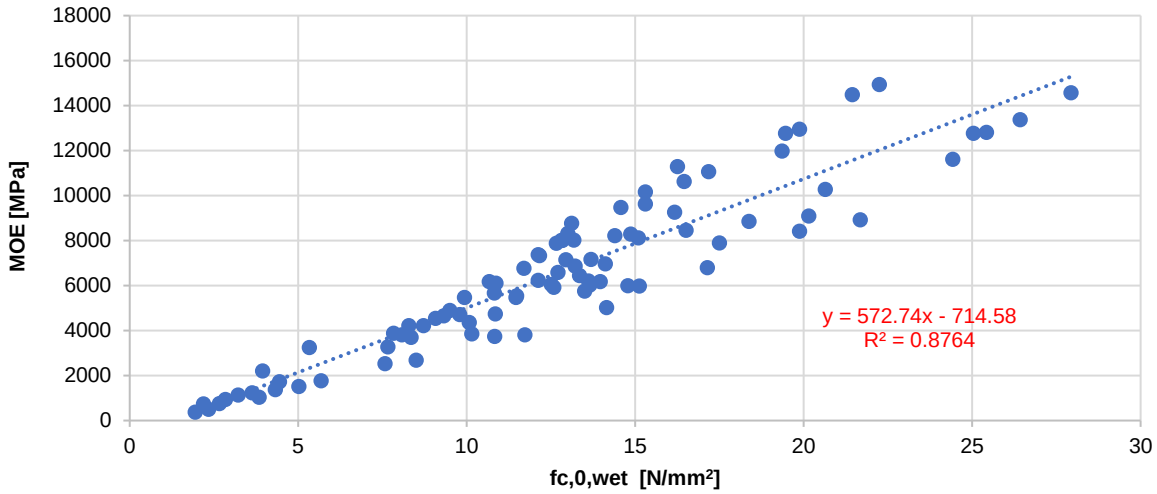

Figure 86 MOE vs Compressive strength parallel to the grain.

6.6 Predictive model for degraded sections.

In the course of conducting experiments on segments of severely degraded spruce, it became evident that the external visual degradation did not explicitly correspond to a significant reduction in structural integrity. Despite their visibly compromised state, these sections exhibited a noteworthy amount of residual strength. Using linear regression analysis provided more clarity on the noticeable differences between the degraded sections and the newer ones. Interestingly, the severely degraded sections showed a much higher coefficient of determination (R^2=0.81) compared to the newer sections. This statistical finding emphasizes that the linear regression method effectively helps reveal the prediction capabilities of the strength based on the drilling amplitude of the degraded sections with a higher degree of accuracy.

Given the stronger correlation within the severely degraded segments prompted the investigation's focus toward the drilling amplitude of the softshell. The subsequent analysis unveils a compelling discovery: the utilization of drilling amplitude as a predictive parameter yields improved prognostications of strength attributes for degrade piles as opposed to non-degraded. This inference is tangibly substantiated through graphical representation, depicted below, which portrays the outcomes derived from drilling amplitudes measuring less than 15%. The empirical data exhibited within this graphical representation succinctly corroborates the assertion of enhanced predictive capability associated with lower drilling amplitudes.

In summary, the experimental findings, coupled with the linear regression analysis, reveal the latent strength within severely degraded spruce sections. The elevation in the R^2 value within these degraded sections highlights the potential for robust predictive modelling. Furthermore, the empirical utilization of drilling amplitude, particularly within the confines of a 15% threshold, serves as an effective tool for advancing the precision and reliability of strength predictions for softshell sections.

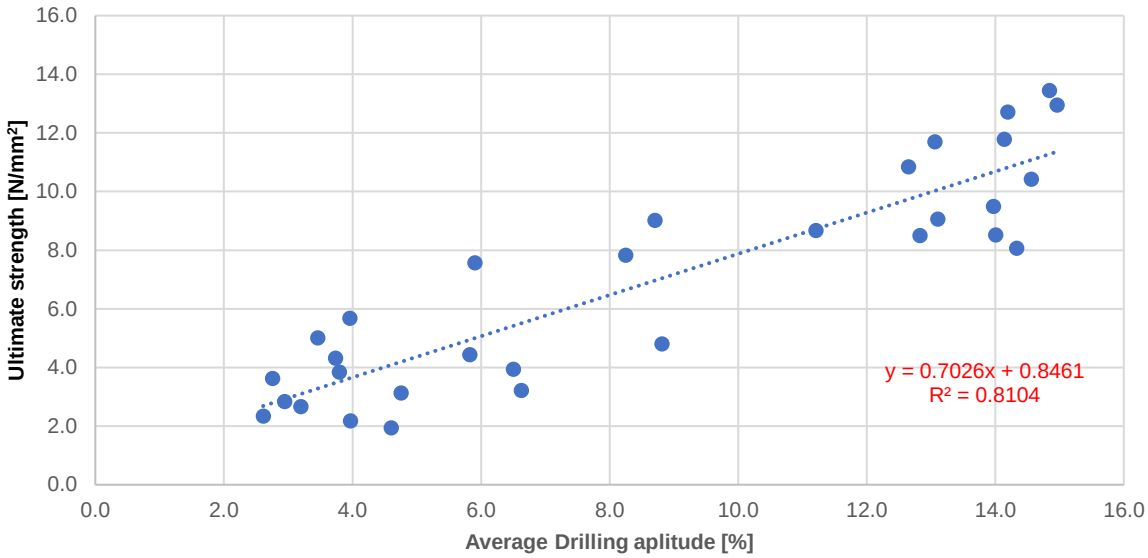

Figure 87 Compressive strength parallel to the grain vs Drilling amplitude for degraded sections

7

Conclusions and outlook

7.1 Main outcomes and concluding remarks.

The review of existing literature in Chapter 2 embarked upon an exploration of various aspects of novelty and addressed gaps in knowledge that have been identified. Through this review, it became evident that the field of research focused on degraded wooden foundation piles is considerably underrepresented, thus highlighting a significant gap in the current body of knowledge. As a direct consequence, the effectiveness and precision of the prevailing techniques employed currently to assess the remaining bearing strength of foundational piles have been brought into question. The recognition of this discrepancy served as a pivotal stimulus for the initiation of the ongoing research endeavour. Practically speaking, the adoption of the RPD drilling technique carries pragmatic advantages worthy of consideration. This particular method has gathered favour among both engineers and on-site operators due to its intrinsic ability to minimize the extent of foundation excavation. Consequently, the operational impact on existing structures is notably diminished, thus rendering the micro-drilling approach a notably less intrusive option. This inherent attribute significantly elevates its utility and desirability within real-world scenarios.

An essential component of this research involves the in-depth analysis of the physical and mechanical attributes intrinsic to Spruce. This understanding is achieved through a comprehensive assessment of the cross-sectional composition of the piles. Notably, Spruce's properties exhibit noticeable variations contingent on its specific location within the pile, particularly with regard to its distance from the core. This intricate spatial relationship prompted the initiation of an extensive and meticulous testing campaign. This endeavour was characterized by a deliberate and systematic refinement of the underlying methodology, a process guided by insights garnered from preliminary experimental phases. This methodological evolution plays a critical role in ensuring the robustness and reliability of the final approach, thus facilitating comprehensive and insightful characterizations of Spruce's distinctive properties. The foundational work laid through this methodological advancement holds pivotal significance, serving as the cornerstone upon which subsequent in-depth investigations should be constructed.

The main outcome of this thesis is to answer the following question.

“How do the variations of mechanical and physical attributes manifest across the cross-sectional profile of both degraded and non-degraded spruce foundation piles and how can micro-drilling techniques be utilized to assess these characteristics?“

7.1.1 Degraded samples

The findings and subsequent examination revealed a distinct and consistent pattern across the various test specimens 3M, 2.7M & 6M. Specifically, the specimens situated at the peripheries (average specimen 1 & 5 result and SD) of the cross-sectional area exhibited an average elevated level of moisture content (233 ± 61 %), coupled with reduced dry density (278 ± 46 kg/m^3) , consequently yielding diminished strength (5 ± 3 kN/m^2) and MOE (2239 ± 1398 Mpa) within the softshell domain. Notably, the observed standard deviation displayed considerable dispersion in the outcomes. Conversely, the internal central sections (average specimen 2,3 &4 result and SD) of the specimens exhibited a diminished moisture content (70 ± 19 %), along with an augmented dry density (399 ± 13 kg/m^3), as well as heightened compressive strength (11 ± 2 kN/m^2) and MOE (5894 ± 1382 Mpa) characteristics Moreover, the standard deviation associated with the internal sections exhibited a

notable degree of uniformity, reflecting both meticulous experimental conduct and consistent structural integrity within the internal regions. The external regions therefore had average 332% moisture content, 70% dry density 49% strength and 38% MOE.

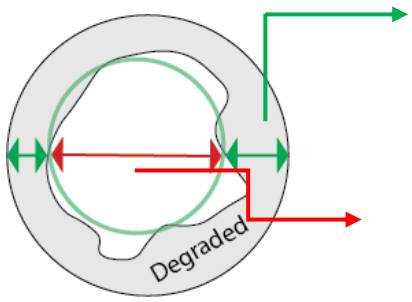

Peripheries (average specimen 1 & 5):

MC:	233 ± 61%	fc,0,wet :	5 ± 3 kN/m^2
Dry density:	278 ± 46 kg/m^3	MOE:	2239 ± 1398 Mpa

Internal central sections (average specimen 2,3 &4):

MC:	70 ± 19%	fc,0,wet :	11 ± 2 kN/m^2
Dry density:	399 ± 13 kg/m^3	MOE:	5894 ± 1382 Mpa

Figure 88 Average Physical and mechanical properties of degraded piles from 1727

7.1.2 Non-degraded samples

The investigation and subsequent analysis of 3.18M, 11M & 10588M from 1886, 1922 & 2019 respectively have unveiled a distinctive and consistent pattern across the piles with a marginal deviation observed in 3.18M. To be specific, the specimens located at the outer edges (average specimens 1 & 5 result and SD) of the 11M & 10588M cross-sectional area exhibited a moisture content (132 ± 22 %), dry density (472 ± 46 kg/m^3), compressive strength (17 ± 2.8 kN/m^2) and MOE (9296.7 ± 1919 Mpa). As a result, there was a slight decrease in both strength and stiffness in these external regions compared to internal regions. The internal sections (average specimens 2 & 4 result and SD) exhibited a moisture content (54 ± 23.4 %), dry density (513.5 ± 48.1 kg/m^3), as well as heightened compressive strength (21.8 ± 2.9 kN/m^2) and MOE (12216.5 ± 2342 Mpa). Remarkably, the samples extracted from the pith (known as sample 3) within the juvenile regions have consistently yielded the lowest values for moisture content (45 ± 12.4%), dry density (438 ± 47.6 kg/m^3), as well as a compressive strength (13 ± 1.9 kN/m^2) and MOE (6795 ± 838.85 Mpa).

Intriguingly, specimen 3.18M has demonstrated a consistent average moisture content for all 5 samples (52 ± 11.8 %). Furthermore, the external regions (average specimens 1 & 5 result and SD) demonstrated the most elevated levels of dry density (474.5 ± 19.8 kg/m^3), as well as heightened compressive strength (16 ± 2 kN/m^2) and MOE (8042.5 ± 2247.7 Mpa). These values are comparable to what was found in samples 1&5 for 11M & 10588M. However, these were the highest mechanical and physical characteristics found in 3.18M with samples 2,3 and 4 having lower results to sample 3 of 11M & 10588M. Dry density (374.3 ± 10.9 kg/m^3), as well as a compressive strength (11.3 ± 1.1 kN/m^2) and MOE (4768.3 ± 760.1 Mpa).

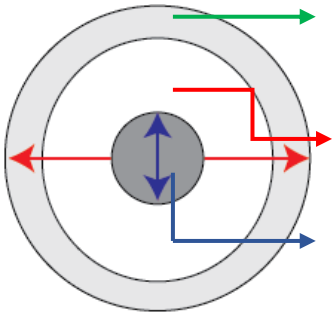

Peripheries (average specimen 1 & 5):

MC:	132 ± 22%	fc,0,wet :	17 ± 3 kN/m^2
Dry density:	472 ± 46 kg/m^3	MOE:	9297 ± 1919 Mpa

Internal central sections (average specimen 2 & 4):

MC:	54 ± 23%	fc,0,wet :	22 ± 3 kN/m^2
Dry density:	514 ± 48 kg/m^3	MOE:	12217 ± 2342 Mpa

Pith/juvenile wood (3):

MC:	45 ± 12%	fc,0,wet :	13 ± 2 kN/m^2
Dry density:	438 ± 48 kg/m^3	MOE:	6795 ± 839 Mpa

Figure 87 Average Physical and mechanical properties of non-degraded piles 11M &10588M

7.1.3 Micro-drilling techniques

The micro-drilling signal was studied in relation to physical and mechanical properties such as the MC, dry density, Compression strength & MOE. In each case, the drilling amplitude serves as the independent variable, while the physical or mechanical property under examination functions as the dependent variable. The conclusion for the degraded, non-degraded and combined samples are as follows; The degraded specimens 3M, 2.7M & 6M contained an average softshell of 38mm, 39mm & 41mm respectively. The linear regression analysis was performed and determined a highly statistically significant result of 70% for MC, 81% for dry density, 78% for compressive strength & 76% for MOE. Notably, a refined examination focused exclusively on compressive strength and a drilling amplitude less than 15% within the softshell layer resulted in an augmented R2 value of 0.81.

The non-degraded specimens 3.18M, 11M & 10588M only contained an average 6.6mm softshell in 3.18M. The linear regression analysis was performed and determined a less statistically significant result of 2.5% for MC, 46% for dry density, 27% for compressive strength & 58% for MOE. Despite the diminished robustness of the outcomes, they furnish valuable insights into the characteristics of non-degraded wood. The results demonstrated a notable degree of dispersion, which can plausibly be ascribed to an array of additional mechanical factors or biological accumulations that fall beyond the scope of this thesis. A final graphical analysis was conducted on all 6 of the piles together. The linear regression analysis was performed and determined a statistically significant result of 59% for MC, 69% for dry density, 53% for compressive strength & 67% for MOE. Consequently, these models facilitate the prediction of novel mechanical and physical properties for untested scenarios through the integration of supplementary drilling amplitude values into the equations.

7.1.4 Formulas

Degraded
Mc = $658.01x^{-0.723}$. (R^2=70%)
Dry density = $166.27x^{0.2901}$ (R^2=82%)
Compression strength = 0.4166x +2.4282. (R^2=78%)
MOE = 257.92x + 457.17. (R^2=76%)

Non-Degraded
Mc = $24.942x^{0.2966}$, (R^2=2.5%)
Dry density = $165.1x^{0.3288}$ (R^2=45%)
Wet compression strength = 0.3764x +7.8576, (R^2=27%)
MOE = 420.62x - 613.36, (R^2=58%)

Combined
MC = $473.83x^{-0.639}$ (R^2=59%)
Dry density = $156.48x^{0.3331}$ (R^2=69%)
Wet compression = 0.5096x +3.1937. (R^2=53%)
MOE = 367.72x - 340.52. (R^2=67%)

7.2 Future implications and recommendations

The RPD drill is an incredibly useful and practical tool which minimises foundation excavation and sample extraction which significantly reduces costs and saves time. The drill provides a drilling amplitude and resistant graph which the average value can be substituted into the determined equations which will be able to predict the MC, Dry density, compressive strength, and MOE. However, it is imperative to exercise caution, as the accuracy of such prediction's hinges on the assumption that the association between drilling amplitude and physical/mechanical properties remains consistent for new tests. Thus, it becomes crucial to validate the model further by comparing with actual measurements or conducting additional experiments to ensure its applicability and reliability in novel test scenarios Hence, the existing predictability constraints arise from the utilization of degraded and non-degraded spruce piles dating back to 1727. It is clear that the predictive possibilities will be more accurate for dry density as in each situation it has the highest linear regression.

The formulas provided give the foundational framework for a prospective predictive model, capable of ascertaining mechanical and physical attributes exclusively through the analysis of drilling amplitude. It is imperative that a rigorous validation process be undertaken to enhance its precision and establish robust correlations. This validation should encompass an investigation into additional biological and mechanical characteristics not addressed within the scope of this thesis. In Annex 8, an investigation has been outlined to scrutinize the ratio correlation between theoretical outcomes derived from formulas obtained through linear regression analysis and the results obtained from full-scale pile testing. Furthermore, an outlined approach for the determination of residual compressive strength predicated upon elementary geometric principles and stiffness ratios has been incorporated within Annex A9. This framework holds potential for refinement, thereby enabling subsequent applications in the computation and estimation of residual bearing capacity.

The softshell is currently not used in the analysis of the remaining bearing strength of the pile as its mechanical abilities were deemed neglectable, however with the analyses of the softshell data It has been determined that strength still resides in these highly degraded zones and therefore a more detailed bearing capacity can be determined which could be the determining factor of a foundation replacement. This remaining strength can be predicted based on the compression tests conducted in this thesis by using the formulas highlighted in section 6.7. This will need to be verified and additional experiments will need to be conducted to verify.

The present thesis exclusively examined specimens of clear wood, thus excluding the inclusion of samples featuring knots. Consequently, it is imperative to conduct a subsequent analysis encompassing cross sections that incorporate knots, with a view to discerning their influence on the residual bearing capacity of the wooden piles. This extension of the study is fundamental in achieving a comprehensive understanding of the structural performance implications posed by the presence of these imperfections. The inclusion of knots in wood induces a mechanical disparity characterized by abrupt changes in grain direction and density. This phenomenon, known as stress concentration, manifests as localized areas experiencing heightened levels of stress when subjected to external loads. This mechanical effect holds particular significance in structural engineering, as it disrupts the uniform distribution of stresses within the material, potentially rendering the wood more prone to failure in these specific regions. Therefore, a thorough comprehension of stress concentrations attributable to knots is essential for the precise assessment and design of the remaining strength of foundation piles.

7.3 Research sub-question(s) and answers

The following sub-questions will be answered in a way to help support the concluding remarks.

1. What research has already been conducted in a comparable project and what data is currently available?

Upon thorough examination of the literature review, it becomes evident that methodologies have been developed to ascertain moisture content, density, compression strength, and modulus of elasticity for foundation piles in a predominantly non-destructive manner. However, the potential for employing destructive testing on variously deteriorated piles presents an opportunity to glean deeper insights into their overall residual strength. The methods and information gleaned from the aforementioned literature offer a solid foundation for devising a methodological framework essential for the impending testing campaign. To comprehensively discern the mechanical and physical attributes across the cross-section of spruce foundation piles of varying ages, a meticulously designed testing protocol will be implemented. This protocol aims to furnish outcomes pertaining to moisture content, density, compression strength, and modulus of elasticity. These outcomes will subsequently be correlated with the drilling amplitude data acquired from the (RPD) drill. The successful alignment of drilling amplitude data with the physical and mechanical characteristics would hold significant practical implications, potentially enabling the prediction of additional properties such as strength and stiffness through a straightforward micro-drilling measurement. It is noteworthy that limited research has been conducted concerning the cross-sectional and longitudinal characteristics of aged piles, thus underscoring the impetus for the proposed research to bridge this gap in the current body of knowledge.

2. What impact does an elevated moisture content have on timber and how can this be related to timber piles?

Elevated moisture content has a multifaceted impact on timber, which is an important phenomenon, particularly in the field of timber piles. the elevated moisture levels significantly impact key mechanical properties: strength, density, and stiffness. The increased moisture content tends to reduce the mechanical strength of the timber. This can lead to a diminished load-bearing capacity, which is crucial for timber piles to effectively support vertical loads and withstand lateral forces. Moreover, moisture-induced swelling and shrinking can result in changes to the density of the timber. These fluctuations in density may subsequently affect the overall stability and load-bearing capabilities of the piles. Furthermore, the elevated moisture content in underwater environments can lead to a reduction in the stiffness of the timber. This decrease in stiffness makes the material less resistant to bending and deformation, qualities that are vital for maintaining shape and stability, particularly in load-bearing applications like timber piles.

From literature and subsequent analysis, it is clear how MC impacts different parts of the wood. Sapwood, the outer living portion of a tree's trunk, is more susceptible to having a higher moisture content in submerged foundation piles due to its physiological role in the tree's water transport system. In a living tree, sapwood is responsible for conducting water and nutrients from the roots to the leaves. This process, known as transpiration, relies on a continuous flow of moisture through the sapwood. When a tree is harvested and processed into timber for construction purposes, the sapwood remains more permeable and hygroscopic compared to the inner heartwood, which is denser and less porous. This means that sapwood has a greater capacity to absorb and retain moisture from its surroundings. Sapwood in submerged foundation piles readily absorbs and retains moisture due to continuous exposure to water and capillary action through its pores. The consistently high moisture levels in submerged environments further enhances this absorption. This natural property highlights the significance of choosing suitable wood species when constructing timber piles for submerged applications.

3. What are the levels and types of degradation, how can it be quantified? (Literature review)

In wooden foundation piles, degradation can be prompted by an array of factors, spanning biological, chemical, and environmental influences. This degradation encompasses distinct categories and levels of effect, which can be delineated as follows, with their quantification necessitating specific methodologies:

Types of Degradation in Wooden Foundation Piles:

Biological Degradation: Fungal Decay: Wood-rotting fungi can engender softening and disintegration of the wood's cellular structure. Insect Infestation: Termites and wood borers can tunnel within the wood, resulting in compromised structural integrity. Chemical Weathering: Exposure to acids, alkalis, pollutants, or substances in the soil and water can lead to chemical transformations within the wood's composition.
Environmental Degradation: Moisture Content: Cycles of wetting and drying contribute to swelling, warping, and dimensional changes, impacting pile strength and stability.

Quantification of Degradation in Wooden Foundation Piles:
Visual Inspection: Assessing changes in appearance, surface condition, and presence of cracks, splits, or boreholes caused by insects. Drilling Resistance Measurement: Determining the ease of drilling into the wood can provide insights into changes in density and strength. Moisture Content Measurement: Quantifying the moisture content of wood using moisture meters can indicate the level of exposure to moisture, influencing degradation. Microscopic Analysis: Microscopic examination of wood samples can reveal the extent of fungal decay, insect tunnels, and changes in cell structure. Mechanical Testing: Performing compression and bending tests on degraded and non-degraded wood samples can quantify changes in strength and stiffness.

4. What type of experiments need to be conducted? What is possible and available for testing in the required time frame? How many experiments need to be done? What type of data needs to be collected and what is the procedure? (Research methodologies)

The study encompasses a thorough experimental investigation aimed at gaining a comprehensive understanding of the physical and mechanical attributes of wooden piles. This entails evaluating degradation, moisture content, density, modulus of elasticity, and compressive strength. Due to time constraints, a focused approach is imperative to yield meaningful insights. The research methodology is divided into two phases: preparation and execution.

Preparation Phase:
The initial phase involves dividing 12-meter wooden piles into 4-meter segments, which are further sectioned into top, middle, and foot portions. Precise measurements and compression tests are conducted on laser-guided 120mm clear specimens, ensuring uniform cross-sectional results. Middle segments undergo 10-day water submersion for saturation to simulate subsurface conditions. Selected cross sections, sourced from sapwood, heartwood, and pith/juvenile wood, are meticulously prepared through accurate cutting, laser measurements, marking, and sanding to achieve precise dimensions. Samples are cut to 120mm length, weighed, sealed, and refrigerated to maintain uniform moisture content. Rigorous sample preparation, aided by RPD data for wood type identification, ensures a systematic approach for subsequent comprehensive testing.

Execution Phase:
Moisture Content and Density Analysis: Various samples from distinct pile sections will be collected for moisture content and density determination. Wet and dry weights, alongside volume calculations using callipers, will yield moisture content (%) and density (kg/m^3). Modulus of Elasticity Determination: Strain gauges and LVDTs will measure strains and displacements during compression tests. Modulus of elasticity (MOE) will be computed from load-deformation data, with elastic range analysis ensuring accurate strain values. Compressive Strength Analysis: Prepared samples will undergo compression tests to ascertain compressive strength. Load-displacement data will provide maximum compressive force and displacement gradient from load-displacement curves.

In conclusion, this research employs a comprehensive array of experiments to comprehensively explore the physical and mechanical attributes of wooden piles. These encompass degradation assessment, moisture content and density analysis, modulus of elasticity determination, and compressive strength analysis, supported by precise specimen preparation and testing. The approach involves meticulous measurements, data collection, and analysis, guided by RPD data for optimal sample selection. The methodology is tailored to research objectives and time constraints, with the aim of yielding robust and significant findings.

5. What is the actual moisture content, dry density distribution, compression strength and stiffness in the cross section of wooden foundation piles both New/old non-degraded piles and visibly degraded piles? What difference and similarities do they possess? (Experiments)

Degraded Specimens:

The study uncovered a clear and consistent trend in different test samples (3M, 2.7M & 6M). Specifically, samples at the edges of the cross-section had more moisture and less density, which made them weaker and less stiff in the softshell part. The variation in results was quite noticeable. However, the middle sections of the specimens had less moisture and higher density, leading to stronger and stiffer qualities. The results were more consistent in these internal sections, indicating well-conducted experiments and structural stability.

Non-degraded Specimens:

The investigation revealed a clear pattern in a variety of test samples (11M & 10588M), with a small difference seen at 3.18M. Samples at the edges of the cross-section had more moisture and less density, resulting in slightly weaker and less stiff characteristics in those areas. The difference in results was noticeable. On the other hand, the core regions showed higher values in terms of density, strength, and stiffness. Interestingly, one sample (3.18M) had consistent moisture content but with more noticeable differences in results. Additionally, the outer regions displayed higher levels of density, strength, and stiffness, gradually decreasing toward the juvenile wood. Remarkably, in all non-degraded samples, the juvenile sections consistently showed lower measurements in terms of density, moisture content, strength, and stiffness.

6. What is the correlation between moisture content, density, compressive strength, and modulus of elasticity and how can it be modelled with the micro-drilling measurements to provide information on level of degradation of piles in service? (Analysis)

The RPD drill stands as an immensely advantageous and pragmatic instrument, effectively streamlining foundation excavation and sample retrieval, all while furnishing data encompassing drilling amplitude and resistance profiles. The outcomes derived from the testing campaign have been compared with the drilling amplitude for each scenario. In this arrangement, the drilling amplitude functions as the independent variable, while the specific physical or mechanical attribute under scrutiny operates as the dependent variable. Remarkably, the graphs representing moisture content, dry density, compression strength, and modulus of elasticity display coefficient of determination (R2 values) that exceed 53% within the framework of linear regression analysis, serving as indicators of a robust correlation. As a direct consequence, these established models enable the anticipation of untested mechanical and physical attributes through the amalgamation of supplementary drilling amplitude values into the underlying equations.

However, it is imperative to exercise caution, as the accuracy of such prediction's hinges upon the assumption that the connection between drilling amplitude and physical/mechanical properties remains consistent across novel tests. Consequently, the necessity to validate the model further arises, necessitating a comparative assessment against empirical measurements or the execution of supplementary experiments. These validation steps are pivotal in ensuring the model's relevance and reliability within unexplored testing scenarios. As a noteworthy observation, the existing limitations in predictability stem from the utilization of both deteriorated and non-degraded spruce piles dating back to the year 1727. Intriguingly, the degraded samples from 1727 exhibit a notably heightened correlation, evident through coefficient of determination (R2 values) exceeding 70% within the context of linear regression analysis. This finding stands in stark contrast to the comparatively diminished outcomes observed for the non-degraded pilings.

7. What effect does the size of the specimen (20*20*120mm^3 &20*20*60mm^3) have on the results?

The size effect of wood samples on mechanical properties is a vital factor in materials testing. Wood's natural heterogeneity and grain orientation cause significant variations in properties. Reduced specimen size increases surface area and defects, leading to lower stiffness and strength. Examining 120mm vs. 60mm samples, results show most differences are <5%, aligned with natural wood variation. Notable differences include (average values) moisture content (14.1%), wet area (1.4%), wet density (6.7%), dry density (2.3%), ultimate force (6.6%), and ultimate strength (6.8%). Moisture content's high variance is due to quicker drying in smaller samples, impacting wet density and strength disparities. Preferably, 120mm samples are recommended, enabling precise strain measurements and modulus of elasticity determination. This choice aligns with local standards, ensuring consistency in wood materials testing. Investigating size effects in wood, including moisture, area, density, strength, and drilling, offers valuable insights for both research and practical applications. Further exploration of mechanisms and factors can enhance wood behaviour understanding, aiding design and engineering practices.

Expanding research to diverse wood species and environmental conditions would advance this field's knowledge.

8. Can the mechanical properties and in particular the compressive strength profile be related to micro-drilling signals?

Yes, this has been proven in two distinctive ways. First, in the report [40] CT scans can be used to precisely calculate the dry density for pile components. The findings indicate that the RPD signals can predict local dry density fluctuations in a manner similar to that found in CT scans. The report ended with an essential conclusion that the physical properties of wood could be predicted with an element of accuracy from the RPD data. Further investigation into related properties, like strength and stiffness over the cross section of a wooden pile, is made possible by this opportunity.

Second, the mechanical properties, especially the compressive strength profile, can be correlated with micro-drilling signals. The analysis conducted in this thesis indicates that the micro-drilling signals, specifically the drilling amplitude, have a substantial predictive capability for various physical and mechanical properties of the wood samples. This relationship was demonstrated through linear regression analysis, which yielded statistically significant results across different properties such as moisture content, dry density, compressive strength, and modulus of elasticity. These findings suggest that the drilling amplitude serves as a reliable indicator for assessing the mechanical characteristics of both degraded and non-degraded wood samples. This predictive potential opens up avenues for accurately estimating properties in scenarios that have not been previously tested, enhancing our understanding of wood behaviour under different conditions.

9. Is it possible to predict the compressive strength of a timber pile by analysing the amplitude of micro-drilling signals conducted through the cross section?

The formulas provided give the foundational framework for a prospective predictive model, capable of ascertaining mechanical and physical attributes exclusively through the analysis of drilling amplitude. It is imperative that a rigorous validation process be undertaken to enhance its precision and establish robust correlations. This validation should encompass an investigation into additional biological and mechanical characteristics not addressed within the scope of this thesis. In Annex 8, an investigation has been outlined to scrutinize the correlation between theoretical outcomes derived from formulas obtained through linear regression analysis and the results obtained from full-scale pile testing. Furthermore, an outlined approach for the determination of residual compressive strength predicated upon elementary geometric principles and stiffness ratios has been incorporated within Annex A9. This framework holds potential for refinement, thereby enabling subsequent applications in the computation and estimation of residual bearing capacity.

References

[1] K. &. Creemers, “Wooden foundation piles and its underestimated relevance for cultural heritage,” *Journal of Cultural Heritage - ELSEVIER,* 2012.

[2] M. Hattinga Verschure, “In Holland stond een huis: De ontwikkeling van funderingstechnieken in stedelijke context tijdens de middeleeuwen in West-Nederland.,” Leiden university , Leiden , 2012.

[3] Bles, T. J., van der Doef, M. R., van Buren, R., Buma, J. T., Brolsma, R. J., Venmans, A. A. M., & van Meerten, J. J., “Investigation of the blue spots in the Netherlands National Highway Network. Deltares rapport,” Netherlands National Highway Network, Amsterdam, 2012.

[4] Blaß, H. J., & Sandhaas, C., Timber engineering-principles for design., KIT Scientific Publishing, 2017.

[5] W. Oomen, “Pile foundations in NL,” TU Delft, Delft, 2017.

[6] Klaassen, R. K., “Bacterial decay in wooden foundation piles—Patterns and causes: A study of historical pile foundations in the Netherlands.,” *Elsevier-International biodeterioration & biodegradation,* vol. 61, no. 1, pp. 45-60, 2008.

[7] H. J. Zantkuijl, “Bouwen in amsterdam - het woonhuis in de stad.,” Architectura & Natura, 1993.

[8] Nico W. Willemse, “Stedelijke ontwikkeling en bodemdaling in en rondom Gouda,” Gemeente Gouda, Gouda, 2017.

[9] A. Teischinger, “OPPORTUNITIES AND LIMITS OF TIMBER IN CONSTRUCTION,” in *World Conference on Timber Engineering*, Vienna, 2016.

[10] D. Grosser, Die Hölzer Mitteleuropas. Ein mikrofotografischer Lehratlas., Berlin: Springer, 1977.

[11] H. M. a. P. S. Tuula Jyske, “Wood Density within Norway Spruce,” *Silva fennica,* vol. 42, pp. 439-455, 2008.

[12] P. H. V. Gryc, “Variability in density of spruce (Picea abies [L.] Karst.),” *JOURNAL OF FOREST SCIENCE,* vol. 53, pp. 129-137, 2007.

[13] S. Hales, Vegetable Staticks, 1727.

[14] Dinwoodie, Desch. Harold Ernest. and John M., “Timber: its structure, properties and utilisation. No. Ed. 6,” MacMillan Press Ltd, 1981..

[15] . Glass, . Samuel V, . Zelinka and . Samuel L, “Moisture Relations and Physical Properties of Wood,” 2021.

[16] Aicher, S., & Stapf, G., “Compressive strength parallel to the fiber of spruce with high moisture content. European Journal of Wood and Wood Products,” in *European Journal of Wood and Wood Products*, Springer, 2016, pp. 527-542.

[17] Fritzell, E., Melander, O., & Rasmuson, A., “The drying kinetics and equilibrium moisture content of MDF fibers.,” in *Drying Technology*, 2009, pp. 993-998.

[18] L. B. ADM Rayner, Fungal decomposition of wood. Its biology and ecology., 1988.

[19] J.-B. S. Tchinda, “Inhibition of fungi with wood extractives and natural durability of five Cameroonian wood species,” *Industrial Crops and Products,* vol. 123, pp. 183-191, 2018.

[20] R. RM., “Innovation in Wood Preservation,” *Polymers,* 12 2020.

[21] A. H. H. Wong, “Wood degrading fungi,” 2007.

[22] Huckfeldt, Tobias, and Olaf Schmidt., “Identification key for European strand-forming house-rot fungi,” *Mycologist,* vol. 20, no. 2, pp. 42-56, 2006.

[23] Eastwood, D. C.: Floudas, D.: Binder, M.: Majcherczyk, A.: Schneider, P.: Aerts, A.: Watkinson, S. C., “The plant cell wall–decomposing machinery underlies the functional diversity of forest fungi.,” *Science,* vol. 33(6043), pp. 762-765., 2011.

[24] Mondo, S. J., Dannebaum, R. O., Kuo, R. C., Louie, K. B., Bewick, A. J., LaButti, K., ... & Grigoriev, I. V., “Widespread adenine N6-methylation of active genes in fungi.,” *Nature genetics,,* Vols. 49(6),, pp. 964-968., 2017.

[25] Landy, E. T., Mitchell, J. I., Hotchkiss, S., & Eaton, R. A., “Bacterial diversity associated with archaeological waterlogged wood,” *International Biodeterioration & Biodegradation,* vol. 61, no. 1, pp. 106-108, 2008.

[26] Broda, M., “Natural compounds for wood protection against fungi—A review. Molecules,” *Molecules,* vol. 25(15), 2020.

[27] EN 408:2010+A1, “Timber structures - Structural timber and glued laminated timber - Determination of some physical and mechanical properties,” 2012.

[28] DIN 52185, “Testing of wood; compression test parallel to grain. German Institute for Standardization (DIN), Berlin,,” Berlin, 1978.

[29] L. Benabou, “Kink Band Formation in Wood Species Under Compressive Loading,” *Experimental Mechanics ,* vol. 48, no. 5, pp. 647-656, 2008.

[30] FormaXylos 1, “Woods of the World (CD-ROM),” CTBA publisher, Paris, 2002.

[31] R. K. W. M. Klaassen, “Final report EU project BACPOLES Chapter 2”.

[32] R. K. W. M. Klaassen, “Life Expectation of Wooden Foundations-a Non-Destructive Approach”.

[33] VROM (Dutch ministry of building), “Protocol Voor het uit Voeren van een Inspectie aan Houten Paalfundering. Directoraat-Generaal Wonen, Directie Strategie, Den Haag.,” Dutch ministry of building, 2003.

[34] J. Van De Kuilen, ;. Willem, O. ;. Beketova-Hummel, G. ;. Pagella, G. ;. Ravenshorst, W. Gard, J. W. Van De Kuilen, O. Beketova-Hummel, G. Pagella and G. Ravenshorst, “An integral approach for the assessment of timber pile foundations”.

[35] “Jeetekno,” Jeetekno, [Online]. Available: https://jeetekno.com/product/pilodyn-wood-tester/. [Accessed 05 01 2023].

[36] Van de Kuilen, J. W., Beketova-Hummel, O., Pagella, G., Ravenshorst, G., & Gard, W., “An integral approach for the assessment of timber pile foundations,” in *World Conference on Timber*, Santiago, Chile, 2021.

[37] E. Schreurs, “DETERIORATION OF TIMBER PILE FOUNDATIONS IN ROTTERDAM,” 2017.

[38] Gard, W. F., & Van de Kuilen, J. W. G., “Micro-drilling resistance measurements of dense hardwoods for hydraulic structures.,” in *WCTE-World Conference on Timber Engineering,*, Seoul, South-Korea., 2018.

[39] Jeronimidis, G., “The fracture behaviour of wood and the relations between toughness and morphology.,” *Proceedings of the Royal Society of London. Series B. Biological Sciences,,* vol. 208, no. 1173, pp. 447-460, 1980.

[40] M. Mirra, G. J. P. Ravenshorst, W.F. Gard, J.W.G. van de Kuilen., “Investigation into the application of micro-drilling (RPD) measurements as replacements of drill cores extractions in determining the soft shell according to the Amsterdam method,” TU Delft, Delft, 2022.

[41] Roy, A., Ravenshorst, G.J.P. Gard, W.F., van de Kuilen, J.W.G.,, “Handleiding Soft Shell Calculator TU Delft versie 0.1,” Delft University of Technology, Delft, 2021.

[42] TU Delft, “Safety rules of the Geoscience and Engineering Laboratory,” The Geoscience and Engineering laboratory, 2021.

[43] Pagella, G., Ravenshorst, G.J.P., “Characterization of the mechanical properties of 60 timber piles retrieved from bridge 30 and 41 in Amsterdam. TUD-F3.2-20230307-GP-v2.0. Delft University of Technology,” Delft, 2023.

[44] G. Zelada-Tumialan, W. Konicki, P. Westover and M. Vatovec, “Structural ForenSicS,” 2014.

[45] G. J. P. Ravenshorst, J. H. Van Dalen, M. ;. Mirra, R. ;. Steiger and J. W. G. Van De Kuilen, “Connection of timber foundation piles to concrete extension piles,” APA, 2021.

[46] . mvanadrichem, “Species independent strength modeling of structural timber for machine grading”.

[47] J. Buma, “Grootschalig actief grondwater-peilbeheer in bebouwd gebied Fase 1,” 2017.

[48] R. Brolsma, Effect van droogte op stedelijk gebied : kennisinventarisatie, Deltares, 2012.

[49] . Auteur, “LAB PROTOCOL FOR THE TEST CAMPAIGN OF WOODEN FOUNDATION PILES FROM ICL PROEFTUIN”.

[50] A. ARoy aroy, t. GJPRavenshorst, W. Gard and J. van de Kuilen, “Handleiding Soft Shell Calculator TU Delft versie 0.1”.

[51] T. Abbott, N. Gamage, W. Lokuge and S. Setunge, “Predicting the remaining life of timber bridges”.

A

Appendix – Results

This Appendix compiles the relevant total data derived from the experimental campaign executed within the laboratory facilities of the Delft University of Technology (TU Delft). The amassed data set encompasses various components, namely visual documentation portraying the spatial orientations of the specimens, detailed records of Micro-drilling procedures, and the ensuing outcomes of the experimental investigations. These investigations encompass critical parameters including moisture content, density measurements, ultimate compression force, and, lastly, the determination of the Modulus of Elasticity. The inclusion of this comprehensive dataset in the appendix of this thesis serves to support and enhance the empirical foundation for the subsequent analyses and conclusions.

A.1 Moisture content and density through the complete section

To determine the moisture content and density through the complete cross section of a pile, small samples of approximately 20mm are cut and manufactured in a continuous manor from two piles 010640M & 010584 which are both new, non-degraded piles. Two cross sections of approximately 120mm and 60mm will be cut from both piles. The procedure for the determination on the moisture content and density is found in the methodological section and results are highlighted below. The aim of these initial experiments is to see how the moisture content and density change depending on their location through the cross section. It would also be cumbersome to undertake compression tests for all specimens so therefore an indication of extreme values would yield valuable results and provide a comparison of the sizes of specimens.

010640M

Figure A.1.1 cross sectional photos of 010640M for 120mm (Left) and 60mm (right)

010640M_120

Table A.1.1 010640M_120_Full data set

CODE	L (WET)	L (DRY)	W (WET)	W (DRY)	H (WET)	H (DRY)	MASS (WET)	MASS (DRY)	MC	AREA (WET)	DENSITY (WET)	DENSITY (DRY)
[#]	[mm]	[mm]	[mm]	[mm]	[mm]	[mm]	[g]	[g]	[%]	[mm^2]	kg/m^3]	kg/m^3]
010640M_ 1	22.09	20.60	24.15	22.20	125.57	125.47	65.1	33.5	94	533	972	584
010640M_ 2	22.23	20.93	22.55	21.85	125.01	124.55	69.8	32.3	116	501	1114	567
010640M_ 3	21.8	19.95	21.99	20.46	124.5	124.20	64.1	32.5	97	479	1074	641
010640M_ 4	20.02	19.22	22.11	20.06	123.47	123.04	41.3	27.9	48	443	756	588
010640M_ 5	17.85	17.10	20.87	18.96	123.55	122.75	31.7	23.3	36	373	689	585
010640M_ 6	18.05	17.22	20.41	18.74	122.61	122.6	30.5	19.0	61	368	675	480
010640M_ 7	21.31	20.26	21.61	20.68	122.13	121.31	42.6	21.0	103	461	757	413
010640M_ 8	21.05	20.16	23.05	21.4	121.53	121.83	40.8	26.0	57	485	692	470
010640M_ 9	21.47	19.93	21.67	20.48	121.29	121.16	41.1	29.4	40	465	728	594
010640M_ 10	20.67	19.73	21.53	20.02	121.67	120.95	57.7	25.1	130	445	1066	525
010640M_ 11	18.9	18.22	20	18.5	121.15	120.61	47.2	20.6	129	378	1031	507
010640M_ 12	18.11	18.21	21.86	19.83	120.63	120.15	41.2	20.4	102	396	863	470
AVERAGES	20.3	19.3	21.8	20.3	122.8	122.4	47.8	25.9	84	444	868	535

Figure A.1.2 010640_120_Moiture content and dry density over the full cross section

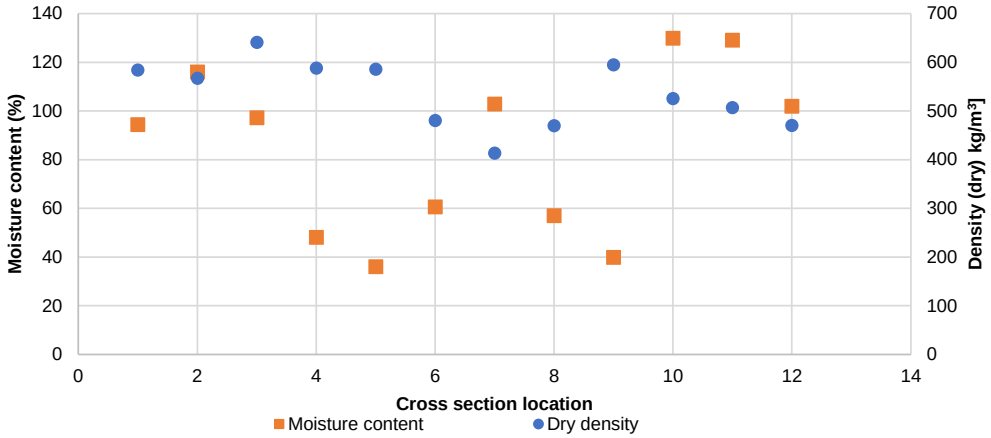

010640M_60

Table A.1.2 010640M_60_ Full data set

code	L (wet)	L (dry)	W (wet)	W (dry)	H (wet)	H (dry)	Mass (wet)	Mass (dry)	MC	Area (wet)	Density (wet)	Density (dry)
[#]	[mm]	[mm]	[mm]	[mm]	[mm]	[mm]	[g]	[g]	[%]	[mm2]	kg/m3]	kg/m3]
010640M_ 1	20.6	19.6	20.9	20.9	57.3	57.1	23.2	12.7	83	430	943	545
010640M_ 2	22.0	20.5	23.8	21.5	57.1	57.0	31.4	15.0	109	523	1051	596
010640M_ 3	19.5	18.6	24.1	22.3	57.0	57.3	27.3	13.5	102	469	1021	569
010640M_ 4	18.3	17.3	23.8	22.1	57.4	57.1	21.0	13.3	58	435	840	608
010640M_ 5	22.4	21.9	24.0	22.4	57.3	56.9	19.4	14.7	32	539	628	528
010640M_ 6	22.1	21.1	24.1	21.7	57.4	57.1	19.0	13.9	37	532	623	531
010640M_ 7	20.2	19.1	23.8	22.5	57.2	56.8	21.7	11.5	89	481	789	472
010640M_ 8	16.1	15.8	23.5	21.7	57.4	57.3	12.8	9.1	40	378	588	464
010640M_ 9	18.0	17.4	23.7	21.8	57.9	57.2	19.2	14.2	35	426	780	657

010640M_ 10	21.9	20.8	23.9	22.7	57.1	57.0	28.5	19.2	48	522	956	714
010640M_ 11	20.4	18.7	23.6	21.2	57.4	57.1	28.2	13.8	104	481	1023	610
010640M_ 12	22.5	21.1	23.5	21.4	57.9	57.6	30.2	15.1	100	527	989	582
Averages	20.3	19.3	23.5	21.8	57.4	57.1	23.5	13.83	70	479	852	573

Figure A.1.3 010640_60_Moiture content and dry density over the full cross section

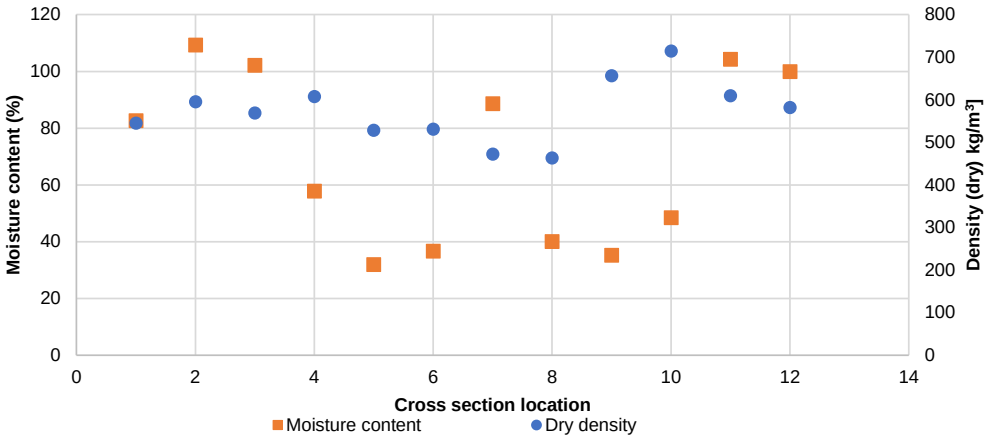

Table A.1.3 010640_Volumetric percentage change between 60mm and 120mm

CODE	SHRINKAGE L	SHRINKAGE W	SHRINKAGE H	MC	AREA (WET)	DENSITY (WET)	DENSITY (DRY)
[#]	[%]	[%]	[%]	[%]	[mm²]	kg/m³]	kg/m³]
010640M_60	5.0%	7.2%	0.4%	70	479	852	573
010640M_120	4.9%	7.1%	0.3%	84	444	868	535
AVERAGES	1.39%	1.53%	28.64%	-20.91%	7.23%	1.79%	-7.03%

010584M

Figure A.1.4_cross sectional photos of 010584M for 120mm (Left) and 60mm (right)

Table A.1.4_010584M_120_Full data set

CODE	L (WET)	L (DRY)	W (WET)	W (DRY)	H (WET)	H (DRY)	MASS (WET)	MASS (DRY)	MC	AREA (WET)	DENSITY (WET)	DENSITY (DRY)
[#]	[mm]	[mm]	[mm]	[mm]	[mm]	[mm]	[g]	[g]	[%]	[mm^{2}]	[kg/m^{3}]	[kg/m^{3}]
010584M_ 1	20.3	19.2	23.1	20.8	121.5	121.1	55.8	26.7	109	470	979	552
010584M_ 2	20.0	19.3	24.7	22.5	121.2	121.1	62.4	28.0	123	494	1041	532
010584M_ 3	21.1	20.0	23.9	21.1	121.1	121.0	41.9	26.1	60	503	687	513
010584M_ 4	19.8	19.2	22.0	20.7	120.8	120.4	30.1	19.7	53	436	571	412
010584M_ 5	21.3	20.0	21.8	20.8	120.6	120.3	32.1	20.6	56	466	571	412
010584M_ 6	20.8	19.6	21.3	20.7	120.6	120.2	30.4	21.1	44	443	569	433
010584M_ 7	19.1	17.5	20.6	18.1	120.1	119.8	30.9	21.7	42	392	656	572
010584M_ 8	21.7	20.0	21.7	20.5	120.7	120.4	49.7	30.5	63	471	874	620
010584M_ 9	20.1	18.8	21.8	20.2	120.6	120.3	57.8	26.1	121	438	1093	571
010584M_ 10	20.5	19.1	23.9	22.2	121.0	121.1	66.0	29.6	123	489	1114	578
010584M_ 11	20.3	18.5	23.6	21.3	121.0	120.7	61.6	28.1	119	479	1063	593
AVERAGES	20.5	19.2	22.6	20.8	120.8	120.6	47.1	25.3	83	462	838	526

Figure A.1.5 010640_120_Moiture content and dry density over the full cross section

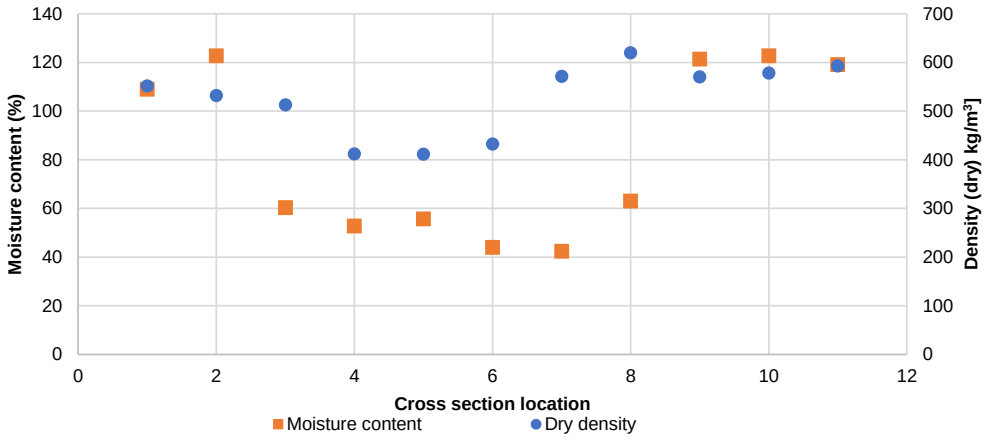

010640M_60

Table A.1.5 010640M_60_ Full data set

CODE	L (WET)	L (DRY)	W (WET)	W (DRY)	H (WET)	H (DRY)	MASS (WET)	MASS (DRY)	MC	AREA (WET)	DENSITY (WET)	DENSITY (DRY)
[#]	[mm]	[mm]	[mm]	[mm]	[mm]	[mm]	[g]	[g]	[%]	[mm^{2}]	kg/m^{3}]	kg/m^{3}]
010584M_ 1	21.7	20.2	22.3	20.2	60.2	60.2	29.1	13.5	116	484	1001	552
010584M_ 2	20.9	18.9	21.5	19.8	60.6	60.3	27.1	12.2	122	449	997	540
010584M_ 3	21.0	20.0	23.3	20.9	60.4	60.4	18.8	12.3	53	489	636	486
010584M_ 4	20.4	19.3	22.2	20.8	60.2	60.1	13.7	9.7	41	451	505	401
010584M_ 5	21.3	20.4	23.4	22.3	60.5	60.2	16.1	10.6	52	497	535	388
010584M_ 6	20.4	19.9	22.3	20.8	60.9	60.8	13.8	9.9	39	456	497	395
010584M_ 7	21.0	20.5	23.2	21.6	60.2	60.1	17.1	12.1	41	486	584	455
010584M_ 8	19.6	18.4	24.5	22.3	60.7	60.7	25.2	13.4	88	479	865	539
010584M_ 9	19.5	16.5	24.8	20.6	60.8	60.7	22.7	10.5	116	483	773	508
010584M_ 10	21.0	19.6	22.5	21.4	61.0	60.7	28.1	12.7	121	471	979	499
010584M_ 11	22.0	20.3	22.2	20.8	61.0	60.9	30.2	13.4	125	488	1016	522
AVERAGES	20.8	19.5	22.9	21.0	60.6	60.5	22.0	11.85	83	476	763	481

Figure A.1.6 010640_60_Moiture content and dry density over the full cross section

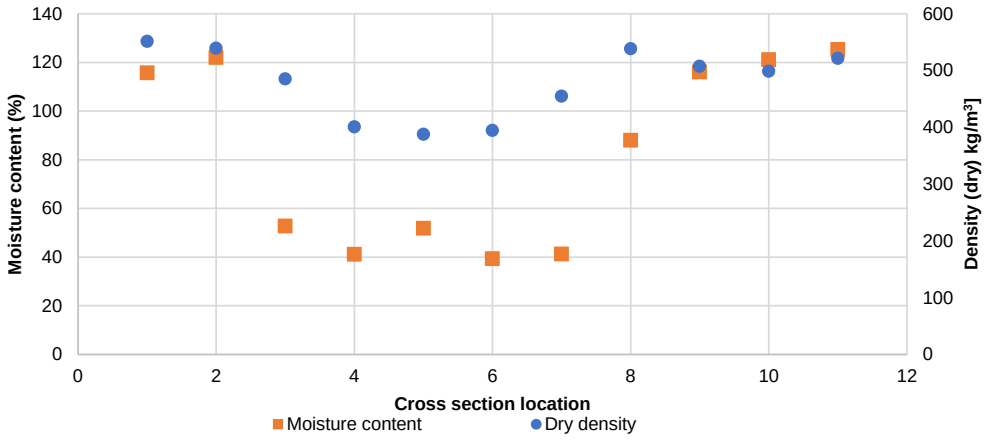

Table A.1.6_010584_Volumetric percentage change between 60mm and 120mm

code	*Shrinkage L*	*Shrinkage W*	*Shrinkage H*	*MC*	*Area (wet)*	*Density (wet)*	*Density (dry)*
[#]	[%]	[%]	[%]	[%]	[mm^{2}]	kg/m^{3}]	kg/m^{3}]
010584M_60	6.4%	8.2%	0.2%	83	476	763	481
010584M_120	6.2%	8.0%	0.2%	83	462	838	526
Averages	3.91%	2.79%	5.15%	0.19%	2.89%	9.02%	8.69%

A.2 - 10588M (2019) New pile HIE-P10588

Pile HIE-P10588 from 2019. With a segment code of 03867, 03824 & 010585 which can be seen in the figure below shall be renamed as V10588M M10588M & K10588M respectively. The pile has been split into 3 sections known as the tip, middle-part and head as can be seen below in the image. From these sections, a segment of approximately 150mm in length was extracted so that the small samples could be manufactured. The results of each full pile segment and subsequent 20*20*120mm local samples are highlighted below.

Figure A.2.1 Full section codes with local cross sections extracted and small specimen locations.

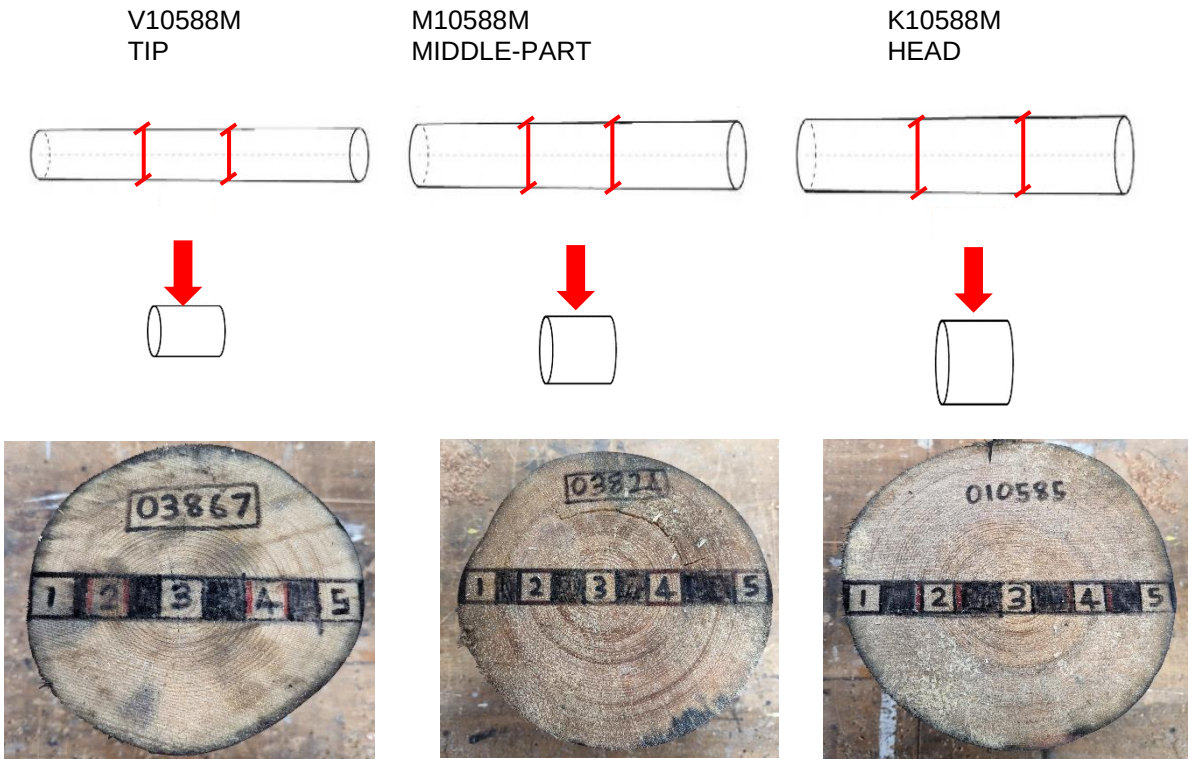

Table A.2.1 Summary of results for full sections and average small samples.

Specimen	Part	Density wet	Density dry	Ultimate strength	MOE_{stat}	MOE_{dyn} (Mpa)	RPD drilling average
[#]	[#]	kg/m^3]	kg/m^3]	[N/mm^2]	Mpa	Mpa	[%]
Full size	K	903	1000	23.1	11900	13200	24.9
	M	1015	1120	22.5	11900	13500	20.6
	V	903	1000	17.0	8900	9600	18.8
Local samples average	K	867	528	22.2	10753	[N/A]	24.9
	M	753	461	20.4	9479	[N/A]	20.6
	V	824	470	17.7	8296	[N/A]	18.8

K10588M

Table A.2.2 Full Specimen Results

Full pile ID	Segment code - container	wet density (kg/m^3)	dry density (kg/m^3)	m.c. (%)	MOE$_{stat}$ (Mpa)	MOE$_{dyn}$ (Mpa)	f_{c0} (Mpa)	soft shell (mm)	failure mechanism	remaining sound c-s (%)	RPD drilling avg (%)
HIE-P10588	K10588M	903	1000	80	11900	13200	23.1	0.0	buckling (top)	100	24.9

Table A.2.3 Local cross-sectional results

Code	Mass Wet	Mass dry	Moisture Content	Area (wet)	Density wet	Density dry	F_{max}	fc,0,wet	MOE	failure mechanism	RPD drilling average
[#]	[g]	[g]	[%]	[mm^2]	[kg/m^3]	kg/m^3]	[kN]	[N/mm^2]	[Mpa]	[N/A]	[%]
10585M_1	50.6	23.8	113	385	1095	591	9.8	25.4	12820	Shear (bottom)	25.2
10585M_2	38.1	24.3	57	400	795	567	10.6	26.4	13379	buckling (bottom)	27.1
10585M_3	29.0	18.1	60	403	600	429	5.6	14.0	6181	buckling (top)	20.1
10585M_4	40.1	24.2	66	402	833	576	11.2	27.9	14578	buckling (top)	25.7
10585M_5	47.6	19.9	139	392	1010	479	6.7	17.1	6809	buckling (top)	26.2
Average	41.1	22.1	87	396	867	528	8.8	22.2	10753	[N/A]	24.9

*Figure A.2.2 K10588M_20*20*120 Dry density & moisture content over cross section*

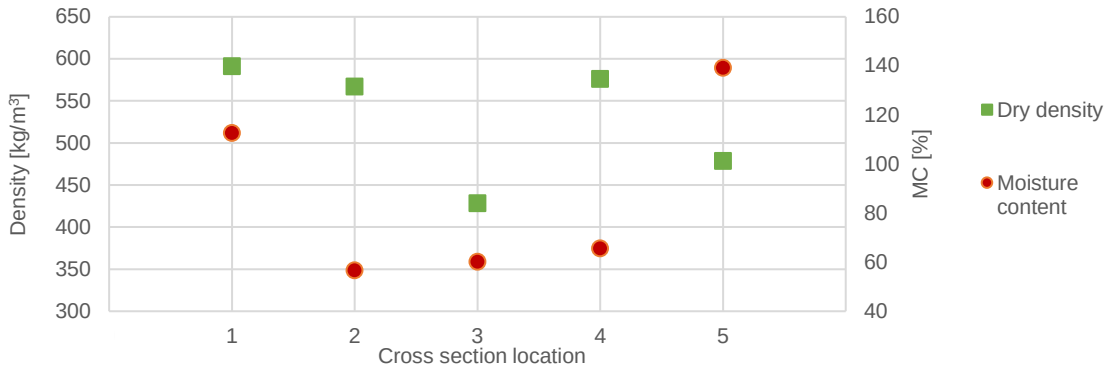

*Figure A.2.3 K10588M _20*20*120 Ultimate strength through cross section & modulus of elasticity*

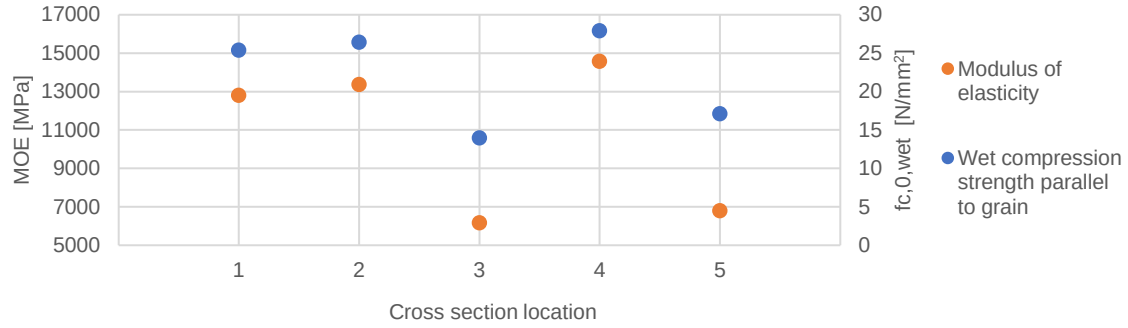

Figure A.2.4 K10588M _Drilling amplitude with ultimate strength.

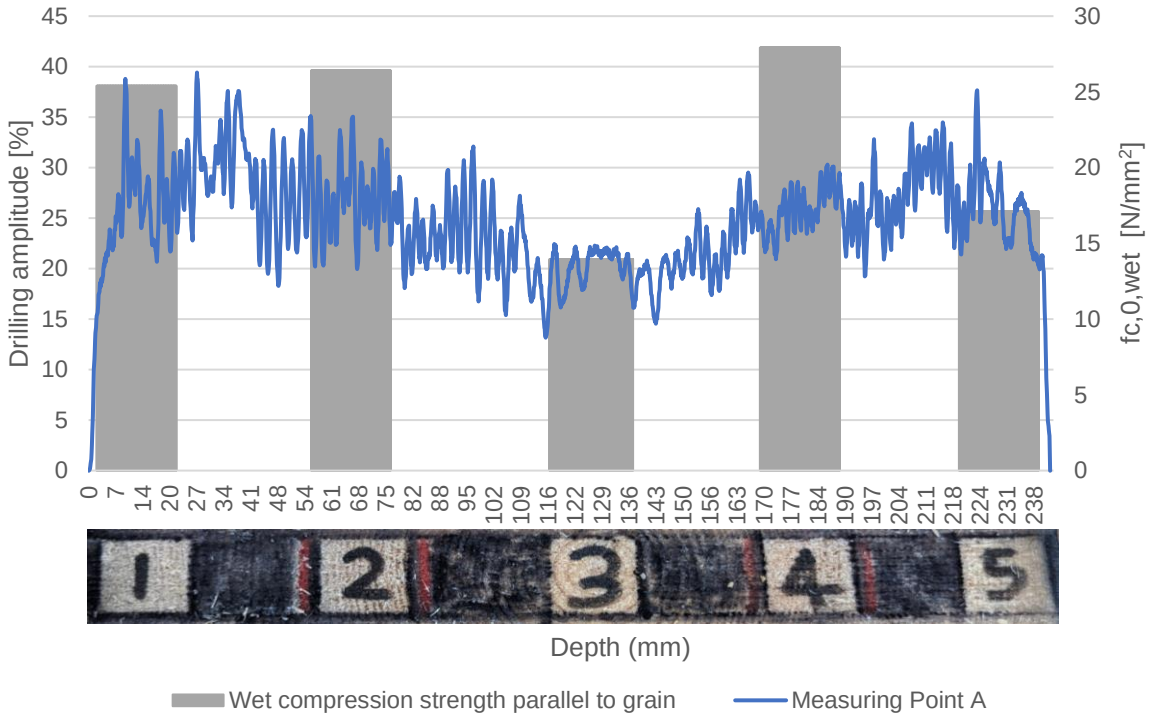

M010588M

Table A.2.4 Full Specimen Results

Full pile ID	Segment code - container	wet density (kg/m³)	dry density (kg/m³)	m.c. (%)	MOE_{stat} (Mpa)	MOE_{dyn} (Mpa)	f_{c0} (Mpa)	soft shell (mm)	failure mechanism	remaining sound c-s (%)	RPD drilling avg (%)
HIE-P10588	M10588M	1015	1120	103	11900	13500	22.5	0.0	buckling (top)	100	20.6

Table A.2.5 Local cross-sectional results

Code	Mass Wet	Mass dry	Moisture Content	Area (wet)	Density wet	Density dry	F_{max}	fc,0,wet	MOE	failure mechanism	RPD drilling average
[#]	[g]	[g]	[%]	[mm²]	[kg/m³]	kg/m³]	[kN]	[N/mm²]	[Mpa]	[N/A]	[%]
M10588M _1	45.2	20.1	125	393	961	434	7.2	18.4	8856	buckling (top)	19
M10588M _2	33.2	28.2	18	390	712	625	9.8	25.0	12782	buckling (top)	22
M10588M _3	22.2	17.1	29	391	472	368	5.5	14.2	5033	buckling (top)	16
M10588M _4	26.2	20.6	27	387	564	437	9.5	24.4	11619	crushing (top)	24
M10588M _5	48.6	21.1	131	384	1053	442	7.7	20.2	9106	buckling (top)	21
Average	35.1	21.4	66	389	753	461	7.9	20.4	9479	[N/A]	20.6

*Figure A.2.5 M010588M_20*20*120_Dry density & moisture content over cross section*

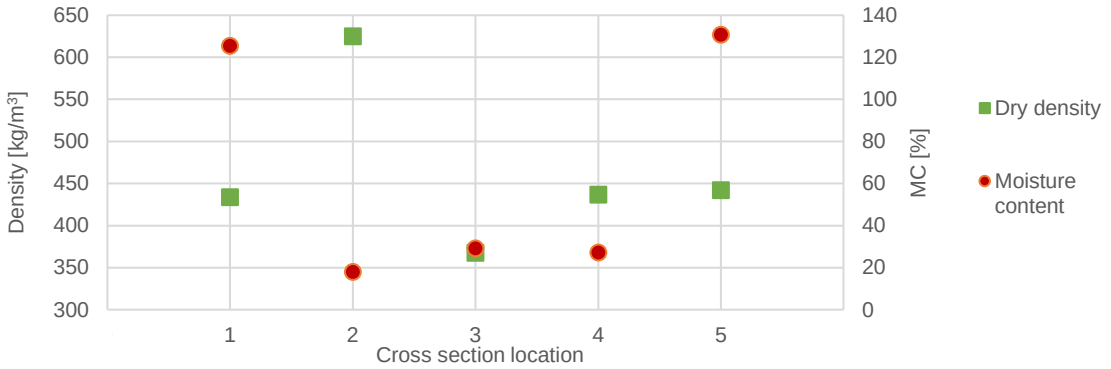

*Figure A.2.6 M010588M_20*20*120_Ultimate strength through cross section & modulus of elasticity*

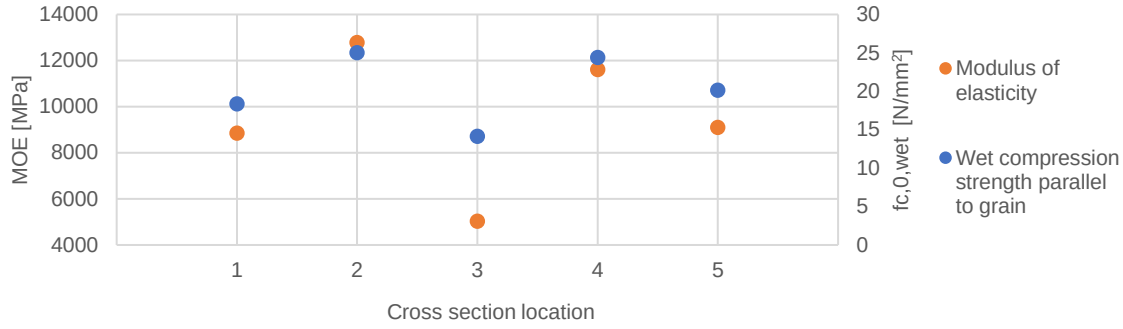

*Figure A.2.7 M010588M_20*20*120_Drilling amplitude with ultimate strength.*

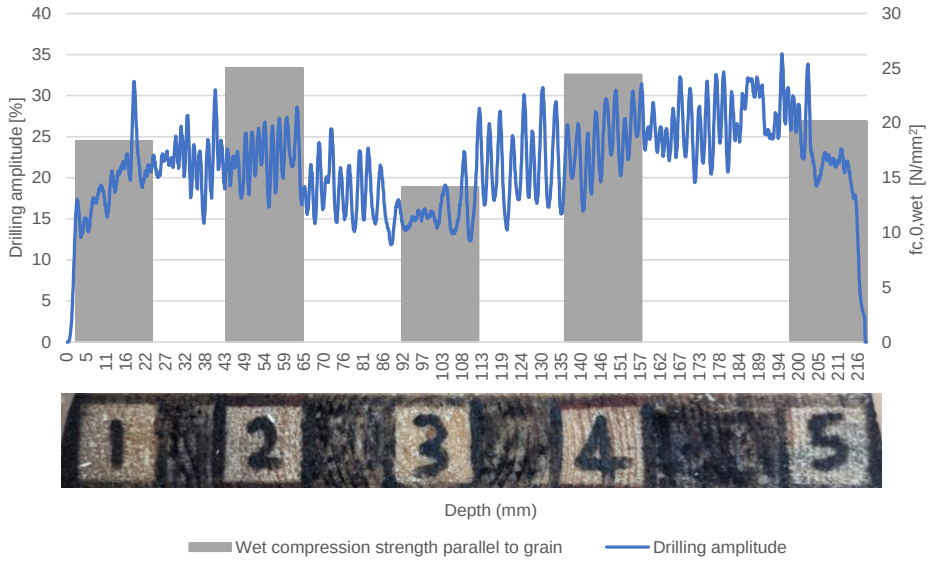

V10588M

Table A.2.6 Full Specimen Results

Full pile ID	Segment code - container	wet density (kg/m3)	dry density (kg/m3)	m.c. (%)	MOEstat (Mpa)	MOEdyn (Mpa)	fc0 (Mpa)	soft shell (mm)	failure mechanism	remaining sound c-s (%)	RPD drilling avg (%)
HIE-P10588	V10588M	903	1000	125	8900	9600	17.0	0.0	0	100	18.8

Table A.2.7 Local cross-sectional results

Code	Mass Wet	Mass dry	Moisture Content	Area (wet)	Density wet	Density dry	F_{max}	fc,0,wet	MOE	failure mechanism	RPD drilling average
[#]	[g]	[g]	[%]	[mm^2]	[kg/m^3]	kg/m^3]	[kN]	[N/mm^2]	[Mpa]	[N/A]	[%]
V10588M _1	47.7	17.8	168	395	1006	420	5.9	14.9	8296	buckling (top)	15.8
V10588M _2	33.3	20.1	66	396	701	452	8.6	21.7	8931	buckling (top)	20.8
V10588M _3	27.0	20.0	35	399	564	453	4.6	11.5	5546	crushing (top)	17.5
V10588M _4	39.8	20.4	95	402	824	479	8.0	19.9	8421	buckling (top)	20.1
V10588M _5	49.4	23.0	115	403	1024	547	8.3	20.6	10288	buckling (top)	19.6
Average	39.4	20.3	96	399	824	470	7.1	17.7	8296	[N/A]	18.8

Graphical results

*Figure A.2.8 V10588M_20*20*120 Dry density & moisture content over cross section*

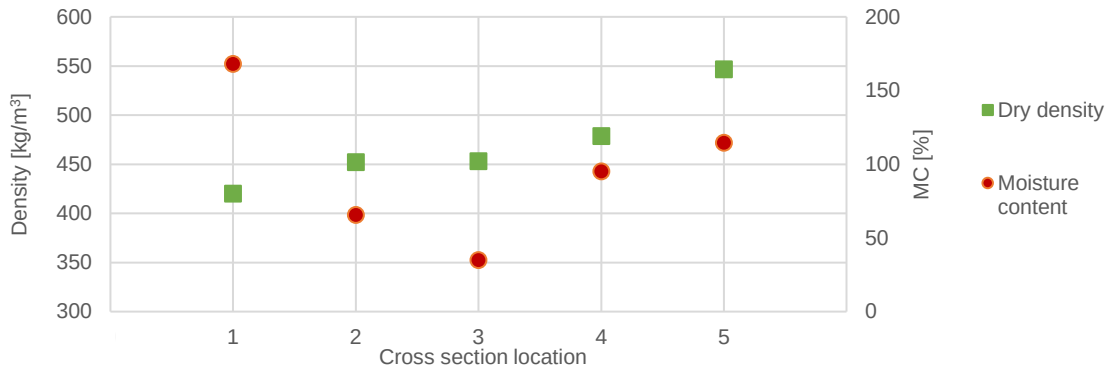

*Figure A.2.9 V10588M _20*20*120 Ultimate strength through cross section & modulus of elasticity*

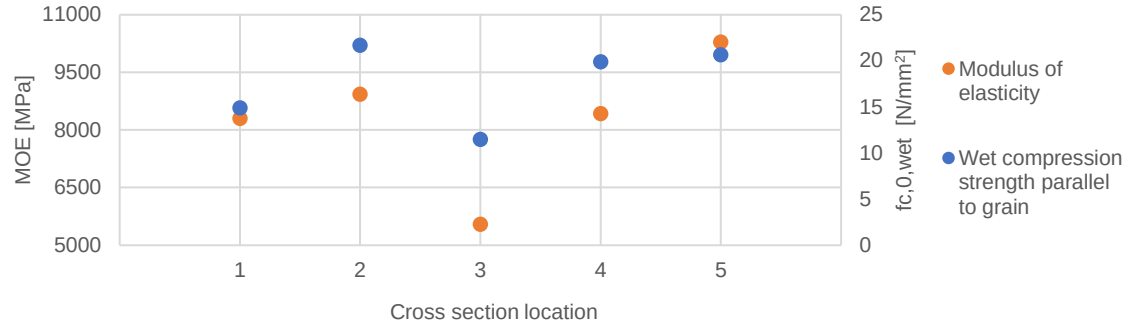

*Figure A.2.10 V10588M _20*20*120_Drilling amplitude with ultimate strength.*

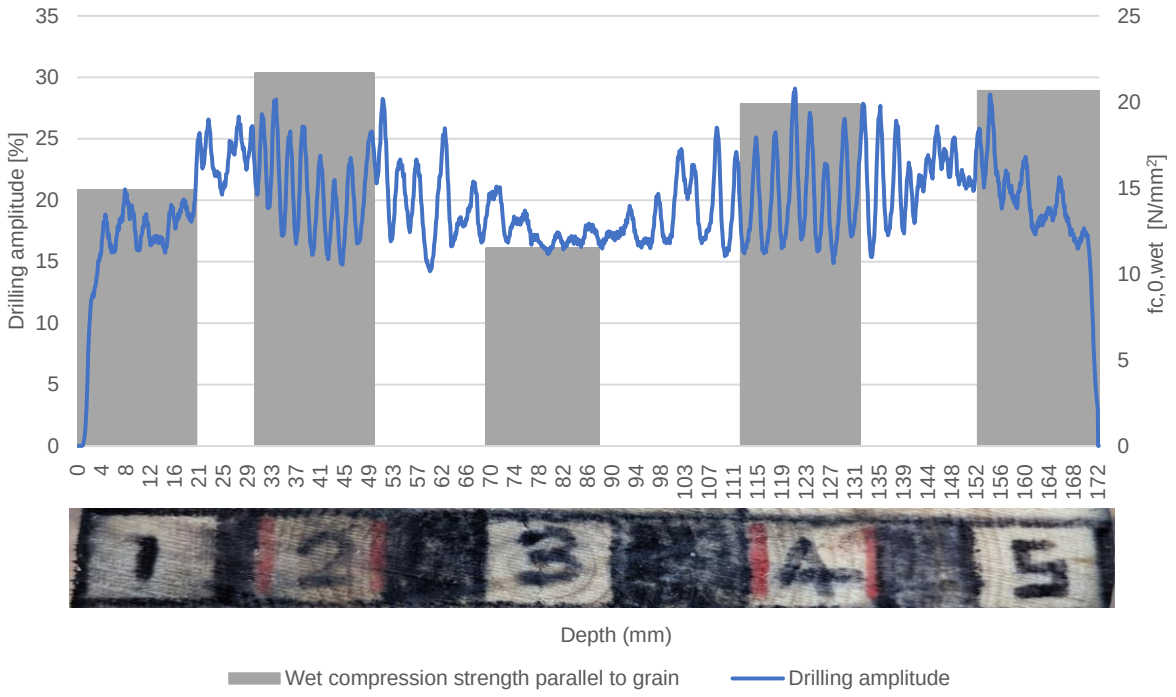

*Table 2.9 V10588M _20*20*120*

Average result	Moisture Content	SD	Density dry	SD	Density wet	SD	fc,0,wet	SD	MOE	SD	RPD drilling average	SD
[#]	[%]	[#]	[kg/m³]	[#]	[kg/m³]	[#]	[N/mm²]	[#]	Mpa	[#]	[%]	[#]
10588M_1	135	29.0	482	95.1	1021	68.3	20	5.4	9990	2466.1	20	4.7
10588M_2	47	25.3	548	87.9	736	51.5	24	2.4	11697	2413.9	23	3.3
10588M_3	41	16.5	416	44.0	546	66.0	13	1.5	5587	574.6	18	2.1
10588M_4	63	34.0	497	71.6	740	152.6	24	4.0	11539	3079.6	23	2.9
10588M_5	128	12.5	489	53.2	1029	21.9	19	1.9	8734	1769.2	22	3.5

*Figure A.2.11 V10588M _20*20*120_Standard deviation of complete pile*

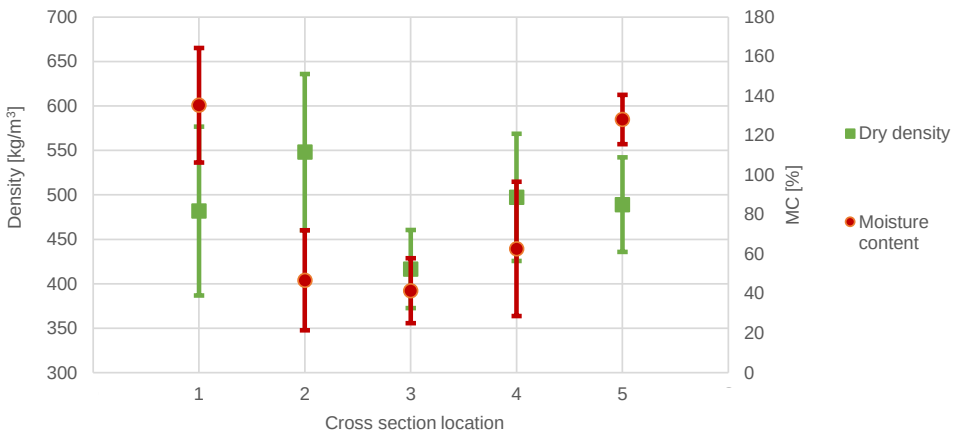

*Figure A.2.12 V10588M _20*20*120_Standard deviation of complete pile*

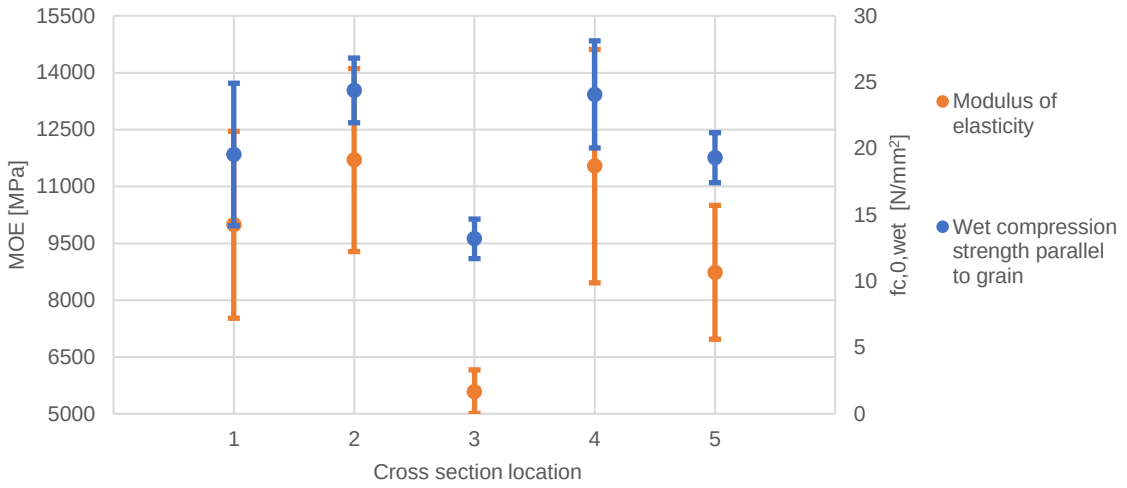
15500
14000
12500
11000
9500
8000
6500
5000
MOE [MPa]
30
25
20
15
10
5
0
fc,0,wet [N/mm²]
1
2
3
4
5
Cross section location
Modulus of elasticity
Wet compression strength parallel to grain

A.3 - 11M (1922) BRU0041-PL2-P1.9

Pile BRU0041-PL2-P1.9 from 1922. With a segment code of 11M from container 228 has been split into 3 sections known as the tip, middle-part and head as can be seen below in the image. From these sections, a segment of approximately 150mm in length was extracted so that the small samples could be manufactured. The results of each full pile segment and subsequent 20*20*120mm local samples are highlighted below.

Figure A.3.1 Full section codes with local cross sections extracted and small specimen locations.

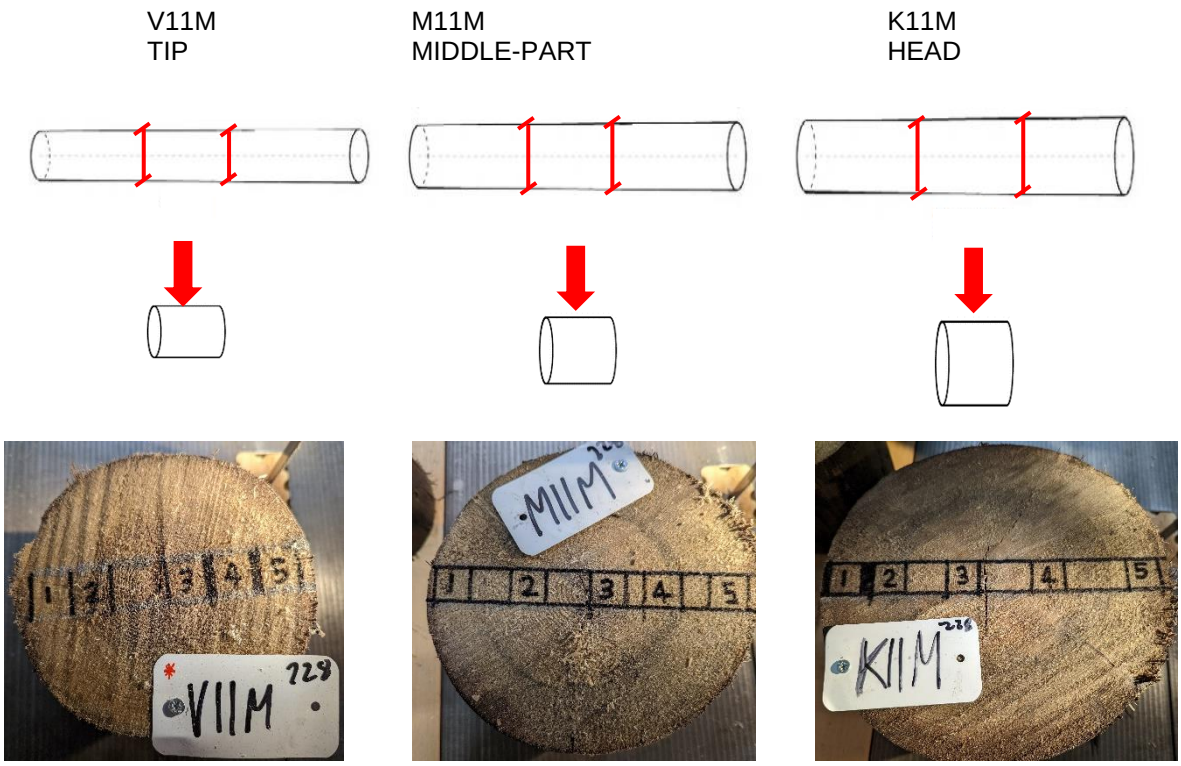

.

Table A.3.1Summary of results for full sections and average small samples

Specimen	Part	Density wet	Density dry	Ultimate strength	MOE_{stat}	MOE_{dyn} (Mpa)	RPD drilling average
[#]	[#]	kg/m^3]	kg/m^3]	[N/mm^2]	Mpa	Mpa	[%]
Full size	K	750	415	16.9	12530	13334	10.3
	M	702	396	16.3	12210	12647	11.2
	V	818	464	15.4	11140	12202	11.6
Local samples average	K	711	486	17.6	11360	[N/A]	29.3
	M	748	461	16.3	10448	[N/A]	26.9
	V	774	484	14.8	9450	[N/A]	28.8

K11M_228

Table A.3.2 Full Specimen Results

Full pile ID	Segment code - container	wet density (kg/m^3)	dry density (kg/m^3)	m.c. (%)	MOE$_{stat}$ (Mpa)	MOE$_{dyn}$ (Mpa)	f_{c0} (Mpa)	soft shell (mm)	failure mechanism	remaining sound c-s (%)	RPD drilling avg (%)
BRU0041-PL2-P1.9	K11M-228	750	415	81	12530	13334	16.9	0	crushing (top)	100	10.3

Table A.3.3 Local cross-sectional results

Code	Mass Wet	Mass dry	Moisture Content	Area (wet)	Density wet	Density dry	Maximum force	fc,0,wet	MOE	failure mechanism
[#]	[g]	[g]	[%]	[mm^2]	[kg/m^3]	[kg/m^3]	[kN]	[N/mm^2]	[Mpa]	[N/A]
K11M_1	41.1	21.1	95	429	799	492	7.0	16.3	11300	34.9
K11M_2	31.8	23.3	36	436	607	532	9.4	21.4	14492	31.7
K11M_3	32.3	23.1	40	433	618	504	7.0	16.2	9276	28.2
K11M_4	33.3	24.0	39	444	626	507	9.9	22.2	14956	30.7
K11M_5	47.8	18.6	157	439	905	394	5.1	11.7	6777	20.9
Average	37	22	73	436	711	486	8	18	11360	29

*Figure A.3.2 K11M_228_20*20*120 Dry density & moisture content over cross section*

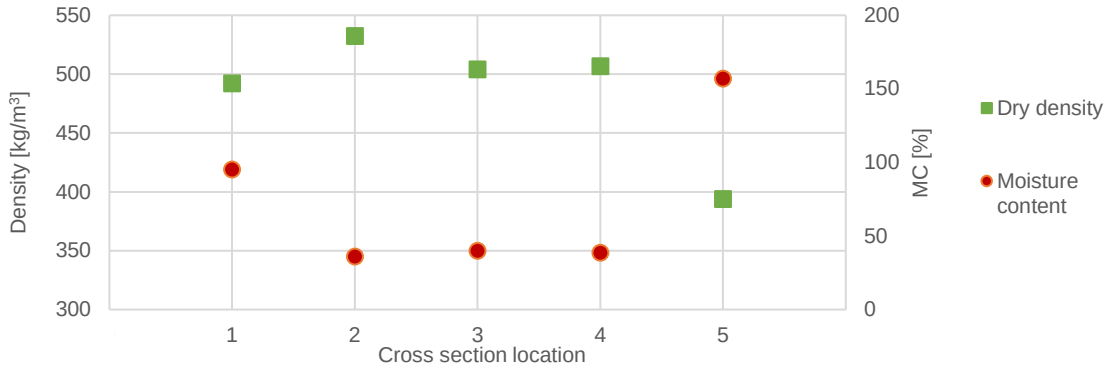

*Figure A.3.3 K11M_228_20*20*120 Ultimate strength through cross section & modulus of elasticity*

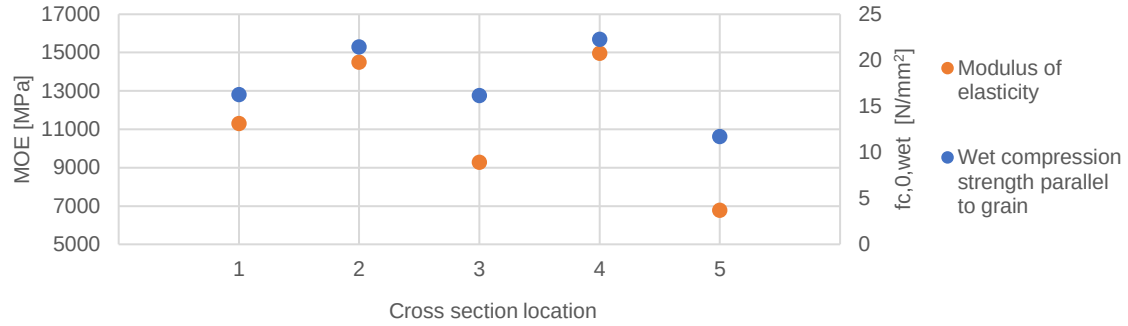

*Figure A.3.4 K11M_20*20*120_Drilling amplitude with ultimate strength.*

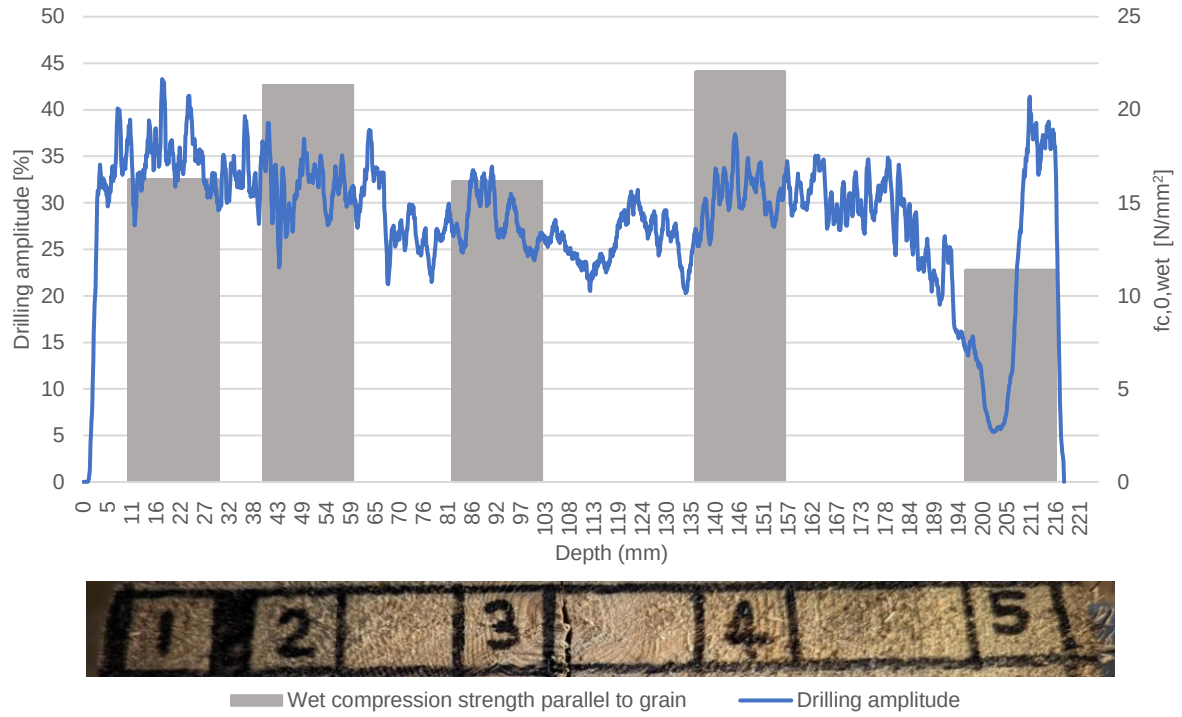

M11M_228

Table A.3.4 Full Specimen Results

Full pile ID	Segment code - container	wet density (kg/m^3)	dry density (kg/m^3)	m.c. (%)	MOE$_{stat}$ (Mpa)	MOE$_{dyn}$ (Mpa)	f_{c0} (Mpa)	soft shell (mm)	failure mechanism	remaining sound c-s (%)	RPD drilling avg (%)
BRU0041-PL2-P1.9	M11M-228	702	396	77	12210	12647	16.3	0	buckling (top)	100	11.2

Table A.3.5 Local cross-sectional results

Code	Mass Wet	Mass dry	Moisture Content	Area (wet)	Density wet	Density dry	Maximum force	fc,0,wet	MOE	RPD drilling avg
[#]	[g]	[g]	[%]	[mm^2]	[kg/m^3]	[kg/m^3]	[kN]	[N/mm^2]	[Mpa]	[%]
M11M_1	47.6	21.1	126	413	958	486	6.3	15.3	9635	24.2
M11M_2	32.4	22.2	46	438	618	481	8.5	19.5	12778	29.0
M11M_3	29.3	19.1	53	441	556	404	5.4	12.1	7384	24.3
M11M_4	32.6	21.6	51	427	635	493	8.5	19.9	12957	30.2
M11M_5	51.2	19.9	157	436	975	443	6.4	14.6	9485	26.7
Average	39	21	87	431	748	461	7	16	10448	26.9

*Figure A.3.5 M11M_228_20*20*120 Dry density & moisture content over cross section*

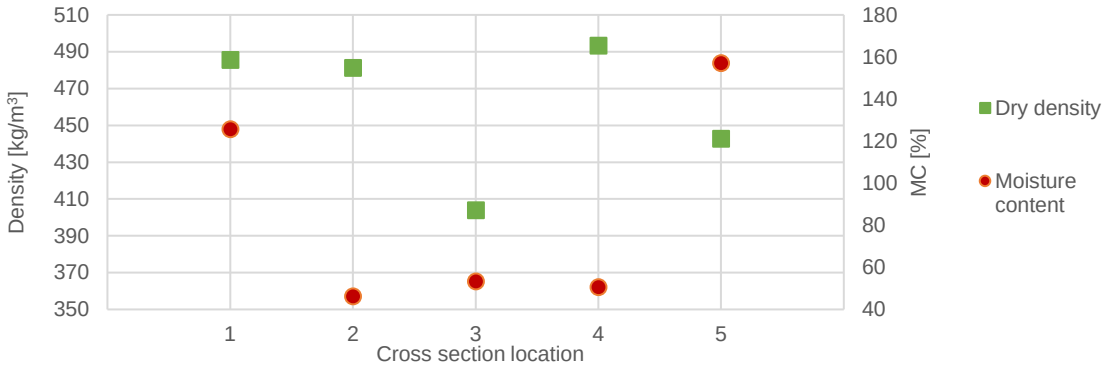

*Figure A.3.6 M11M_228_20*20*120 Ultimate strength through cross section & modulus of elasticity*

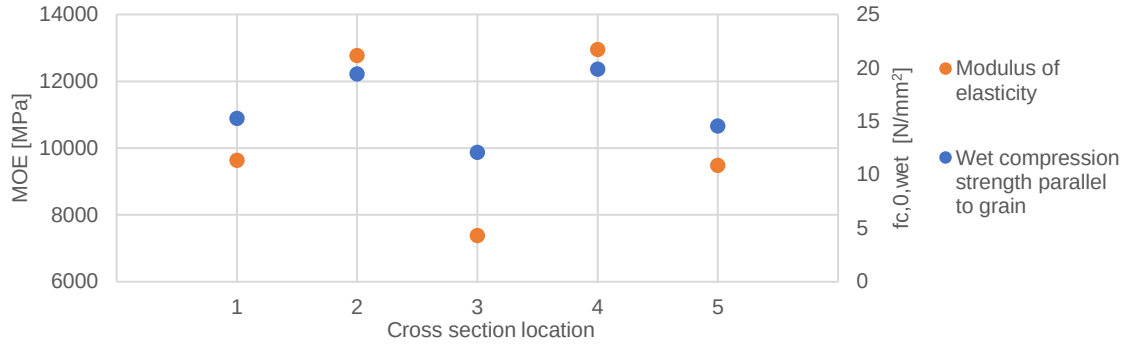

Figure A.3.7 M11M_Drilling amplitude with ultimate strength.

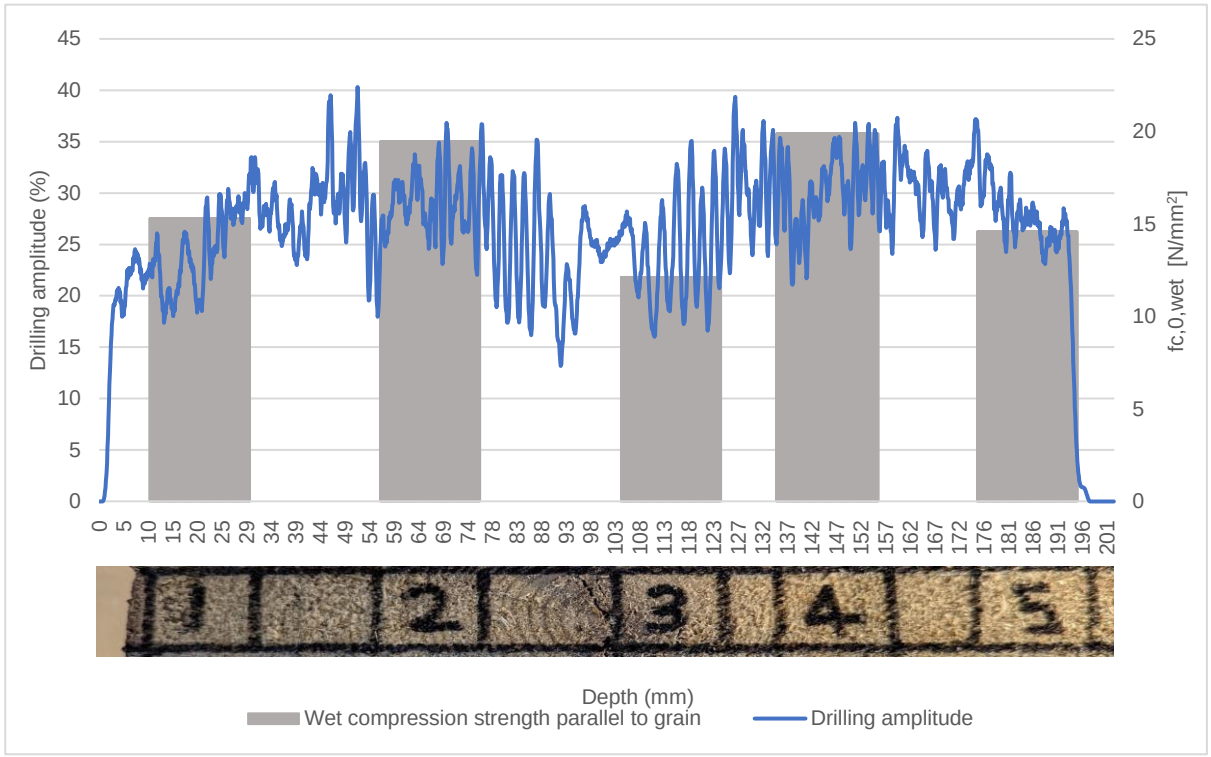

V11M_228

Table A.3.6 Full Specimen Results

Full pile ID	Segment code - container	wet density (kg/m^3)	dry density (kg/m^3)	m.c. (%)	MOE$_{stat}$ (Mpa)	MOE$_{dyn}$ (Mpa)	f_{c0} (Mpa)	soft shell (mm)	failure mechanism	remaining sound c-s (%)	RPD drilling avg (%)
BRU0041 -PL2-P1.9	V11M-228	818	464	76	11140	12202	15.4	0	buckling (top)	100	11.6

Table A.3.7 Local cross-sectional results

Code	Mass Wet	Mass dry	Moisture Content	Area (wet)	Density wet	Density dry	Maximum force	fc,0,wet	MOE
[#]	[g]	[g]	[%]	[mm^2]	[kg/m^3]	[kg/m^3]	[kN]	[N/mm^2]	[Mpa]
V11M_1	50.1	21.0	138	435	962	484	5.6	12.8	8016
V11M_2	35.4	22.8	55	438	671	516	7.4	16.5	10632
V11M_3	32.6	21.0	55	440	618	472	5.8	12.2	7348
V11M_4	41.0	21.9	87	433	789	498	7.4	17.2	11075
V11M_5	42.8	20.0	114	428	832	448	6.6	15.3	10177
Average	40.4	21.4	90	435	774	484	6.6	14.8	9450

*Figure A.3.8 V11M_228_20*20*120 Dry density & moisture content over cross section*

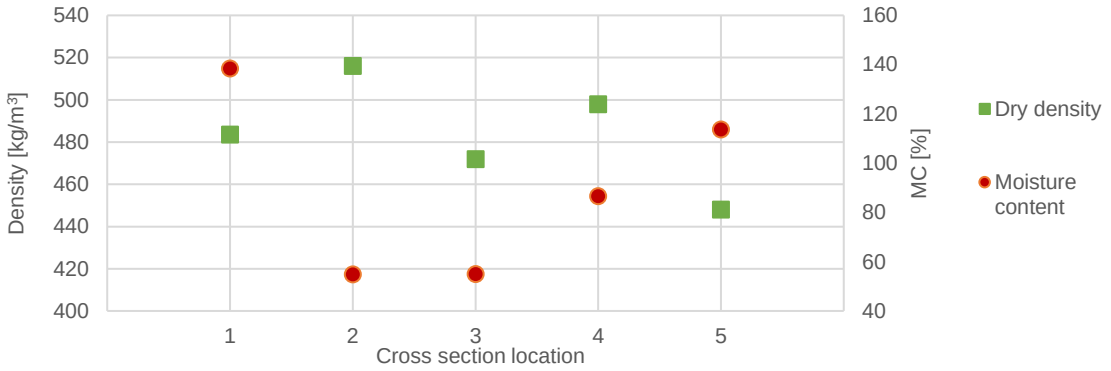

*Figure A.3.9 V11M_228_20*20*120 Ultimate strength through cross section & modulus of elasticity*

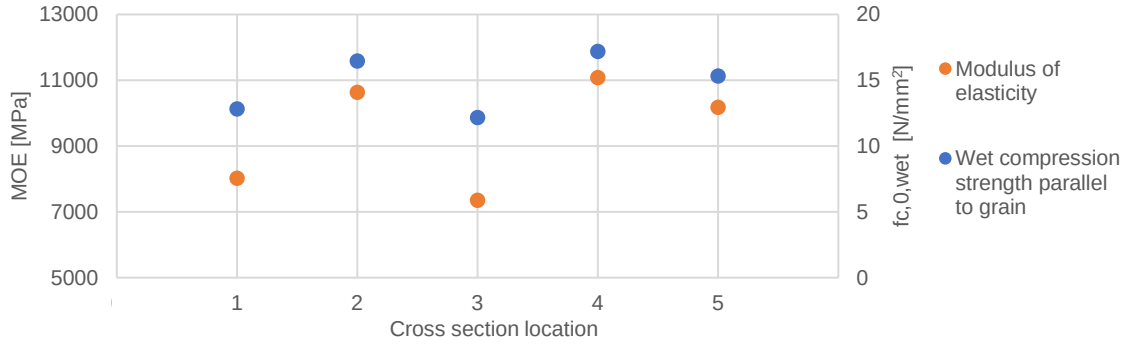

*Figure A.3.10 V11M_20*20*120_Drilling amplitude with ultimate strength.*

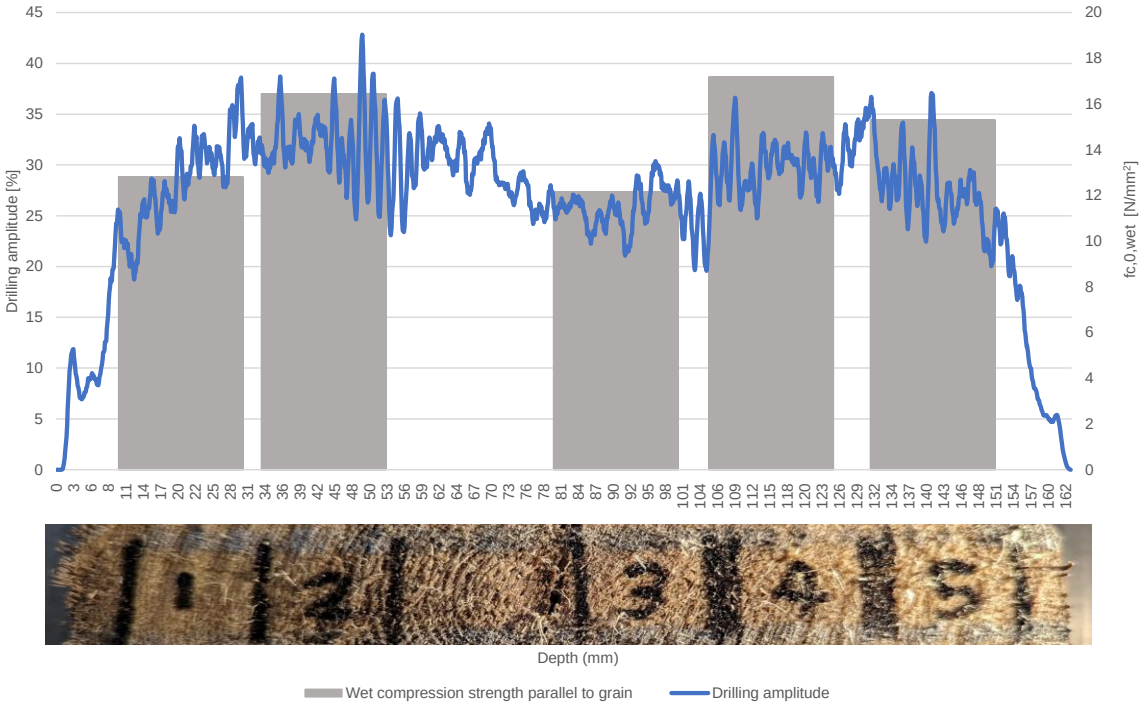

*Table A.3.9 Standard deviation 11M_20*20*120*

Average result	Moisture Content	SD	Density dry	SD	Density wet	SD	fc,0,wet	SD	MOE	SD	RPD drilling average	SD
[#]	[%]	[#]	[kg/m^3]	[#]	[kg/m^3]	[#]	[N/mm^2]	[#]	Mpa	[#]	[%]	[#]
11M_1	120	22.2	487	4.5	906	92.9	15	1.8	9650	1641.6	29	5.4
11M_2	46	9.4	510	26.2	632	34.1	19	2.5	12634	1933.8	31	1.8
11M_3	49	8.3	460	51.2	597	35.8	13	2.3	8003	1103.1	26	2.0
11M_4	59	25.0	499	6.8	683	91.6	20	2.5	12996	1940.8	30	0.4
11M_5	143	24.9	428	29.9	904	71.7	14	1.9	8813	1797.3	25	3.7

*Figure A.3.11 Standard deviation 11M_20*20*120*

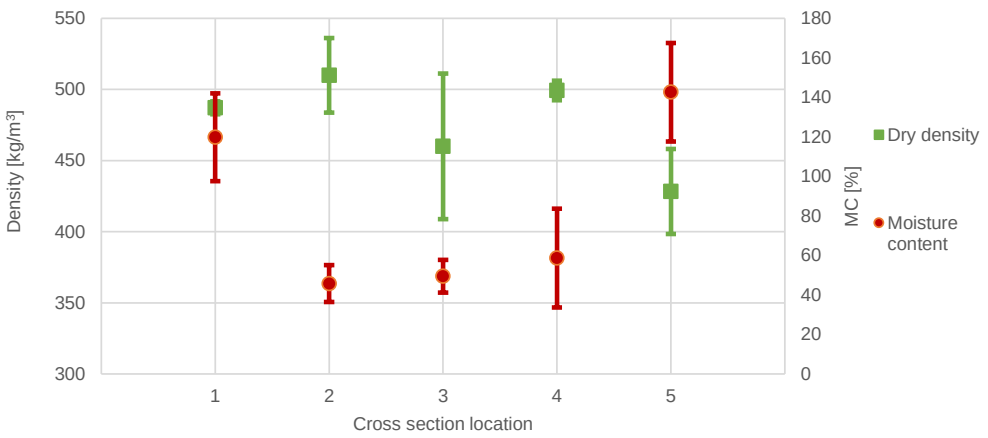

*Figure A.3.11 Standard deviation 11M_20*20*120*

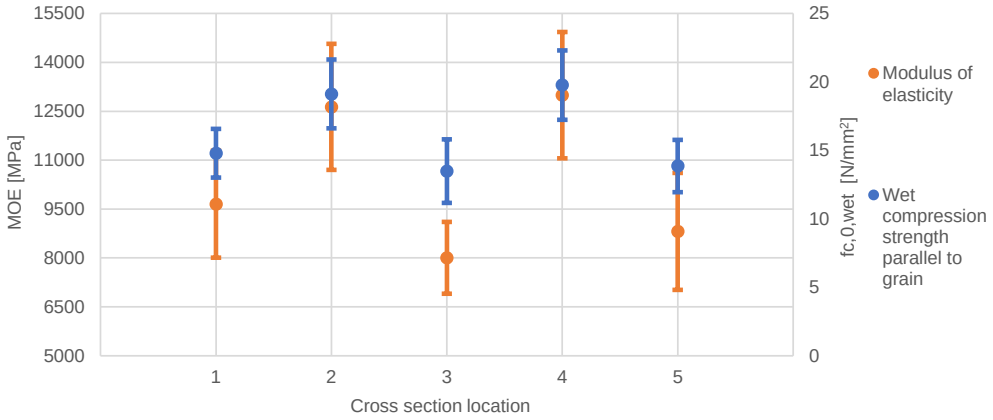

BRU0041-PL2-P1.9- 11M – 20*20*60mm

Pile BRU0041-PL2-P1.9 from 1922. With a segment code of 11M from container 228 has been split into 3 sections known as the tip, middle-part and head as can be seen below in the image. From these sections, a segment of approximately 150mm in length was extracted so that the small samples could be manufactured. The results of each full pile segment and subsequent small samples are highlighted below. Figure 89 Full section codes with local cross sections extracted and small specimen locations.

*Figure A.3.12 Full pile specimens 11M_20*20*60*

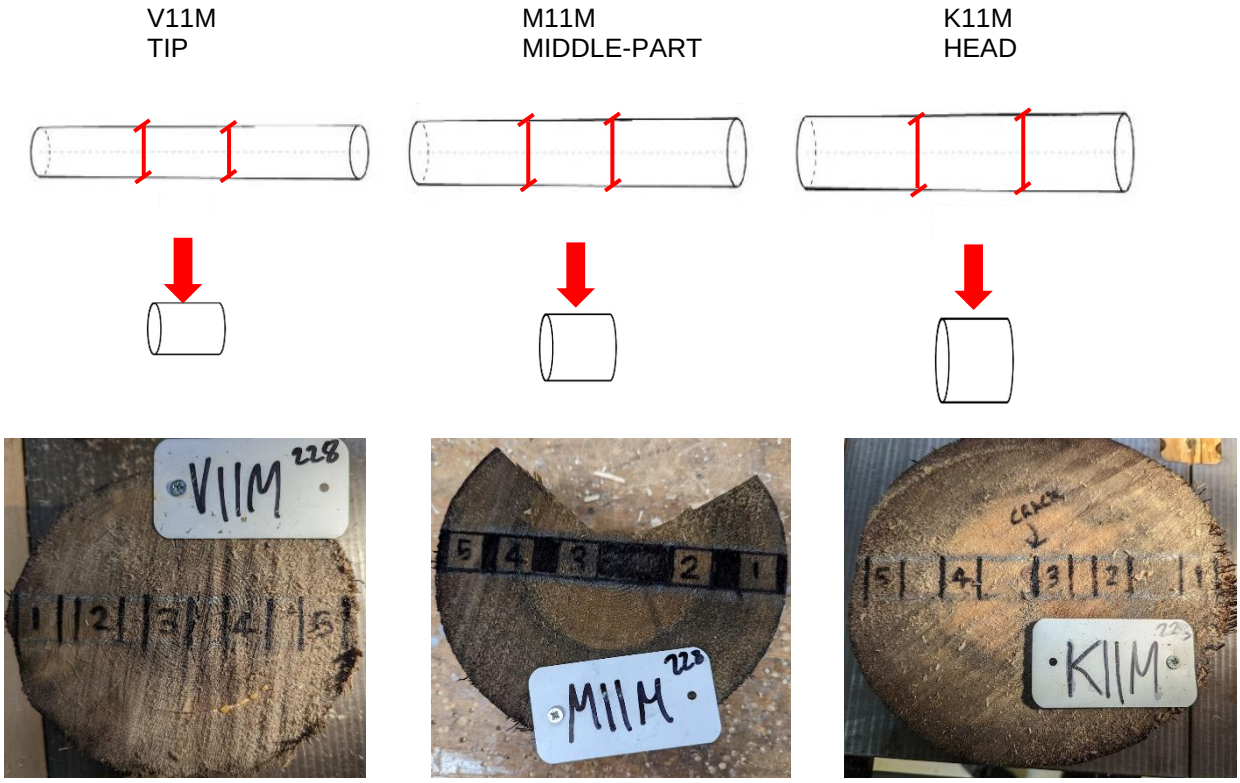

Table A.3.10 Summary of results for full sections and average small samples.

Specimen	Part	Density wet	Density dry	Ultimate strength	MOE_{stat}	MOE_{dyn} (Mpa)	RPD drilling average
[#]	[#]	kg/m^3]	kg/m^3]	[N/mm^2]	Mpa	Mpa	[%]

Full size	K	750	415	16.9	12530	13334	10.3
	M	702	396	16.3	12210	12647	11.2
	V	818	464	15.4	11140	12202	11.6
Local samples average	K	711	486	17.6	11360	[N/A]	29.3
	M	748	461	16.3	10448	[N/A]	26.9
	V	774	484	14.8	9450	[N/A]	28.8

K11M_228

Table A.3.11 Full Specimen Results

Full pile ID	Segment code - container	wet density (kg/m^3)	dry density (kg/m^3)	m.c. (%)	MOE_{stat} (Mpa)	MOE_{dyn} (Mpa)	f_{c0} (Mpa)	soft shell (mm)	failure mechanism	remaining sound c-s (%)	RPD drilling avg (%)
BRU0041-PL2-P1.9	K11M-228	750	415	81	12530	13334	16.9	0	crushing (top)	100	10.3

Table A.3.12 Local 60mm cross-sectional results

Code	Mass Wet	Mass dry	Moisture Content	Area (wet)	Density wet	Density dry	Ultimate force	Ultimate strength	RPD drilling average
[#]	[g]	[g]	[%]	[mm^2]	kg/m^3]	kg/m^3]	[kN]	[N/mm^2]	[%]
K11M_1	20.9	8.2	155	418	835	372	4.77	11.41	17.7
K11M_2	18.1	12.1	49	428	706	532	12.59	29.41	30.7
K11M_3	17.8	12.7	40	434	679	555	8.64	19.89	26.7
K11M_4	18.6	13.3	40	437	703	556	9.84	22.50	28.5
K11M_5	22.8	11.5	98	437	871	485	8.58	19.64	34.9
Average	19.6	11.6	77	431	759	500	8.9	20.6	27.7

*Figure A.3.13 K11M_228_20*20*60_Dry density & moisture content over cross section*

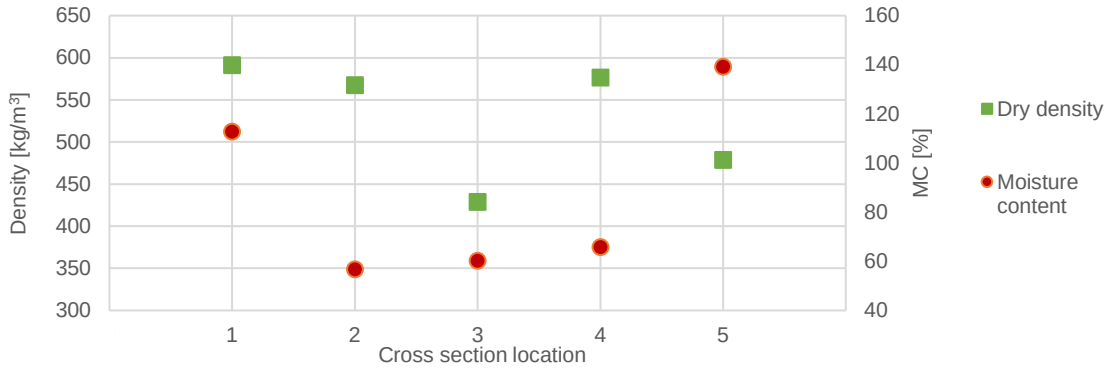

*Figure A.3.14 K11M_228_20*20*60 _Drilling amplitude with ultimate strength.*

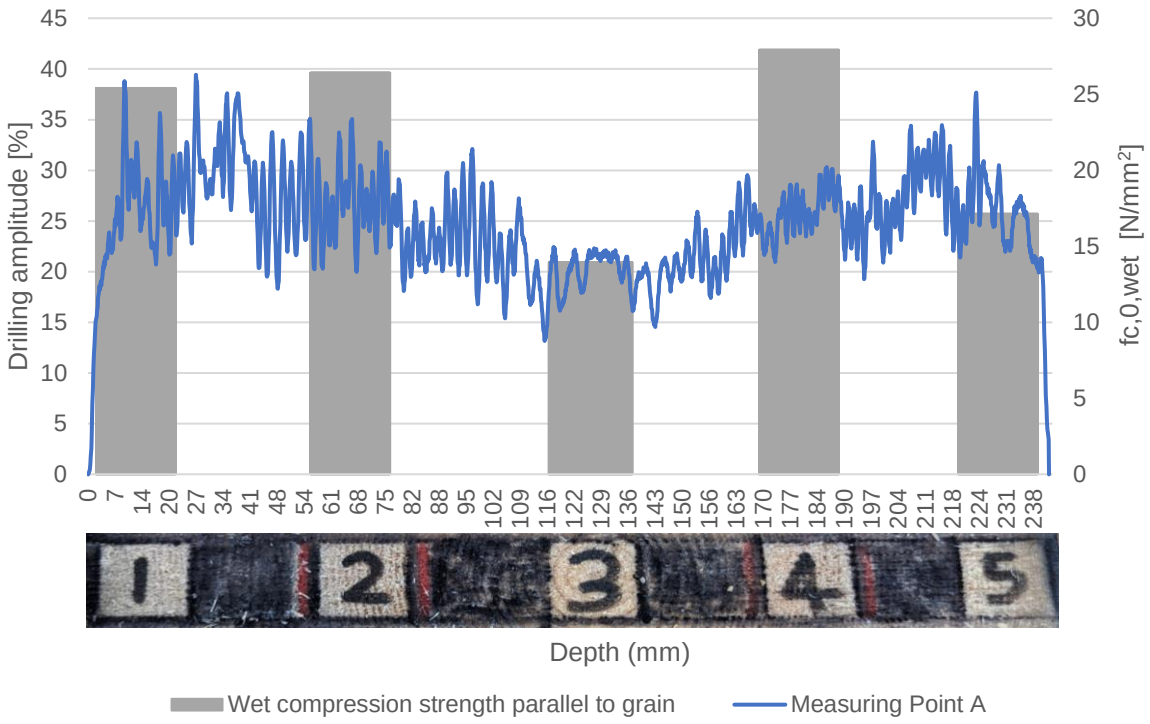

M11M_228

Table A.3.13 Full Specimen Results

Full pile ID	Segment code - container	wet density (kg/m^3)	dry density (kg/m^3)	m.c. (%)	MOE$_{stat}$ (Mpa)	MOE$_{dyn}$ (Mpa)	f_{c0} (Mpa)	soft shell (mm)	failure mechanism	remaining sound c-s (%)	RPD drilling avg (%)
BRU0041-PL2-P1.9	M11M-228	702	396	77	12210	12647	16.3	0	buckling (top)	100	11.2

Table A.3.14 Local 60mm cross-sectional results

Code	Mass Wet	Mass dry	Moisture Content	Area (wet)	Density wet	Density dry	Ultimate force	Ultimate strength	RPD drilling average
[#]	[g]	[g]	[%]	[mm^2]	kg/m^3]	kg/m^3]	[kN]	[N/mm^2]	[%]
M11M_1	20.83	10.27	103	436	797	460	7.38	16.92	28.7
M11M_2	17.04	11.36	50	435	653	526	8.85	20.36	29.9
M11M_3	15.48	10.40	49	442	584	456	7.06	15.96	27.3
M11M_4	18.76	10.67	76	438	716	490	8.02	18.33	29.4
M11M_5	19.99	8.73	129	432	771	402	4.59	10.61	20.2
Average	18.4	10.3	81	437	704	467	7.2	16.4	27.1

*Figure A.3.15 M11M _228_20*20*60 Dry density & moisture content over cross section*

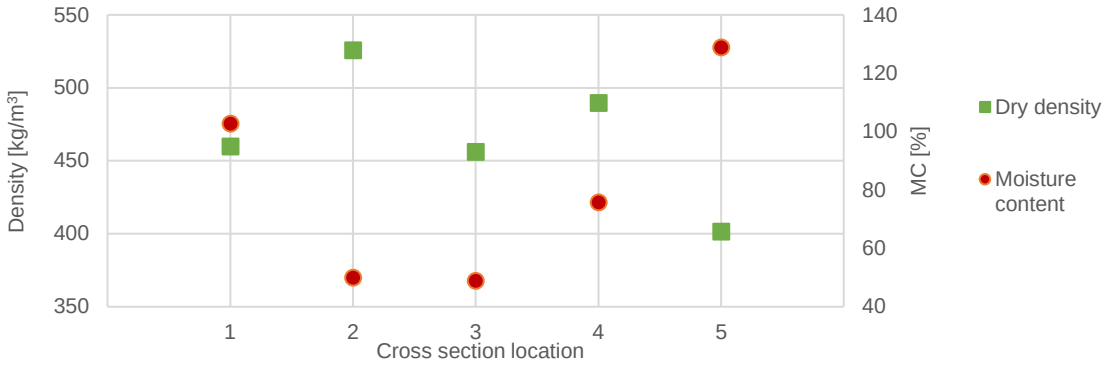

*Figure A.3.16 M11M _228_20*20*60 _Drilling amplitude with ultimate strength.*

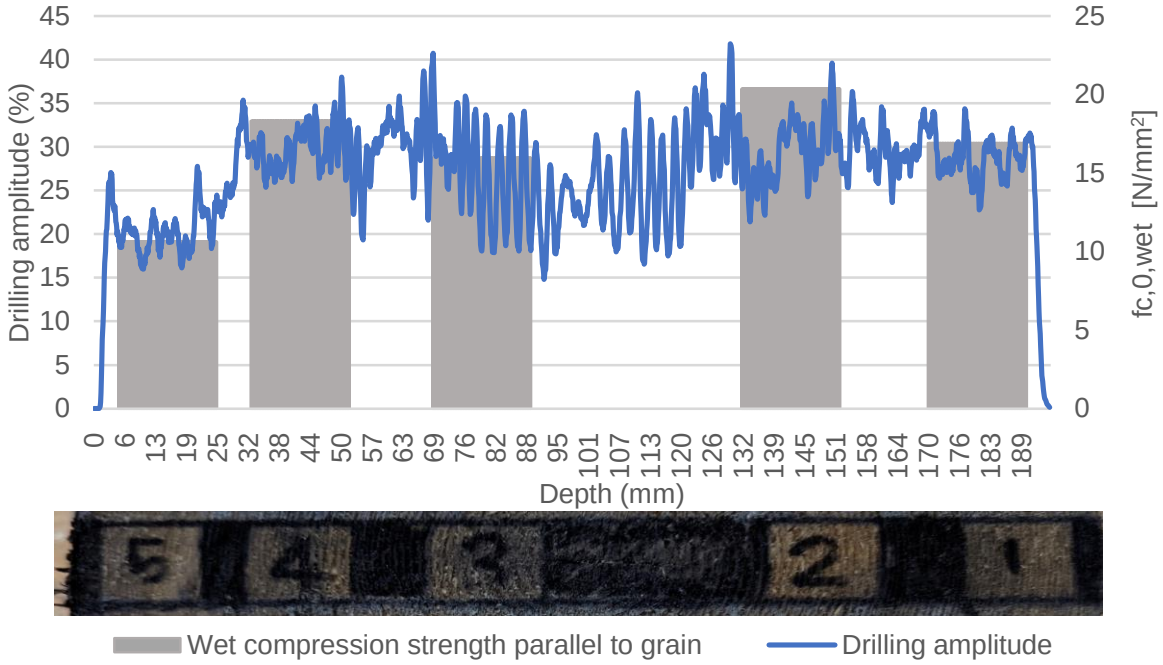

V11M_228

Table A.3.15 Full Specimen Results

Full pile ID	Segment code - container	wet density (kg/m³)	dry density (kg/m³)	m.c. (%)	MOE_{stat} (Mpa)	MOE_{dyn} (Mpa)	f_{c0} (Mpa)	soft shell (mm)	failure mechanism	remaining sound c-s (%)	RPD drilling avg (%)
BRU0041 -PL2-P1.9	V11M-228	818	464	76	11140	12202	15.4	0	buckling (top)	100	11.6

Table A.3.16 Local 60mm cross-sectional results

Code	Mass Wet	Mass dry	Moisture Content	Area (wet)	Density wet	Density dry	Ultimate force	Ultimate strength	RPD drilling average
[#]	[g]	[g]	[%]	[mm²]	kg/m³]	kg/m³]	[kN]	[N/mm²]	[%]
V11M_1	19.7	10.3	91	421	782	478	5.15	12.24	25.2
V11M_2	22.3	10.0	122	429	870	450	6.13	14.29	30.0
V11M_3	14.7	10.2	43	441	556	457	6.84	15.50	35.2
V11M_4	17.0	10.2	67	442	643	460	7.27	16.43	31.7
V11M_5	19.8	9.6	105	422	785	463	5.63	13.35	27.1

Average	18.7	10.1	85.7	431.0	727.3	461.7	6.2	14.4	29.8

*Figure A.3.17 V11M_228_20*20*60 Dry density & moisture content over cross section*

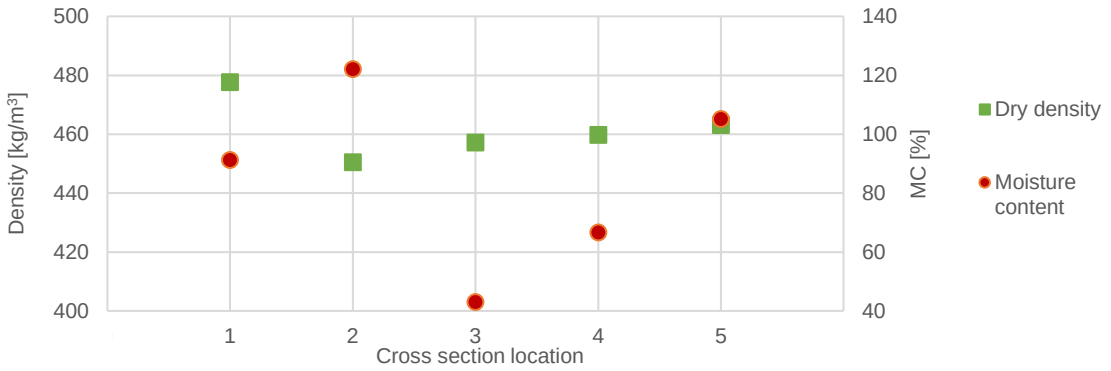

*Figure A.3.18 V11M_228_20*20*60 _Drilling amplitude with ultimate strength.*

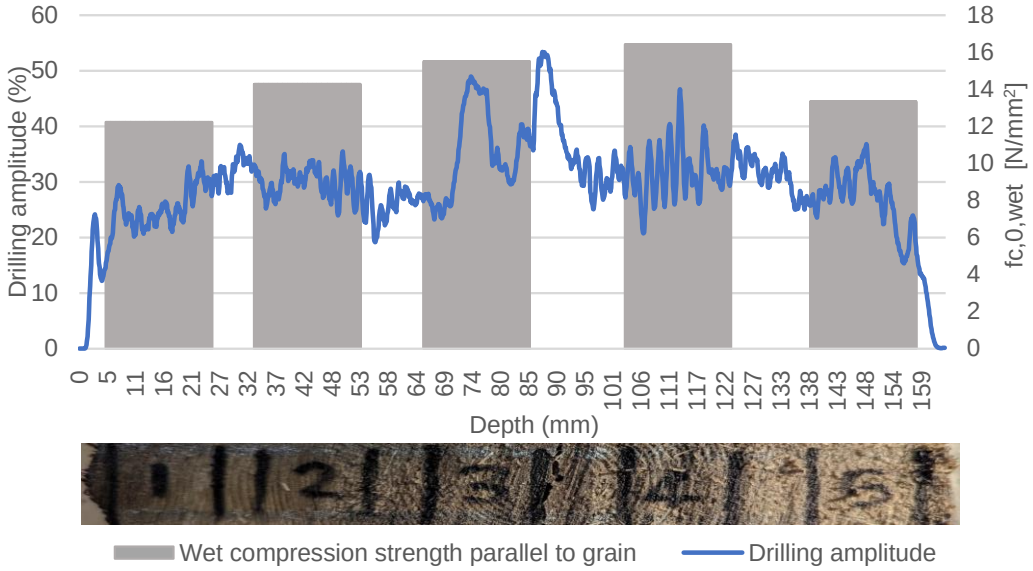

A.4 - 3.18M (1886)BRU0030-PL1-P3.18

Pile BRU0030-PL1-P3.18 from 1886. With a segment code of 3.18M from container 115 has been split into 3 sections known as the tip, middle-part and head as can be seen below in the image. From these sections, a segment of approximately 150mm in length was extracted so that the small samples could be manufactured. The results of each full pile segment and subsequent 20*20*120mm local samples are highlighted below.

Figure A.4.1 Full section codes with local cross sections extracted and small specimen locations.

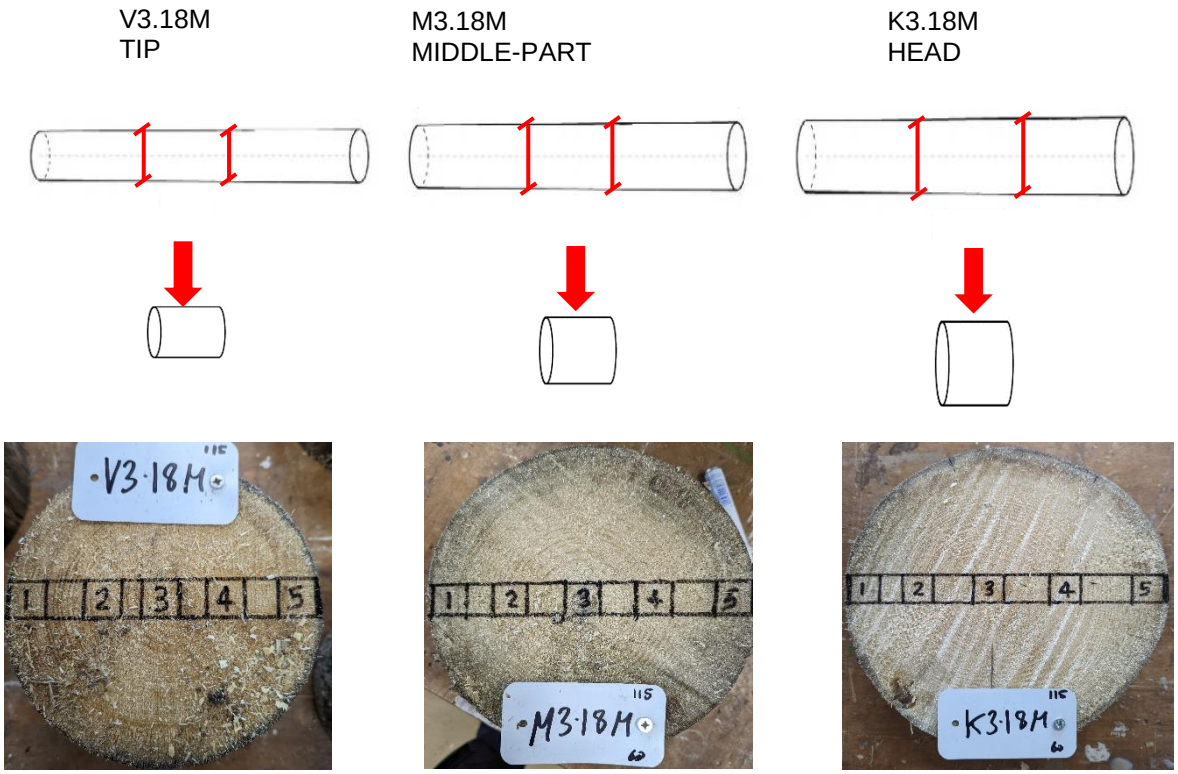

Table A.4.1 Summary of results for full sections and average small samples.

Specimen	Part	Density wet	Density dry	Ultimate strength	MOE_{stat}	MOE_{dyn} (Mpa)	RPD drilling average
[#]	[#]	kg/m^3]	kg/m^3]	[N/mm^2]	Mpa	Mpa	[%]
Full size	K	582	373	14.9	10766	11398	18.8
	M	595	390	14.2	10179	10935	15.0
	V	668	363	12.1	8990	10434	14.3
Local samples average	K	540	410	13.2	5289	[N/A]	16.3
	M	530	411	13.2	5604	[N/A]	17.3
	V	568	422	13.3	7342	[N/A]	15.9

K3.18M_115

Table A.4.2 Full Specimen Results

Full pile ID	Segment code - container	wet density (kg/m^3)	dry density (kg/m^3)	m.c. (%)	MOE_{stat} (Mpa)	MOE_{dyn} (Mpa)	f_{c0} (Mpa)	soft shell (mm)	failure mechanism	remaining sound c-s (%)	RPD drilling avg (%)
BRU0030-PL1-P3.18	K3.18-115	582	373	56	10766	11398	14.9	13.75		89	18.8

Table A.4.3 Local cross-sectional results

Code	Mass Wet	Mass dry	Moisture Content	Area (wet)	Density wet	Density dry	Ultimate force	Ultimate strength	MOE	RPD drilling average
[#]	[g]	[g]	[%]	[mm^2]	[kg/m^3]	[kg/m^3]	[kN]	[N/mm^2]	Mpa	[%]
K3.18M_1	34.53	20.21	71	416	691	487	7.3	17.5	7909	20.3
K3.18M_2	24.36	17.09	43	417	485	388	6.3	15.1	5990	15.7
K3.18M_3	27.35	16.91	62	415	549	376	3.5	8.5	2687	12.8
K3.18M_4	22.10	15.37	44	418	439	351	4.2	10.2	3857	15.4
K3.18M_5	27.44	18.97	45	426	537	450	6.3	14.8	6001	17.0
Average	27.2	17.7	53	418	540	410	5.5	13.2	5289	16.3

*Figure A.4.2 K3.18M_115_20*20*120 Dry density & moisture content over cross section*

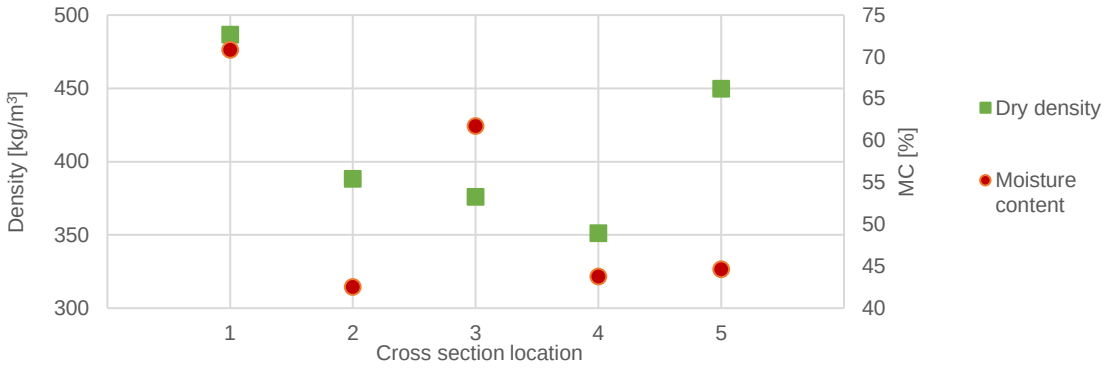

*Figure A.4.3 K3.18M_115_20*20*120 Ultimate strength through cross section & modulus of elasticity*

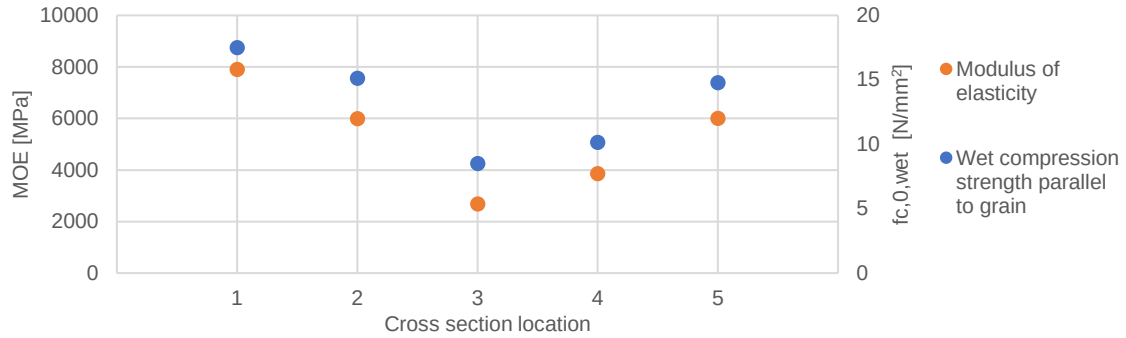

*Figure A.4.4 K3.18M_115_20*20*120 _Drilling amplitude with ultimate strength.*

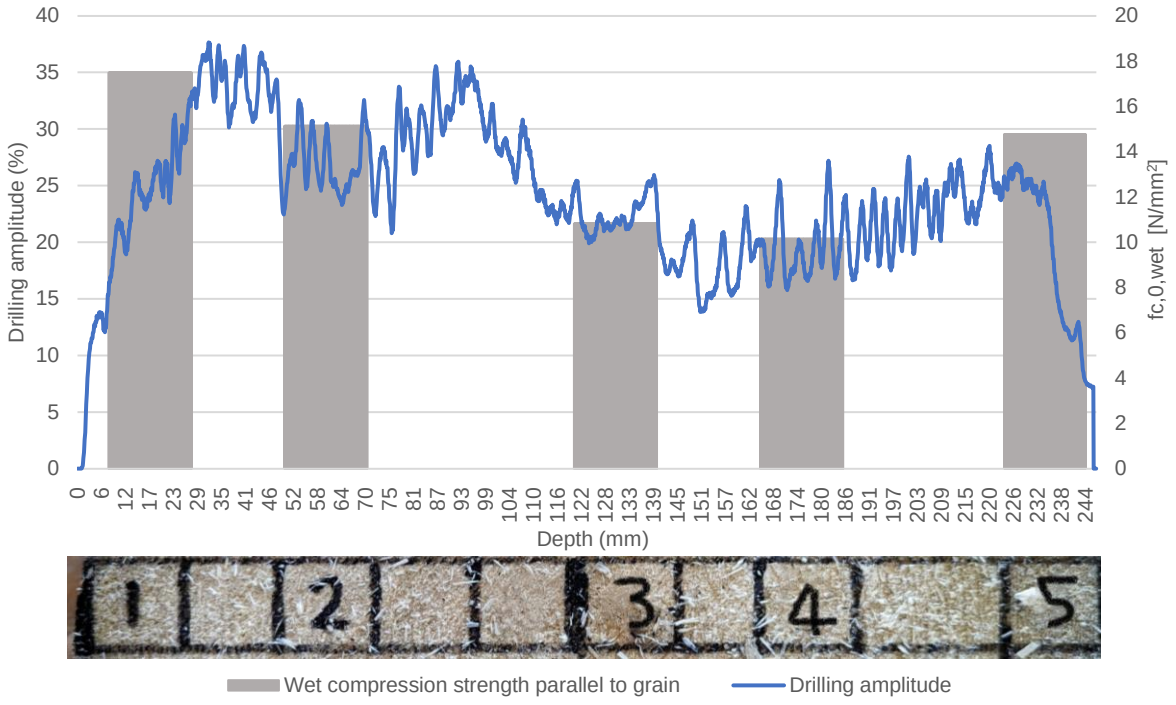

M3.18M_115

Table A.4.4 Full Specimen Results

Full pile ID	Segment code - container	wet density (kg/m³)	dry density (kg/m³)	m.c. (%)	MOE_{stat} (Mpa)	MOE_{dyn} (Mpa)	f_{c0} (Mpa)	soft shell (mm)	failure mechanism	remaining sound c-s (%)	RPD drilling avg (%)
BRU0030-PL1-P3.18	M3.18-115	595	390	52	10179	10935	14.22	1.7		98	15

Table A.4.5 Local cross-sectional results

Code	Mass Wet	Mass dry	Moisture Content	Area (wet)	Density wet	Density dry	Ultimate force	Ultimate strength	MOE	RPD drilling average
[#]	[g]	[g]	[%]	[mm²]	kg/m³]	kg/m³]	[kN]	[N/mm²]	Mpa	[%]
M3.18M_1	29.0	19.7	47	415	582	468	5.60	13.50	5766	18
M3.18M_2	24.1	16.4	47	419	479	378	5.70	13.62	6210	16
M3.18M_3	24.8	16.7	48	416	496	376	4.50	10.83	3755	15
M3.18M_4	23.9	17.1	40	415	479	384	4.87	11.73	3821	16
M3.18M_5	31.4	20.2	55	424	615	450	7.00	16.51	8466	21
Average	26.6	18.0	47.4	417.7	530.1	411.2	5.5	13.2	5603.6	17.3

*Figure A.4.5 M3.18M_115 _20*20*120 Dry density & moisture content over cross section*

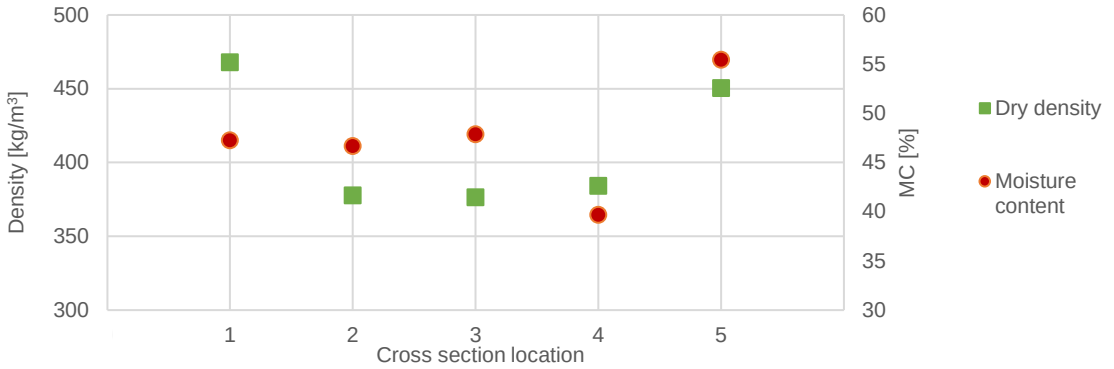

*Figure A.4.6 M3.18M_115 _20*20*120 Ultimate strength through cross section & modulus of elasticity*

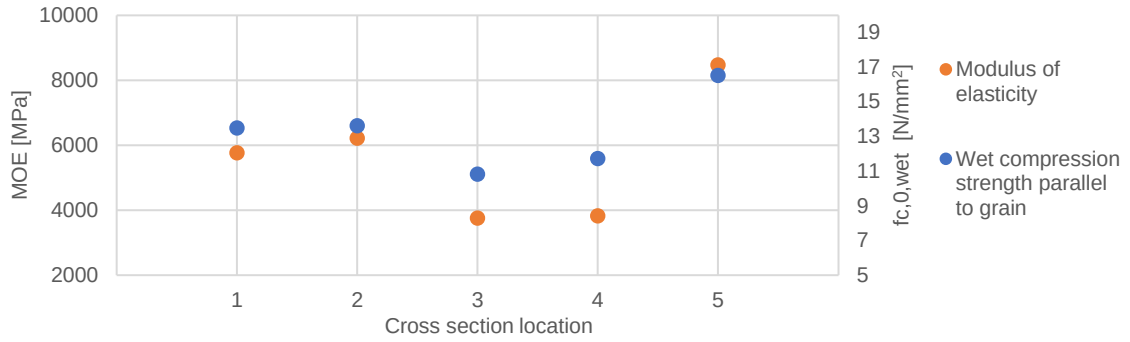

*Figure A.4.7 M3.18M_115 _20*20*120 _Drilling amplitude with ultimate strength.*

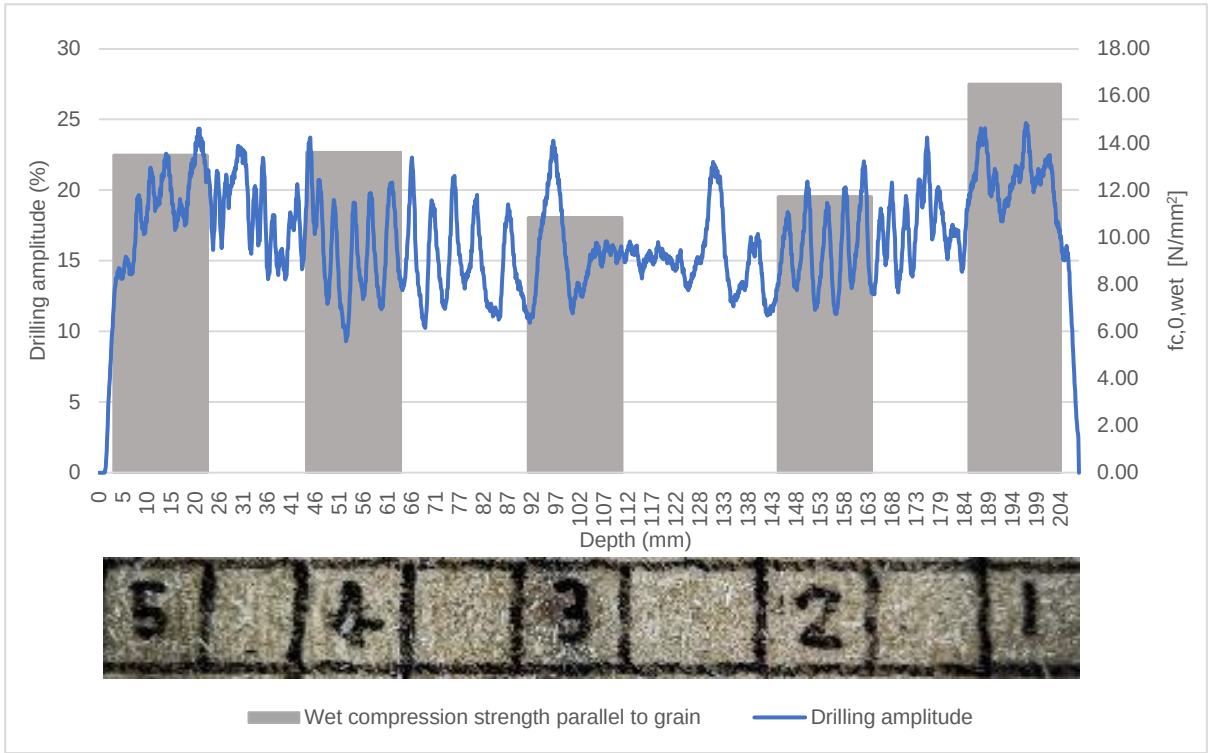

V3.18M_115

Table A.4.6 Full Specimen Results

Full pile ID	Segment code - container	wet density (kg/m^3)	dry density (kg/m^3)	m.c. (%)	MOE_{stat} (Mpa)	MOE_{dyn} (Mpa)	f_{c0} (Mpa)	soft shell (mm)	failure mechanism	remaining sound c-s (%)	RPD drilling avg (%)
BRU0030-PL1-P3.18	V3.18-115	668	363	84	8990	10434	12.1	3.8		96	14.3

Table A.4.7 Local cross-sectional results

Code	Mass Wet	Mass dry	Moisture Content	Area (wet)	Density wet	Density dry	Ultimate force	Ultimate strength	MOE	RPD drilling average
[#]	[g]	[g]	[%]	[mm^2]	[kg/m^3]	[kg/m^3]	[kN]	[N/mm^2]	Mpa	[%]
V3.18M_1	32.41	23.31	39.04	409.05	646.80	533.34	7.92	19.36	11984.81	19.70
V3.18M_2	23.30	16.27	43.21	408.23	466.80	369.09	5.38	13.18	8025.59	16.20
V3.18M_3	25.87	16.58	56.03	411.26	513.50	367.60	3.32	8.07	3818.71	14.30
V3.18M_4	31.58	16.67	89.44	410.05	627.83	381.33	4.45	10.85	4751.91	12.60
V3.18M_5	29.46	19.21	53.36	410.87	585.60	460.09	6.20	15.09	8129.36	16.90
Average	28.5	18.4	56.2	409.9	568.1	422.3	5.5	13.3	7342.1	15.9

*Figure A.4.8 V3.18M_115_20*20*120 Dry density & moisture content over cross section*

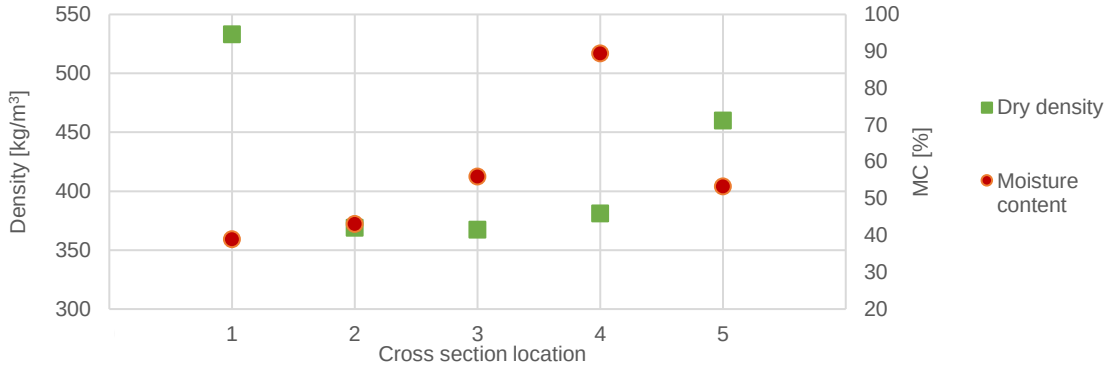

*Figure A.4.9 V3.18M_115_20*20*120 Ultimate strength through cross section & modulus of elasticity*

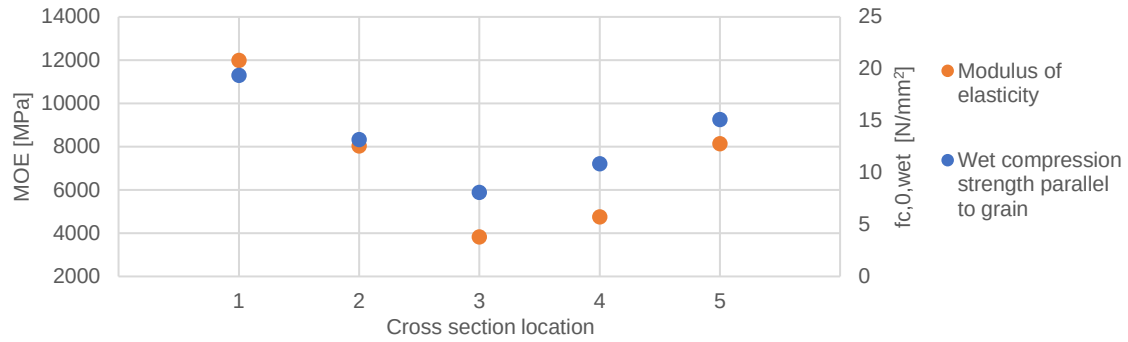

*Figure A.4.10 V3.18M_115_20*20*120 _Drilling amplitude with ultimate strength.*

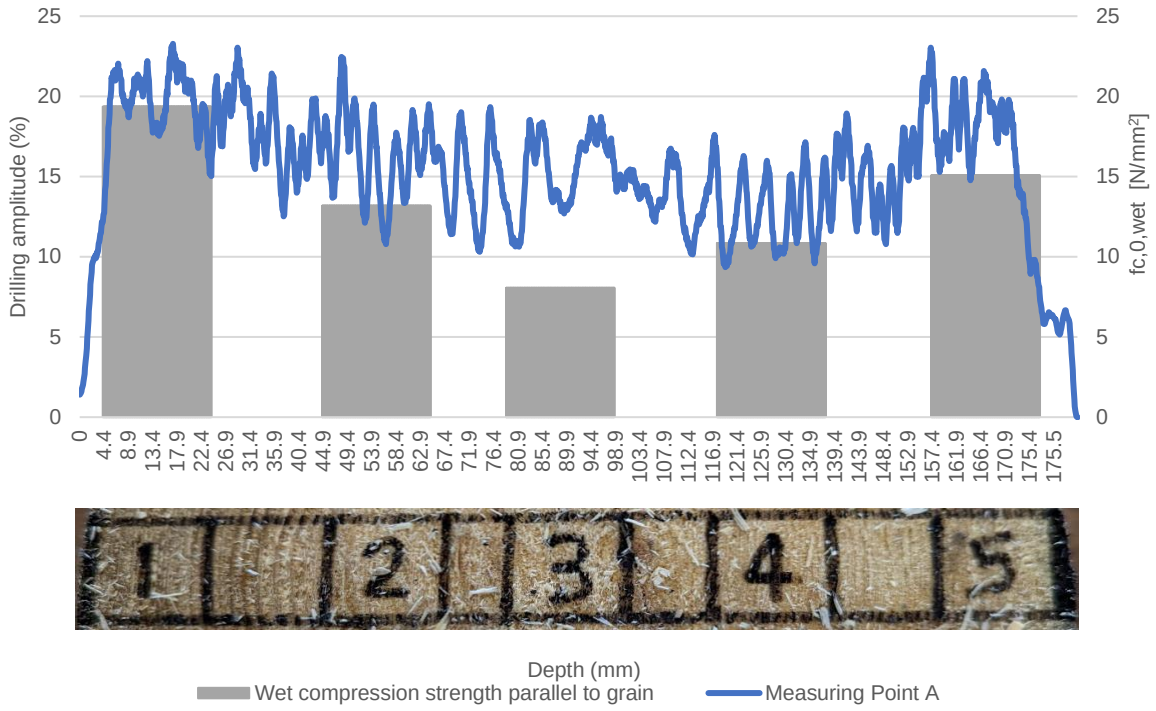

Table A.4.8 Standard deviation

Average result	Moisture Content	SD	Density dry	SD	Density wet	SD	fc,0,wet	SD	MOE	SD	RPD drilling average	SD
[#]	[%]	[#]	[kg/m^3]	[#]	[kg/m^3]	[#]	[N/mm^2]	[#]	Mpa	[#]	[%]	[#]
3.18M_1	52	16.5	496	33.7	640	55.0	17	3.0	8553	3158.9	19	1.1
3.18M_2	44	2.2	378	9.6	477	9.4	14	1.0	6742	1117.3	16	0.3
3.18M_3	55	7.0	373	4.9	519	27.0	9	1.5	3420	635.7	14	1.3
3.18M_4	58	27.6	372	18.3	515	99.6	11	0.8	4143	527.3	15	1.8
3.18M_5	51	5.7	453	5.8	579	39.8	15	0.9	7532	1336.5	18	2.3

Figure A.4.11 Standard deviation

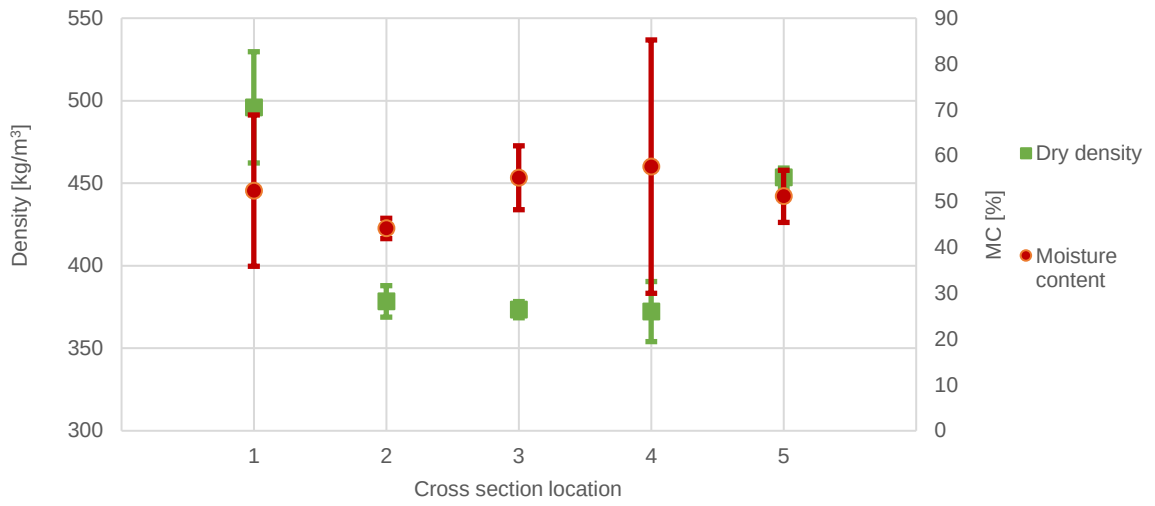

Figure A.4.12 Standard deviation

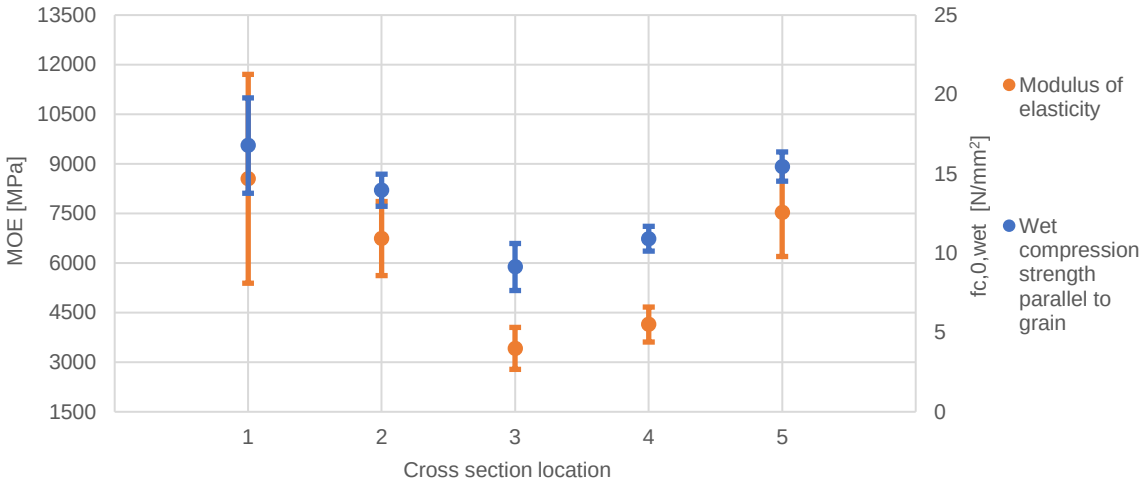

BRU0030-PL1-P3.18- full pile

Pile BRU0030-PL1-P3.18 from 1886. With a segment code of 3.18M from container 115 has been split into 3 sections known as the tip, middle-part and head as can be seen below in the image. From these sections, a segment of approximately 80mm in length was extracted so that the small samples could be manufactured. The results of each full pile segment and subsequent small samples are highlighted below.

Figure A.4.13 Full section codes with local cross sections extracted and small specimen locations.

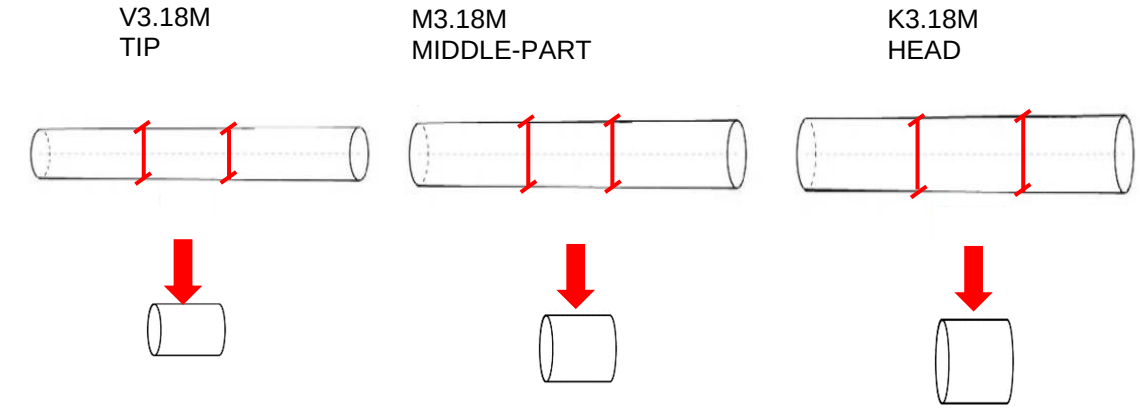

Table A.4.9 Summary of results for full sections and average small samples.

Specimen	Part	Density wet	Density dry	Ultimate strength	MOE_{stat}	MOE_{dyn} (Mpa)	RPD drilling average
[#]	[#]	kg/m^3]	kg/m^3]	[N/mm^2]	Mpa	Mpa	[%]
Full size	K	582	373	14.9	10766	11398	18.8
	M	595	390	14.2	10179	10935	15.0
	V	668	363	12.1	8990	10434	14.3
Local samples average	K	532	411	14.1	[N/A]	[N/A]	15.9
	M	530	421	14.4	[N/A]	[N/A]	17.1
	V	566	429	14.1	[N/A]	[N/A]	15.4

K3.18M_115

Table A.4.10 Full Specimen Results

Full pile ID	Segment code - container	wet density (kg/m^3)	dry density (kg/m^3)	m.c. (%)	MOE_{stat} (Mpa)	MOE_{dyn} (Mpa)	f_{c0} (Mpa)	soft shell (mm)	failure mechanism	remaining sound c-s (%)	RPD drilling avg (%)
BRU0030-PL1-P3.18	K3.18-115	582	373	56	10766	11398	14.9	13.75		89	18.8

Table A.4.11 Local 60mm cross-sectional results

Code	Mass Wet	Mass dry	Moisture Content	Area (wet)	Density wet	Density dry	Ultimate force	Ultimate strength	RPD drilling average
[#]	[g]	[g]	[%]	[mm^2]	kg/m^3]	kg/m^3]	[kN]	[N/mm^2]	[%]
K3.18M_1	15.52	9.86	57	416	619	462	6.54	15.72	18.4
K3.18M_2	11.22	7.98	41	417	449	377	6.09	14.60	15.5

K3.18M_3	14.44	8.59	68	415	580	384	4.86	11.70	13.1
K3.18M_4	10.99	7.82	41	417	437	367	5.31	12.72	14.2
K3.18M_5	14.31	9.84	45	414	576	467	6.56	15.85	18.5
Average	13.3	8.8	50	416	532	411	5.9	14.1	15.9

Graphical results

*Figure A.4.14 K3.18M_115_20*20*60 Dry density & moisture content over cross section*

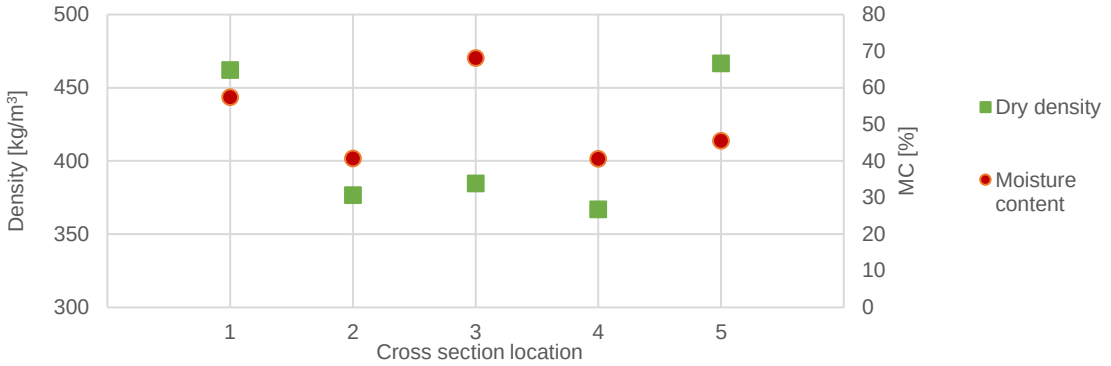

*Figure A.4.15 K3.18M_115_20*20*60 _Drilling amplitude with ultimate strength.*

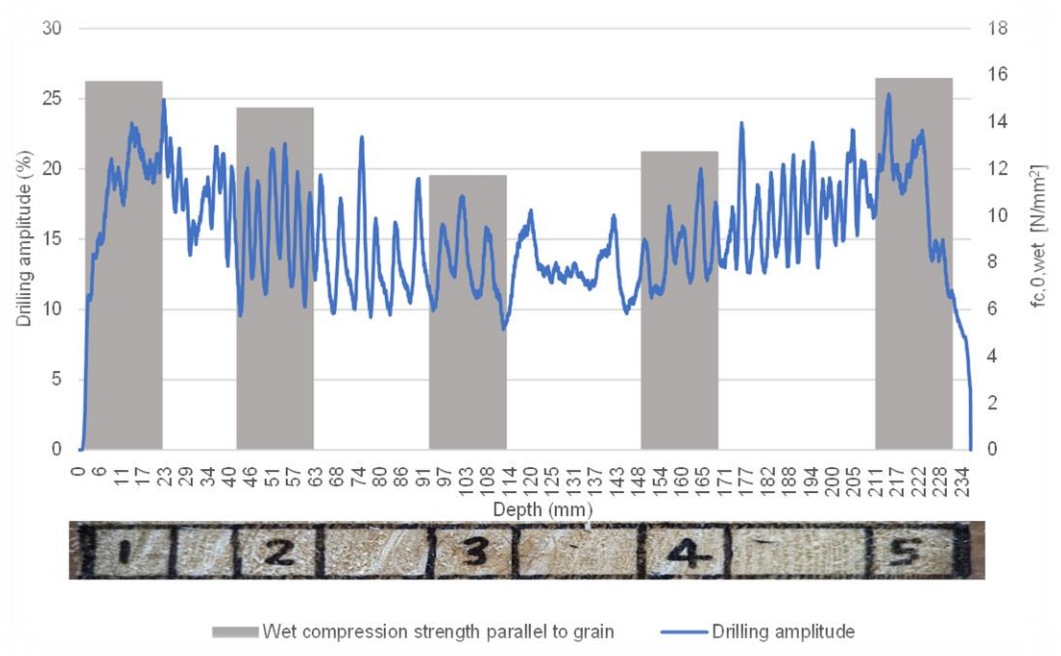

M3.18M_115

Table A.4.12 Full Specimen Results

Full pile ID	Segment code - container	wet density (kg/m^3)	dry density (kg/m^3)	m.c. (%)	MOE_{stat} (Mpa)	MOE_{dyn} (Mpa)	f_{c0} (Mpa)	soft shell (mm)	failure mechanism	remaining sound c-s (%)	RPD drilling avg (%)
BRU0030-PL1-P3.18	M3.18-115	595	390	52	10179	10935	14.22	1.7		98	15

Table A.4.13 Local 60mm cross-sectional results

Code	Mass Wet	Mass dry	Moisture Content	Area (wet)	Density wet	Density dry	Ultimate force	Ultimate strength	RPD drilling average
[#]	[g]	[g]	[%]	[mm^2]	[kg/m^3]	[kg/m^3]	[kN]	[N/mm^2]	[%]
M3.18M_1	16.09	10.53	52.80	419.61	641.54	489.56	6.89	16.42	19.4
M3.18M_2	12.19	8.91	36.81	424.76	480.71	395.77	6.55	15.42	15.8
M3.18M_3	11.74	8.30	41.45	425.79	462.15	372.41	4.44	10.43	14.6
M3.18M_4	11.30	8.10	39.51	420.03	450.41	374.92	5.65	13.45	14.8
M3.18M_5	15.63	9.91	57.72	425.60	617.23	470.56	7.03	16.52	20.7
Average	13.4	9.2	45.7	423.2	530.4	420.6	6.1	14.4	17.1

Graphical results

*Figure A.4.14 M3.18M_115 _20*20*60 Dry density & moisture content over cross section.*

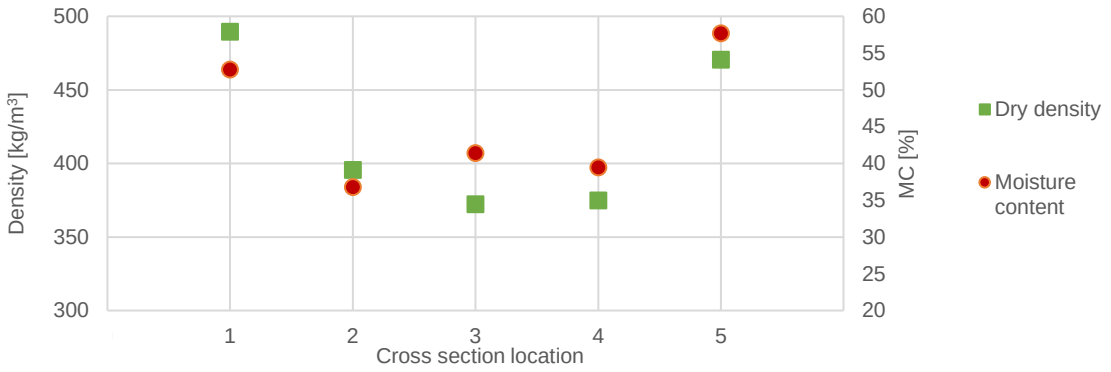

*Figure A.4.15 M3.18M_115 _20*20*60 _Drilling amplitude with ultimate strength.*

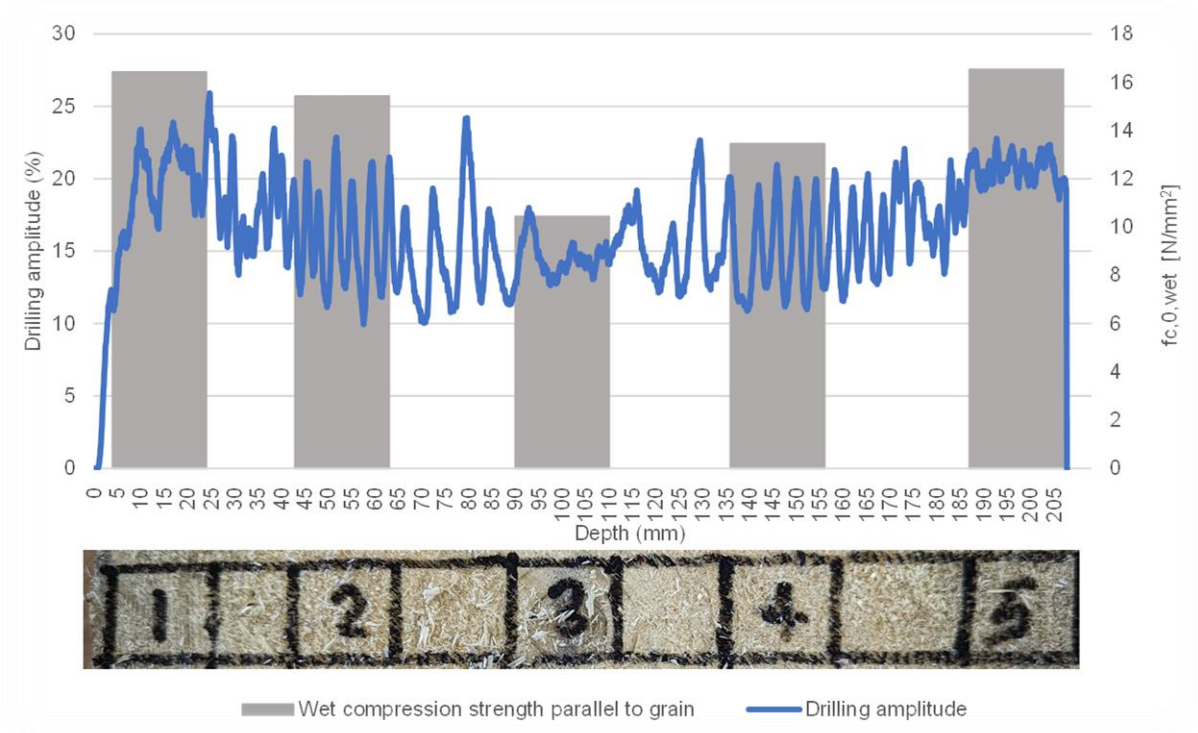

V3.18M_115

Table A.4.14 Full Specimen Results

Full pile ID	Segment code - container	wet density (kg/m^3)	dry density (kg/m^3)	m.c. (%)	MOE_{stat} (Mpa)	MOE_{dyn} (Mpa)	f_{c0} (Mpa)	soft shell (mm)	failure mechanism	remaining sound c-s (%)	RPD drilling avg (%)
BRU0030-PL1-P3.18	V3.18-115	668	363	84	8990	10434	12.1	3.8		96	14.3

Table A.4.15 Local 60mm cross-sectional results

Code	Mass Wet	Mass dry	Moisture Content	Area (wet)	Density wet	Density dry	Ultimate force	Ultimate strength	RPD drilling average
[#]	[g]	[g]	[%]	[mm^2]	kg/m^3]	kg/m^3]	[kN]	[N/mm^2]	[%]
V3.18M_1	14.22	9.12	56	412	566	428	4.86	11.79	14.1
V3.18M_2	13.42	9.15	47	414	524	422	6.29	15.20	15.4
V3.18M_3	16.16	8.70	86	416	637	389	3.77	9.07	13.1
V3.18M_4	12.06	8.43	43	411	482	380	5.32	12.96	15.0
V3.18M_5	15.62	11.73	33	411	622	527	8.79	21.38	19.6
Average	14.3	9.4	53	413	566	429	5.8	14.1	15.4

*Figure A.4.16 V3.18M_115_20*20*60 Dry density & moisture content over cross section*

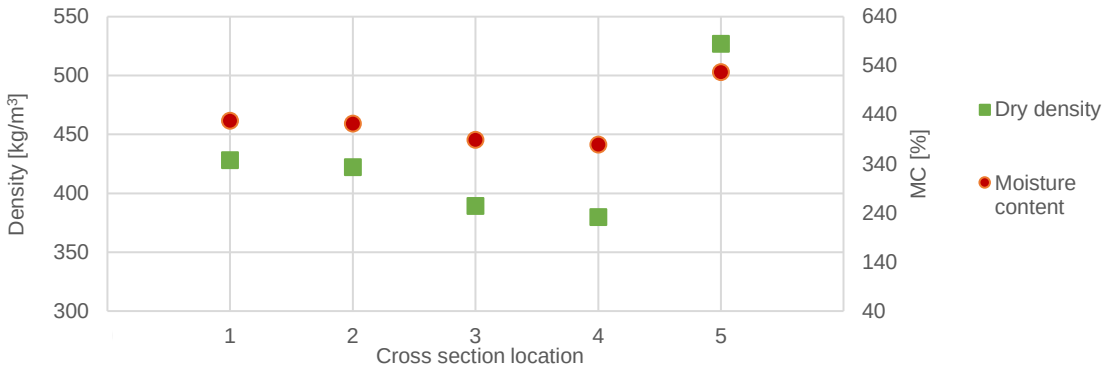

*Figure A.4.17 V3.18M_115_20*20*60 _Drilling amplitude with ultimate strength.*

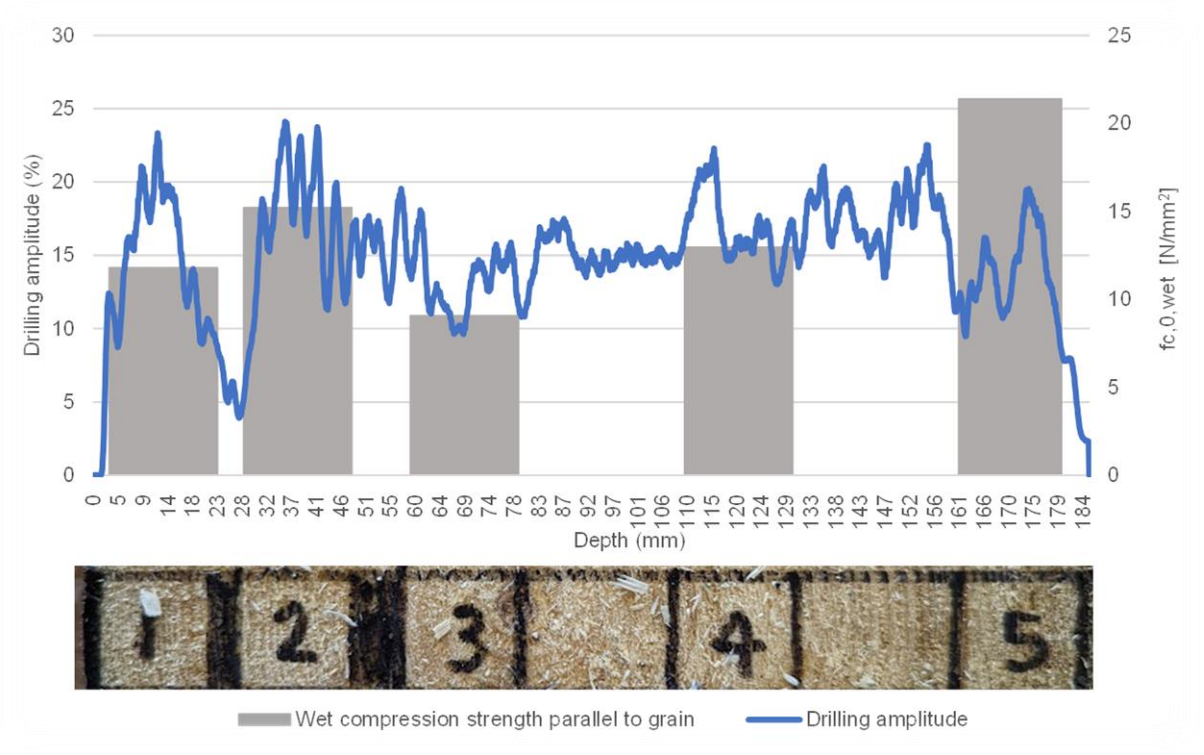
Drilling amplitude (%)
fc,0,wet [N/mm²]
Depth (mm)
1
2
3
4
5
Wet compression strength parallel to grain
Drilling amplitude

A.5 - 3M – (1727)BRU0030-PL1-P2.13

Pile BRU0030-PL1-P2 from 1727. With a segment code of 3M from container 228 has been split into 3 sections known as the tip, middle-part and head as can be seen below in the image. From these sections, a segment of approximately 150mm in length was extracted so that the small samples could be manufactured. The results of each full pile segment and subsequent 20*20*120mm local samples are highlighted below.

A.5.1 Full section codes with local cross sections extracted and small specimen locations.

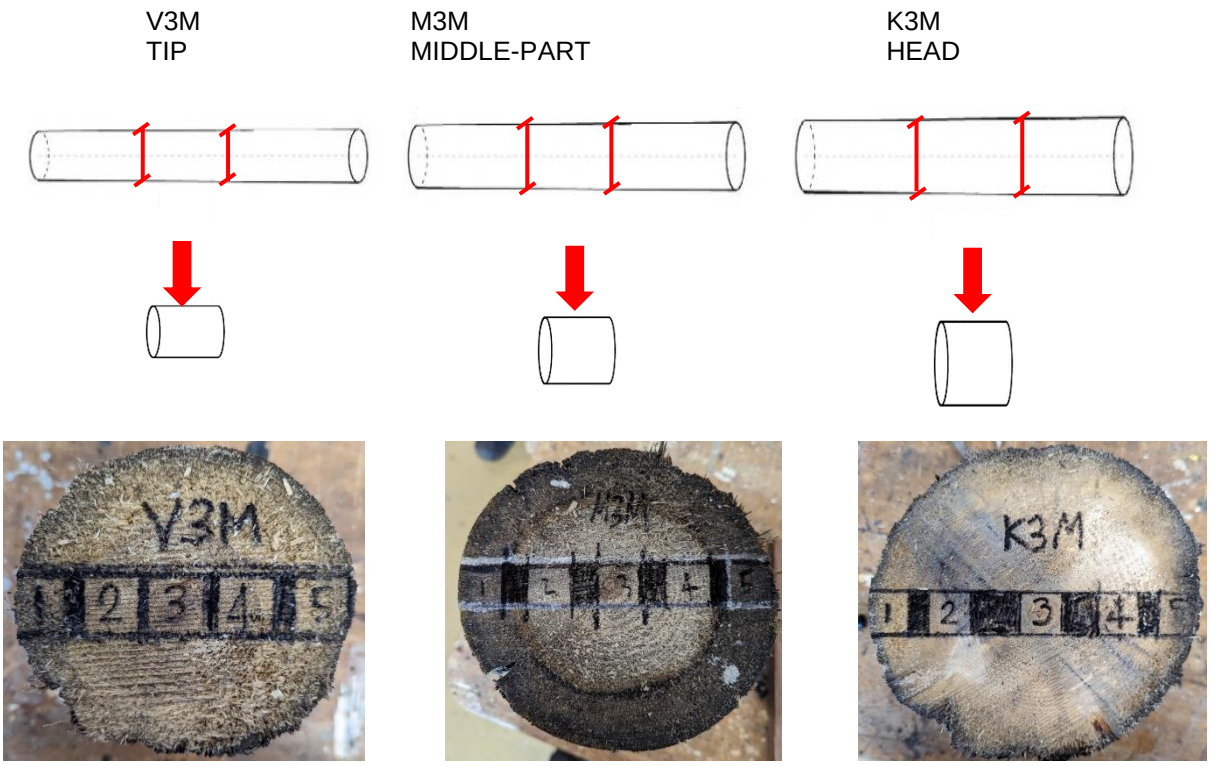

Table A.5.1 Summary of results for full sections and average small samples.

Specimen	Part	Density wet	Density dry	Ultimate strength	MOE	RPD drilling averages	soft shell
[#]	[#]	kg/m^3]	kg/m^3]	[N/mm^2]	Mpa	[%]	[mm]
Full size	K	778	266	7.1	8400	8.1	13.0
	M	664	245	5.3	3720	7.8	47.0
	V	755	235	5.1	2930	7.4	54.0
Local samples average	K	642	333	8.2	4092	16.9	13.0
	M	634	310	7.5	3706	12.3	47.0
	V	633	317	6.6	2936	10.9	54.0

K3M_228

Table A.5.2 Full Specimen Results

Full pile ID	Segment code - container	wet density (kg/m3)	dry density (kg/m3)	m.c. (%)	MOE$_{stat}$ (Mpa)	MOE$_{dyn}$ (Mpa)	f_{c0} (Mpa)	soft shell (mm)	failure mechanism	remaining sound c-s (%)	RPD drilling avg (%)

BRU0030-PL1-P2.13	K3M-228	778	266	192	8400	7713	7.1	13	buckling (bottom)	86	8.1

Table A.5.3 Local cross-sectional results

Code	Mass Wet	Mass dry	Moisture Content	Area (wet)	Density wet	Density dry	Ultimate force	Ultimate strength	MOE	failure mechanism	RPD drilling average
[#]	[g]	[g]	[%]	[mm^2]	kg/m^3]	kg/m^3]	[kN]	[N/mm^2]	Mpa	[N/A]	[%]
K3M_1	39.3	13.8	185	406	807	308	3.1	7.6	2538	buckling (bottom)	5.9
K3M_2	26.5	16.3	62	410	537	370	5.8	14.1	6978	buckling (top)	30.9
K3M_3	26.1	13.9	88	411	530	319	2.2	5.3	3253	crushing (top)	16.0
K3M_4	27.7	16.4	68	415	556	380	4.1	9.9	5480	buckling (top)	25.4
K3M_5	39.2	12.1	224	418	782	287	1.7	3.9	2213	buckling (bottom)	6.5
Average	31.8	14.5	126	412	642	333	3.4	8.2	4092	[N/A]	16.9

*Figure A.5.2 K3M_228_20*20*120 Dry density & moisture content over cross section*

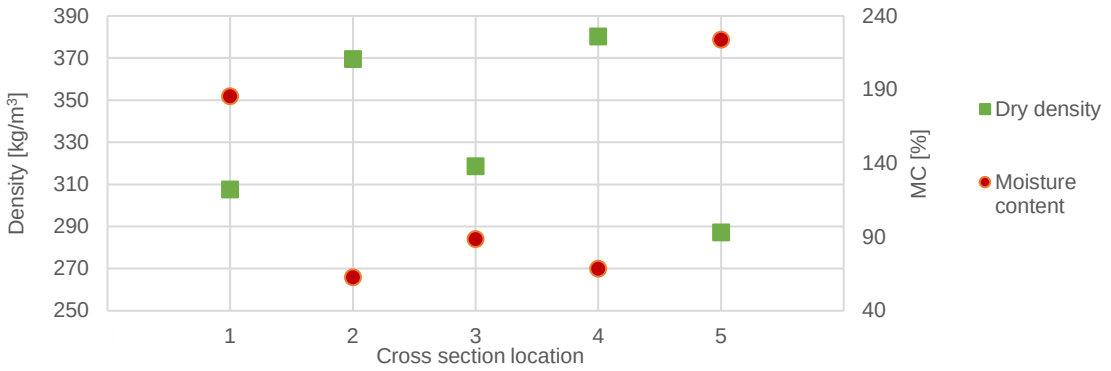

*Figure A.5.3 K3M_228_20*20*120 Ultimate strength through cross section & modulus of elasticity*

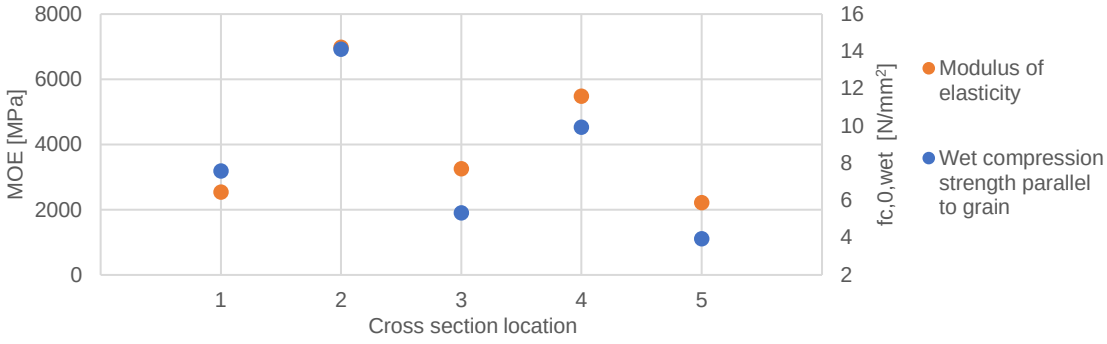

*Figure A.5.4 K3M_20*20*120_Drilling amplitude with ultimate strength.*

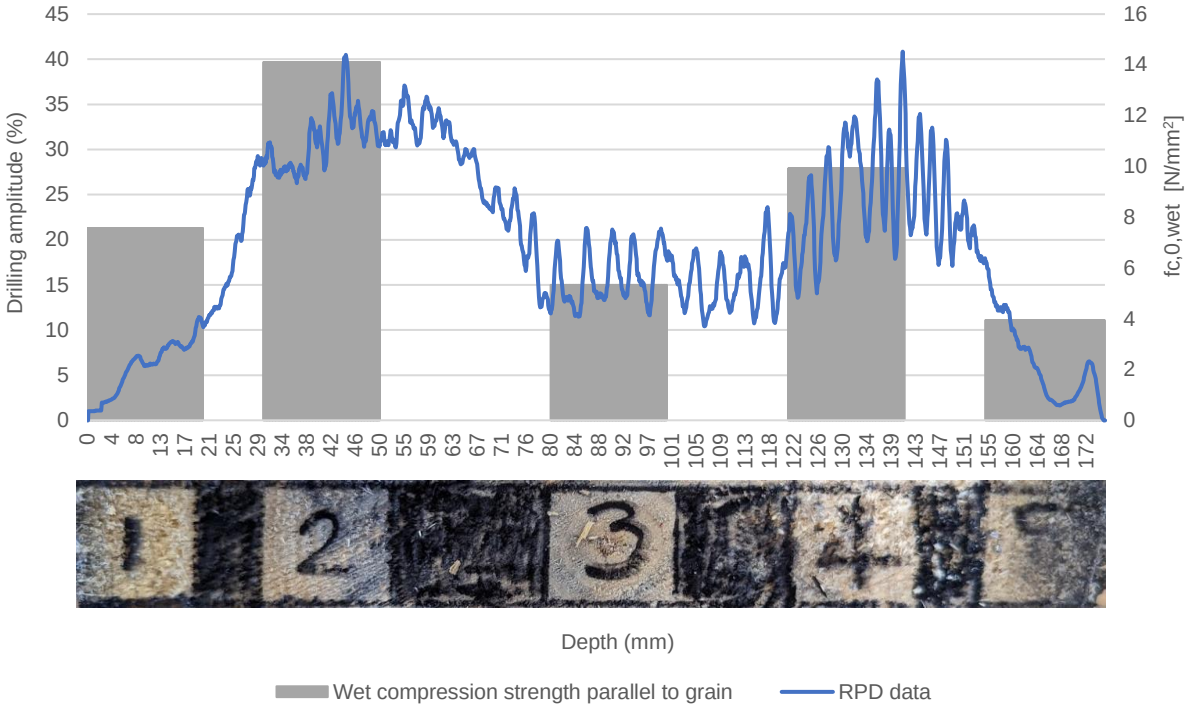

M3M_228

Table A.5.4 Full Specimen Results

Full pile ID	Segment code - container	wet density (kg/m3)	dry density (kg/m3)	m.c. (%)	MOEstat (Mpa)	MOEdyn (Mpa)	fc0 (Mpa)	soft shell (mm)	failure mechanism	remaining sound c-s (%)	RPD drilling avg (%)
BRU0030-PL1-P2.13	M3M-228	664	245	170	3720	3904	5.3	47	buckling (top)	49	7.8

Table A.5.5 Local cross-sectional results

Code	Mass Wet	Mass dry	Moisture Content	Area (wet)	Density wet	Density dry	Ultimate force	Ultimate strength	MOE	failure mechanism	RPD drilling average
[#]	[g]	[g]	[%]	[mm^2]	kg/m^3]	kg/m^3]	[kN]	[N/mm^2]	Mpa	[N/A]	[%]
M3M_1	39.7	9.7	309	419	789	226	1.2	2.8	943	buckling (top)	2.9
M3M_2	27.5	16.2	70	419	544	372	4.5	10.8	5683	buckling (bottom)	20.4
M3M_3	24.2	15.2	59	433	463	338	3.9	9.1	4557	buckling (bottom)	15.4
M3M_4	30.6	17.0	80	417	608	389	5.3	12.7	6598	crushing (top)	18.9
M3M_5	38.6	9.6	303	419	765	224	0.9	2.2	748	buckling (bottom)	4.0
Average	32.1	13.5	164	421	634	310	3.2	7.5	3706	[N/A]	12.3

*Figure A.5.5 M3M_228_20*20*120 Dry density & moisture content over cross section*

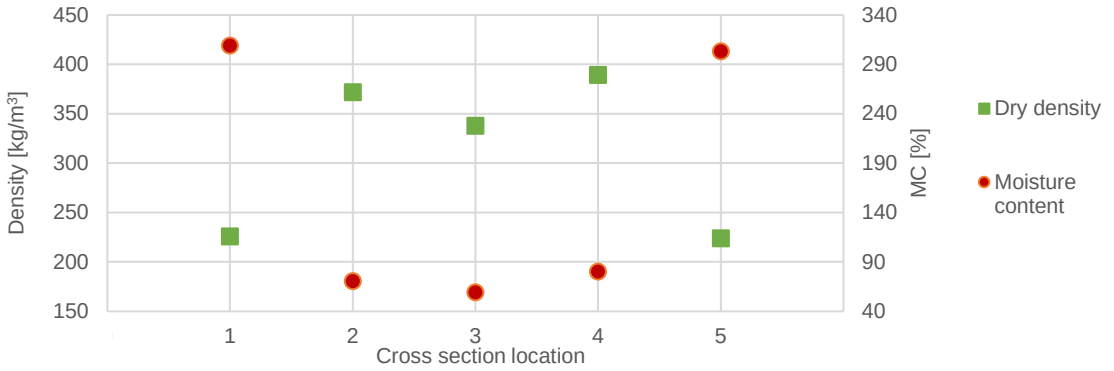

*Figure A.5.6 M3M_228_20*20*120 Ultimate strength through cross section & modulus of elasticity*

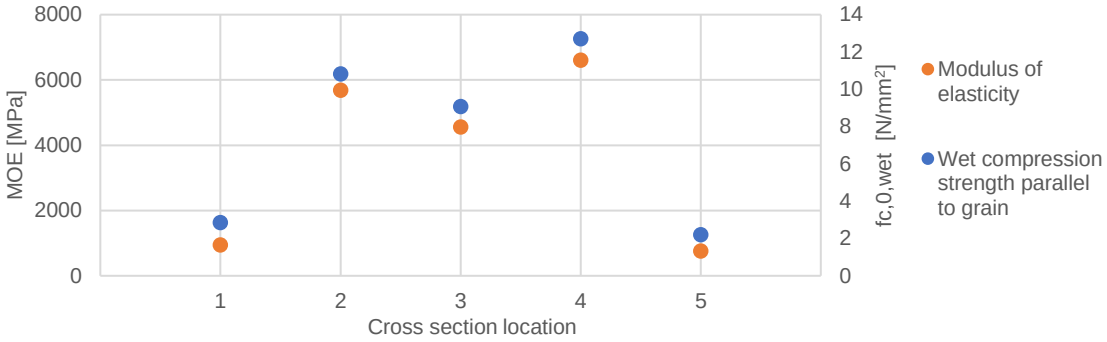

*Figure A.5.7 M3M_20*20*120_Drilling amplitude with ultimate strength.*

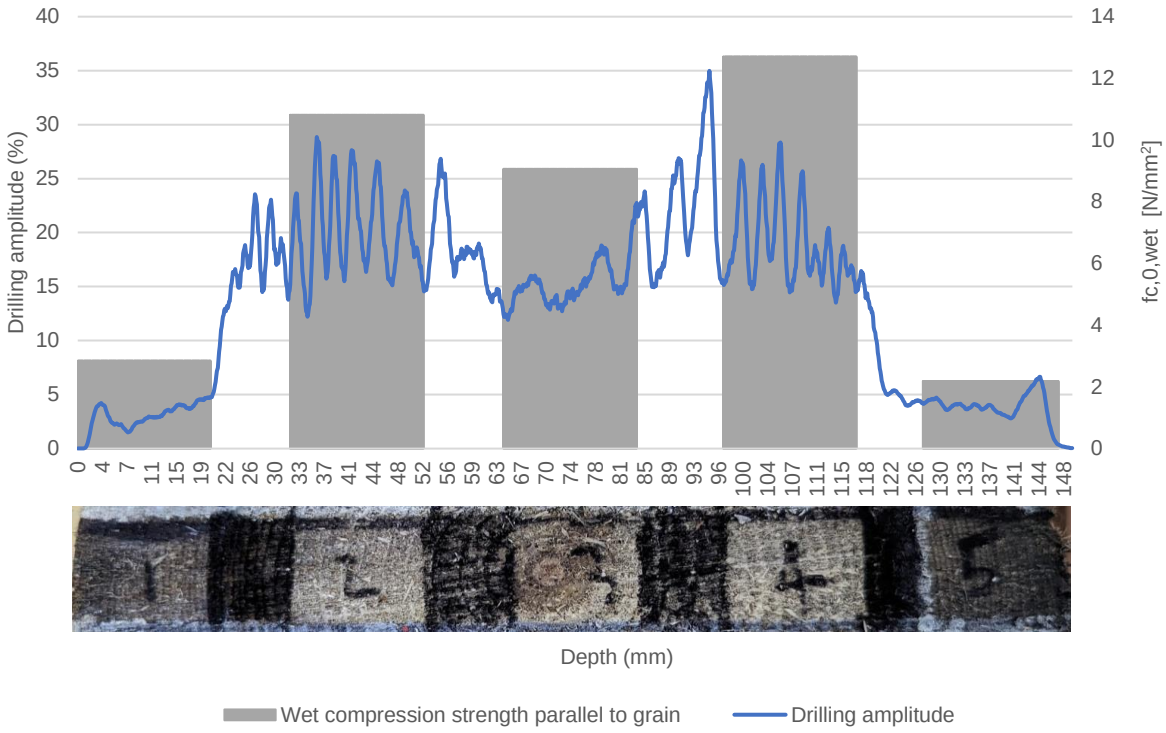

V3M_228

Table A.5.6 Full Specimen Results

Full pile ID	Segment code - container	wet density (kg/m3)	dry density (kg/m3)	m.c. (%)	MOE_{stat} (Mpa)	MOE_{dyn} (Mpa)	f_{c0} (Mpa)	soft shell (mm)	failure mechanism	remaining sound c-s (%)	RPD drilling avg (%)
BRU0030 -PL1- P2.13	V3M-228	755	235	222	2930	4006	5.1	54	buckling (top)	34	7.4

Table A.5.7 Local cross-sectional results

Code	Mass Wet	Mass dry	Moisture Content	Area (wet)	Density wet	Density dry	Ultimate force	Ultimate strength	MOE	failure mechanism	RPD drilling average
[#]	[g]	[g]	[%]	[mm^2]	[kg/m^3]	[kg/m^3]	[kN]	[N/mm^2]	Mpa	[N/A]	[%]
V3M_1	40.9	9.2	345	407	836	220	0.8	1.9	386	buckling (bottom)	5
V3M_2	26.2	16.9	55	418	522	381	4.1	9.8	4719	buckling (top)	17
V3M_3	27.0	16.1	68	409	551	359	3.1	7.7	3287	crushing (top)	16
V3M_4	26.6	16.4	62	419	528	381	4.0	9.5	4910	buckling (top)	14
V3M_5	35.5	10.7	232	405	730	245	1.8	4.3	1380	buckling (bottom)	4
Average	31.2	13.9	152	412	633	317	2.7	6.6	2936	[N/A]	10.9

*Figure A.5.8 V3M_228_20*20*120 Dry density & moisture content over cross section*

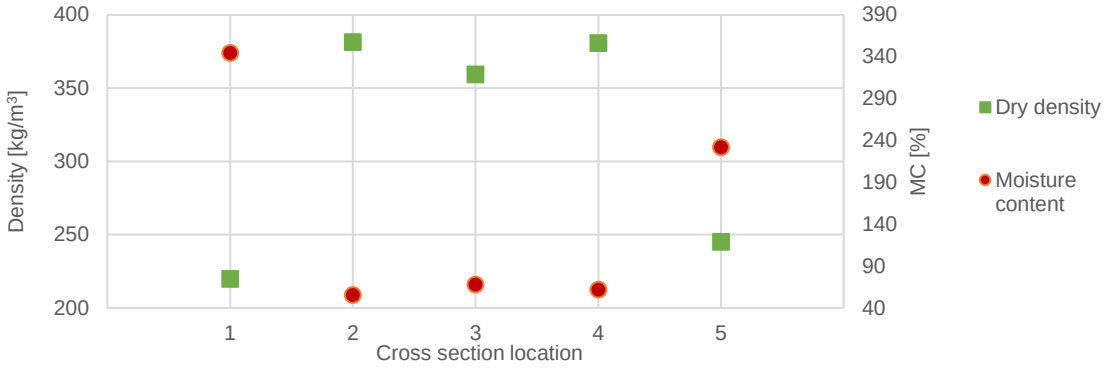

*Figure A.5.9 V3M_228_20*20*120 Ultimate strength through cross section & modulus of elasticity*

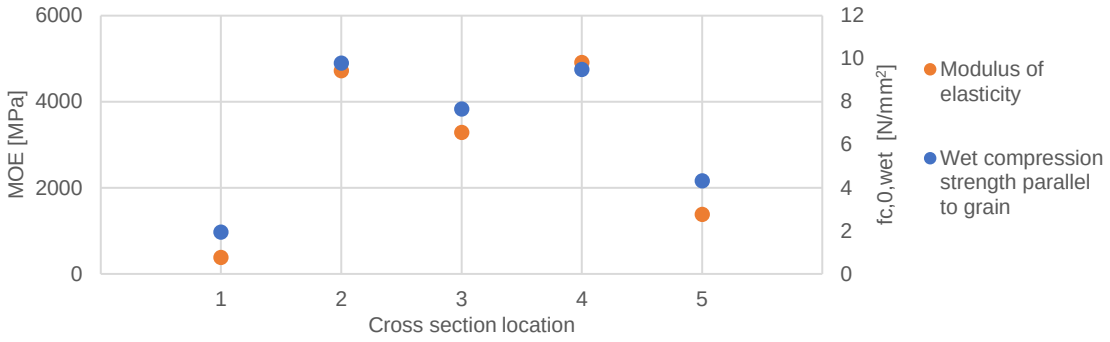

*Figure A.5.10 V3M_20*20*120_Drilling amplitude with ultimate strength.*

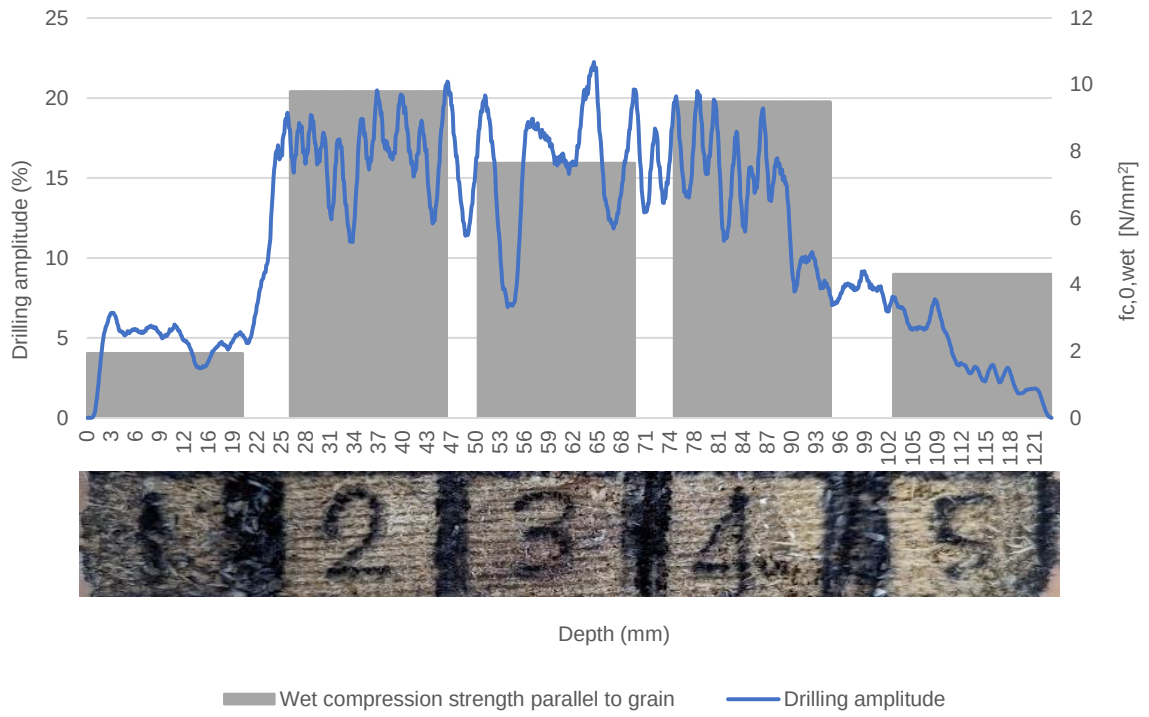

Table A.5.8 standard deviation

Average result	Moisture Content	SD	Density dry	SD	Density wet	SD	fc,0,wet	SD	MOE	SD	RPD drilling average	SD
[#]	[%]	[#]	[kg/m³]	[#]	[kg/m³]	[#]	[N/mm²]	[#]	Mpa	[#]	[%]	[#]
3M_1	280	83.5	251	49.0	811	8.0	4	3.0	1289	1117.1	4	1.5
3M_2	63	7.3	374	6.3	534	11.1	12	2.3	5793	1133.8	23	7.4
3M_3	72	15.1	338	20.4	515	45.5	7	1.9	3699	743.3	16	0.3
3M_4	70	9.1	383	5.0	564	40.5	11	1.7	5663	858.9	19	5.7
3M_5	253	43.6	252	32.3	759	26.9	3	1.1	1447	734.5	5	1.5

Figure90

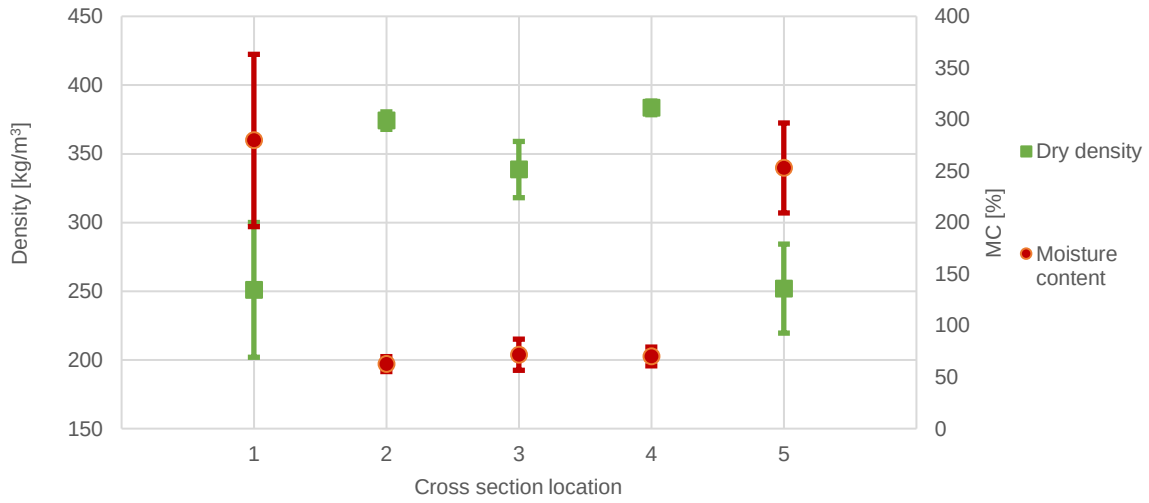

Figure A.5.12 standard deviation

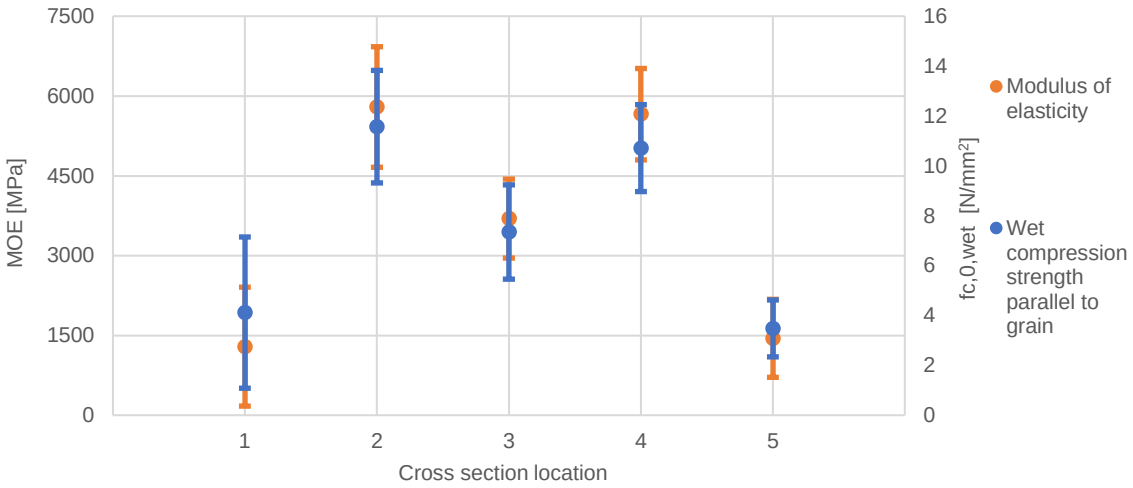

A.6 - 2.7M (1727) - BRU0030 PL1 P2.7

Pile BRU0030 PL1 P2.7 from 1727. With a segment code of 2.7M from container 115 has been split into 3 sections known as the tip, middle-part and head as can be seen below in the image. From these sections, a segment of approximately 150mm in length was extracted so that the small samples could be manufactured. The results of each full pile segment and subsequent 20*20*120mm local samples are highlighted below.

Figure A.6.1 Full section codes with local cross sections extracted and small specimen locations.

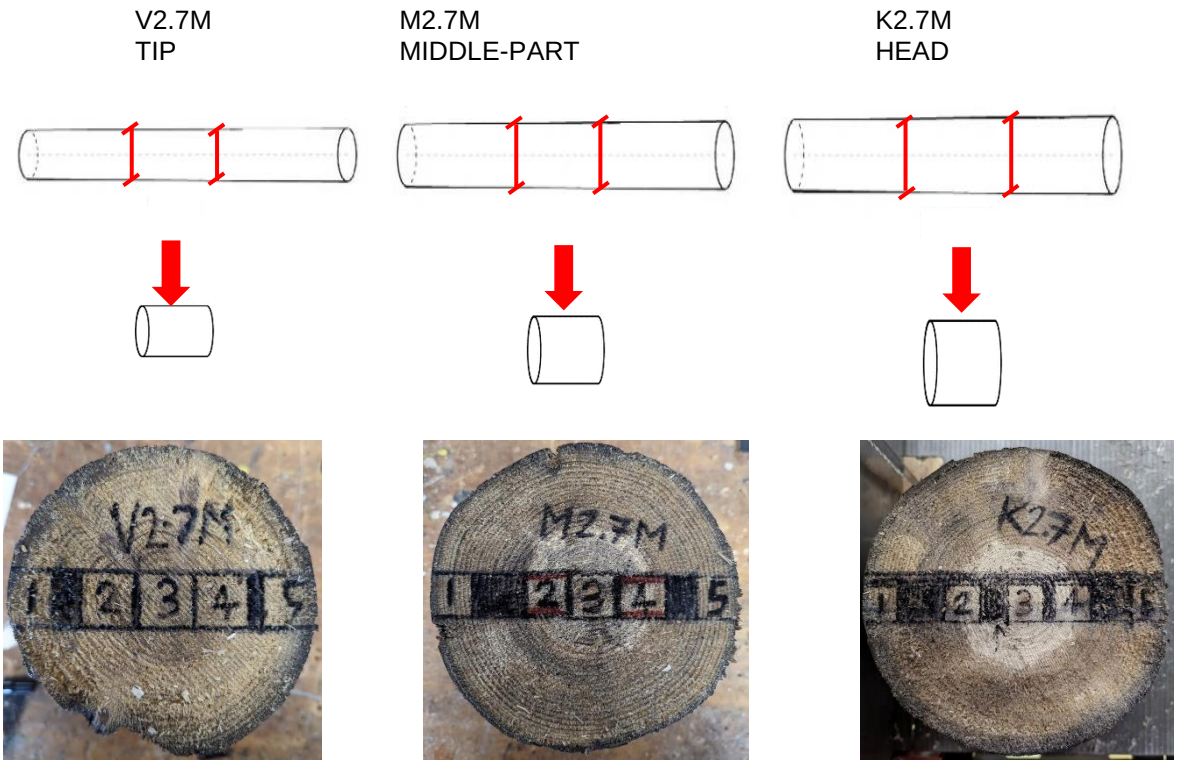

Table A.6.1 Summary of results for full sections and average small samples.

Specimen	Part	Density wet	Density dry	Ultimate strength	MOE_{stat}	MOE_{dyn} (Mpa)	RPD drilling average
[#]	[#]	kg/m^3]	kg/m^3]	[N/mm^2]	Mpa	Mpa	[%]
Full size	K	778	266	7.1	8400	7713	8.1
	M	664	245	5.3	3720	3904	7.8
	V	755	235	5.1	2930	4006	7.4
Local samples average	K	642	333	8.2	4092	[N/A]	16.9
	M	634	310	7.5	3706	[N/A]	12.3
	V	633	317	6.6	2936	[N/A]	10.9

K2.7M_115

Table A.6.2 Full Specimen Results

Full pile ID	Segment code - container	wet density (kg/m3)	dry density (kg/m3)	m.c. (%)	MOE_{stat} (Mpa)	MOE_{dyn} (Mpa)	f_{c0} (Mpa)	soft shell (mm)	failure mechanism	remaining sound c-s (%)	RPD drilling avg (%)
BRU0030 PL1 P2.7	K2.7-115	571	289	97	4972	4976	6.1	29	buckling (top)	73	13.7

Table A.6.3 Local cross-sectional results

Code	Mass Wet	Mass dry	Moisture Content	Area (wet)	Density wet	Density dry	Ultimate force	Ultimate strength	MOE	failure mechanism	RPD drilling average
[#]	[g]	[g]	[%]	[mm^2]	[kg/m^3]	[kg/m^3]	[kN]	[N/mm^2]	Mpa	[N/A]	[%]
K2.7M_1	31.8	11.6	175	416	636	256	1.9	4.4	1732	buckling (bottom)	5.8
K2.7M_2	40.4	16.1	151	423	797	369	3.9	9.3	4669	buckling (top)	18.0
K2.7M_3	31.6	18.1	74	428	615	409	3.7	8.7	4223	crushing (top)	17.8
K2.7M_4	33.4	19.1	75	422	661	432	4.6	10.9	6112	buckling (top)	19.4
K2.7M_5	38.6	10.7	261	410	787	232	1.5	3.6	1239	buckling (bottom)	2.8
Average	35.2	15.1	147	420	699	340	3.1	7.4	3595	[N/A]	12.8

Graphical results

*Figure A.6.2 K2.7M_228_20*20*120 Dry density & moisture content over cross section*

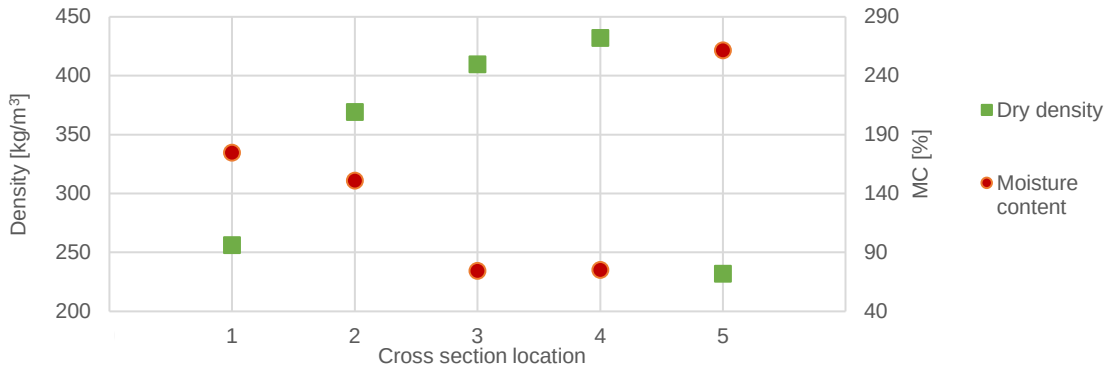

*Figure A.6.3 K2.7M_228_20*20*120 Ultimate strength through cross section & modulus of elasticity*

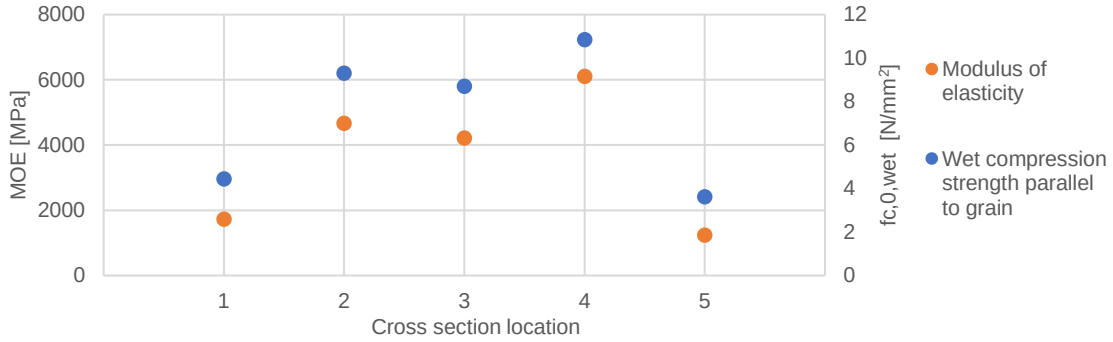

*Figure A.6.4 K2.7M_20*20*120_Drilling amplitude with ultimate strength.*

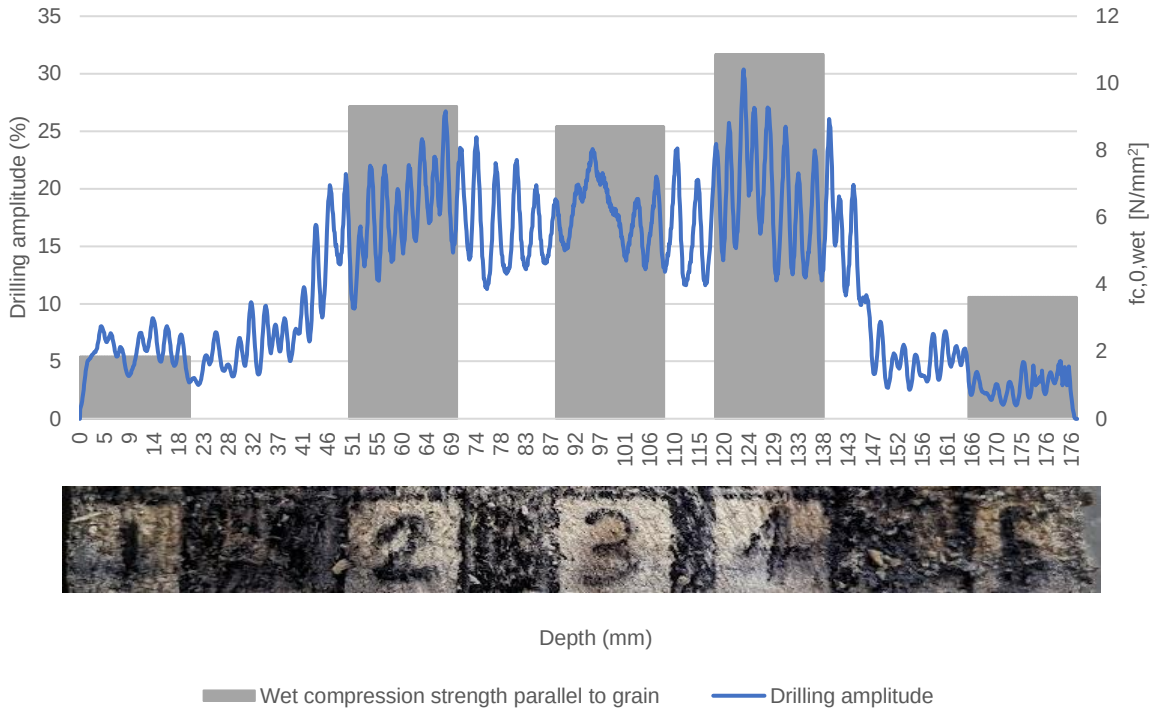

M2.7M_115

Table A.6.4 Full Specimen Results

Full pile ID	Segment code - container	wet density (kg/m3)	dry density (kg/m3)	m.c. (%)	MOE_{stat} (Mpa)	MOE_{dyn} (Mpa)	f_{c0} (Mpa)	soft shell (mm)	failure mechanism	remaining sound c-s (%)	RPD drilling avg (%)
BRU0030 PL1 P2.7	M2.7-115	531	258	106	2569	2723	4.1	54	buckling (middle)	54	9.5

Table A.6.5 Local cross-sectional results

Code	Mass Wet	Mass dry	Moisture Content	Area (wet)	Density wet	Density dry	Ultimate force	Ultimate strength	MOE	failure mechanism	RPD drilling average
[#]	[g]	[g]	[%]	[mm^2]	[kg/m^3]	[kg/m^3]	[kN]	[N/mm^2]	Mpa	[N/A]	[%]
M2.7M_1	33.4	11.2	198	401	693	252	1.5	3.8	1048	Shear (top)	3.8
M2.7M_2	26.7	17.9	49	407	548	425	5.2	12.8	8022	Shear (top)	24.0
M2.7M_3	26.9	17.6	53	407	552	398	5.2	12.7	7888	Shear (top)	22.6
M2.7M_4	28.1	17.0	65	405	578	398	5.3	13.1	8776	Shear (top)	18.7
M2.7M_5	38.2	9.6	297	405	786	219	1.1	2.7	769	Shear and buckling (top)	3.2
Average	30.7	14.7	132	405	631	339	3.7	9.0	5301	[N/A]	14.5

*Figure A.6.5 M2.7M_115_20*20*120 Dry density & moisture content over cross section*

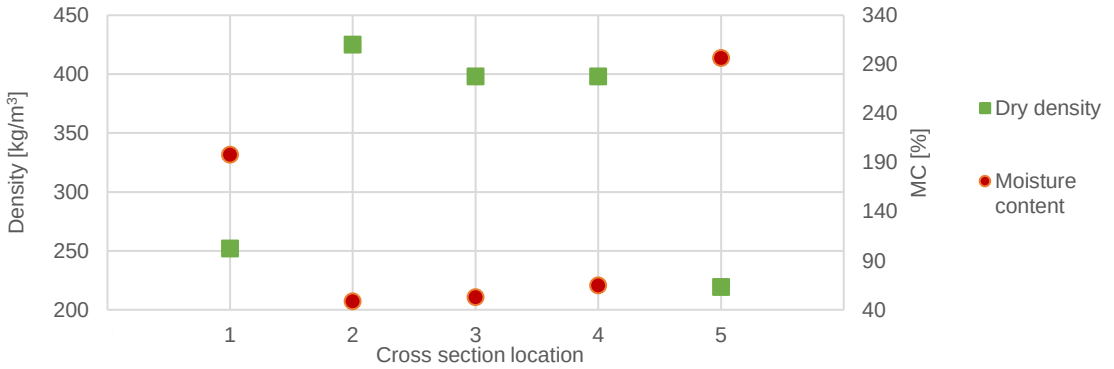

*Figure A.6.6 M2.7M_115_20*20*120 Ultimate strength through cross section & modulus of elasticity*

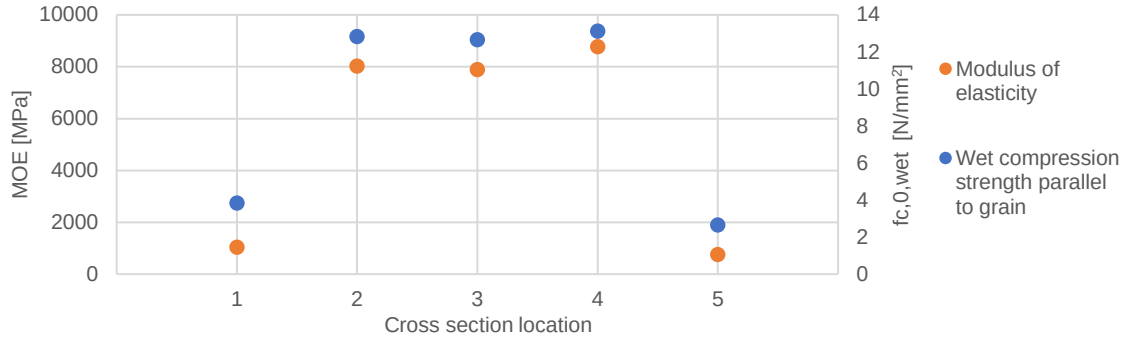

Figure A.6.7 M2.7M_115_Drilling amplitude with ultimate strength.

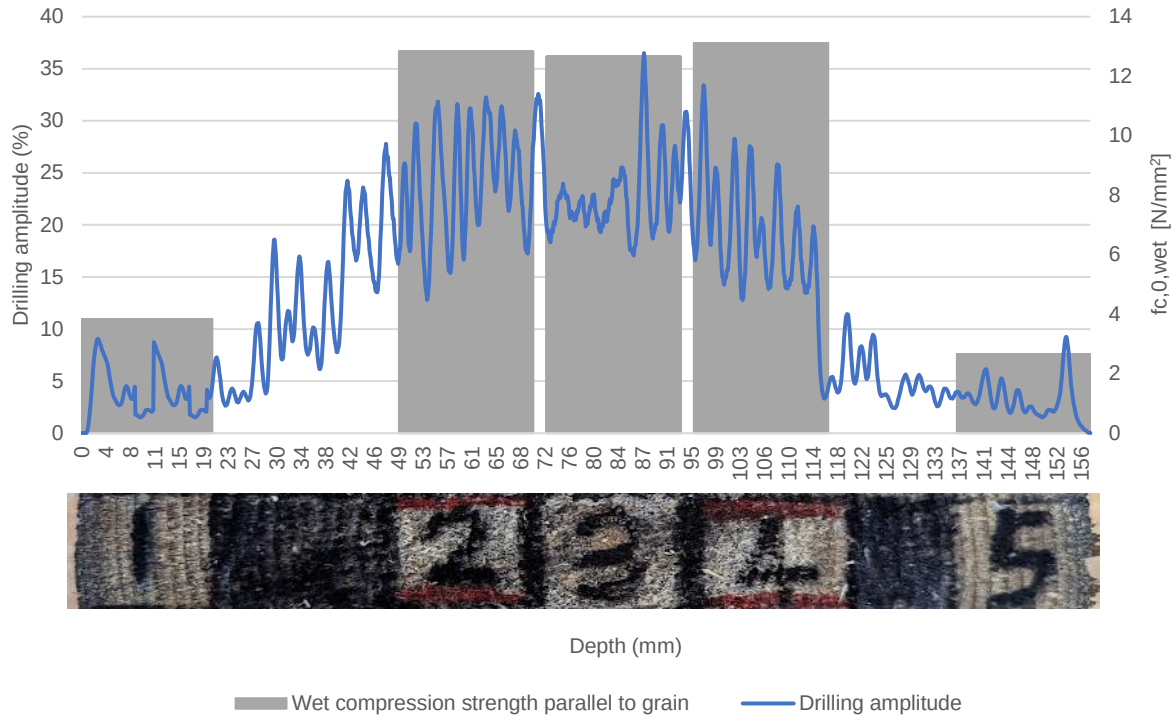

V2.7M_115

Table A.6.6 Full Specimen Results

Full pile ID	Segment code - container	wet density (kg/m3)	dry density (kg/m3)	m.c. (%)	MOE_{stat} (Mpa)	MOE_{dyn} (Mpa)	f_{c0} (Mpa)	soft shell (mm)	failure mechanism	remaining sound c-s (%)	RPD drilling avg (%)

BRU0030 PL1 P2.7	V2.7-115	744	270	175	3935	4300	5.8	34.1	buckling (middle)	57	10.4

Table A.6.7 Local cross-sectional results

Code	Mass Wet	Mass dry	Moisture Content	Area (wet)	Density wet	Density dry	Ultimate force	Ultimate strength	MOE	failure mechanism	RPD drilling average
[#]	[g]	[g]	[%]	[mm^2]	[kg/m^3]	[kg/m^3]	[kN]	[N/mm^2]	Mpa	[N/A]	[%]
V2.7M_1	33.7	13.0	159	419	670	280	2.4	5.7	1771	Shear (bottom)	4.0
V2.7M_2	34.7	17.9	93	419	692	398	5.3	12.6	5927	buckling (top)	18.2
V2.7M_3	27.2	19.0	43	425	535	419	5.3	12.5	6054	crushing (top)	21.5
V2.7M_4	25.8	18.1	42	426	506	405	5.5	12.9	7154	Shear (top)	17.2
V2.7M_5	39.0	11.7	233	411	795	269	2.1	5.0	1529	Shear (bottom)	3.5
Average	32.1	16.0	114	420	640	354	4.1	9.7	4487	[N/A]	12.9

*Figure A.6.8 V2.7M_115_20*20*120 Dry density & moisture content over cross section*

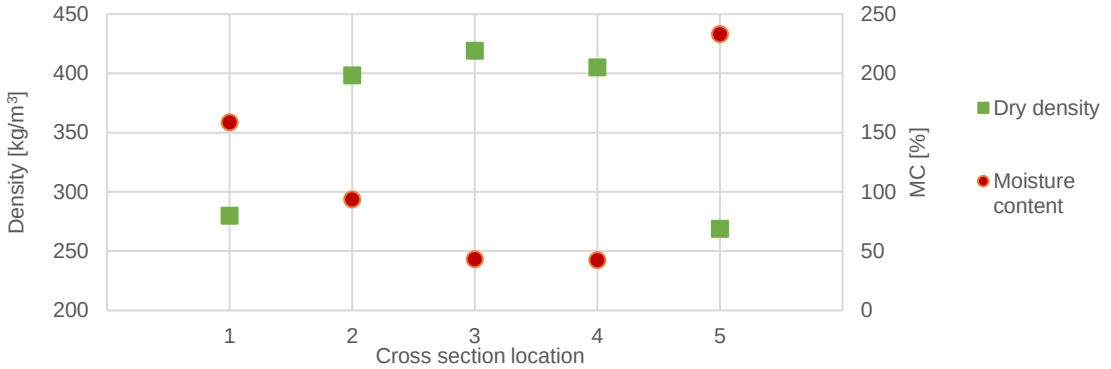

*Figure A.6.9 V2.7M_115_20*20*120 Ultimate strength through cross section & modulus of elasticity*

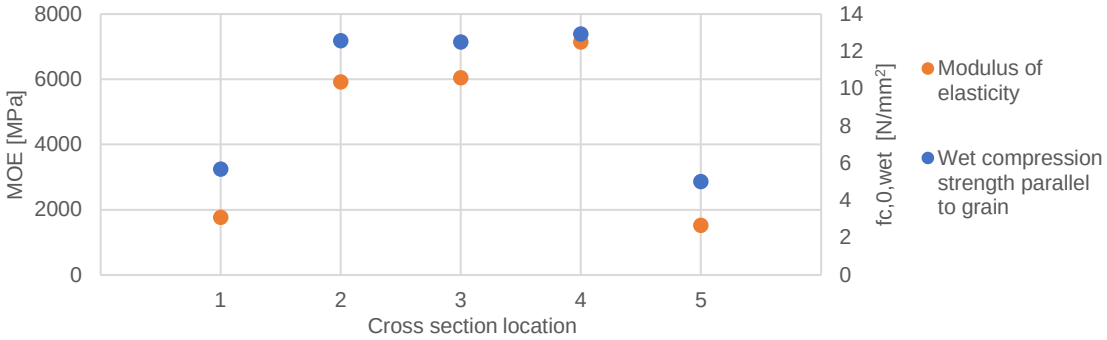

Figure A.6.10 V2.7M_115_Drilling amplitude with ultimate strength.

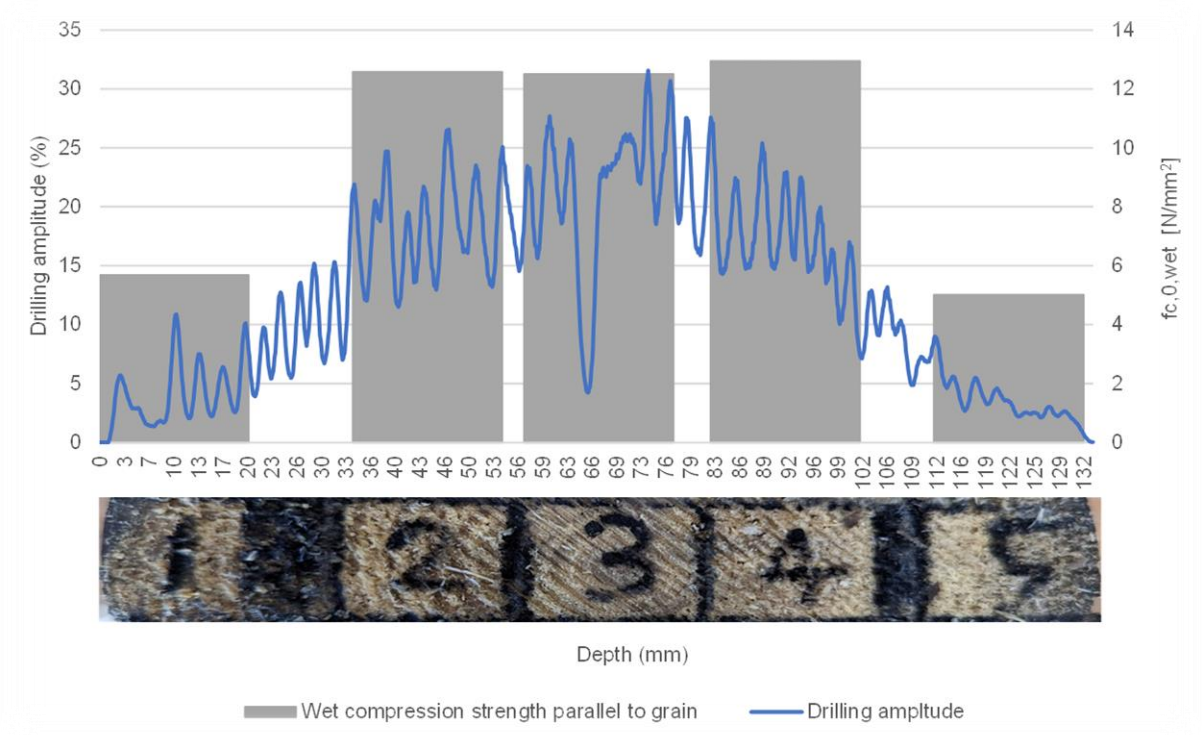

Table A.6.8 Standard deviation

Average result	Moisture Content	SD	Density dry	SD	Density wet	SD	fc,0,wet	SD	MOE	SD	RPD drilling average	SD
[#]	[%]	[#]	[kg/m³]	[#]	[kg/m³]	[#]	[N/mm²]	[#]	Mpa	[#]	[%]	[#]
2.7M_1	177	19.8	263	14.9	666	28.3	5	0.9	1517	407.0	5	1.1
2.7M_2	98	51.0	397	28.0	679	124.9	12	2.0	6206	1693.8	20	3.4
2.7M_3	57	15.8	409	10.4	567	42.4	11	2.2	6055	1832.7	21	2.5
2.7M_4	61	16.8	412	17.9	582	77.6	12	1.3	7347	1342.9	18	1.1
2.7M_5	264	31.9	240	25.7	789	4.6	4	1.2	1179	383.8	3	0.4

Figure A.6.11 standard deviation

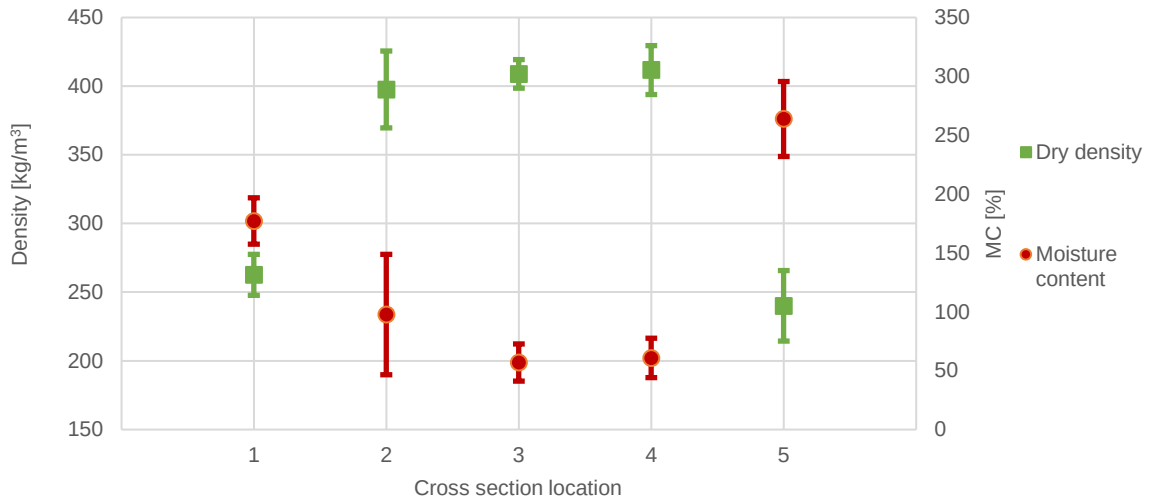

Figure A.6.12 standard deviation

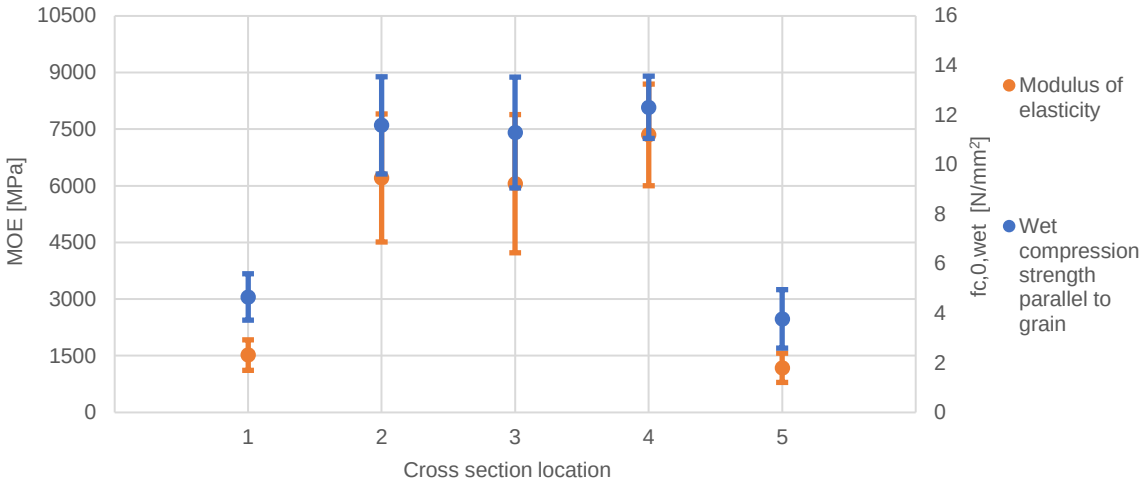
10500
9000
7500
6000
4500
3000
1500
0
MOE [MPa]
16
14
12
10
8
6
4
2
0
fc,0,wet [N/mm²]
1
2
3
4
5
Cross section location
Modulus of elasticity
Wet compression strength parallel to grain

A.7 - 6M (1727) - BRU0030-PL2-P2.21

Pile BRU0030-PL2-P2.21-6M from 1727. With a segment code of 6M from container 228 has been split into 3 sections known as the tip, middle-part and head as can be seen below in the image. From these sections, a segment of approximately 150mm in length was extracted so that the small samples could be manufactured. The results of each full pile segment and subsequent 20*20*120mm local samples are highlighted below.

Figure A.7.1 Full section codes with local cross sections extracted and small specimen locations.

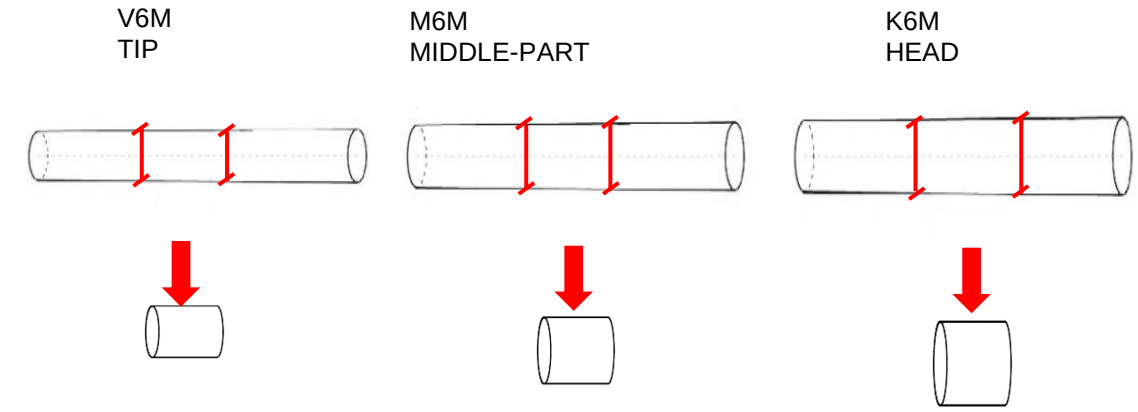

Figure A.7.1 Summary of results for full sections and average small samples.

Specimen	Part	Density wet	Density dry	Ultimate strength	MOE_{stat}	MOE_{dyn} (Mpa)	RPD drilling average
[#]	[#]	kg/m^3]	kg/m^3]	[N/mm^2]	Mpa	Mpa	[%]
Full size	K	648	329	9.8	8300	8639	10.2
	M	671	304	6.3	4590	5691	9.1
	V	716	307	6.6	4230	4680	9.3
Local samples average	K	745	402	13.4	6912	[N/A]	22.0
	M	712	390	9.1	4749	[N/A]	20.2
	V	721	373	8.7	4112	[N/A]	16.5

K6M_228
Table A.7.2 Full Specimen Results

Full pile ID	Segment code - container	wet density (kg/m^3)	dry density (kg/m^3)	m.c. (%)	MOE_{stat} (Mpa)	MOE_{dyn} (Mpa)	f_{c0} (Mpa)	soft shell (mm)	failure mechanism	remaining sound c-s (%)	RPD drilling avg (%)
BRU0030-PL2-P2.21	K6M-228	648	329	97	8300	8639	9.8	30	buckling (top)	74	10.2

Table A.7.3 Local cross-sectional results

Code	Mass Wet	Mass dry	Moisture Content	Area (wet)	Density wet	Density dry	Ultimate force	Ultimate strength	MOE	RPD drilling average
[#]	[g]	[g]	[%]	[mm^2]	kg/m^3]	kg/m^3]	[kN]	[N/mm^2]	Mpa	[%]
K6M_1	46.9	13.0	262	429	909	284	5.86	13.65	6033	22.4
K6M_2	40.3	20.1	101	431	779	448	6.21	14.40	8235	24.4
K6M_3	28.4	18.5	54	432	546	400	5.92	13.69	7171	22.3
K6M_4	30.0	20.2	49	438	570	436	5.79	13.22	6875	22.5
K6M_5	47.9	19.1	151	430	923	442	5.21	12.13	6244	18.2
Average	38.7	18.2	123	432	745	402	5.8	13.4	6912	22.0

*Figure A.7.2 K6M_228_20*20*120 Dry density & moisture content over cross section*

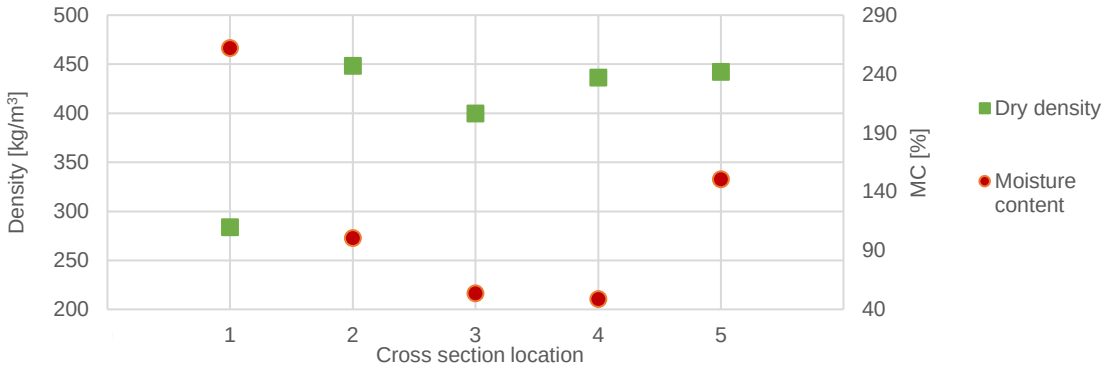

*Figure A.7.3 K6M_228_20*20*120 Ultimate strength through cross section & modulus of elasticity*

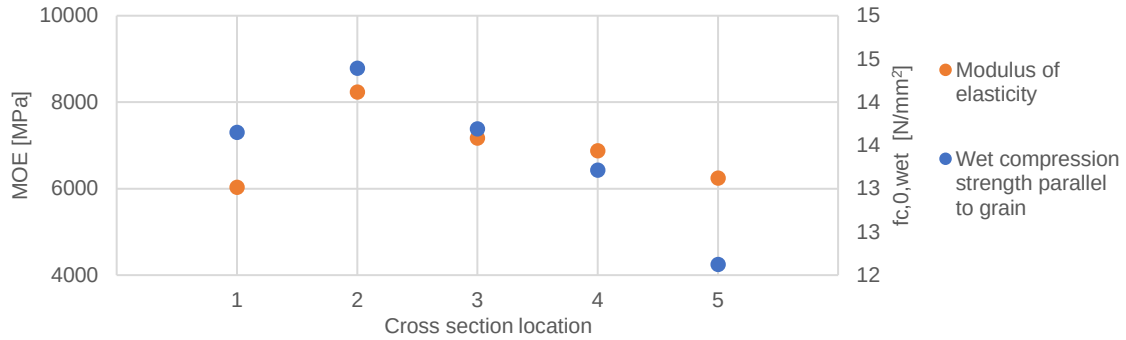

*Figure A.7.4 K6M_228_20*20*120 _Drilling amplitude with ultimate strength.*

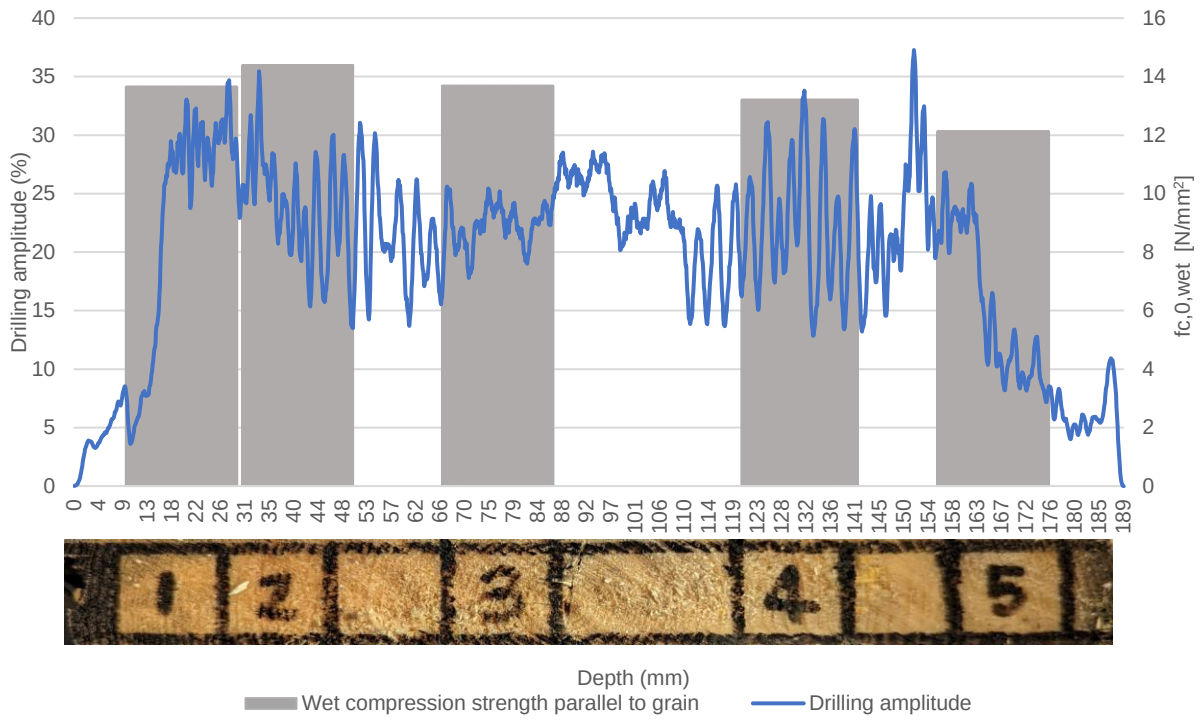

M6M_228

Table A.7.4 Full Specimen Results

Full pile ID	Segment code - container	wet density (kg/m³)	dry density (kg/m³)	m.c. (%)	MOE_{stat} (Mpa)	MOE_{dyn} (Mpa)	f_{c0} (Mpa)	soft shell (mm)	failure mechanism	remaining sound c-s (%)	RPD drilling avg (%)
BRU0030-PL2-P2.21	M6M-228	671	304	120	4590	5691	6.3	52	crushing (top)	51	9.1

Table A.7.5 Local cross-sectional results

Code	Mass Wet	Mass dry	Moisture Content	Area (wet)	Density wet	Density dry	Ultimate force	Ultimate strength	MOE	RPD drilling average
[#]	[g]	[g]	[%]	[mm²]	kg/m³]	kg/m³]	[kN]	[N/mm²]	Mpa	[%]
M6M_1	46.9	13.0	262	438	897	280	1.41	3.22	1145	6.6
M6M_2	40.3	20.1	101	457	738	446	4.60	10.07	4375	26.0
M6M_3	28.4	18.5	54	458	517	396	3.83	8.35	3713	23.4
M6M_4	30.0	20.2	49	466	539	428	6.05	13.00	8326	26.2
M6M_5	47.9	19.1	151	460	867	401	4.91	10.67	6188	18.7
Average	38.7	18.2	123.1	455.8	711.7	390.2	4.2	9.1	4749.4	20.2

*Figure A.7.5 M6M_228 _20*20*120 Dry density & moisture content over cross section*

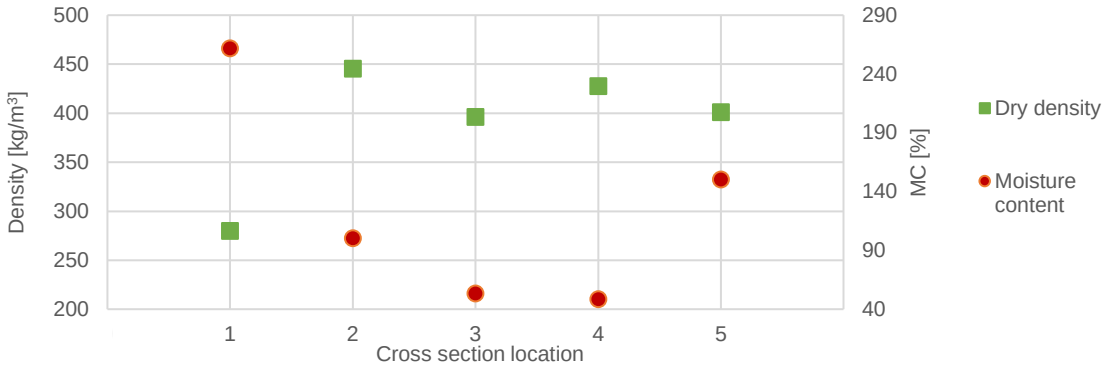

*Figure A.7.6 M6M_228 _20*20*120 Ultimate strength through cross section & modulus of elasticity*

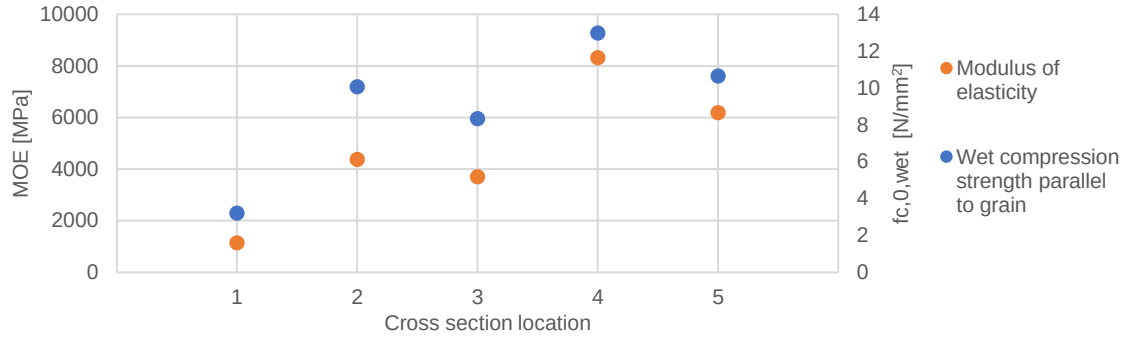

*Figure A.7.7 M6M_228 _20*20*120 _Drilling amplitude with ultimate strength.*

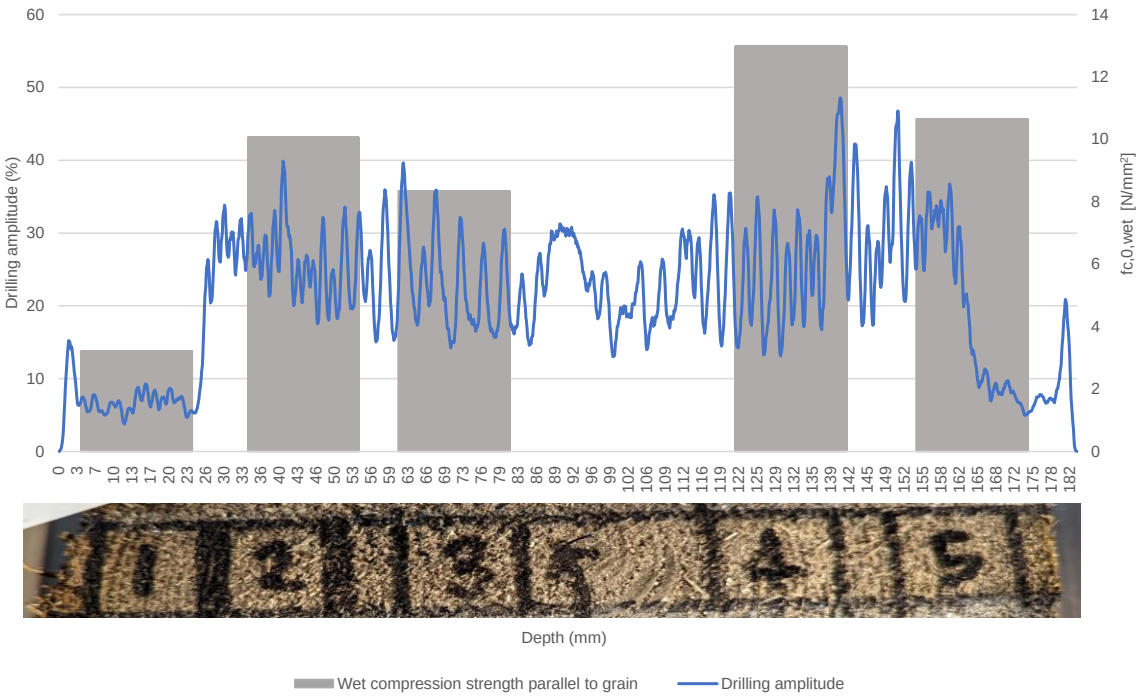

V6M_228

Table A.7.6 Full Specimen Results

Full pile ID	Segment code - container	wet density (kg/m³)	dry density (kg/m³)	m.c. (%)	MOE_{stat} (Mpa)	MOE_{dyn} (Mpa)	f_{c0} (Mpa)	soft shell (mm)	failure mechanism	remaining sound c-s (%)	RPD drilling avg (%)

BRU0030-PL2-P2.21	V6M-228	716	307	133	4230	4680	6.6	42	buckling (top)	51	9.3

Table A.7.7 Local cross-sectional results

Code	Mass Wet	Mass dry	Moisture Content	Area (wet)	Density wet	Density dry	Ultimate force	Ultimate strength	MOE	RPD drilling average
[#]	[g]	[g]	[%]	[mm^2]	[kg/m^3]	[kg/m^3]	[kN]	[N/mm^2]	Mpa	[%]
V6M_1	38.6	17.3	123	444	720	349	3.48	7.83	3894	8.2
V6M_2	32.4	19.7	65	446	607	423	5.11	11.46	5475	21.0
V6M_3	35.2	19.7	79	443	659	409	3.67	8.28	4233	22.0
V6M_4	38.8	20.3	91	438	741	452	5.85	13.35	6452	27.6
V6M_5	44.9	10.3	334	427	878	230	1.00	2.34	504	2.6
Average	38.0	17.5	138.2	439.8	721.0	372.6	3.8	8.7	4111.8	16.3

*Figure A.7.8 V6M_20*20*120_Dry density & moisture content over cross section*

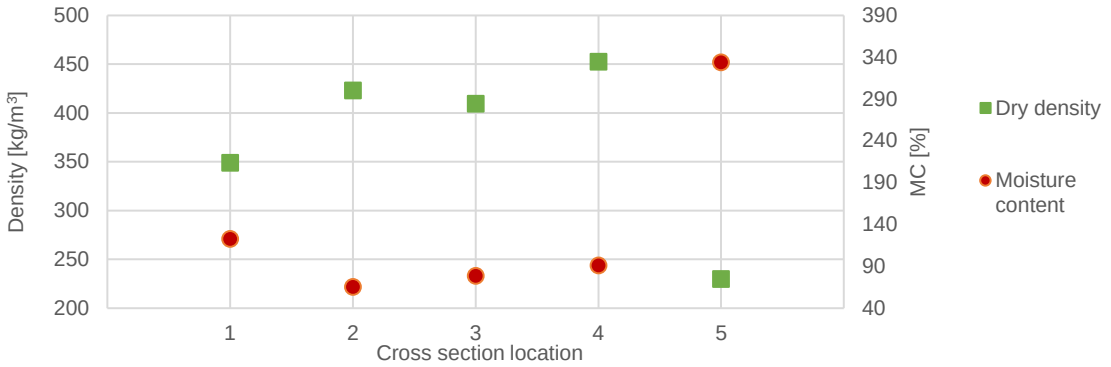

*Figure A.7.9 V6M_20*20*120_Ultimate strength through cross section & modulus of elasticity*

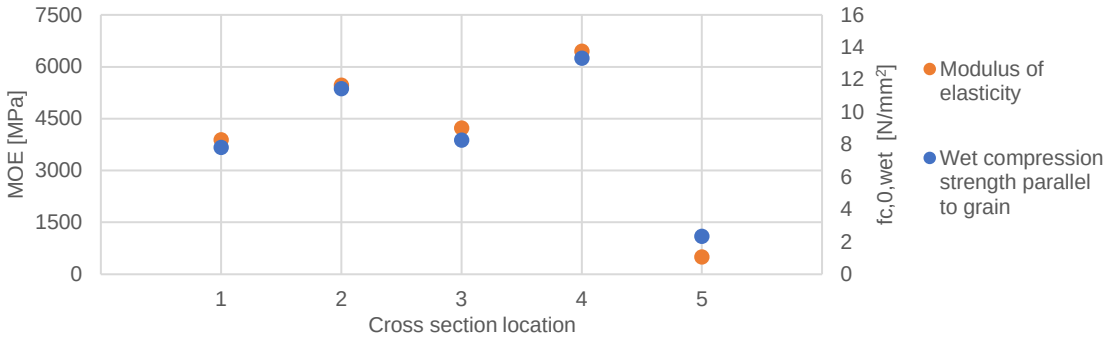

*Figure A.7.10 V6M_20*20*120 _Drilling amplitude with ultimate strength.*

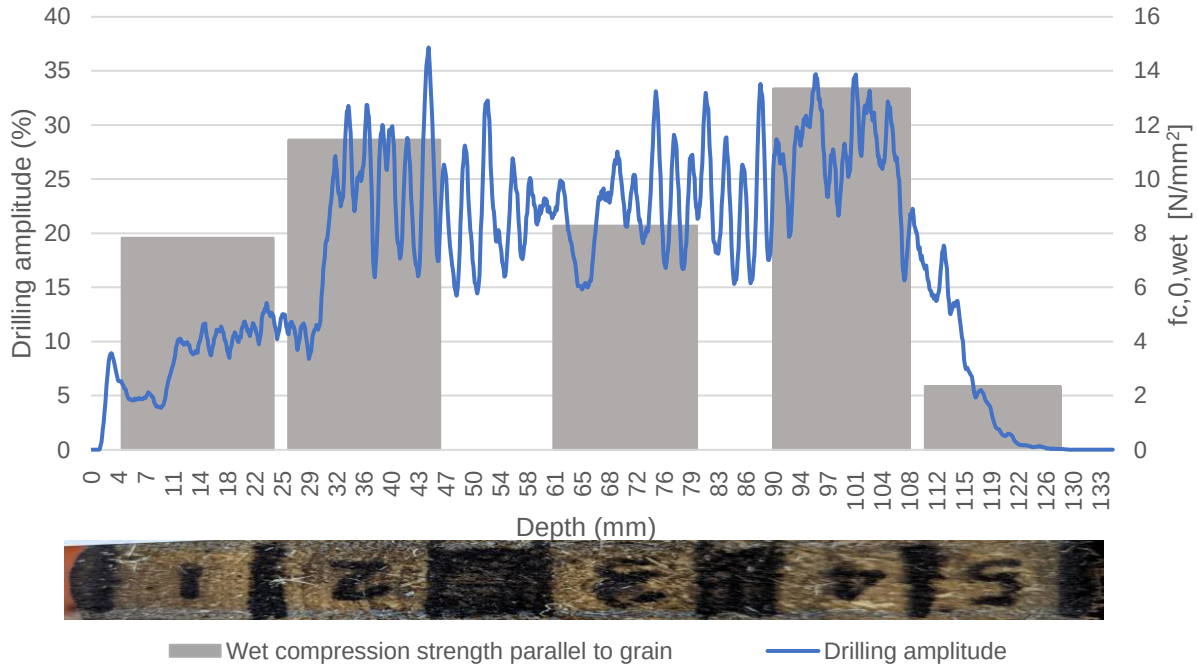

Table 11 A.7.8 standard deviation

Average result	Moisture Content	SD	Density dry	SD	Density wet	SD	fc,0,wet	SD	MOE	SD	RPD drilling average	SD
[#]	[%]	[#]	[kg/m^3]	[#]	[kg/m^3]	[#]	[N/mm^2]	[#]	Mpa	[#]	[%]	[#]
6M_1	216	80.5	304	38.5	842	105.6	8	5.2	3691	2450.1	12	8.7
6M_2	89	20.5	439	13.9	708	90.0	12	2.2	6028	1988.5	24	2.6
6M_3	62	14.4	402	6.8	574	75.1	10	3.1	5039	1864.9	23	0.7
6M_4	63	24.4	439	12.5	616	108.6	13	0.2	7218	982.5	25	2.6
6M_5	212	105.8	358	112.7	889	29.8	8	5.3	4312	3298.0	13	9.1

BRU0030-PL2-P2.21-6M full pile

Pile BRU0030-PL2-P2.21-6M from 1727. With a segment code of 6M from container 228 has been split into 3 sections known as the tip, middle-part and head as can be seen below in the image. From these sections, a segment of approximately 100mm in length was extracted so that the small samples could be manufactured. The results of each full pile segment and subsequent small samples are highlighted below.

Figure A.7.11 Full section codes with local cross sections extracted and small specimen locations.

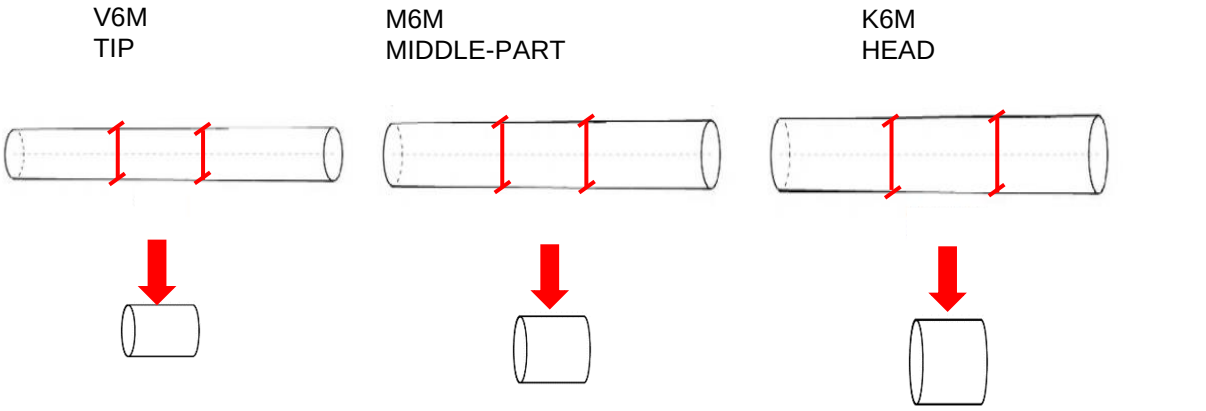

Figure A.7.9 Summary of results for full sections and average small samples.

Specimen	Part	Density wet	Density dry	Ultimate strength	MOE_{stat}	MOE_{dyn} (Mpa)	RPD drilling average
[#]	[#]	kg/m^3]	kg/m^3]	[N/mm^2]	Mpa	Mpa	[%]
Full size	K	648	329	9.8	8300	8639	10.2
	M	671	304	6.3	4590	5691	9.1
	V	716	307	6.6	4230	4680	9.3
Local samples average	K	745	402	13.4	6912	[N/A]	22.0
	M	712	390	9.1	4749	[N/A]	20.2
	V	721	373	8.7	4112	[N/A]	16.5

K6M_228

Table A.7.10 Full Specimen Results

Full pile ID	Segment code - container	wet density (kg/m^3)	dry density (kg/m^3)	m.c. (%)	MOE_{stat} (Mpa)	MOE_{dyn} (Mpa)	f_{c0} (Mpa)	soft shell (mm)	failure mechanism	remaining sound c-s (%)	RPD drilling avg (%)
BRU0030-PL2-P2.21	K6M-228	648	329	97	8300	8639	9.8	30	buckling (top)	74	10.2

Table A.7.11 Local 60mm cross-sectional results

Code	Mass Wet	Mass dry	Moisture Content	Area (wet)	Density wet	Density dry	Ultimate force	Ultimate strength	RPD drilling average
[#]	[g]	[g]	[%]	[mm^2]	kg/m^3]	kg/m^3]	[kN]	[N/mm^2]	[%]

K6M_1	14.3	7.8	83	427	561	352	3.85	9.02	8.7
K6M_2	12.6	9.3	36	431	489	411	6.02	13.96	21.5
K6M_3	14.3	9.3	53	443	539	421	5.75	12.99	24.6
K6M_4	14.5	10.0	46	430	563	458	6.34	14.74	21.6
K6M_5	24.2	9.8	146	431	937	457	6.10	14.16	22.3
Average	16.0	9.2	73	432	618	420	5.6	13.0	19.8

Graphical results

*Figure A.7.12 K6M_228_20*20*60_Dry density & moisture content over cross section*

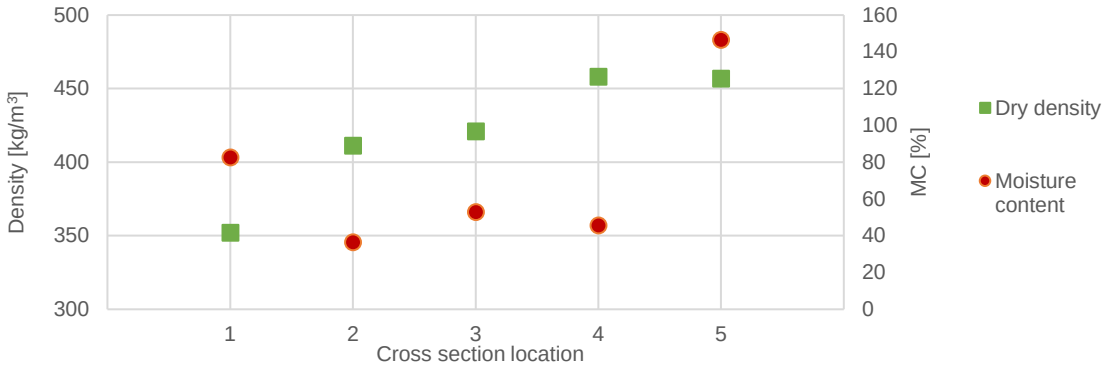

*Figure A.7.13 K6M_228_20*20*60 _Drilling amplitude with ultimate strength.*

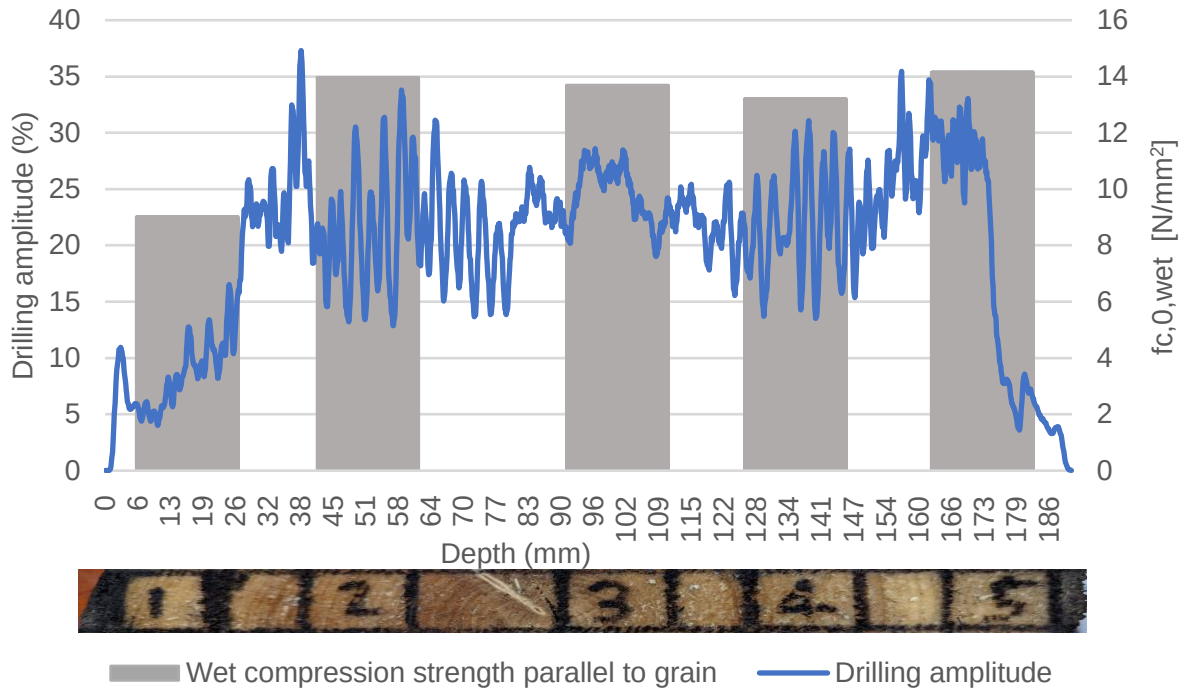

M6M_228

Table A.7.12 Full Specimen Results

Full pile ID	Segment code - container	wet density (kg/m³)	dry density (kg/m³)	m.c. (%)	MOE_{stat} (Mpa)	MOE_{dyn} (Mpa)	f_{c0} (Mpa)	soft shell (mm)	failure mechanism	remaining sound c-s (%)	RPD drilling avg (%)
BRU0030-PL2-P2.21	M6M-228	671	304	120	4590	5691	6.3	52	crushing (top)	51	9.1

Table A.7.13 Local 60mm cross-sectional results

Code	Mass Wet	Mass dry	Moisture Content	Area (wet)	Density wet	Density dry	Ultimate force	Ultimate strength	RPD drilling average
[#]	[g]	[g]	[%]	[mm^2]	kg/m^3]	kg/m^3]	[kN]	[N/mm^2]	[%]
M6M_1	19.92	5.85	241	434	763	247	2.09	4.81	8.8
M6M_2	16.32	11.03	48	437	623	506	6.89	15.77	30.1
M6M_3	14.31	8.77	63	435	553	397	4.06	9.34	21.4
M6M_4	15.57	10.70	46	442	592	454	5.86	13.26	25.3
M6M_5	19.33	8.10	139	436	738	365	3.72	8.53	14.0
Average	17.1	8.9	107	437	654	394	4.5	10.3	19.9

*Figure A.7.14 M6M _228_20*20*60 Dry density & moisture content over cross section*

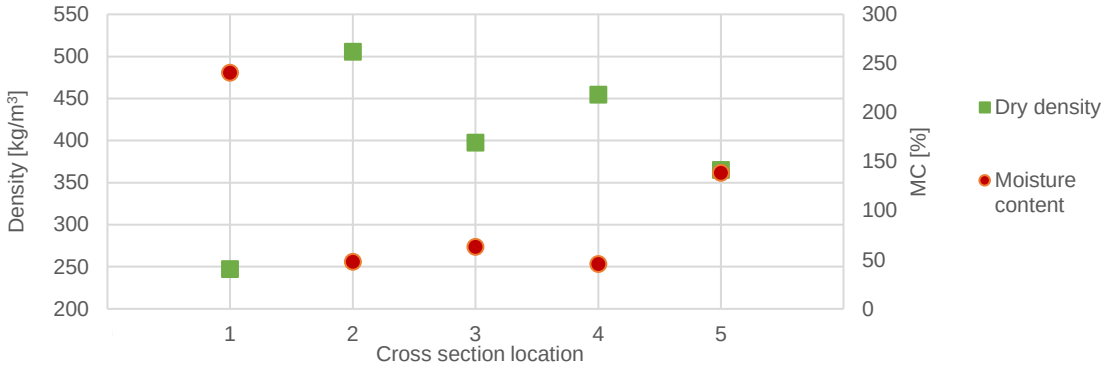

*Figure A.7.15 M6M _228_20*20*60 _Drilling amplitude with ultimate strength.*

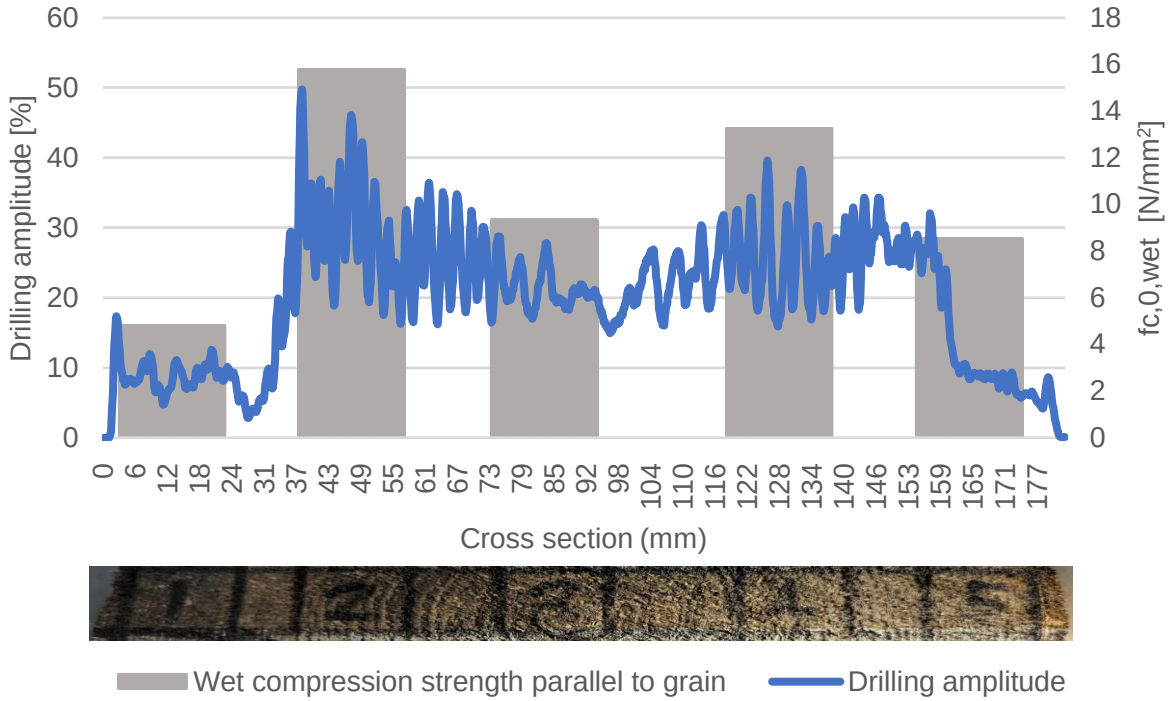

V6M_228

Table A.7.14 Full Specimen Results

Full pile ID	Segment code - container	wet density (kg/m^3)	dry density (kg/m^3)	m.c. (%)	MOE$_{stat}$ (Mpa)	MOE$_{dyn}$ (Mpa)	f_{c0} (Mpa)	soft shell (mm)	failure mechanism	remaining sound c-s (%)	RPD drilling avg (%)
BRU0030-PL2-P2.21	V6M-228	716	307	133	4230	4680	6.6	42	buckling (top)	51	9.3

Table A.7.15 Local 60mm cross-sectional results

Code	Mass Wet	Mass dry	Moisture Content	Area (wet)	Density wet	Density dry	Ultimate force	Ultimate strength	RPD drilling average
[#]	[g]	[g]	[%]	[mm^2]	kg/m^3]	kg/m^3]	[kN]	[N/mm^2]	[%]
V6M_1	16.7	7.8	114	428	650	345	3.71	8.68	11.2
V6M_2	14.5	8.5	71	428	560	391	5.02	11.72	24.1
V6M_3	14.6	8.9	64	431	561	392	4.36	10.13	21.9
V6M_4	18.2	10.0	82	429	704	443	5.67	13.21	25.0
V6M_5	19.4	5.1	282	428	757	231	1.34	3.13	4.8
Average	16.7	8.0	122.7	428.8	646.6	360.4	4.0	9.4	17.4

Graphical results

*Figure A.7.16 V6M_228_20*20*60 Dry density & moisture content over cross section*

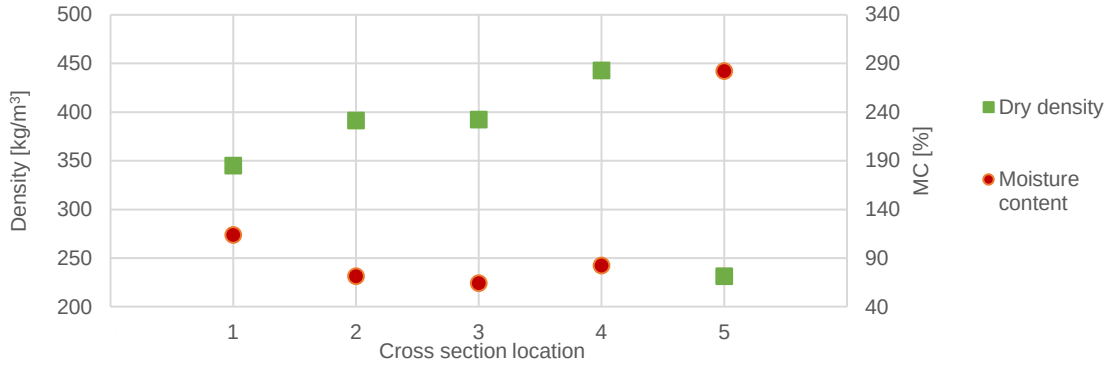

*Figure A.7.17 V6M_228_20*20*60 _Drilling amplitude with ultimate strength.*

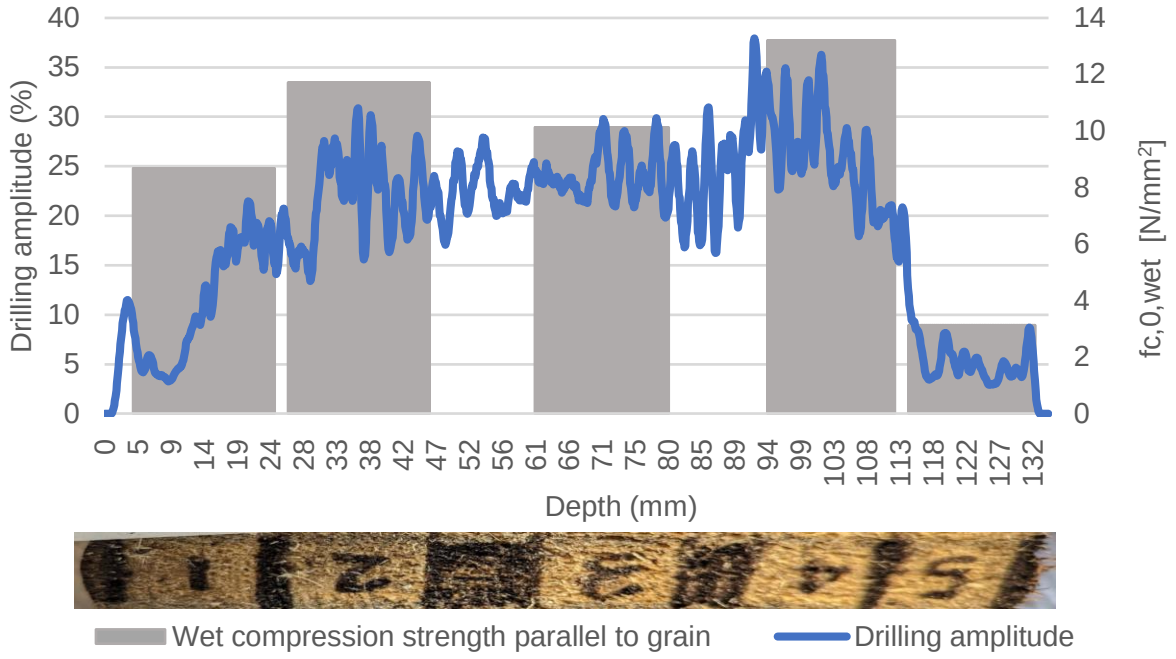

A8 - Future predictive model strategy based on linear regression.

The analysis of micro-drilling signals was conducted to establish relationships with physical and mechanical properties such as moisture content, dry density, compressive strength, and modulus of elasticity. In each case, drilling amplitude served as the independent variable, while the property under examination acted as the dependent variable. The results from degraded, non-degraded, and combined samples revealed distinct patterns. For example, degraded specimens (3M, 2.7M & 6M) displayed softshell thicknesses of 38mm, 39mm & 41mm respectively. Through linear regression analysis, highly significant formulas were derived, with coefficients of determination at 70% for MC, 81% for dry density, 78% for compressive strength, and 76% for MOE. Notably, a focused examination on compressive strength, coupled with a drilling amplitude of less than 15% within the softshell layer, led to an enhanced R^2 value of 0.81. These formulas, derived from the linear regression analysis, can be effectively applied to predict properties in new piles, providing valuable insights for assessing their characteristics and behaviour.

To evaluate the predictive accuracy of the formulas, it is essential to conduct a practical test. Utilizing the findings from [43] for the complete pile tests. The Average drilling amplitude can be employed and subsequently integrated into the following equations for assessment. This creates the theoretical result which can be found in the tabulated results below.

Degraded piles
Mc = $658.01x^{-0.723}$. (R^2=70%)
Dry density = $166.27x^{0.2901}$ (R^2=82%)
Compression strength = 0.4166x +2.4282. (R^2=78%)
MOE = 257.92x + 457.17. (R^2=76%)

Physical & Mechanical Properties

To evaluate the predictive accuracy of the formulas, it is essential to conduct a practical test. Utilizing the findings from [43] for the complete pile tests. The Average drilling amplitude is employed and subsequently integrated into the following equations for assessment. This creates the theoretical result which can be found in the tabulated results below. Table A8.1 & A8.2 have been produced for degraded piles in order to determine the predictive capabilities of the equations determined through the linear regression analysis. The pile has 3 sections to which a ratio for the difference between theoretical and experimental results have been tabulated. For Moisture content, Dry density, fc,0,wet and MOE the average result for the 3 piles is 0.96 ± 17, 1.15 ± 12 ,1.07 ± 25 and 0.69 ± 20 respectively.

The study's findings reveal distinct predictive patterns across different material properties. Moisture content predictions average at 0.96 of actual values, exhibiting a modest underestimation, coupled with a 0.17 variability around this mean. In contrast, predictions for dry density are notably higher, averaging at 1.15 of actual values, with a narrower variability of ±0.12 compared to moisture content. For fc,0,wet, predictions tend to exceed actual values, averaging at 1.07, while displaying a wider variability of ±0.25, surpassing both moisture content and dry density in terms of variation. Notably, predictions for MOE are consistently lower, averaging at 0.69 of actual values, accompanied by a 0.20 variability. This indicates that the model's accuracy varies for different properties; it exhibits a high degree of accuracy for dry density, moderate accuracy for moisture content and fc,0,wet, but demonstrates comparatively lower accuracy for MOE. These insights underscore the model's strengths and limitations in predicting diverse material characteristics, shedding light on the reliability of the linear regression-based analysis.

Table A8.1 Physical results for degraded piles both experimental and theoretical results

Pile Segment	*MC Actual*	*MC theoretical*	*Ratio*	*Pile avg. ratio*	*Dry Density Actual*	*Dry Density Theoretical*	*Diff.*	*Pile avg. ratio.*
[NUM]	[%]	[%]	[N/A]	[%]	(kg/m^3)	(kg/m^3)	[%]	[%]
K3M-228	192	145	0.75	0.78	266	305	1.15	1.21
M3M-228	170	149	0.87		245	302	1.23	
V3M-228	222	155	0.70		235	297	1.27	

K6M-228	97	123	1.27	1.12	329	326	0.99	1.02
M6M-228	120	133	1.11		304	316	1.04	
V6M-228	133	131	0.98		307	318	1.03	
K2.7-115	97	99	1.02	0.98	289	355	1.23	1.23
M2.7-115	106	129	1.22		258	320	1.24	
V2.7-115	175	121	0.69		270	328	1.21	

Table A8.2 Mechanical results for degraded piles both experimental and theoretical results

Pile Segment	*fc,0,wet Actual*	*fc,0,wet Theoretical*	*Ratio*	*Pile avg. ratio*	*MOE Actual*	*MOE Theoretical*	*ratio*	*Pile avg. ratio*
[NUM]	[N/mm^2]	[N/mm^2]	[%]	[%]	[Mpa]	[Mpa]	[%]	[%]
K3M-228	7.1	5.8	0.82	0.99	8400	2546	0.30	0.59
M3M-228	5.3	5.7	1.07		3720	2469	0.66	
V3M-228	5.1	5.5	1.08		2930	2366	0.81	
K6M-228	9.8	6.7	0.68	0.87	8300	3088	0.37	0.55
M6M-228	6.3	6.2	0.99		4590	2804	0.61	
V6M-228	6.6	6.3	0.95		4230	2856	0.68	
K2.7-115	6.1	8.1	1.33	1.35	4972	3981	0.80	0.91
M2.7-115	4.1	6.4	1.56		2569	2910	1.13	
V2.7-115	5.8	6.8	1.17		3935	3144	0.80	

Non-degraded piles

Mc = 24.942x$^{0.2966}$, (R^2=2.5%)
Dry density = 165.1x$^{0.3288}$ (R^2=45%)
Wet compression strength = 0.3764x +7.8576, (R^2=27%)
MOE = 420.62x - 613.36, (R^2=58%)

Table A8.3 & A8.4have been produced for degraded piles in order to determine the predictive capabilities of the equations determined through the linear regression analysis. The pile has 3 sections to which an average ratio results for the difference between theoretical and experimental results have been tabulated. For Moisture content, Dry density, fc,0,wet and MOE the average result for the 3 piles is 0.79 ± 0.20, 0.98 ± 0.17 ,0.88 ± 0.19 and 0.48 ± 0.19 respectively.

Table A8.3 Physical results for non-degraded piles both experimental and theoretical results

Pile Segment	*MC Actual*	*MC theoretical*	*Ratio*	*Pile avg. ratio*	*Dry Density Actual*	*Dry Density Theoretical*	*Ratio*	*Pile avg. Ratio*
[NUM]	[%]	[%]	[%]	[%]	(kg/m^3)	(kg/m^3)	[%]	[%]
K11M-228	81	50	0.62	0.65	415	355	0.86	0.86
M11M-228	77	51	0.66		396	365	0.92	
V11M-228	76	52	0.68		464	370	0.80	
K3.18-115	56	60	1.06	0.93	373	433	1.16	1.09
M3.18-115	52	56	1.06		390	402	1.03	
V3.18-115	84	55	0.65		363	396	1.09	

Table A8.4 Mechanical results for non-degraded piles both experimental and theoretical results

Pile Segment	*fc,0,wet Actual*	*fc,0,wet Theoretical*	*Ratio*	*Pile avg. Ratio*	*MOE Actual*	*MOE Theoretical*	*Ratio*	*Pile avg. Ratio*
[NUM]	[N/mm^2]	[N/mm^2]	[%]	[%]	[Mpa]	[Mpa]	[%]	[%]
K11M-228	16.9	11.7	0.69	0.74	12530	3719	0.30	0.34
M11M-228	16.3	12.1	0.74		12210	4098	0.34	
V11M-228	15.4	12.2	0.79		11140	4266	0.38	
K3.18-115	14.9	14.9	1.00	1.02	10766	7290	0.68	0.61
M3.18-115	14.2	13.5	0.95		10179	5698	0.56	
V3.18-115	12.1	13.3	1.10		8990	5420	0.60	

The results shown above hold significant promise, but they necessitate comprehensive testing across a diverse array of both degraded and non-degraded specimens to ascertain their potential practical application. It's important to note that these findings are exclusively derived from drilling amplitude tests performed on the cross sections of complete piles. One notable concern is that the experiments in this thesis were carried out on clear wood samples. Consequently, for accurate results, the failure mode of the pile must occur under pure compression. Should the pile fail due to stress concentration at the knots, the theoretical results could significantly overestimate its actual strength.

A9 - Cross-sectional bearing capacity future calculation strategy based on drilling amplitude.

The primary objective underlying this calculation is to ascertain the residual strength of the foundation piles. This determination is predicated on a two-fold consideration, encompassing both the average strength exhibited by the intact and structurally sound sections of the wood, as well as the supplementary remaining strength attributed to the softshell region of the piles. By calculating the residual strength through this method, it becomes possible to gain insights into the overall load-bearing capacity and structural integrity of the foundation piles, even in instances where certain portions of the wood exhibit degradation and high softshell volume. This analytical approach allows for a more precise and comprehensive understanding of the piles' performance and durability, thus providing a valuable asset in the field of structural engineering and infrastructure management.

The calculation of the area relies on fundamental basic geometric principles, inherently offering a reasonable estimate suitable for rapid computations of the strength. To address the non-uniformity inherent to circular piles, a more precise approach is employed. This involves acquiring two drilling amplitudes, which collectively provide a more accurate representation of the entire diameter of the pile. As a consequence, the results are presented as two distinct values, referred to as "d1" and "d2." This dual-amplitude strategy enhances the precision of the assessment, accommodating the variations observed in the circular geometry of the pile.

$$Average\ area\ of\ pile = \frac{1}{4}\pi\left(\frac{d1+d2}{2}\right)^2$$

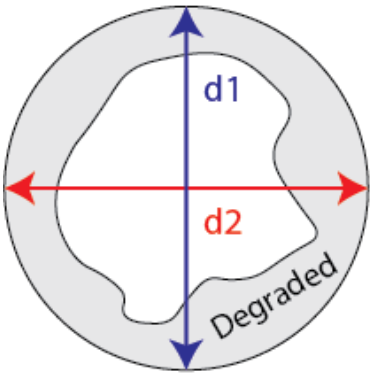

Figure A9.1 Cross section

The determination of the softshell can be accomplished through the utilization of a specialized softshell calculator, with softshell 1 (SS_1) representing the cumulative measure of zones 1 and 2. Similarly, a parallel procedure is employed for softshell 2 (SS_2), resulting in two distinct lengths corresponding to each respective softshell zone.

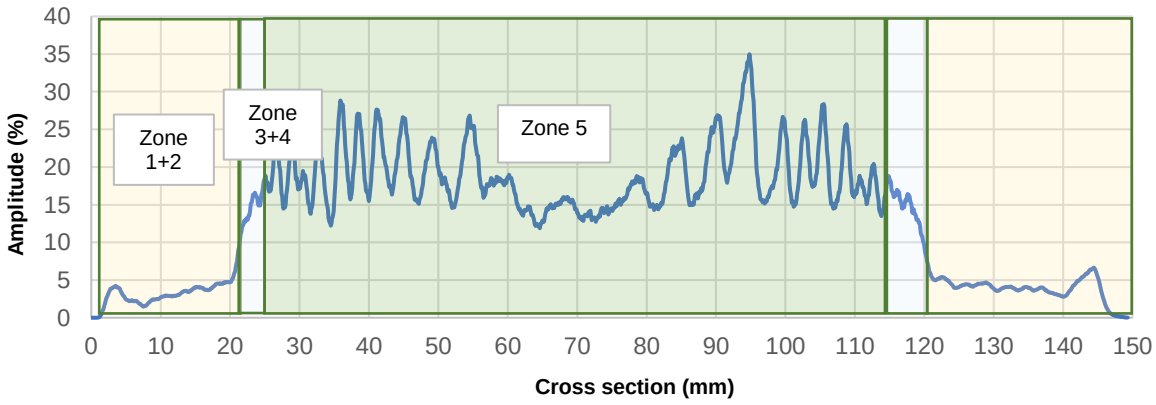

Figure A9.2 Drilling amplitude Vs. Cross section.

$$Average\ Sound\ wood\ area = A_s = \frac{1}{4}\pi\left(\frac{(d1 - SS_1) + (d2 - SS_2)}{2}\right)^2$$

$$Average\ Soft\ shell\ area\ = A_d = \frac{1}{4}\pi\left(\frac{d1 + d2}{2}\right)^2 - \frac{1}{4}\pi\left(\frac{(d1 - SS_1) + (d2 - SS_2)}{2}\right)^2$$

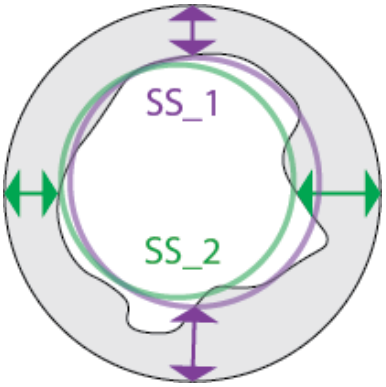

Figure A9.3 Soft shell cross section

The two strengths will then need to be calculated and this can be done using the Average drilling amplitude for the softshell (zone 1&2) area which has been correlated with the strength of the softshell. This can then be substituted into the following formula.

$$f_{c0\_softshell} = f_d = 0.7026x + 0.8461$$

The sound wood area can be determined separately (zone 3,4&5). This can then be substituted into the following formula.

$$f_{c0_{soundwood}} = f_s = 0.4166x + 2.4282$$

Given the composite action of the sound and degraded part it is paramount to consider the modulus ratio which refers to the relationship between the elastic moduli of the constituent materials in the composite material.

Mathematically, the modulus ratio (n) can be expressed as:

$$n = \frac{E_s}{E_d}$$

E_s is the elastic modulus of the sound part . Y = 257.92x + 457.17 R² = 0.7578
E_d is the elastic modulus of the degraded part Y = 257.92x + 457.17 R² = 0.7578

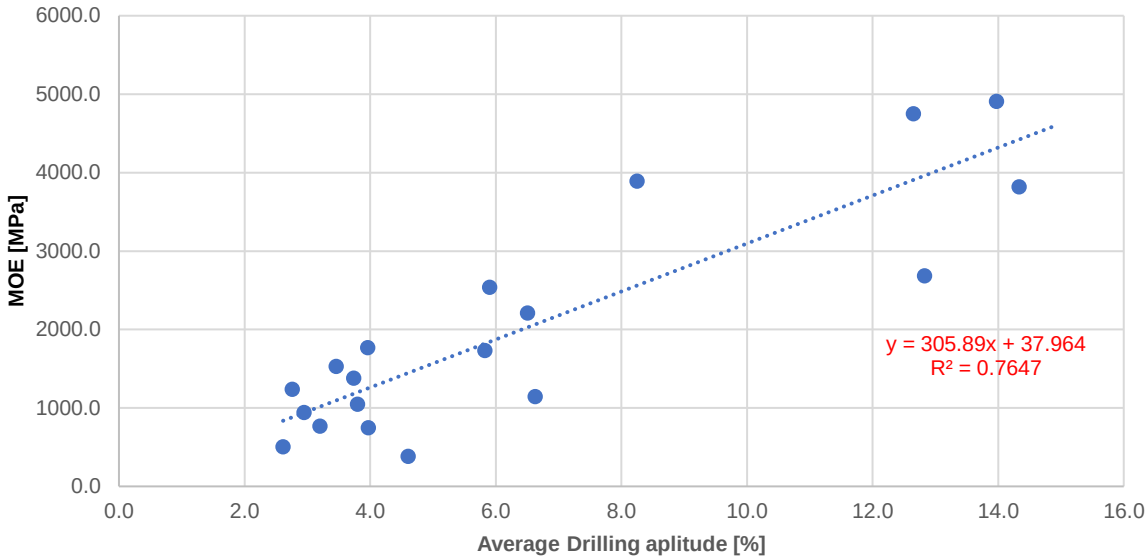

Figure A9.4 MOE vs Drilling amplitude

Equation (1)

$$Total\ load = shared\ by\ sound\ and\ degraded\ parts$$
$$F = f_s + f_d$$

Equation (2)

$$\text{Assumption} = One\ pile = one\ deformation \therefore equal\ strains$$
$$\varepsilon_s = \varepsilon_d \implies \frac{\sigma_s}{E_s} = \frac{\sigma_d}{E_d}$$

Expanding this given:

$$\sigma_s = \frac{f_s}{A_s} \; and \; \sigma_d = \frac{f_d}{A_d}$$

Substituting into equation (2)

$$\frac{f_s}{A_s * E_s} = \frac{f_d}{A_d * E_d}$$

Therefore,

$$f_d = f_s * \frac{A_d}{A_s} * \frac{E_d}{E_s}$$

$Let\ n = \frac{E_s}{E_d} (> 1)$

$$f_d = f_s * \frac{A_d}{A_s} * \frac{1}{n}$$

Substitute this back into equation (1)

$$F = f_s + f_d$$

$$F = f_s * \left(\frac{A_d}{A_s} * \frac{1}{n}\right) + f_d$$

$$F = f_s * \left(\frac{A_d}{A_s * n} + 1\right)$$

Therefore,

$$F = f_s * \frac{A_d + A_s * n}{A_s * n}$$

$$F = f_s * \frac{\left(\frac{1}{4}\pi\left(\frac{d1 + d2}{2}\right)^2 - \frac{1}{4}\pi\left(\frac{(d1 - SS_1) + (d2 - SS_2)}{2}\right)^2\right) + \frac{1}{4}\pi\left(\frac{(d1 - SS_1) + (d2 - SS_2)}{2}\right)^2 * n}{\frac{1}{4}\pi\left(\frac{(d1 - SS_1) + (d2 - SS_2)}{2}\right)^2 * n}$$

Or force in sound part,

$$f_s = F * \frac{A_s * n}{A_1 + A_s * n}$$